NOTICE

The quality of this microform is heavily dependent upon the quality of the original thesis submitted for microfilming. Every effort has been made to ensure the highest quality of reproduction possible.

If pages are missing, contact the university which granted the degree.

Some pages may have indistinct print especially if the original pages were typed with a poor typewriter ribbon or if the university sent us an inferior photocopy.

Reproduction in full or in part of this microform is governed by the Canadian Copyright Act, R.S.C. 1970, c. C-30, and subsequent amendments.

AVIS

La qualité de cette microforme dépend grandement de la qualité de la thèse soumise au microfilmage. Nous avons tout fait pour assurer une qualité supérieure de reproduction.

S'il manque des pages, veuillez communiquer avec l'université qui a conféré le grade.

La qualité d'impression de certaines pages peut laisser à désirer, surtout si les pages originales ont été dactylographiées à l'aide d'un ruban usé ou si l'université nous a fait parvenir une photocopie de qualité inférieure.

La reproduction, même partielle, de cette microforme est soumise à la Loi canadienne sur le droit d'auteur, SRC 1970, c. C-30, et ses amendements subséquents.

Experimental and Analytical Investigation on the Design of a New Electronic Fuel Control Unit for Small Gas Turbine Engines

Gino Carrese

A Thesis

in

The Department

of

Mechanical Engineering

Presented in Partial Fulfillment of the Requirements
for the Degree of Master of Engineering at
Concordia University
Montreal, Quebec, Canada

September 1989

ISBN 0-315-51388-8

ABSTRACT

EXPERIMENTAL AND ANALYTICAL INVESTIGATION ON THE DESIGN OF A NEW ELECTRONIC FUEL CONTROL UNIT FOR SMALL GAS TURBINE ENGINES

Gino Carrese

The objective of this thesis is to examine a new design of a low cost electronic fuel control unit for small gas turbine engines. Application in remotely piloted vehicles is targeted. The proposed design uses some mass produced components from fuel injection systems for automobiles. It incorporates a diaphragm valve keeping constant differential pressure across a metering valve that is actuated by a digital linear actuator. Mathematical models of the steady state and transient performance of the system are created for computer simulation. A prototype is tested to validate the models. Multiobjective optimization of the system's hydromechanical design is then performed with the validated models. The optimization criteria include speed of transient response, system sensitivity to design parameter changes, and linearity of the metering valve flow schedule.

ACKNOWLEDGEMENTS

The author would like to express his gratitude and deep appreciation to his thesis supervisor, Dr. T. Krepec, for his successful guidance and for providing the resources necessary to carry out this research.

The author is also grateful to Antonios Georgantas for the many discussions and for his assistance during the course of this work.

Thanks are also extended to other members of the fuel Control Systems Laboratory at Concordia University; Carmine Lisio and Domenic Miele.

Thanks are also due to Bendix Avelex for manufacturing parts of the fuel control unit prototype and for their financial assistance.

Finally, the author would like to thank his parents for the sacrifices they made for their children.

This work was supported financially by the Natural Sciences and Engineering Research Council of Canada Postgraduate Scholarship, Concordia Graduate Fellowship, and Fonds pour la Formation de Chercheurs et l'Aide a la Recherche du Quebec.

TABLE OF CONTENTS

LIST OF FIGURES

LIST OF TABLES

NOMENCLATURE

A_c - curtain area through diaphragm orifice

A_{ci} - effective flow area for diaphragm orifice and nozzle orifice in series

A_d - diaphragm effective area

A_i - nozzle flow area

A_{io} - nominal nozzle flow area

A_m - metering valve flow area

A_n - nozzle manifold pipe inlet cross sectional area

A_o - flow area through diaphragm orifice

A_{or} - maximum flow area through diaphragm orifice

A_{pr} - effective pressure area for regulating valve plunger

a_r - effective flow area through regulating valve

b - effective damping of diaphragm

c_{di} - flow coefficient for nozzle orifice

c_{dm} - flow coefficient for metering valve

c_{do} - flow coefficeint for diaphragm orifice

c_{dr} - flow coefficient for flow through pressure regulator

d - wire diameter of helical preload spring

d_n - diameter of nozzle manifold pipe inlet

dq - change in nozzle flow

D_r - diameter of regulating valve plunger

f - stepper motor stepping frequency

f_{sp} - helical spring preload force

FS - Fuel Schedule

g(x) - inequality constraint

G - shear modulus of elasticity

$G(x)$ - goal function

h - diaphragm deflection

$h(x)$ - equality constraint

h_{max} - gap in diaphragm orifice with undeflected diaphragm

i - number of metering valve slits

ITAE - transient response index

ITAEMIN - minimum ITAE index

K - number of simulation steps

k_s - spring constant of helical preload spring

k_{sr} - spring constant of regulating valve preload spring

l - metering valve plunger actuation distance

l_c - helical spring preload compression

l_o - initial metering valve position

l_f - final metering valve position

m_d - effective diaphragm mass

m_f - air mass flow

N - number of active helical spring coils

p_c - combustor pressure

p_{co} - compressor pressure

p_d - upper diaphragm chamber pressure

p_n - nozzle back pressure

p_{nd} - demanded nozzle pressure

p_{ni} - nozzle back pressure at ith simulation step

p_p - pump pressure

p_{pr} - regulated pump pressure

p_c - combustor pressure

P^* - intermediary pressure for two stage throttling assumption in diaphragm orifice

q - nozzle flow

q_{dn} - flow through diaphragm orifice

q_l - flow with perturbed parameter

q_{nc} - flow through nozzle

q_o - nominal nozzle flow

q_{pd} - flow through metering valve

q_r - bypassed flow

q_s - flow change per stepper motor step

s - stepper motor step size

S - set of nondominated solutions

SENS - sensitivity index

SENSMIN - minimum sensitivity index

t - simulation time

VAR - variation of differential pressure index

VARMIN - minimum VAR index

v - diaphragm velocity

v_d - volume of upper diaphragm chamber

v_n - volume of nozzle manifold

w - width of metering valve slits

w_i - weight on objective function

x_o - nominal regulating valve plunger position

x_r - regulating valve plunger deflection from nominal position

x - design vector

$z(x)$ - vector of objective functions

GREEK SYMBOLS

β - bulk modulus of fuel

ε - constraint on objective function

Δp - differential pressure across metering valve

Δp_{ave} - average differential pressure

Δp_{ext} - extreme differential pressure

Δt_i - time step at ith iteration

χ - feasible design space

ρ - fuel density

CHAPTER 1

INTRODUCTION

1.1 General

In this introduction, the function of a fuel control unit for small gas turbine engines will be explained. The fuel requirements of gas turbines are then discussed. Finally, the objective of this thesis and the program followed to achieve it will be outlined.

The application of gas turbine engines in aviation has increased rapidly in the past twenty years [1]. A single shaft, open cycle gas turbine, in the simplest form, is shown in Figure 1.1. It works on the Brayton thermodynamic cycle, which involves air induction, air compression, fuel addition and combustion, and product gas expansion and expulsion. A fuel control unit is responsible for the fuel delivery portion of the cycle.

The major functional control components of the gas turbine are shown in Figure 1.2. The computing section compares the operator demand for a speed or power level with information from engine sensors. Based on the logic of the computing section, actuators are moved to meet the demand. The new operating point is monitored by the sensors and fed back to the computing section to close the loop [2]. Typically, speed, pressure and temperature are measured by engine instrumentation, either mechanically, electrically or fluidically. Elements such as bellows and thermocouples are employed. The control system also protects the engine from hazardous operation.

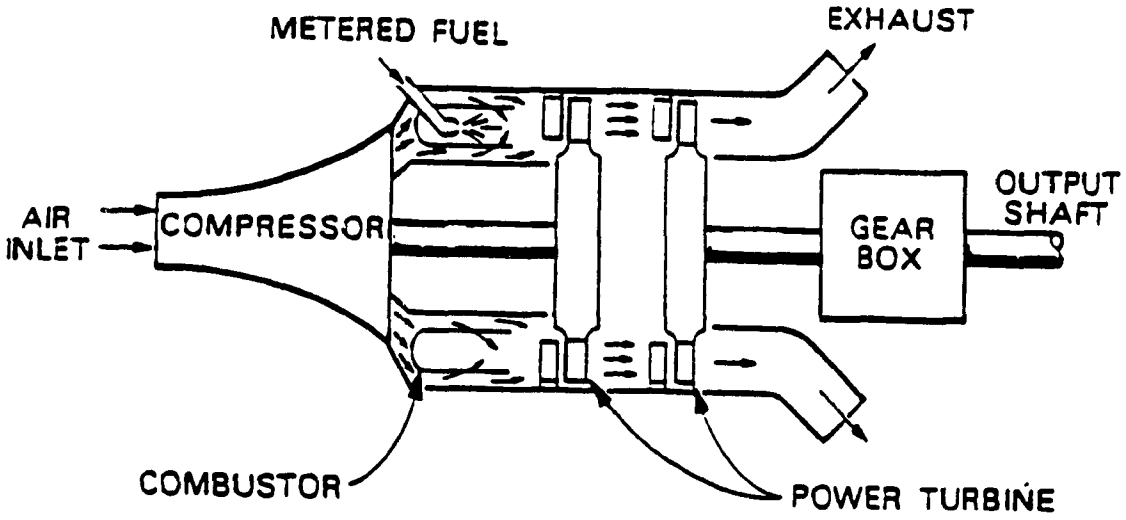

Figure 1.1 Simplified Schematic of a Gas Turbine Engine [3]

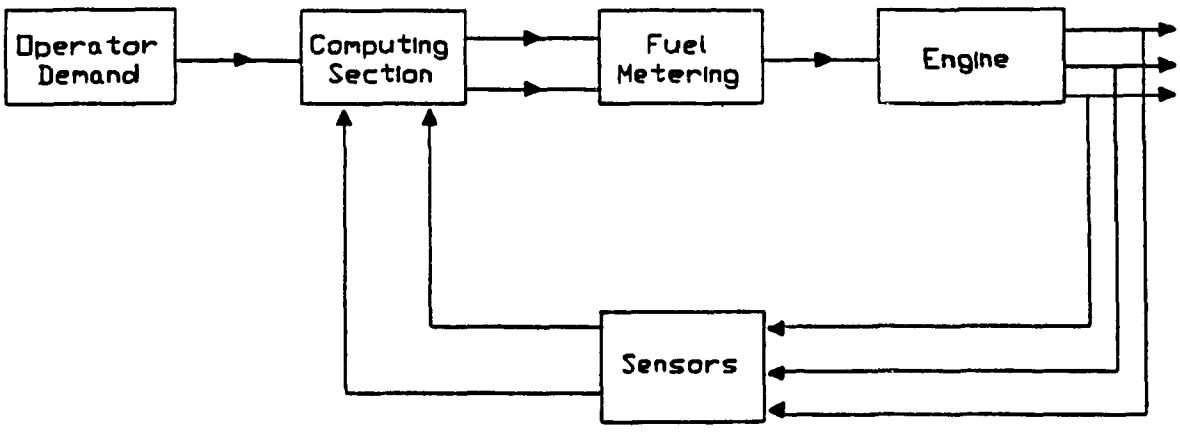

Figure 1.2 Control System Functional View of a Gas Turbine Engine

To meter fuel flow to an engine, one needs a pump, a metering valve, and a system for bypassing the excess fuel delivered by the pump (Figure 1.3). Engine driven constant displacement pumps are commonly used. Ususally, the bypass system maintains a constant pressure drop across a metering valve. The metering valve flow area then determines the flow to the engine. The metering valve is moved by an actuator under control of the computing section.

To close the loop, the speed of the turbine engine is measured as feedback. The fuel flow to the engine, i.e., the output of the fuel control unit, is only an intermediate variable in the overall system that includes the engine. Torque and compressor pressure are also used as feedback signals.

In conventional fuel controls, several actuators are used that are also primary sensing devices. For example, bellows are used that sense the compressor pressure, and by expanding, actuate the metering valve. The same can be said of centrifugal governors. The weights sense speed by moving apart against a spring due to the centrifugal force. This action actuates a valve. For the newly introduced electronically controlled units, the conceptual difference in operation is that the increased flexibility allows the control to rely on only one metering valve actuating device. All sensing devices are transducers that convert the sensed signals to an electrical form that is fed into a computer. Based on all sensed signals, the computer decides what the single actuator should do to provide the

required fuel flow. This has a simplifying effect on the design of a fuel control unit.

1.2 Fuel Flow Requirements of a Small Gas Turbine Engine

A fuel control system must deliver fuel to the combustion chamber of an engine in the quantity and under the pressure required to produce the necessary burning conditions in order to control the speed or power output of the engine. The fuel supply to the combustion chamber has to match the air supply provided by the compressor to maintain the correct fuel-air ratio for combustion [4]. Because air mass flow (m_f) is difficult to monitor directly as a signal to control the fuel flow, usually the compressor pressure, P_{co}, (which is approximately proportional to the air mass flow) is used. The fuel delivery rate required is expressed as a fuel schedule, FS, which is a measure of the fuel-air ratio.

$$FS = m_f / P_{co}$$

A typical fuel schedule is shown in Figure 1.4. The following are important branches of the characteristic:

1) Acceleration Schedule (maximum schedule)

This schedule provides the maximum fuel to the combustor during the short time of acceleration. If too much fuel is provided, the combustor pressure builds up too high, leading to compressor stall and excessive gas temperatures

(which can damage the turbine blades).

2) Deceleration Schedule (minimum schedule)

This schedule maintains the minimum flow required during deceleration to prevent "flameout" due to too lean fuel-air mixture.

3) Governing Schedule

This schedule controls the engine speed at any setpoint. A speed governor decreases fuel flow as speed approaches the desired value. If engine speed exceeds the setpoint, the fuel flow is decreased below steady state requirements, decelerating the engine. The steady state is reached when the governor fuel flow equals the engine steady state load requirements. Typically, proportional plus integral (isochronous) or proportional (droop) governing control modes are used. Several settings are usually pre-set for the speed governing schedule. They are

a) maximum speed range

b) idle speed range, which may include two speeds;

i) ground idle, and
ii) flight idle.

Besides these settings, most fuel controls incorporate "all speed governors" where infinitely many speed ranges can be selected by the pilot via a throttle lever position.

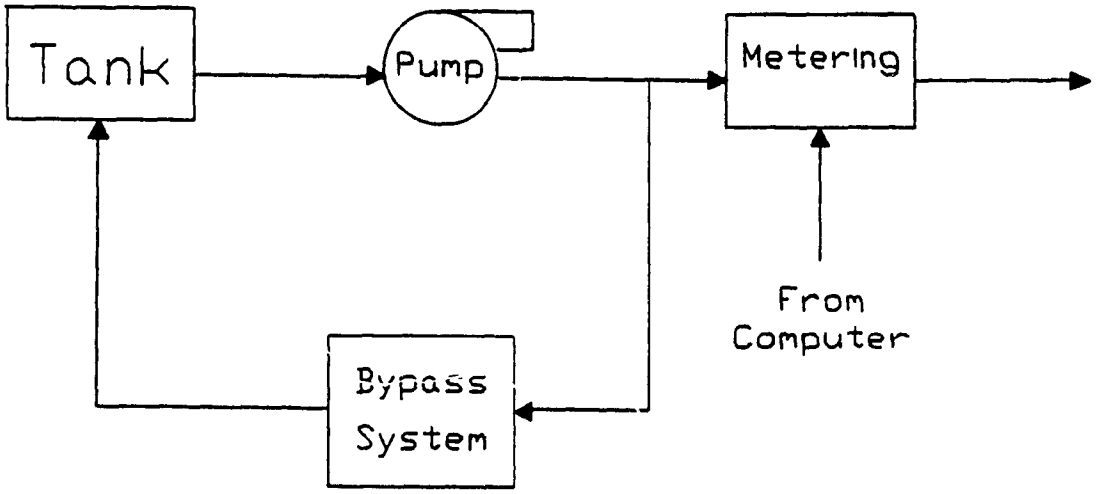

Figure 1.3 General Fuel Control Unit Concept [2]

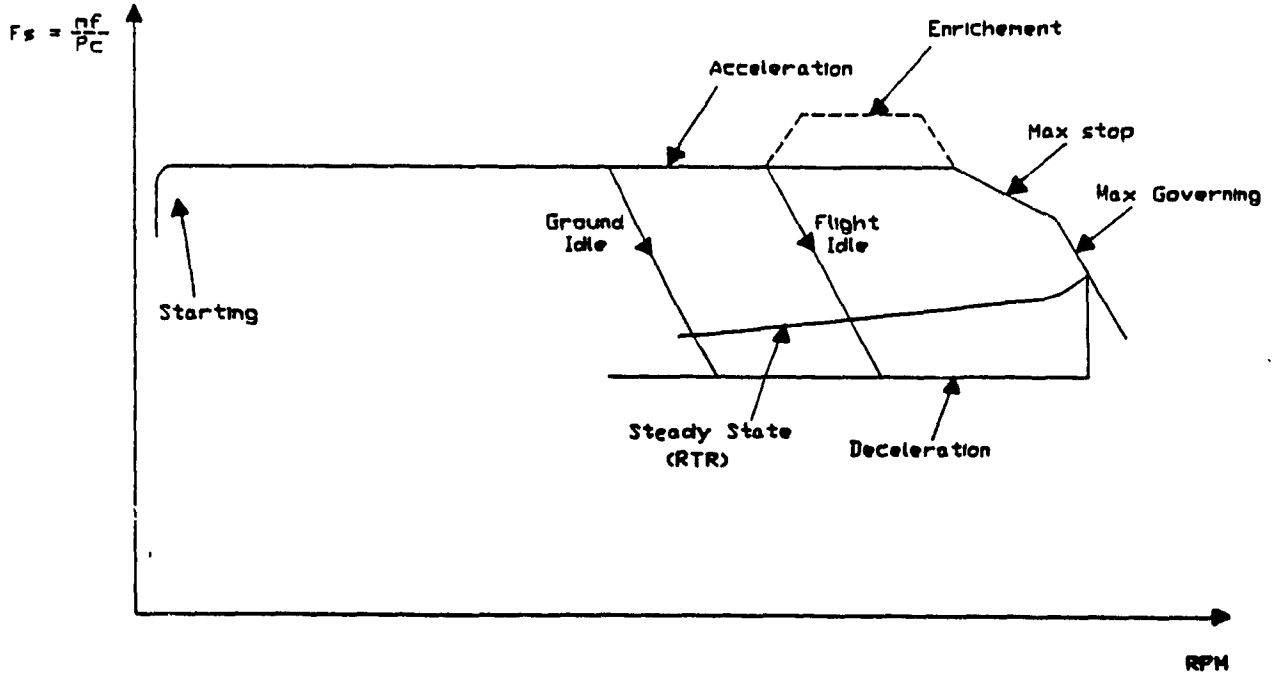

Figure 1.4 Fuel Schedule for Fuel Control of a Turboprop Engine [4]

4) Steady State Schedule (RTR)

This schedule, also called the "required to run" (RTR) schedule, depends on the engine load. For a propeller loaded shaft, the RTR curve is as shown in Figure 1.4. The fuel supply is set at every speed to balance the propeller load. A fuel flow rate in excess of the steady state requirements for that speed causes acceleration. Conversely, a flow below the steady state requirements at a particular speed causes deceleration.

Some implications of the fuel schedule should be considered. At governing, the fuel control is a feedback control system, with speed feedback. During acceleration or deceleration, however, the fuel control operates in the open loop (no fuel flow or speed feedback). For the acceleration mode, it is desired, for best efficiency, to accelerate as fast as possible. However, there is a safety margin to prevent compressor stall. For every speed there is an acceleration limit. A fuel stall boundary curve can be drawn by experimentally increasing the fuel flow rate to the combustor at various speeds and noting when compressor surge occurs. The fuel control must provide an accurate fuel delivery rate to operate close to this limit without deviating into the stall region. Since there is no practical mechanism for accurately predicting or assessing the onset of surge, the stall limit is programmed into the fuel control in advance. For deceleration, it is desired to decelerate as fast as possible. But, the fuel flow cannot be reduced too much since this causes flameout. It can be

concluded that acceleration and deceleration place more stringent requirements on the performance of the fuel control since the benefits of feedback are not available.

1.3 Thesis Objective

This thesis involves an analysis of a fuel control design. A low cost, reliable, electronic fuel control for a small gas turbine engine is desired. This thesis shows how to apply engineering analysis to the analysis, testing, and optimization of such a fuel control.

1.4 Thesis Outline

This chapter explained what a fuel control is and what the gas turbine fuel requirements it must fulfill are. A review of research work in electronic fuel control for small gas turbines is performed in chapter 2. Similar automotive developments are also covered. The recogniton of a need in industry for a low cost fuel control unit that justifies the undertaking of this project is identified in chapter 3. The fuel control proposal is described in chapter 4. Mathamatical models for its steady state (chapter 5) and transient performance (chapter 8) are created. After describing the experimental setup (chapter 6), prototype testing is used to validate the models (chapters 7 and 9). Then, three design optimization criteria are examined seperately; linearity of the metering valve flow schedule (chapter 10), sensitivity to parameter changes during service life (chapter 11), and transient response time (chapter 12). In chapter 13, the three criteria are unified using multiobjective optimization. Chapter 14 summarizes the thesis and makes conclusions and recommendations. Figure 1.5 shows the organizational flowchart of the thesis.

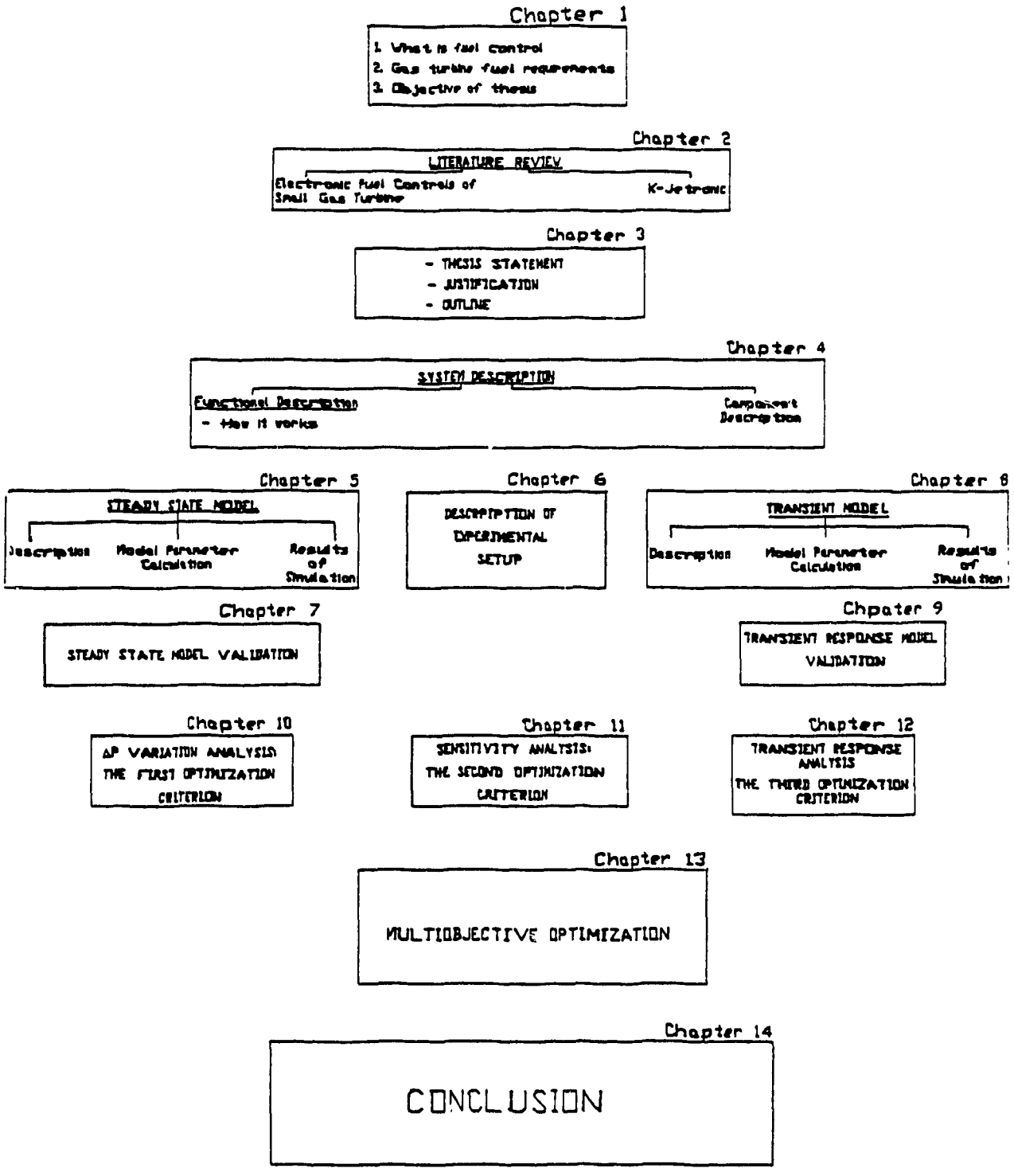

Figure 1.5 The Organization of the Thesis

Chapter 2

LITERATURE REVIEW

In this chapter, the work published in the literature related to this thesis will be examined. First, developments in electronic fuel control for small gas turbines will be reviewed. Then, developments in automotive fuel control will be discusssed.

2.1 Review of Developments in Electronic Fuel Control For Small Gas Turbine engines

As early as 1965, the potential benefits of the increased flexibility offered by microelectronics and digital control in fuel control were recognized. However, at the time, electronic computers were still bulky, unreliable and expensive. Semiconductor integrated circuits were already anticipated but not available yet [5] [6]. Hydromechanical fuel control units with pneumatic computing capabilities were well developed and became very reliable. Typically, these units relied on multicomponent hydromechanical systems to modulate the flow. These systems were heavy, expensive, and took up much space [7].

Despite the tremendous advances in digital control, electronics, and semiconductors during the long period of research and development that has occured since the 1960's, electronic fuel controls are still not fully accepted regarding their reliability. For airliners, a sufficient level of hydromechanical backup and multiple and completely

redundant electronic controls are used to provide a rescue in case of failure [8]. If one of the electronic channels fails, another channel takes over. In big airliners, 4-channel systems are being used. The higher price of such a solution is justified because it avoids the high financial penalties incurred if a fuel control unit failure interrupts the flight schedule [8]. For small gas turbine engines, however, the extra cost this implies is not easily absorbed.

Historically, much of the progress in digital electronic fuel control systems was developed by the American Air Force with primary emphasis toward the large gas turbine engines used to power tactical and strategic manned aircraft. Because of the high sophistication and cost of these systems, very little technical spin-off occured for the control systems of small, non man-rated engines used to power drones, RPVs and missiles [7].

For unmanned applications in missiles and remotely piloted vehicles (RPVs), there has been more general acceptance of full authority electronic computation in fuel controls than is the case for manned application [9]. This is because in the case of unmanned vehicles, the price of failure is not high. Also, since the cost of the airborne remotely piloted vehicle is small compared to that of airliners, the more sophisticated (and expensive) airliner electronic fuel controls cannot be used.

Particularly for very simple controls, the fuel handling section, not the computing section, represents the

major portion of the total control unit costs. During 1973 and 1974, a program was conducted by Chandler Evans, under contract to the U.S. Air Force Aero Propulsion Laboratory (AFAPL) [10]. Tradeoff studies were performed in the initial phase of the program between various fuel pumping and metering systems in search of the most inexpensive and reliable configuration. Different systems were built and tested corresponding to three increasing levels of sophistication: 1) Low Cost Target Drone Control, 2) Cruise Missile Fuel Control and 3) More Complex RPV Controls. However, in this study, mostly analog computation was evaluated because digital computation was still expensive and not as reliable at the time. There is a need today for similar research and trade-off studies which would take into account the advances and lowering of costs in microprocessor and electronic actuator technology that has taken place since. Design configurations using different electronic actuators and control schemes are being intensively developed presently as companies fight for the RPV and missile portion of the fuel control market. Cost, performance and reliability will be the deciding factors.

In 1982, a new digital Multiapplication Control System (MACS) was developed and flight tested by Hamilton Standard for use in small aircraft gas turbine engines [11]. The design combines the computing power of modern digital electronic technology with the reliability of a simplified hydromechanical unit serving as a manual backup fuel control. The MACS system did not provide the sophisticated

failure logic and redundancy features of the digital systems in large gas turbines, but offered the possibility to incorporate them in future versions.

Similar research work has been, and is being done by other manufacturers. More complicated digital control schemes are being implemented in order to achieve better reliability and control [12] [13]. There is little doubt that eventually, advances in the reliability of electronic controls will diminish the need for extensive backup.

In the case of remotely piloted vehicles and missiles, the need for low cost is a strong factor in design. Some applications have operational lives of only a few hours. In 1984, Krepec and Georgantas adapted a diesel fuel injection pump for use in a small gas turbine engine [14][15]. Their concept was to take advantage of the low cost and high reliability of the mass produced automotive diesel fuel injection pump to build an inexpensive fuel control unit. The pulsating character of the fuel flow delivered by the pump was made continuous by a special flow equalizing system. The requirement for a non-linear fuel delivery characteristic of the acceleration and deceleration schedules was met by changing to electronic control. The metering valve was adapted to be actuated by a microprocessor controlled digital actuator. However, the unit would be too bulky for use in small remotely piloted vehicles.

In 1986, Georgantes and Krepec [16][17] adapted the conventional pneumatic computing Bendix DP-F2 fuel control

unit for electronic control. The metering valve was brought under microprocessor control by replacing the valve-actuating bellows by a digital linear actuator. In a later study, they brought the bypass valve under microprocessor control also. In their research on the increased flexibility offered by electronic control, they sought the interaction strategy and control logic of the two actuators that gives best response and back-up capability. Continuing with the above research, in 1989, Carrese, Georgantes and Krepec [18] developed a computerized method for automated optimization of the digital controller of a small gas turbine fuel control. In a follow-up paper, the same authors [19] studied different electronic controller structures to solve special control problems associated with fuel control.

Starting in 1987 and in cooperation with Bendix Avelex, the Fuel Control Laboratory at Concordia University designed a new low cost electronic fuel control unit for application in remotely piloted vehicles [20][21][22][23]. Their first target was the Williams International WTS 34 - a small gas turbine used in Canadair CL-227 Drones. In their first report, different possible pump and metering configurations were evaluated in terms of cost and ability to meet the performance specifications. Three designs were chosen for investigation, in which mass produced automotive fuel injection components and a standard Bendix DP-F2 bypass valve diaphragm were used in order to lower production costs.

In the last program report for Bendix Avelex [23], Carrese identified three criteria for optimization of the design of fuel control unit; linearity of the metering valve flow schedule, sensitivity of the unit to parameter changes over its operational life, and the speed of the transient response. A multiobjective optimization technique was applied to select the best design parameters for the unit.

In 1989, Swonger and Huffman published a paper on thier work in low cost control systems for expendable turbine engines [24]. This work, called the INTERFACE II program, was initiated by the U.S. Air Force and carried out by Teledyne CAE in conjunction with Wright Research and Development. The purpose of the program was to develop and demonstrate the technology base needed for advanced low cost non man-rated fuel control systems for small turbine engines. A new, low cost, lightweight digital electronic fuel control system was built applicable to a wide variety of drones, rpv's and missiles. The system was successfully tested on an engine in an altitude chamber. In the course of the development, different control modes, fuel pump and metering configurations, actuators, engine sensor and microcontroller systems were evaluated and compared.

2.2 Review of Developments in Automotive Fuel Control Systems

Hundreds of automotive vehicle models of various makes are today fitted with gasoline injection systems as standard features in Europe, the USA and Japan. Modern injection systems for spark-ignition engines do not inject the fuel directly into the cylinders but rather into the intake manifold or intake ports. They have the task of producing an optimum air-fuel ratio [25]. The important implication of this is that for these fuel injection systems, the fuel injection into the port is continuous, not intermittent (as would be the case for direct injection). For a gas turbine engine, continuous fuel flow is also required. Therefore, developments in such automotive fuel injection systems can have important consequences in fuel controls development for small gas turbine engines.

The automotive fuel injection system most related to the fuel control system design investigated in this thesis is the fully mechanical K-Jetronic system produced by Robert Bosch of West Germany and used in over 40 models of cars. Volkswagen was the first company to equip one of their cars for the U.S. market with this type of fuel injection in 1967 to reduce exhaust gas pollution. A schematic of the K-Jetronic system is shown in Figure 2.1.

The system primary pressure is generated by an electric fuel pump and maintained at its nominal value by a plunger-type pressure regulator integrated into the fuel distributor. The fuel passes through the filter to remove

solid particles, down to a small size of 0.025mm. The fuel accumulator maintains the pressure in the system after the engine has been stopped. This prevents the formation of vapour bubbles which would hinder hot starting [26].

A gas rotameter measures air flow by changing the float position by an amount proportional to the incoming air drawn in by the engine. This flowmeter force acts against the hydraulic system control pressure to move the metering valve. This pressure is controlled by the bimetallic strip warm-up regulator. It is only slightly reduced for full load enrichment and acceleration and is increased for altitude compensation. Hence, the metering valve (which controls the fuel flow to the engine) is moved according to the incoming mass airflow in order to produce the correct fuel-air ratio. The movement of the metering valve plunger exposes longitudinal slits in the barrel through which the fuel for each engine cylinder is metered (there is one slit for every cylider). Differential pressure valves (again, one for each cylinder) in the fuel distributor keep the pressure drop across the metering valve slits constant. This allows the fuel flow through the slits to be proportional to the metering valve plunger position. Injectors deliver fuel continously to each intake valve [26]. One of the virtues of this system is that it is not sensitive to a decrease in the injector flow area caused by carbon deposits. It delivers essentially the same amount of fuel, despite the fact that the nozzle manifold pressure may increase due to the nozzle contamination.

Figure 2.2 shows another spark ignition engine fuel injection system made by Robert Bosch. It is the L-Jetronic, a relative of the K-Jetronic that is now applied on a variety of European and American cars. The L-Jetronic incorporates electronic control. The air intake is measured directly by an airflow meter that is an independent interchangeable assembly. The configuration consists of a pivoted flap in the airstream. The flap deflection angle is converted to a DC voltage through the use of a conducting, highly friction-resistant plastic potentiometer. Because the flap angle versus airflow is a logarithmic relation, an exponential geometric design of the wiper track is employed to give a linear voltage output to airflow relation. The fuel injection is governed by the speed density concept. The engine speed is controlled by suitably changing the fuel-air ratio of the fuel injected into the intake port [26].

Electronically controlled electromagnetic injectors are used with a solid mechanical stop. Atomization is achieved using the kinetic energy of the liquid [26].

A roller cell pump is used to supply fuel and the pump pressure is kept constant by a diaphragm type pressure regulator. The metering is achieved by electronically controlling the solenoid injection valve opening time. The electronic control unit has a monostable trigger circuit, which determines pulses of several milliseconds. A contact in the ignition distributor triggers the pulses once per working cycle. From the distributor pulses, the engine speed is determined [26].

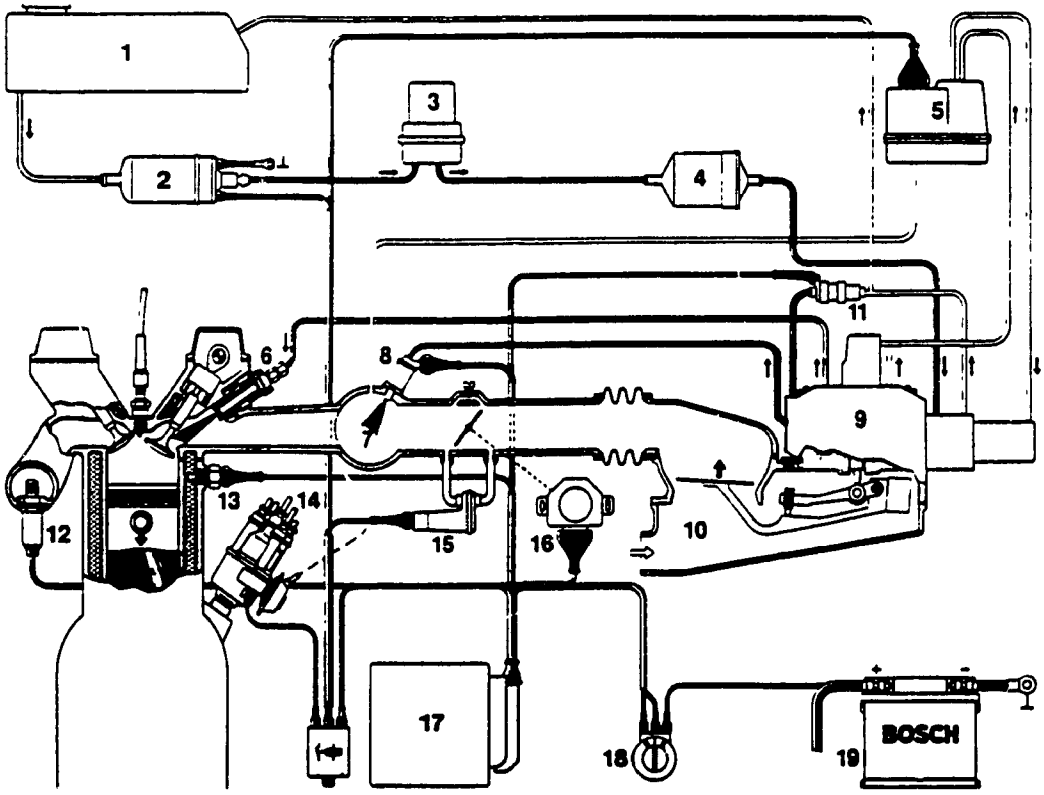

Figure 2.1 The Bosch K-Jetronic Fuel Injection System [26]

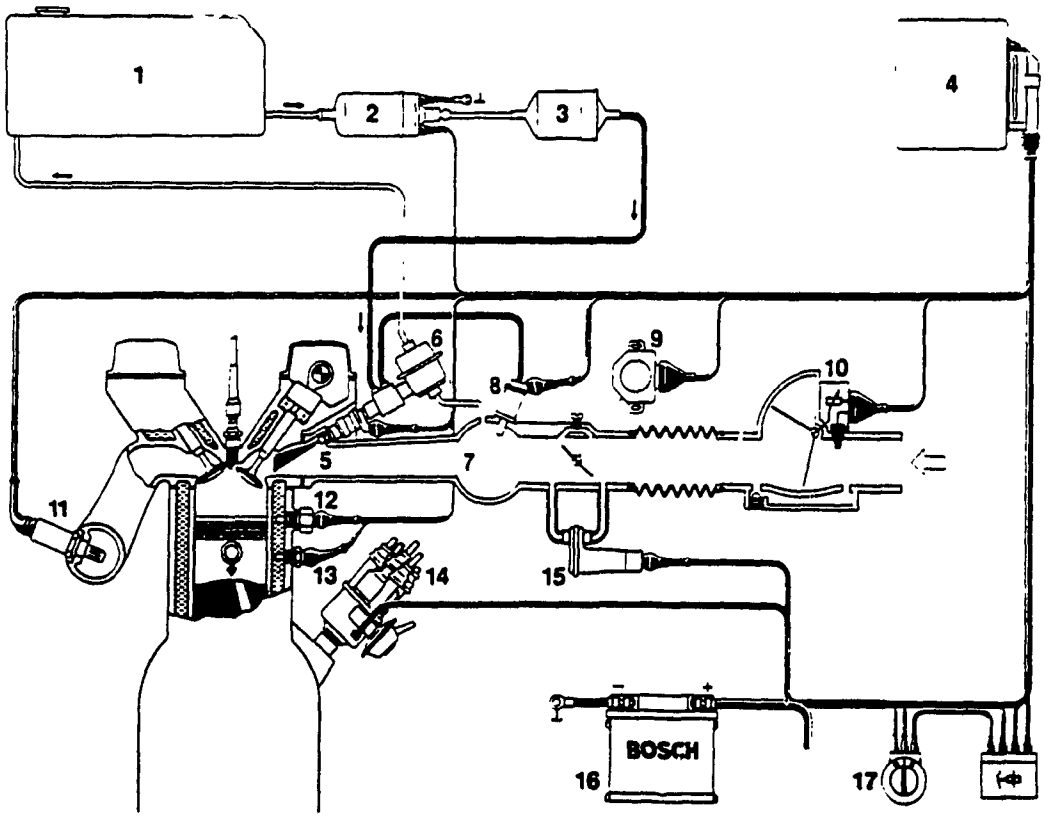

Figure 2.2 The Bosch L-Jetronic Fuel Injection System [26]

CHAPTER 3

Justification of Research Work

In this chapter, the main concept of this thesis is stated and justified. Original aspects of the analysis performed in this thesis are then underlined.

From the literature review, it was concluded that some gas turbines which are large and highly sophisticated, demand equally sophisticated and expensive fuel controls. Others are less so and need only the sophistication required to meet their mission profiles. For a remotely piloted vehicle or a missile, the required life can be very short (even a few hours). What is therefore required for fuel delivery, is an inexpensive unit that is still reliable enough to the job. The unit should also be compact and lightweight since payload is expensive.

The main disadvantages of electronic control (loss in reliability) is not as critical as for manned vehicles because no human lives are endangered. Therefore, most modern remotely piloted vehicles can have full-authority electronic fuel controls with no back-up. However, there is still some question as to what is the best pump and metering system configuration in terms of cost, performance and reliability.

For small gas turbines used for remotely piloted vehicles, the maximum fuel flow requirements are not much higher than those of the autmotive spark ignition engine. For example, the Canadair CL 227 drone requires an engine with 50 to 100 HP power. As discussed in the literature

review, modern automotive fuel injection systems deliver fuel continuously to each cylinder intake port. A gas turbine also requires continuous fuel flow, although its fuel schedule differs considerably from that of its automotive counterpart. An opportunity arises to adapt the well known and proven reliable automotive fuel injection systems for use in small gas turbine engines. With the increased flexibility offered by electronic control, the different fuel schedules and control logic do not pose a big problem. If automotive fuel injection components, which are manufactured in millions of pieces in fully automated factories, can be used in the design of a fuel control unit for small gas turbine engines, economies of scale can be exploited to lower costs. This idea is a central concept behind the fuel control unit design proposal examined and brought to a technical solution in this thesis.

Besides this main objective, some original aspects in the analysis in this thesis should be underlined. The method used in chapter 10 to choose design variables in order to minimize the deviations of the metering valve schedule from linearity is a possibility that was overlooked by Bosch in his original paper on a similar concept [28]. Sensitivity studies are not new, but they are traditionaly performed as a post-optimality analysis. In this thesis, the system sensitivity is quantified by a sensitivity index and included in an original way as a criterion in optimization. Finally, multiobjective optimization

techniques have been recently developed and have been applied mostly to water resource and other large scale decision making problems. The optimization analysis in this thesis uses one of these multicriteria optimization techniques for application in mechanical design.

CHAPTER 4

Description of Proposed System

In this chapter, the proposed fuel control system will be introduced and the functioning of the unit will be explained. Then, each component comprising the system will be described in detail.

4.1 System Description

Figure 4.1 shows schematically the proposed fuel control unit design which is similar in some details to Bosch's K-Jetronic fuel injection system for spark ignition engines. It uses a proven reliable concept and mass produced (inexpensive) automotive components. It consists of two fluid circuits. The primary circuit maintains essentially constant pump pressure. It involves fuel flow from the pump, through a filter, and back to tank via a plunger-type pressure regulating valve.

The secondary circuit meters fuel to the engine. It involves flow from the primary circuit, through the metering valve, into the upper diaphragm valve chamber, through the diaphragm valve orifice, and into the engine combustor via the nozzle. A minimum pressurizing valve can be used to ensure that fuel flows into the combustor only if it is above a certain pressure level.

The diaphragm valve maintains constant pressure drop across the diaphragm, and therefore also across the metering valve. This pressure drop is set by the diaphragm spring preload and is governed by the force balance on the

diaphragm. With constant pressure drop across the metering valve, flow through it and to the engine is determined solely by the metering valve flow area, which depends on the valve position. The metering valve barrel, taken from the K-Jetronic system, has 6 slits in it. However, unlike in the K-Jetronic, a linear digital actuator (stepper motor) under microprocessor control moves the metering valve plunger, exposing the slits and metering the flow to the combustor. Figure 4.2 shows an assembly drawings of the fuel control unit testing prototype.

The diaphragm valve differential pressure regulation action can be understood as a kind of feedback control system. If the metering valve opening increases, more fuel enters the upper diaphragm chamber. This causes the pressure there to build up initially. The increased upper diaphragm chamber pressure upsets the force balance on the diaphragm, causing it to move down. The diaphragm valve orifice flow area is determined by the clearance between the diaphragm and the face of the nozzle manifold pipe inlet (the curtain area). Hence, the downward motion of the diaphragm opens the diaphragm orifice, increasing the flow to the nozzles and returning the upper chamber pressure back to its initial value (where the forces on the diaphragm balance again). If the metering valve is moved towards its closed position, on the other hand, the flow to the nozzles decreases, causing the pressure in the upper diaphragm chamber to drop initially. This reduces the upper chamber pressure force on the diaphragm, causing the

diaphragm to move up, reducing the diaphragm orifice curtain area. The upper chamber pressure therefore builds back up to the initial value to restore force equilibrium.

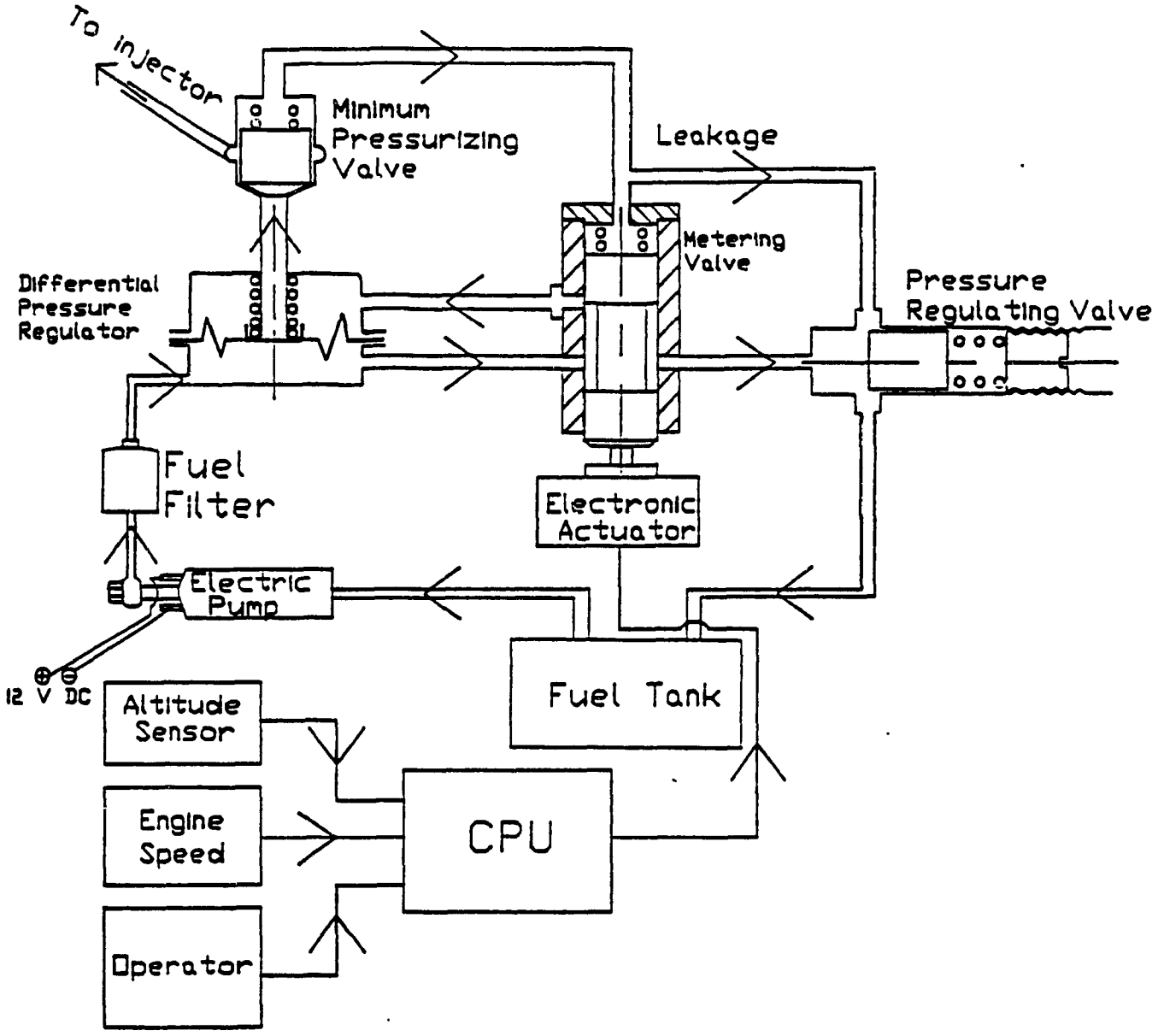

Figure 4.1 Hydraulic Schematic of the Fuel Control Unit [20]

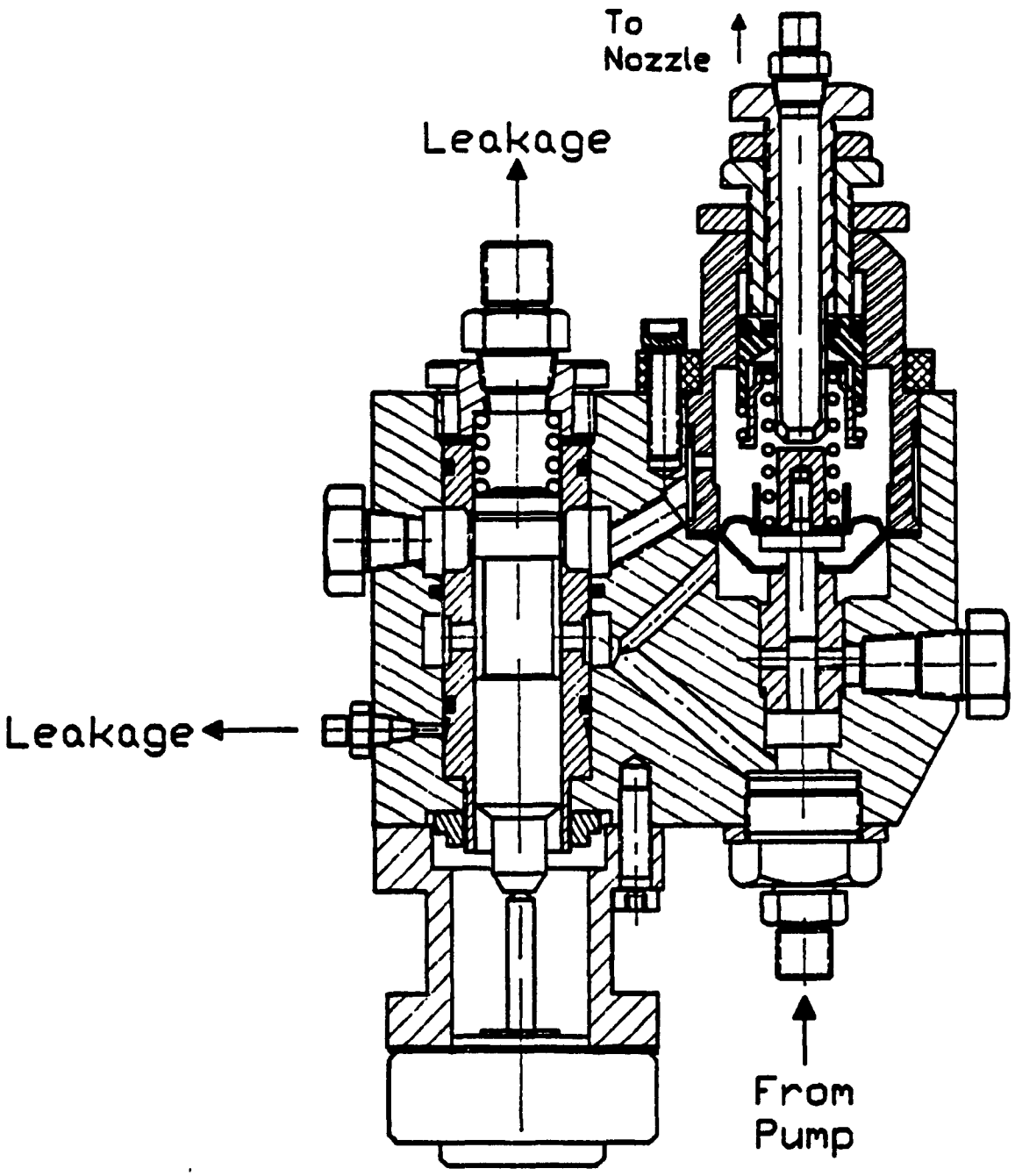

Figure 4.2 Assembly Drawing of Fuel Control Unit Prototype Manufactured for Testing [22]

4.2 Component Description

In this section, the components of the fuel control system are described individually.

Electric Fuel Pump

Since the pressure regulating valve of the primary circuit maintains essentially constant pump pressure for a wide range of pump discharge flows, a constant displacement pump (which is less expensive) can be used. For the low flow required by a small gas turbine, an automotive roller cell type pump could be used with only minor modifications. The pump used by Bosch in the K-Jetronic system (Figure 4.3) can be used. The pump is a roller cell type driven by an electric motor with 12 volt dc voltage supply provided by a car battery.

It was found experimentally that a higher flow can be obtained with this pump by increasing the voltage supply to 14 volts dc. To obtain the higher pressure needed for the fuel control unit requirement, two of these pumps can be used in a series arrangement under a single envelope (Figure 4.4). The advantage of using the automotive pumps is that they are proven reliable and very inexpensive, because they are made in large quantities.

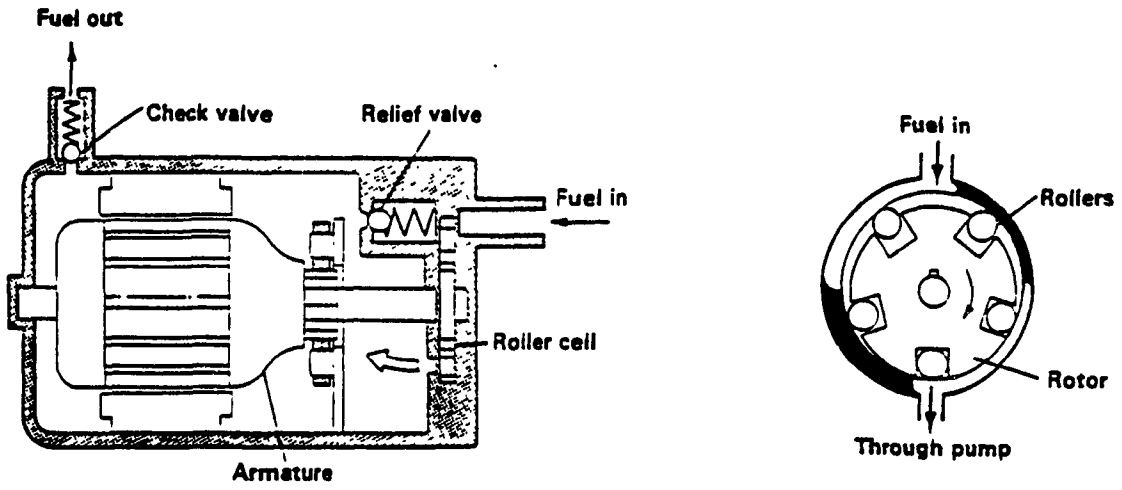

Figure 4.3 The Bosch Electric Fuel Pump [26]

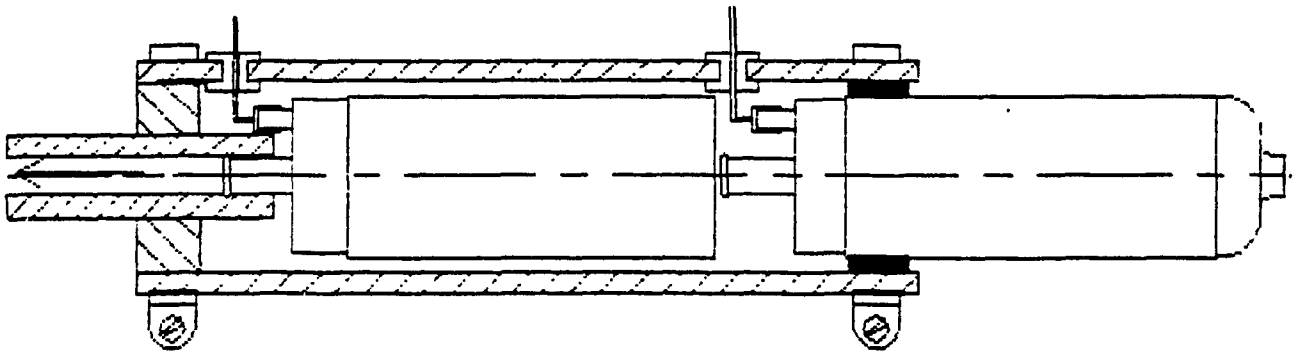

Figure 4.4 Two Bosch Pumps in Series Under a Single Envelope [22]

Fuel Filter

Because of close tolerances used in the design, good filtering is needed. The fuel filter retains solid particles which could wear or clogg the system. For example,a metal chip in the fuel can jam the metering valve. The filter contains a paper element with a mean pore size of 10 μm backed up by a fluff trap. This combination ensures good fuel cleaning [26]. Figure 4.5 shows a schematic of the filter.

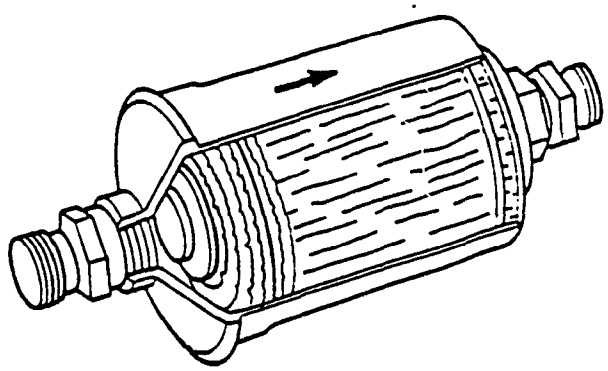

Figure 4.5 Schematic of the Bosch Filter [20]

Pressure Regulating Valve

The pressure regulating valve is a plunger type, with the regulated pressure level adjustable by a screw that alters the spring preload. The fuel pump always delivers more fuel than is required by the engine. This causes the spring loaded plunger to shift in the pressure regulator and open a port through which excess fuel can return to the tank. The regulator is shown in Figure 4.6.

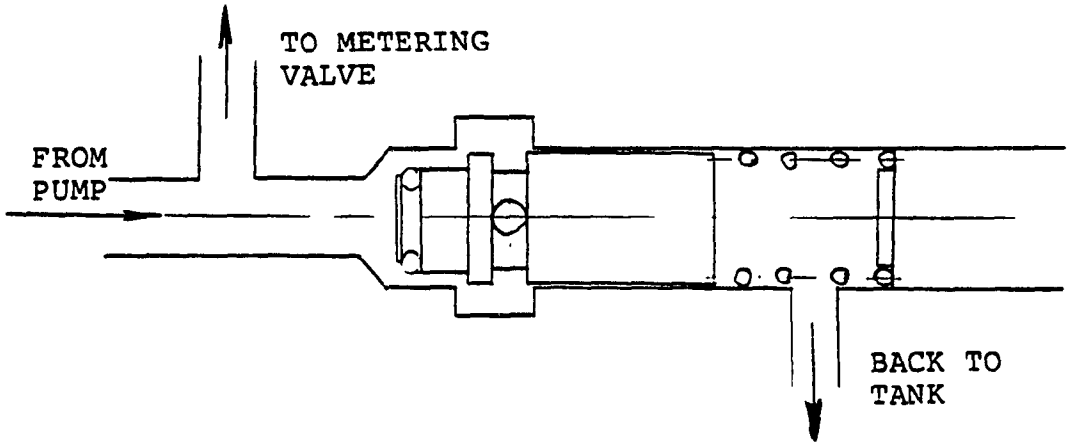

Figure 4.6 Fuel Pressure Regulator [22]

The Metering Valve

The metering valve is taken directly from the Bosch K-Jetronic System. It consists of a plunger and a barrel. The barrel in the metering valve used by Bosch has 6 slits symmetrically cut in it by electrodischarge machining. The symmetry allows pressure balance of lateral forces acting on the valve plunger. There are six slits because in automotive design, fuel had to be equally metered to all engine cylinders. However, this is not the case for the gas turbine. Only two metering slits are needed (instead of one, to maintain pressure balance). O-ring seals are fitted onto the barrel to prevent leaks. The metering valve plunger is pushed forward by a linear stepper motor. A spring preloads the plunger from the opposite side to maintain contact with the motor shaft when retracted. A schematic of a valve slit is shown in Figure 4.7.

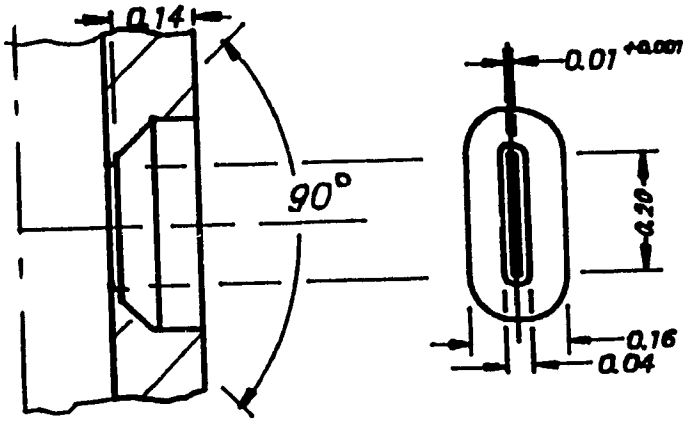

Figure 4.7 The Metering Valve Slit [22]

The Diaphragm Valve

The diaphragm valve design uses some parts from the bypass valve of the Bendix DPF-2 fuel control unit. These are the rubber diaphragm and the spring. The DPF-2 bypass valve stem (which is expensive) usually attached to the diaphragm is not used. Instead, a simple cylindrical pilot is fixed to the diaphragm so that it slides inside a hole machined in the housing. This ensures that the diaphragm is deflected vertically, i.e., perpendicular to the face of the diaphragm valve orifice. A helical spring preloads the diaphragm. The preload force is adjusted by changing the preload compression of the spring. A special tightening nut system is provided in the design for this purpose. The diaphragm is shown in Figure 4.2.

Nozzle Manifold

The nozzle mainfold leads from the upper diaphragm chamber to outside of the unit. The bottom face of the pipe inlet lies perpendicular to the flat diaphragm flapper position. The small clearance between the face of the nozzle manifold pipe inlet and the diaphragm flapper is critical since it determines the effective flow area through the diaphragm valve. This clearance is governed by the diaphragm deflection resulting frcm a force balance on the diaphragm. The nominal clearance corresponding to an undeflected diaphragm, however, is adjustable. The nozzle manifold pipe is threaded into the housing, allowing changes in the nominal position of the pipe by screwing it

in or out the housing. The top of the nozzle manifold pipe is connected to tubing that leads to the nozzle. The nozzle manifold is shown in Figure 4.2.

Digital Linear Actuator

The linear digital actuator used is manufactured by Airpax (Series 922221-P2). It is a linear stepper motor fitted with a lead screw shaft. It is commonly used in computer peripherals. It requires a 12 volt dc supply and a seperate driver. The step size is .025mm. The maximum pull-in stepping rate is 500 steps/sec and the maximum pull-out rate is 700 steps/sec. The maximum linear travel of the motor shaft is 32.2 mm and the maximum force it can generate is 20.9 N. The specifications of the motor stated above are adequate for use in the proposed fuel control unit. However, advances are taking place in digital actuator technology and less expensive, higher performance motors are becoming available.

Chapter 5

Steady State Simulation Model and Results

In this chapter, the steady state model equations describing the system will be developed. All parameters used in the model will be calculated. A method to solve the model equations will be presented and simulation results will be plotted.

5.1.1 Pump Pressure in the Primary Circuit

Pump pressure is assumed constant since the regulating valve used (Figure 5.1) is designed to have a flat characteristic. This assumption will be checked experimentally in chapter 6. Also, it is expected that the system is insensitive to variations in pump pressure. This will be checked in chapter 11.

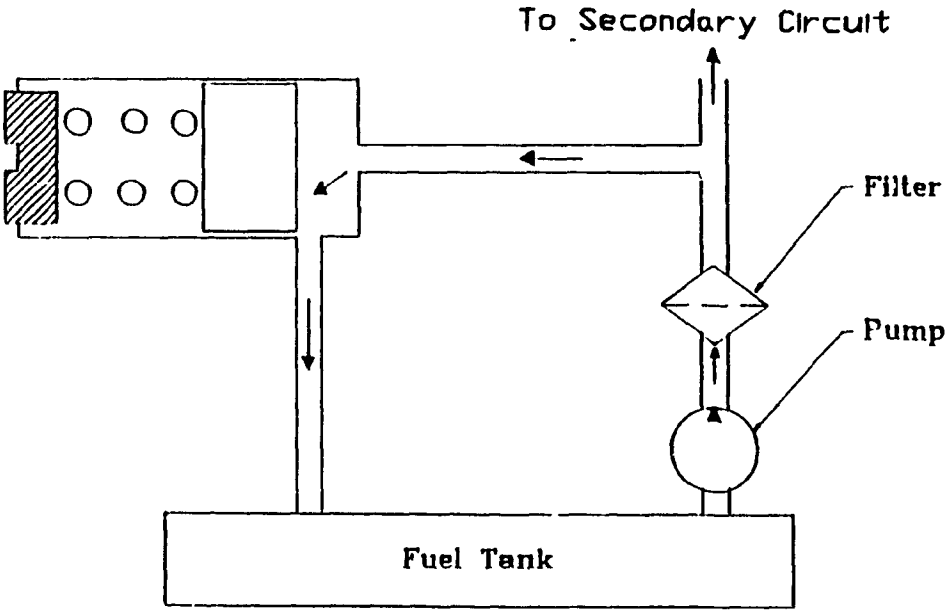

Figure 5.1 Schematic of the Pressure Regulating Valve and Primary Circuit

A force balance on the pressure regulator plunger gives,

$$P_{pr} A_{pr} = K_{sr} x_r + f_{spr} \qquad (5.1)$$

where, K_{sr} = spring constant of regulating valve preload spring
f_{spr} = preload force applied by the spring
A_{pr} = effective pressure area for valve plunger
P_{pr} = regulated pump pressure
x_r = plunger deflection from nominal position

However, the plunger displacement, x_r, determines the flow area (a_r) through the regulator and back to tank.

$$a_r = \pi D_r (x_o + x_r)$$

where x_o = the nominal plunger position
D_r = the diameter of the plunger

The flow bypassed back to tank, q_r, is given by

$$q_r = c_{dr} a_r \sqrt{(2/\rho) P_{pr}} \qquad (5.2)$$

where c_{dr} = flow coefficient for flow through valve

Depending on the nozzle flow, the bypassed flow varies. From equation 5.2, the two factors that can change bypass flow are pump pressure and regulating valve flow area. However, examining equation 5.1, it is evident that if the preload dominates the equation, then pump pressure is almost constant. That is, if a spring of low constant is used and the preload is achieved by using a large preload compression, then the changes in spring length required by changes in valve flow area are negligeable in the force balance. This gives essentially constant pump pressure and changes in bypass flow occur due to changes in plunger position only.

5.1.2 Flow in the Secondary Circuit

The primary circuit is a reservoir with almost constant pump pressure to feed the secondary circuit with fuel. A schematic of the secondary circuit is shown in Figure 5.2.

Diaphragm Force Balance

To produce a mathematical model of the secondary circuit, a simplified (equivalent piston) force pattern will be considered as acting on the diaphragm. In steady state, six forces act on the diaphragm (Figure 5.3).

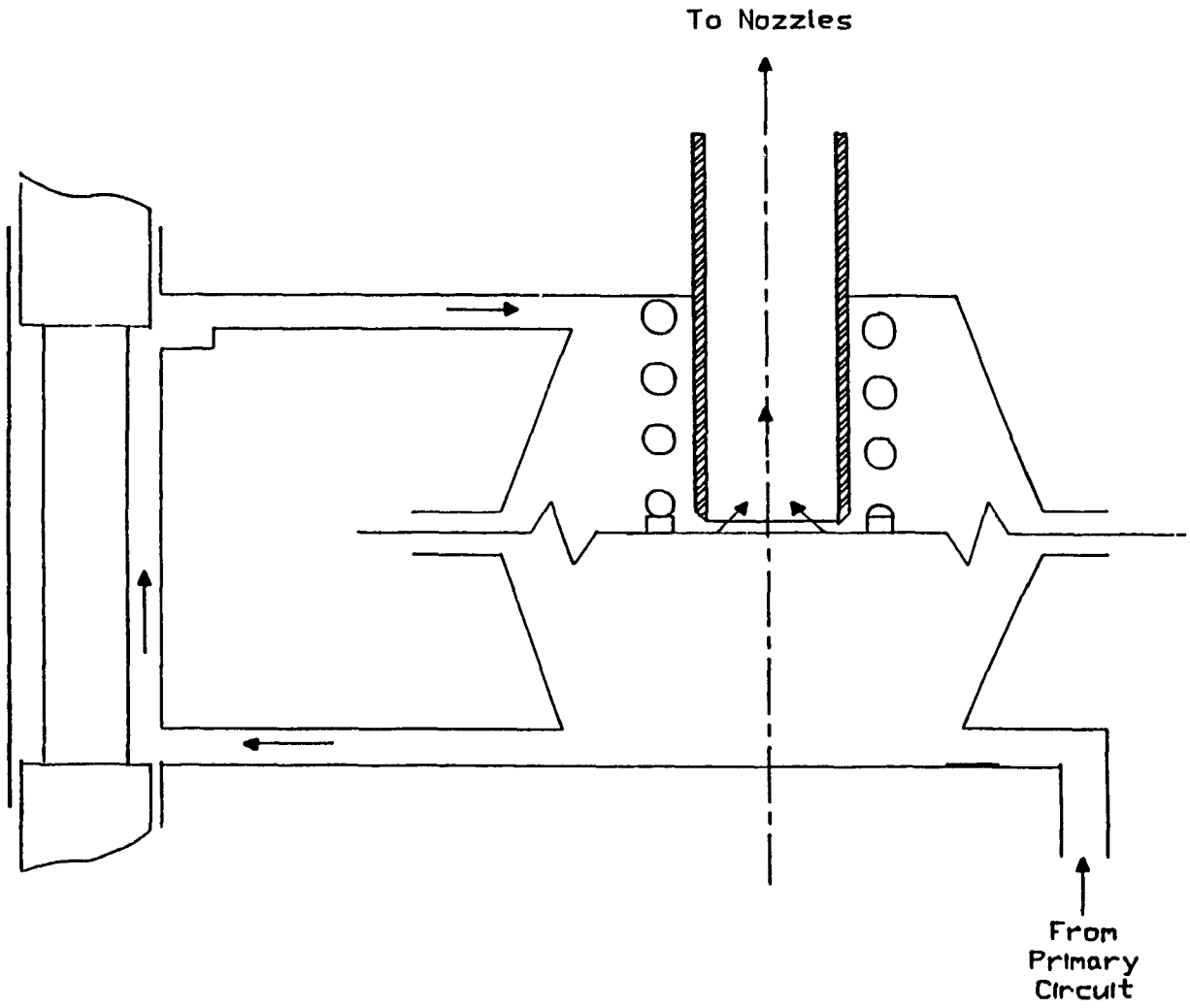

Figure 5.2 Secondary Circuit of Fuel Control Unit

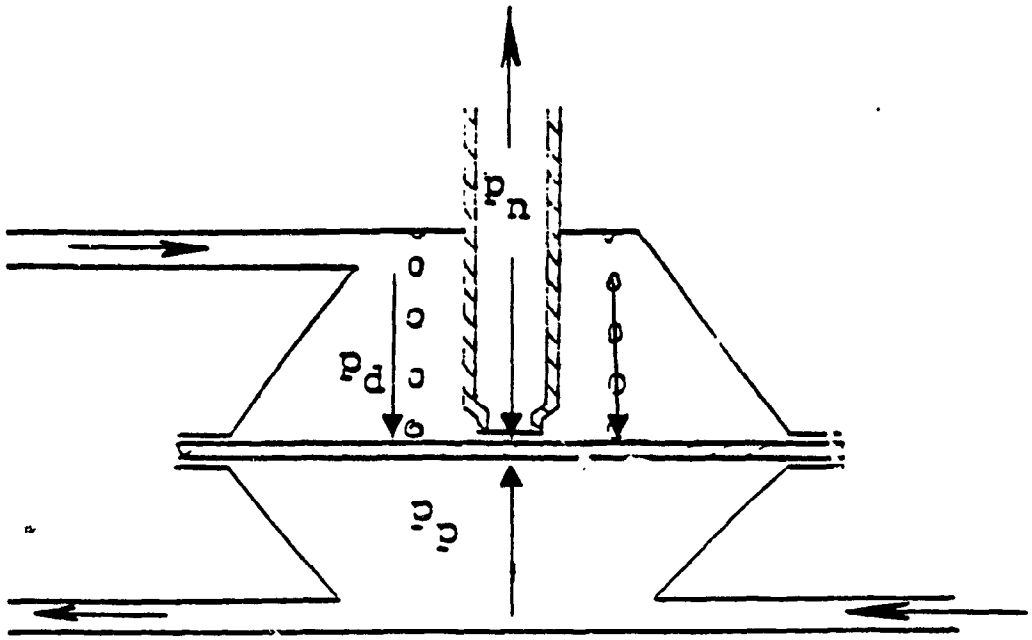

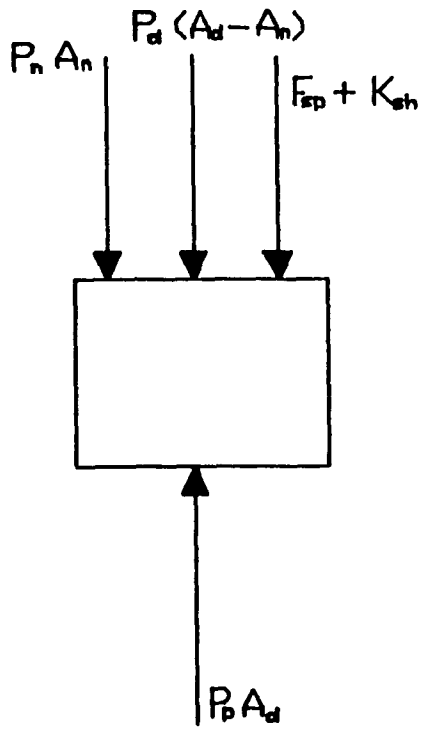

Figure 5.3 Force Balance on the Diaphragm

Balancing the forces on the diaphragm,

$$P_p A_d = P_d(A_d - A_n) + K_s h + P_n A_n + f_{sp} - \rho q^2 / A_n \qquad (5.3)$$

where P_p = the pump pressure

A_d = effective diaphragm area

A_n = cross sectional area of nozzle manifold pipe inlet

P_d = upper diaphragm chamber pressure

f_{sp} = the preload force on the diaphragm

k_s = the spring constant of the spring

P_n = nozzle back pressure

h = diaphragm delection

ρ = fuel density

q = fuel flow to nozzle

The terms $P_p A_d$ and $P_d(A_d - A_n)$ are forces the lower and upper diaphragm chamber pressures exert on the diaphragm. The pressure P_d does not act on the total diaphragm area because of the pressure drop through the diaphragm orifice. The term $P_n A_n$ takes this into account. The term f_{sp} is the preload force the helical spring exerts on the diaphragm at nominal compression. The spring force $K_s h$ is for diaphragm deflections about nominal compression. The spring constant of the diaphragm itself is assumed negligeable compared to the stiffness of the helical compression spring. The final term, $\rho q^2 / A_n$, is a flow force term. It is negligeable.

For initial calculations, some simplifications of the diaphragm force balance can be made. Since $A_n << A_d$, then $(A_d - A_n) \cong A_d$.

Since $K_s h << f_{sp}$, the increase in spring force with diaphragm deflection can be neglected.

With these approximations, the force balance becomes

$$P_p A_d \cong P_p A_d + f_{sp} \quad \text{or,}$$

$$(P_p - P_d) \cong f_{sp} / A_d \tag{5.4}$$

Thus, the differential pressure across the diaphragm is dictated mostly by the spring preload. In an original publication by Bosch on the K-Jetronic fuel injection system for spark ignition engines [27], the ratio of areas Ad/An was kept over 100 in order to keep differential pressure dependent only on the spring preload. A spring with low constant was used in order to keep the spring force term $K_s h$ negligeable. If these recommendations are followed, then equation 5.4 can be quite accurate. If these conditions are violated, the differential pressure will not be exactly constant. The fuel flow to the nozzles will not be linearly related to the metering valve position. For the applications in small gas turbines considered in this thesis, only one diaphragm valve is used (Bosch used one valve for each engine cylinder). Since much higher flow now passes through the valve, the diaphragm orifice must

be enlarged. This decreases the ratio A_d/A_n and thus the differential pressure across the diaphragm deviates from that predicted by equation 5.4. A method to overcome this problem is proposed and implemented in chapter 10.

The required preload to set differential pressure Δp is

$$f_{sp} = \Delta p A_d \qquad (5.5)$$

The required spring preload compression, l_c, is given by

$$l_c = f_{sp} / K_s \qquad (5.6)$$

It is impractical to measure the spring compression inside the housing. Rather, the preload is adjusted using a special nut in the design and a differential pressure transducer. When the desired differential pressure is reached, the nut is locked.

Effective Diaphragm Area

Following an analysis by Georgantes on a modified Bendix DP-F2 fuel control unit [28], an effective diaphragm area can be found so that equation 5.3 can be used. This involves careful consideration of the forces acting on the diaphragm and the geometry involved. The effective diaphragm area is 3.09 cm^2. This value is close to the value used in an independent study on the DP-F2 unit [29]. There is some debate as to what the effective area should be.

Pressure Division, Secondary Circuit

The secondary circuit involves three orifices in series in a nonlinear pressure divider.

Assuming constant exit pressure, P_c (this assumption is valid for the narrow range of governing and in testing), and using the orifice equation and continuity, two independent equations can be written,

$$q = C_{dm}A_m\sqrt{(2/\rho)(P_p-P_d)} = C_{do}A_o\sqrt{(2/\rho)(P_d-P_n)}$$

$$= C_{di}A_i\sqrt{(2/\rho)(P_n-P_c)}$$

where C_{dm} = metering valve orifice flow coefficient

A_m = metering valve flow area

C_{do} = flow coefficient for diaphragm orifice

A_o = flow area through diaphragm orifice

C_{di} = flow coefficient for nozzle

A_i = nozzle flow area

For testing conditions, the nozzle discharge pressure, P_c, is atmospheric.

The above, when combined with the force balance equation, gives 3 independent nonlinear equations for steady state conditions in the 3 unknowns P_d, h, and Pn.

$$C_{dm}A_m\sqrt{(2/\rho)*(P_p-P_d)} - C_{do}A_o\sqrt{(2/\rho)(P_d-P_n)} = 0 \quad (5.7)$$

$$C_{do}A_o\sqrt{(2/\rho)(P_d-P_n)} - C_{di}A_i\sqrt{(2/\rho)(P_n-P_c)} = 0 \quad (5.8)$$

$$P_pA_d - P_d(A_d-A_n) - K_sh - P_nA_n - f_{sp} = 0 \quad (5.3)$$

The metering valve flow area depends on the linear position of the plunger in the barrel (Figure 4.7).

$$A_m = l\ w\ i \quad (5.9)$$

where l = the plunger actuation distance

w = width of slits in the barrel

i = number of slits in the barrel

The diaphragm orifice acts as a flapper orifice (Figure 5.4). It is given by,

$$Ao = \pi D_n(h_{max} - h) \quad (5.10)$$

where h_{max} = the clearance between the undeflected diaphragm position and face of the inlet of the nozzle manifold pipe

The critical flow area through the diaphragm orifice should be the curtain area, which is given by $\pi D_n(h_{max}-h)$. If this exceeds the manifold pipe inlet cross sectional area ($\pi D_n^2/4$), the curtain area no longer governs, surrendering control of pressure drop across the metering valve. This situation is called saturation.

To avoid diaphragm orifice saturation, a design

requirement is,

$$\pi D_n (h_{max} - h) << \pi D_n^2/4 \qquad \text{or} \tag{5.11}$$

$$h >> h_{max} - D_n/4 \tag{5.12}$$

The diaphragm valve flow area, A_o, is therefore given by,

$$A_o = \begin{cases} \pi D_n (h_{max} - h) & \text{if } h >> h_{max} - D_n/4 \\ \\ \pi D_n^2/4 & \text{if } h << h_{max} - D_n/4 \end{cases} \tag{5.13}$$

Close to the orifice saturation conditions, the two restrictions affect the flow. A two stage throttling assumption matches results best. Assuming that the curtain area $\pi D_n (h_{max} - h)$ and the manifold inlet pipe cross sectional area $\pi D_n^2/4$ are two orifices in series, we let the intermediary pressure is be P*. Assuming equal flow coefficients and using continuity,

$$q = c_{do} A_c \sqrt{(2/\rho)(P_d - P^*)} = C_{do} A_n \sqrt{(2/\rho)(P^* - P_n)} \tag{5.14}$$

Solving for P* and substituting in (5.14),

$$P^* = [P_p (A_c/A_n)^2 + P_n]/[1+(A_c/A_n)^2]$$

$$q = \frac{c_{do} A_c A_n}{\sqrt{(A_c^2 + A_n^2)}\ \sqrt{(2/\rho)(P_d - P_n)}} \qquad (5.15)$$

It is clear that the effective orifice is

$$A_o = \frac{A_c A_n}{\sqrt{(A_c^2 + A_n^2)}} \qquad (5.16)$$

If $A_n >> A_c$ or $A_c << A_n$, this formula reduces to the cases stated above.

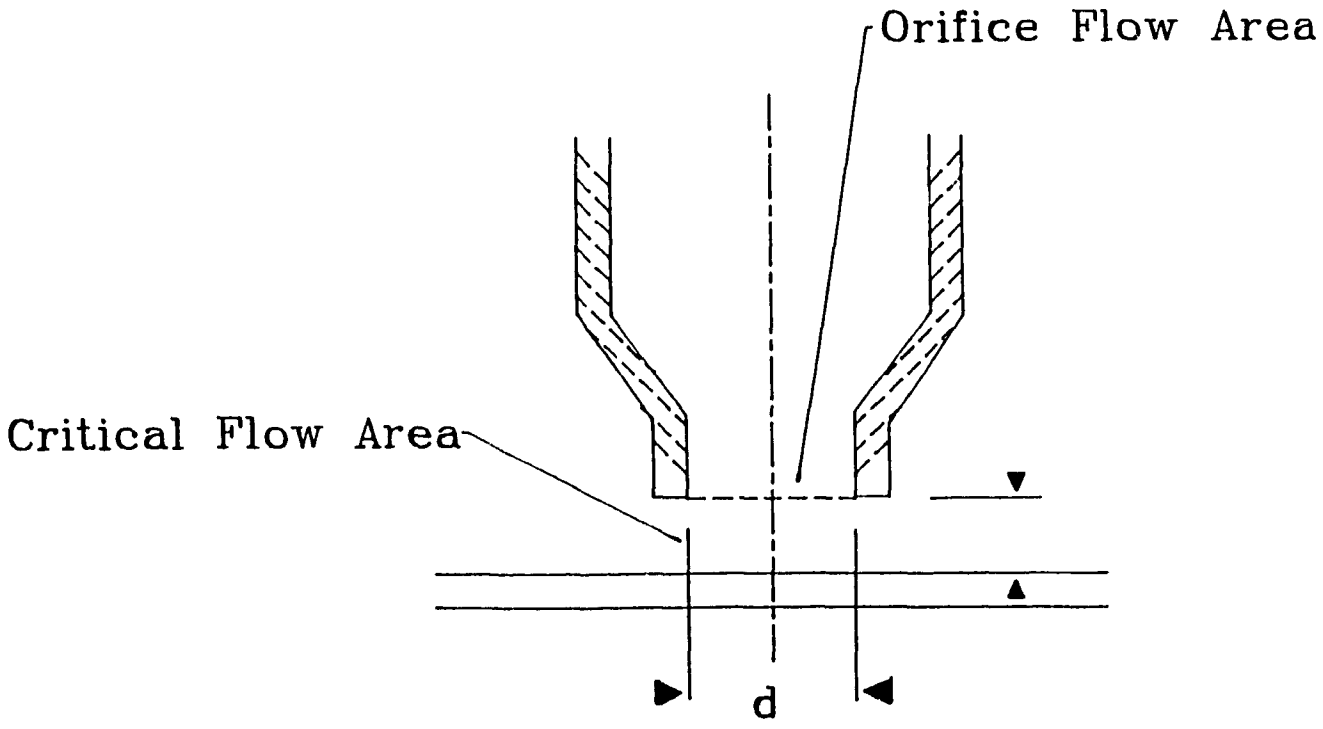

Figure 5.4 Critical Flow Area Through Diaphragm Valve

5.2 Solution Procedure

The nonlinear set of steady state model equations can be solved by a simple search technique, since from design considerations, the region of search is small and well known. Using an IBM AT compatible computer with math co-processor, the complete steady state schedule is obtained in under one minute. Figure 5.5 explains the strategy.

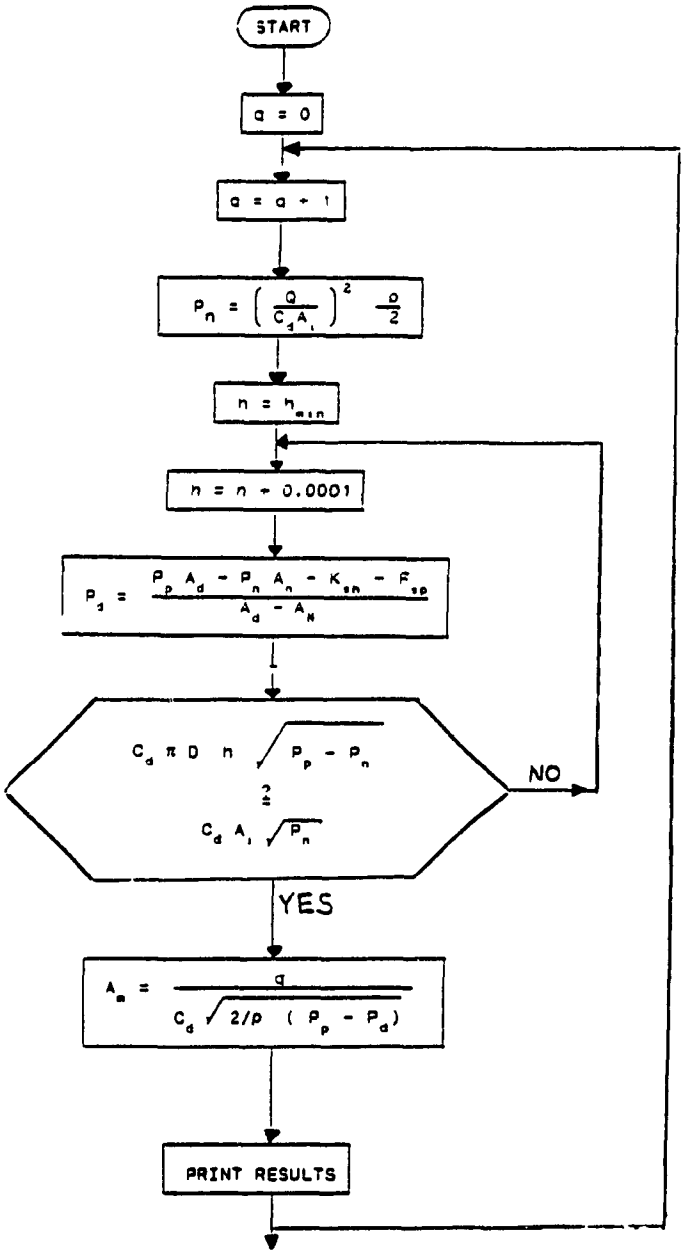

Figure 5.5 Flowchart for Calculation of Steady State Results

5.3 Calculation of Parameters

In this section, the steady state model nominal design parameters will be calculated. Some of these calculations are only approximate. They are used as a starting point in the design. The final recommendations will be made after optimization is performed in chapter 13.

Fuel Density

The fuel used for testing is a calibration fluid used for fuel metering controls in laboratory testing. It is less flammable than regular jet fuel (for example, JP-5 or JP-4 fuel), but otherwise has most of its important charaterisics. The density of the fluid is 770 kg/m^3.

Calculation of Nozzle Area

The nozzles used in gas turbines are usually chosen by the engine producer and a new fuel control design should accomodate this fact. For the Williams International WTS-34-16 gas turbine upgraded to 100 HP (the engine will be used in the Canadair Drone), a constant flow area nozzle is used.The maximum injection pressure for the nozzle is 150 psid (1.034 Mpa) and this corresponds to a maximum fuel flow of 54 kg/hr. Assuming a constant flow coefficient of 0.6, the flow area calculated as,

$$A_i = \frac{q}{c_{di}\sqrt{(2/\rho)p_n}} = \frac{(54)/[(3600)(720)]}{0.6\sqrt{(2/770)(150)(6895)}} \qquad (5.17)$$

$$= .6393 \text{ mm}^2$$

Calculation of Differential Pressure

A wide range of differential pressure settings are possible. A larger differential pressure results in a faster system response because the required metering valve flow area for a particular flow is smaller with large differential pressure. The stepper motor has to move less far in exposing the slits in the barrel, speeding up the response. However, with large differential pressure, the resolution of flow drops since each actuator step results in a larger flow change. This lower resolution can be a problem for acceleration and deceleration, where the fuel control operates in the open loop. For best efficiency, it is desired to operate as close to the stall and flameout boundaries as possible, and therefore accuracy is needed. The stepper motor step size s = 0.025mm. Assuming that a flow change of q_s=0.4 kg/hr per step is maximum acceptable, the corresponding differential pressure should satisfy,

$$q_s = c_{dm} s\ w\ i \sqrt{(2/\rho)(P_p - P_d)} \qquad (5.18)$$

The metering valve used for testing has six slits in it. The slit width is w = .08 mm. Substituting q_s = 0.4 kg/hr, c_{dm}= 0.6, s = .025mm, i=6 and ρ= 770 kg/hr and solving for differential pressure

$$\Delta p = [q_s/(c_{dm} s\ w\ i)]^2 (\rho/2) \qquad (5.19)$$

$$= \left[\frac{(10)^6(0.4)/[(770)(3600)]}{(0.6)(.025)(6)(.08)} \right]^2 (770/2) = .1546 \text{ mPa} \quad (22.4 \text{ psid})$$

Calculation of Required Pump Pressure

The pump pressure should be greater than the maximum nozzle back pressure plus the differential pressure across the metering valve. Therefore, assuming a differential pressure of 22 psid (.1546 Mpa) is used, the pump pressure should be at least 150+22 = 172 psig (1.189 Mpa). However, a larger pressure than this should be used to provide a safety margin against changes in the regulating valve characteristic and nozzle contamination. Therefore, the pump pressure is chosen as 180 psi (1.241 mPa) until optimization results are obtained.

Calculation of Diaphragm Orifice Diameter

The diaphragm orifice diameter, d_n, must be chosen according to the flow requirements of the fuel control. If the pressure drop across the metering valve is kept constant at 22 psid by the diaphragm valve and the pump pressure is fixed at 180 psi by the primary circuit pressure regulator, the upper diaphragm chamber pressure is fixed at about 180-22 = 158 psi (1.089 Mpa). At maximumflow, the nozzle pressure is high (150 psi) and there is only an 8 psi drop across the diaphragm orifice. At minimum flow, the nozzle pressure is close to zero and the diaphragm orifice is almost closed shut. The range of flow areas that the diaphragm valve must provide is therefore

$$A_{or} = \frac{q_{max}}{c_d\sqrt{(2/\rho)(p_d - p_n)}} = \frac{54/\,[(3600)(770)]}{(0.6)\sqrt{(2/770)(8)(6895)}}$$

$$= 2.71 \text{ mm}^2$$

The changes in flow area between maximum and minimum flow are achieved by deflections of the diaphragm. This deflection required depends on the diameter chosen for the diaphragm orifice. Making sure that saturation of this orifice is avoided, many possibilities still exist. If the diaphragm orifice diameter is made small, then this results in a large ratio Ad/An. This is advantageous because the linearity of the metering valve schedule improves and the approximation in equation 5.4 improves. However, this lowers the safety margin against saturation. The diaphragm

orifice diameter is arbitrarily chosen as 2.8 mm. The final design recommendation will be made after optimization studies are performed in chapter 13. A check must be made to ensure that saturation of the diaphragm orifice does not occur. Using the saturation condition (equation 5.12),

$$h = \frac{A_{or}}{\pi d_n} \qquad \frac{2.71}{\pi (2.8)} = .308 \text{ mm}$$

which is less than $d_n/4 = 0.7$mm. Thus, saturation is not a problem with the chosen diaphragm orifice size.

Calculation of Spring Constant and Preload Compression

The spring used is a Bendix DP-F2 fuel control unit spring with 3150 N/m constant. This was arbitrarily chosen as a starting design. However a check must be made. The spring must be of low enough constant so that the term $K_s h$ in the force balance on the diaphragm (equation 5.3) is not too large. The maximum deflection of the diaphragm (considering only steady state conditions) was calculated above from the maximum flow area through the diaphragm valve and the diaphragm orifice diameter as 0.31 mm. The corresponding maximum value of the $K_s h$ term is therefore (3150)(.00031m) = 0.977 N. The preload force of the helical spring can be approximated from the differential pressure,

$$f_{sp} = \Delta p(A_d) = 22(6895)(.00039) = 59.1 \text{ N}$$

It can be seen that the $k_s h$ term is negligeable in comparison.

5.4 Steady State Simulation Results

Figures 5.6 to 5.11 show some simulation runs with nominal design variable settings. System variables are plotted versus metering valve position. The flow curve (Figure 5.6) shows that the fuel flow varies almost linearly with the metering valve movement. This is the desired steady state result. Slight deviations from linearity occur because the differential pressure across the metering valve is not kept perfectly constant. Flow saturation of the diaphragm orifice occurs at about 56 kg/hr. At this point, the cross sectional area of the nozzle manifold pipe inlet is becoming smaller than the diaphragm orifice curtain area. The diaphragm valve loses control of the differential pressure across the metering valve. The effective orifice through the diaphragm valve is fixed at the nozzle manifold pipe inlet cross sectional area, independent of the motion of the diaphragm. The secondary circuit becomes three orifices in series. Pump pressure is divided between these three orifices, with the metering valve orifice being the only one changing in the divider. Opening the metering valve changes the division slightly, a smaller pressure drop occuring across the metering valve. However, increasing the metering valve flow area does not increase the flow to the nozzles significantly because the nozzle orifice becomes the dominant restriction in the divider. Therefore, the saturation flow can be approximated from only the pump pressure and the nozzle orifice size (Figure 5.7).

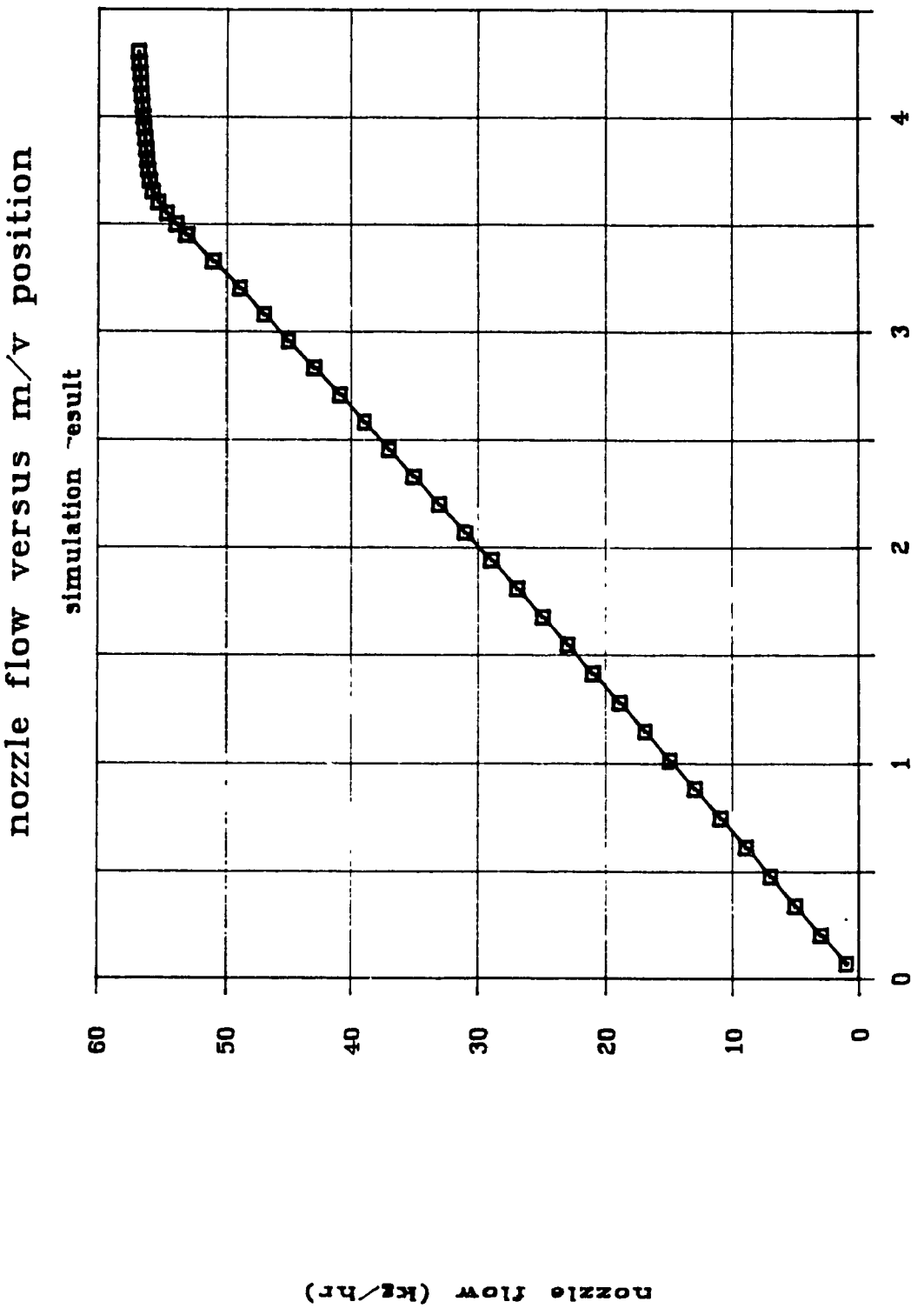

Figure 5.6 Fuel Flow Versus Metering Valve Position

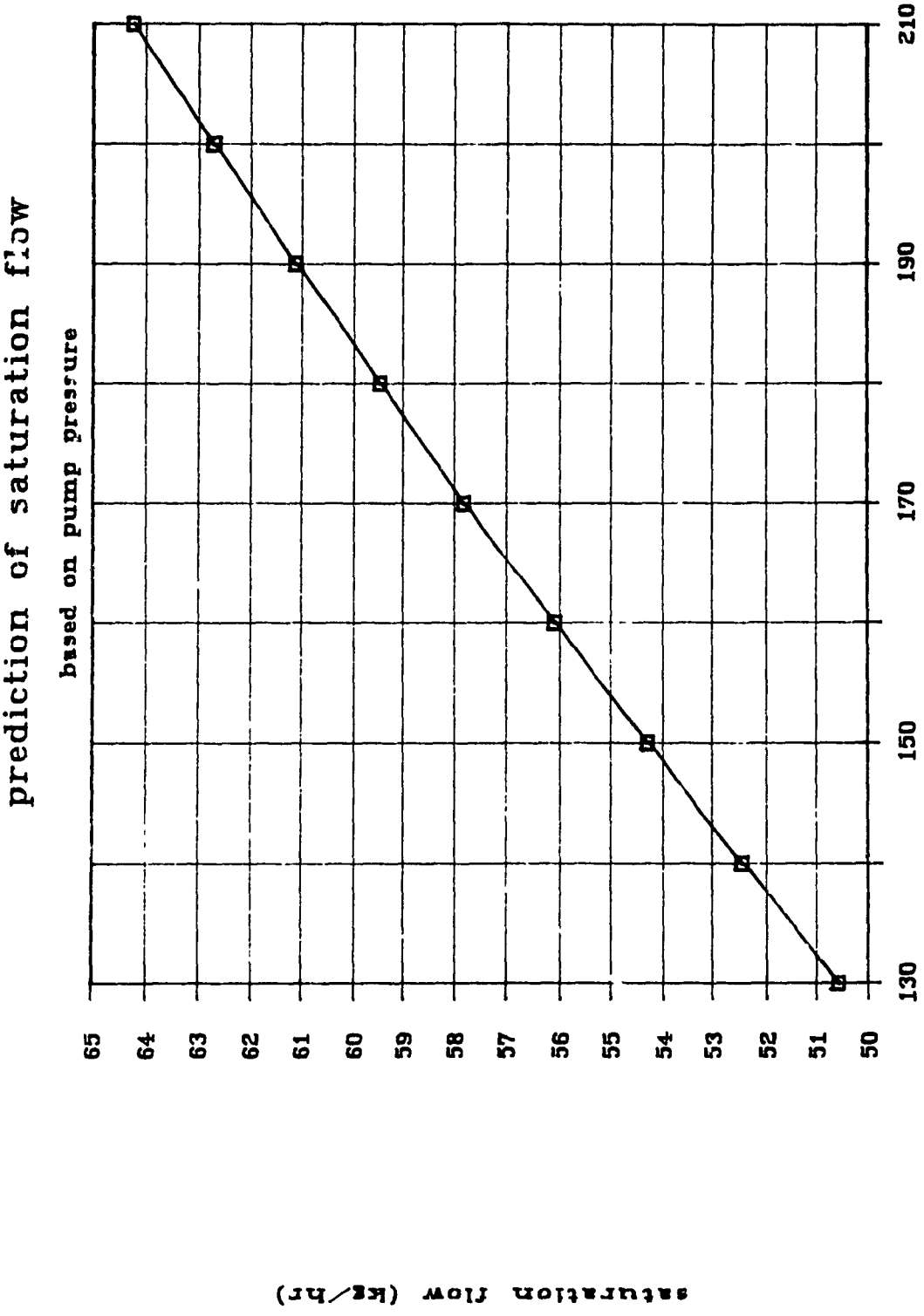

Figure 5.7 Approximation of Saturation Flow

The nozzle pressure (Figure 5.8) follows the nozzle flow. In fact this signal is directly related to the nozzle flow by the orifice equation.

Figure 5.9 shows the differential pressure across the metering valve versus the metering valve position. The differential pressure is almost constant, providing linearity of nozzle flow versus metering valve position. For most of the schedule, however, the differential pressure rises slightly with metering valve position, and hence with the fuel flow. This is because the increasing of flow changes the force balance on the diaphragm. In saturation, the differential pressure drops with metering valve opening. This is expected from the equivalent secondary circuit for diaphragm saturation conditions.

Figure 5.10 shows the diaphragm deflection. The motion is very small, but it increases exponentially at higher flow when the diaphragm orifice is becoming saturated. This can be explained as follows. For increasing flow, the nozzle pressure increases, but the upper diaphragm chamber pressure stays essentially constant because of the diaphragm valve regulation. Hence, the diaphragm must move down and open the orifice not only to accomodate the higher flow demand, but also to compensate for the decreasing pressure potential across the diaphragm orifice responsible for pushing the fuel through.

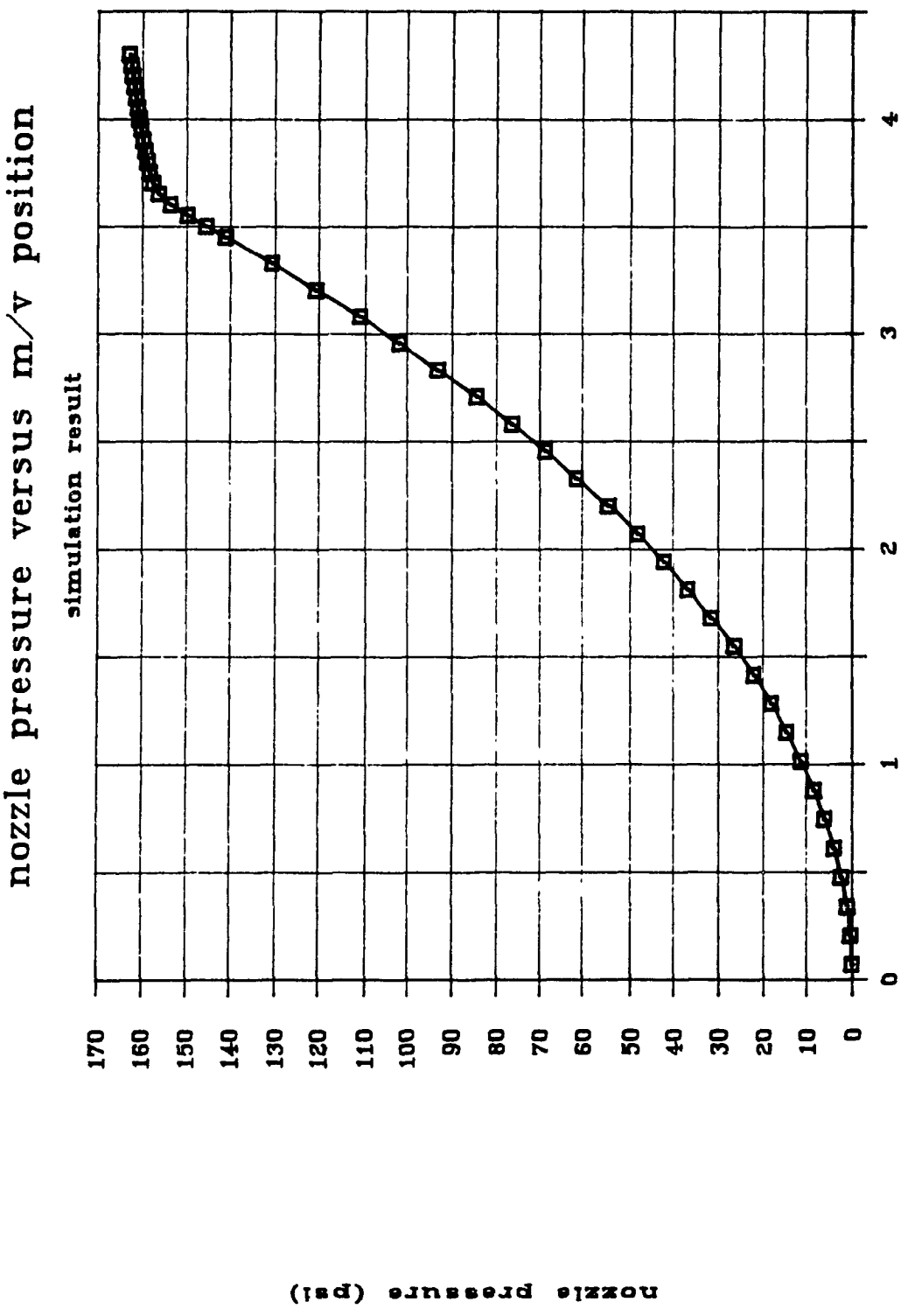

Figure 5.8 Nozzle Pressure Versus Metering Valve Position

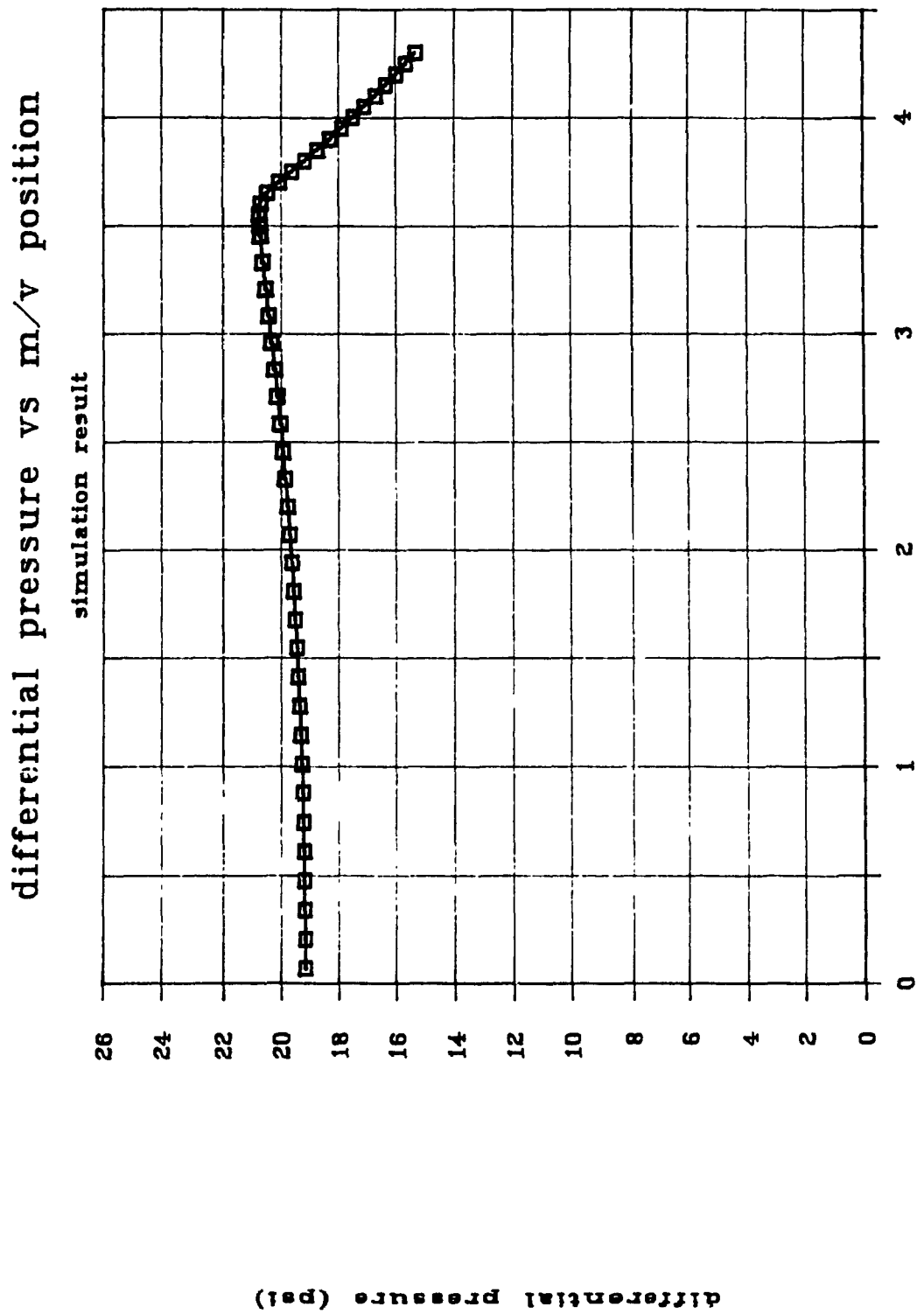

Figure 5.9 Differential Pressure Versus Metering Valve Position

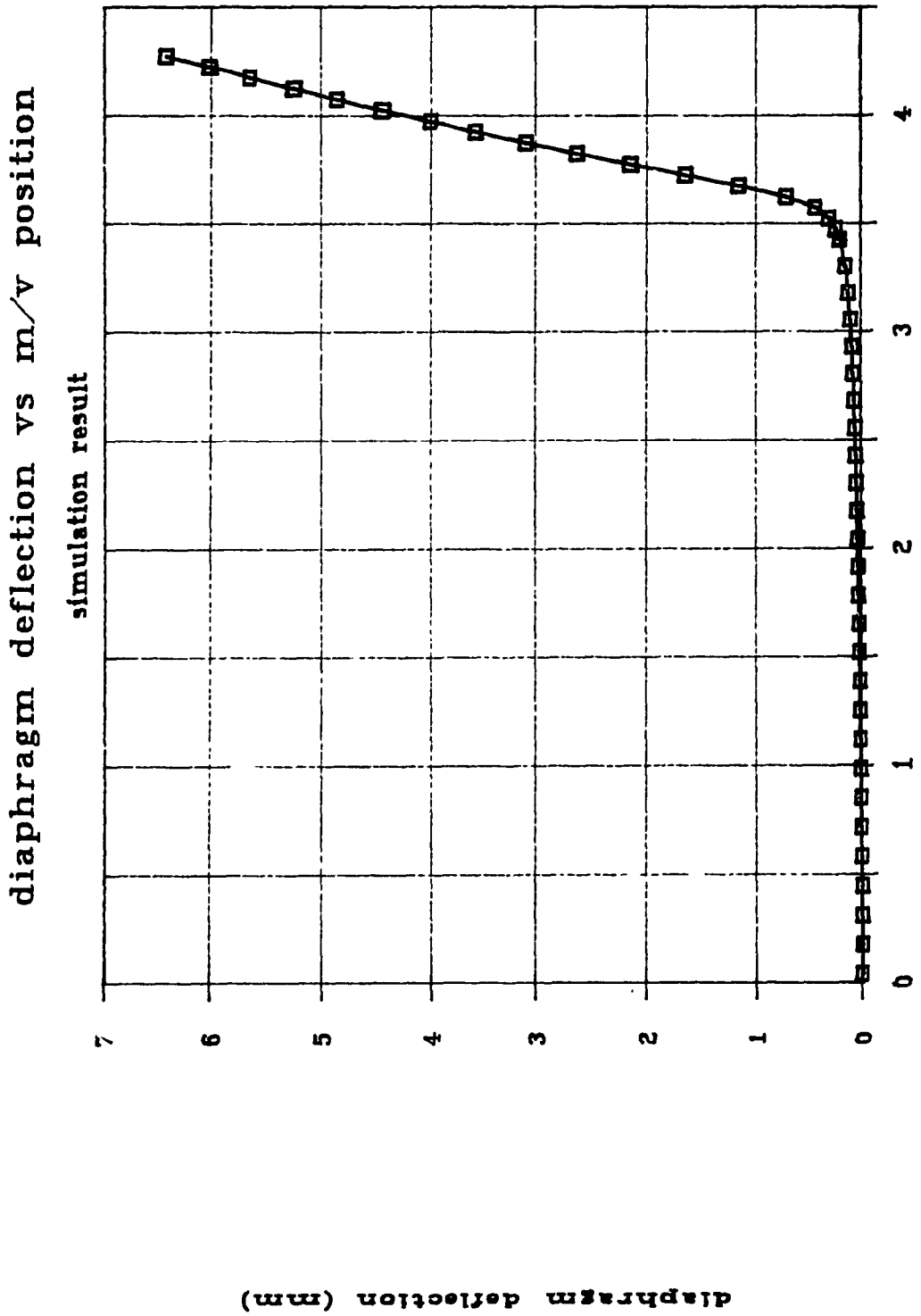

Figure 5.1b (a) Diaphragm Deflection

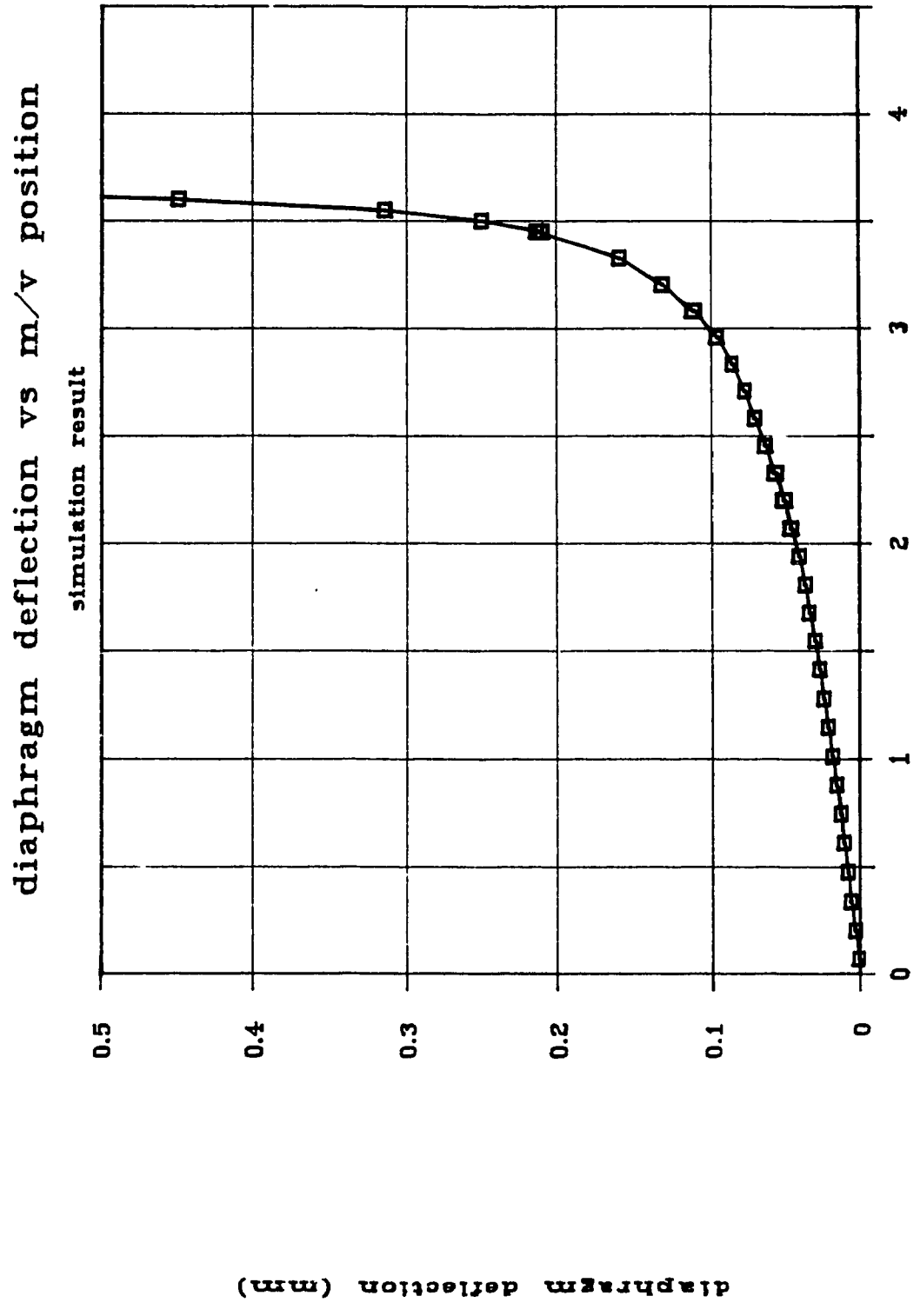

Figure 5.1C (b) Diaphragm Deflection (detail)

CHAPTER 6

Description of Experimental Setup

In this chapter, the experimental setup used to test the prototype will be described.

Figure 6.1 shows the hydromechanical experimental setup. An electrically driven constant displacement pump is used as the fuel flow source. Pump pressure can be adjusted by changing the spring preload on the regulating valve plunger with a special adjustment screw. Two automotive filters in parallel trap contaminating solid particles. Two filters are used instead of one since the flow rating of the automotive filter is below the requirements for gas turbine engine application. Dial guages indicate pump pressure and nozzle pressure. Pump flow is measured by a rotameter and a turbine flow meter. The differential pressure across the metering valve and the nozzle pressure are measured by fast responding Validyne diaphragm type pressure transducers. A rotameter and another turbine flow meter measure nozzle flow. There is some redundancy in the instrumentation for recording steady state results. This provides an extra check on experimental readings. However, for recording transient processes, this redundancy does not exist since the rotameters and the dial pressure guages cannot be used.

The metering valve is operated by a linear digital actuator. Its position is known by counting steps. To account for possible lost steps and to record the actuator

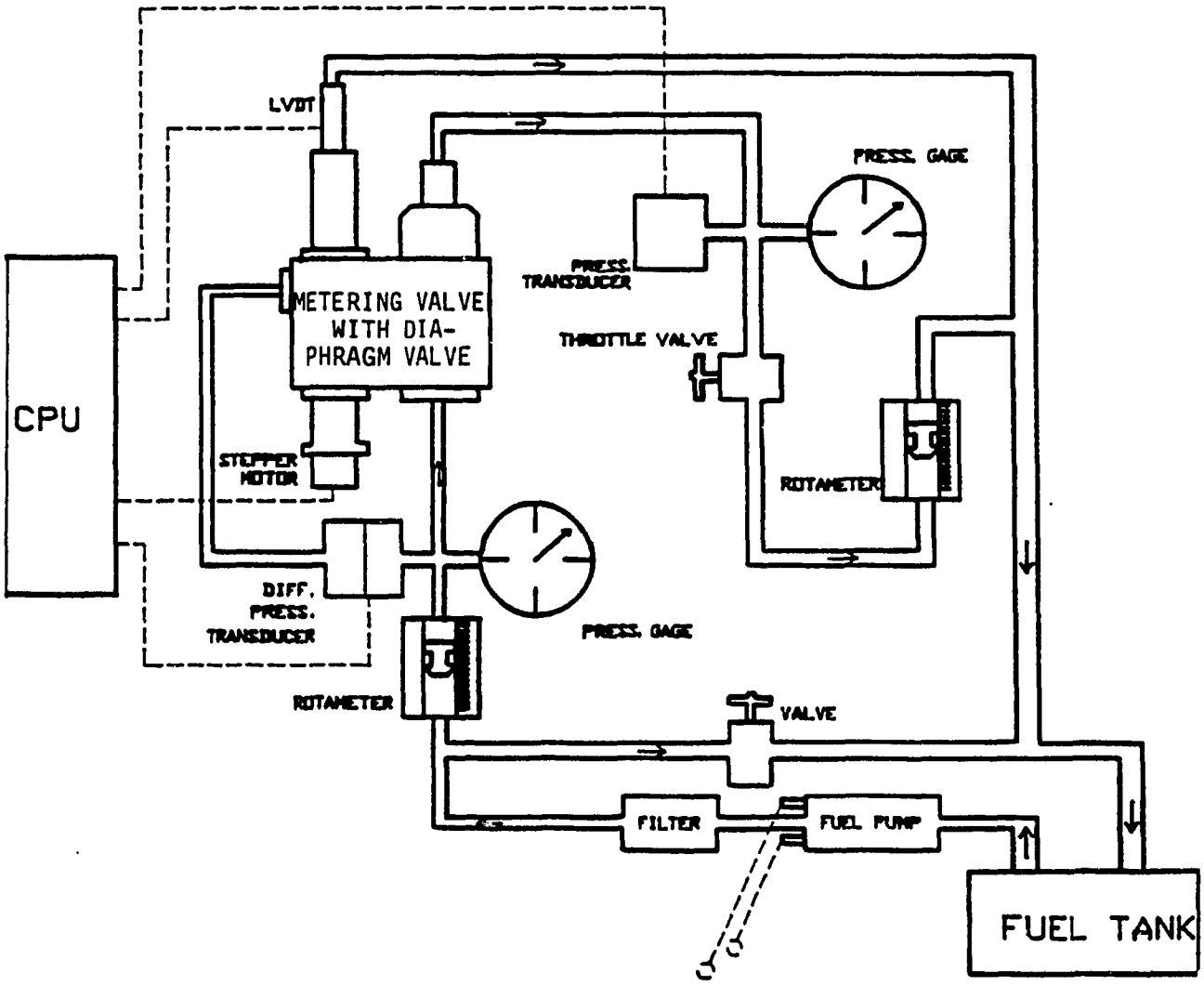

Figure 6.1 Schematic of the Experimental Setup [22]

movement, the metering valve is fitted with an LVDT. The diaphragm deflection is measured with a similar LVDT.

Some adaptations were made to the prototype to allow for instrumentation. The modifications for the metering valve and diaphragm LVDTs are shown in Figure 6.3.

The nozzle orifice is simulated with a fine adjustment (1 degree taper) metering valve fitted with a micrometer head. The spring preload on the diaphragm can be adjusted mechanically with a nut tightening system. The spring constant can be varied using a special spring length changing device. This design is shown in Figure 6.4. For a helical spring, changing the effective free length of the spring (i.e. , the number of active coils, N), changes the spring constant according to the formula [27],

$$k_s = d^4G/(8D^3N)$$

where d = the wire diameter

G = shear modulus of elasticity

D = mean spring diameter

Flow coefficients for the metering valve orifice, diaphragm orifice and the nozzle orifice were approximated to be 0.6, as is often done in the literature. This assumption was experimentally checked.

Figure 6.2 shows a block diagram of the signal flow and signal conditioning involved in testing. Information flows in two directions. Signals from the fuel control unit, "the plant", are measured by transducers and converted into

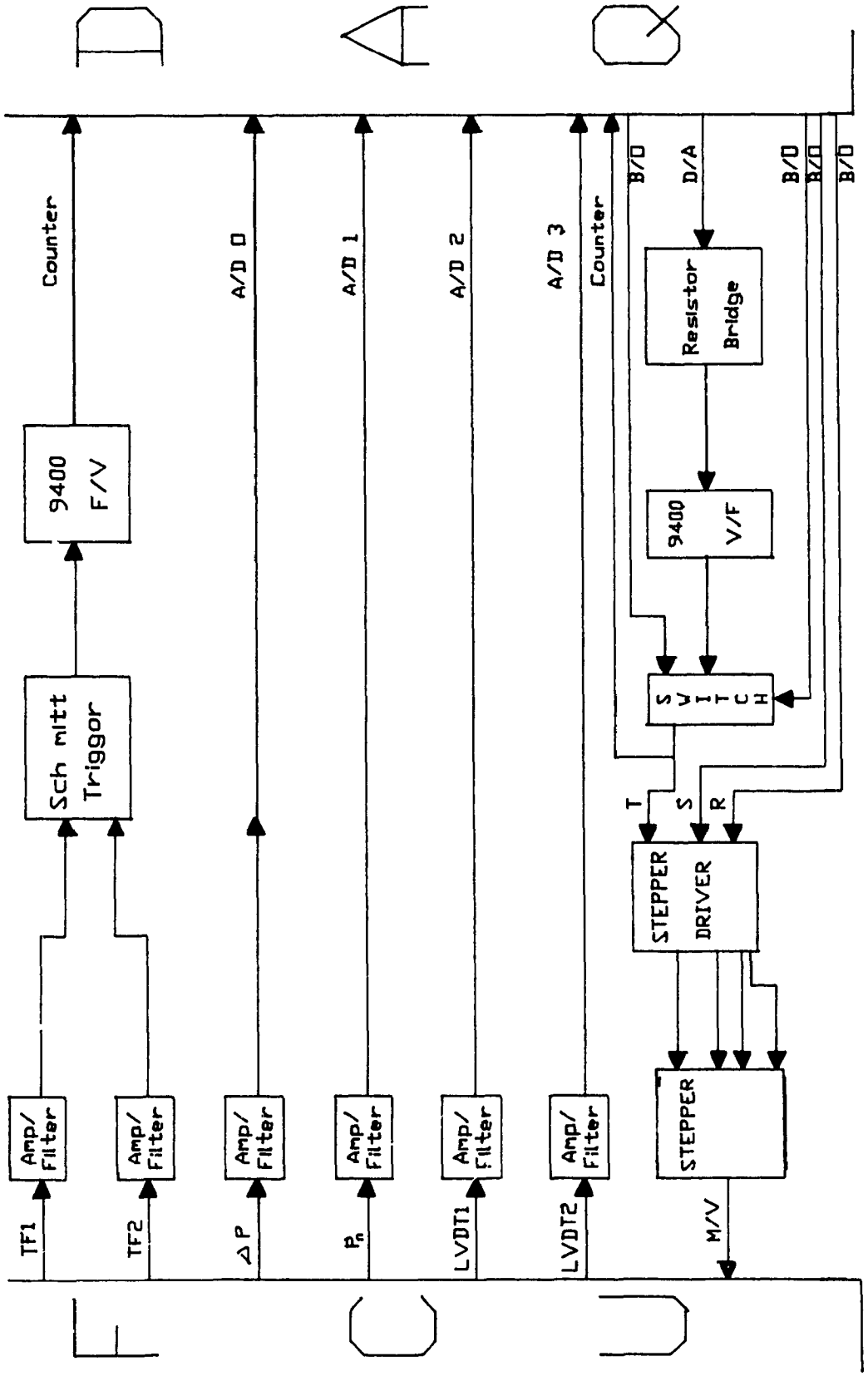

Figure 6.2 Block Diagram of Signal Flow and Conditioning

electrical form. They then enter an interface board where they are amplified and filtered. Finally, the signals are recorded via a data aquisition system. The computer also outputs control signals via the data aquisition system. The interface board conditions these signals into a form suitable to drive the actuator or change the control logic.

To record transient responses, an IBM Data Aquisition System (DAQ) was used. This system comes as a plug in card for a personal computer. Signals from the test bench are amplified, filtered, and multiplexed onto the analog to digital (D/A) conversion channels of the DAQ.

A SAA 1027 chip is used as the stepper motor driver. Two methods are used to control the motor. The first, single stepping, is used for steady state tests. A binary output (B/O) pin of the DAQ is connected to the stepper driver trigger and toggled from high to low by the control program. Stepping frequency is controlled by software delays between transitions. The correct actuation length is assured (assuming no lost steps) by counting the number of transitions. This method is accurate, but requires large software time, limiting its use in recording fast transients.

For recording transient processes, velocity control mode is used. The equired stepping speed is computed and a proportional analog voltage is outputted via a digital to analog (D/A) converter channel. This is converted to a square wave output of proportional frequency by a Teledyne 9400 voltage to frequency converter chip. This waveform

triggers the stepper motor driver. The trigger pin is connected to a counter channel of the DAQ so that the actuation length is controlled by counting steps. Velocity control is not as accurate as single stepping, but it does not tie up the CPU as much, allowing faster sampling. A multiplexer is used (controlled by a B/O pin of the DAQ) to switch the control modes.

An interactive control program was written in the C programming language to control all the testing and record the results. This program allows for variable stepping rate of the stepper motor, control of metering valve actuation direction and control of metering valve position (accurate within a step). The stepping control mode is also changeable and the sampling time can be varied. The minimum sampling time possible is 6 ms. However, 25 ms sampling time was found accurate enough to record the transient processes involved with this fuel control unit. The program also allows for multiple runs and stores the data in a location specified by the user. A spreadsheet and graphics package were interfaced with this program so that plots of transient processes are automatically generated on the screen and plotted after the transient.

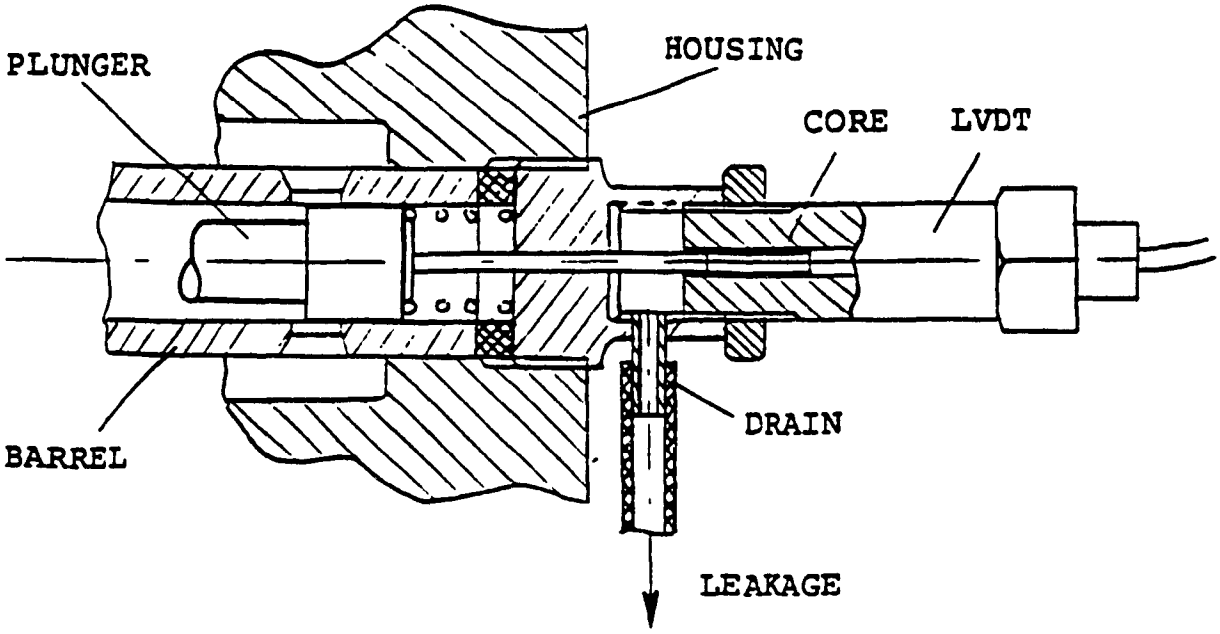

Figure 6.3 Metering Valve LVDT Design Modification

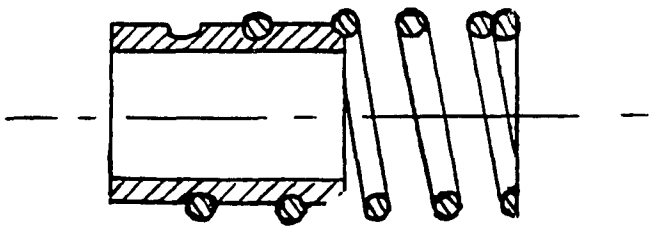

Figure 6.4 Variable Spring Constant Design Modification

CHAPTER 7

Steady State Experimental Results and Model Validation

In this chapter, the experimental results of prototype testing will be used to validate the steady state simulation model described in chapter 5.

Figures 7.1 to 7.5 show the obtained test results versus metering valve position. In each case a hysterisis loop is shown starting from and ending at maximum flow. The simulation results with the same parameters used in testing are superimposed on experimental plots for comparison. Figure 7.1a shows the fuel flow varying almost linearly with the metering valve position. Flow saturation of the diaphragm orifice occurs at about 56 kg/hr. There is almost no hysterisis in this curve. At very low flow, there is a loss of linearity because the diaphragm valve cannot regulate the differential pressure in this case (see Figure 7.3). Figure 7.1b compares this curve with the simulation results. The match is good with only a small discrepency in the saturation flow. The low flow nonlinerity is not simulated because the low flow increase in differential pressure was neglected in simulation. This discrepancy has to be accepted because there is no possibility to simulate fuel leakage through the valve.

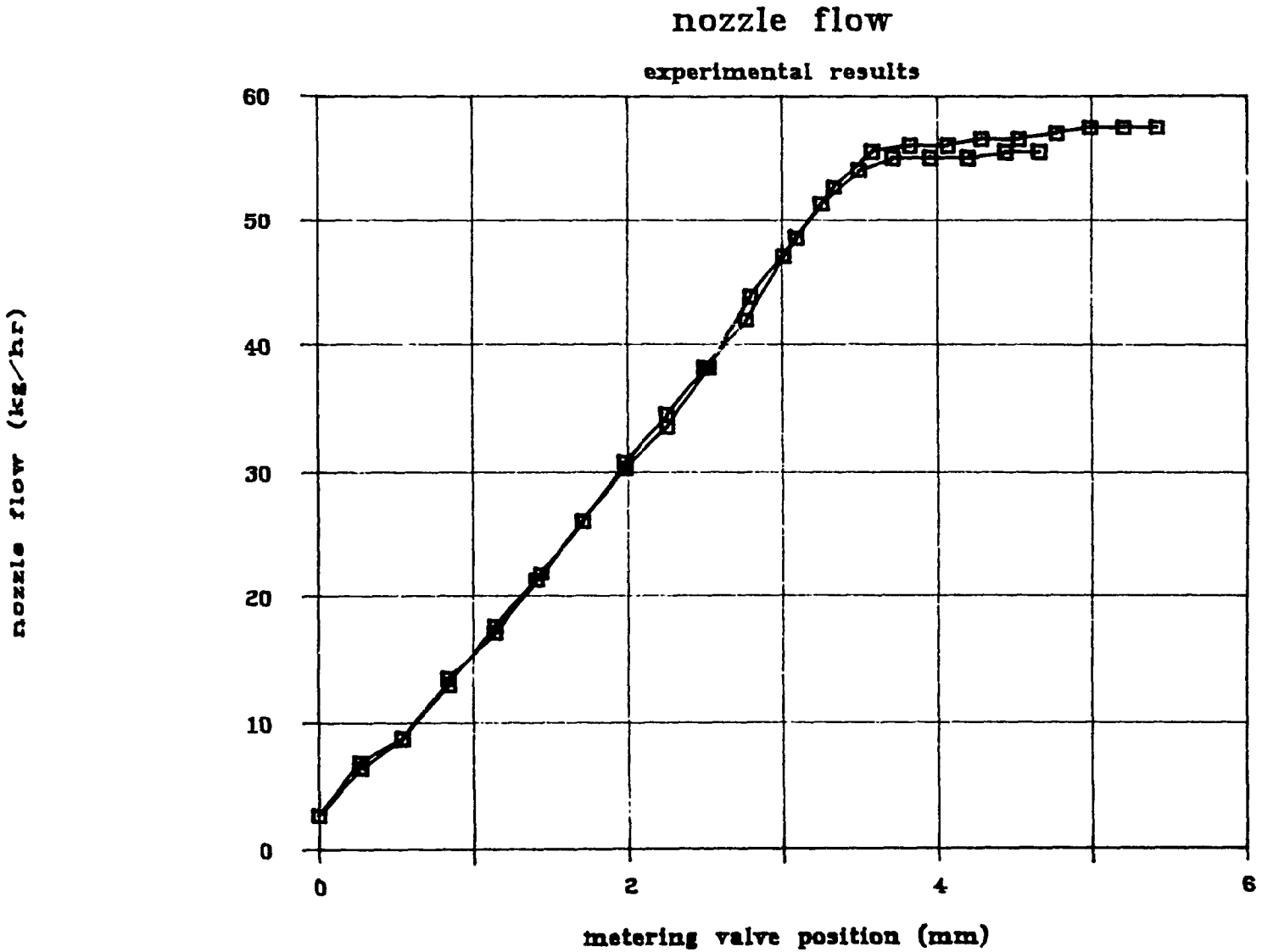

Figure 7.1 (a) Flow versus Metering Valve Position
Experimental Hysterisis loop

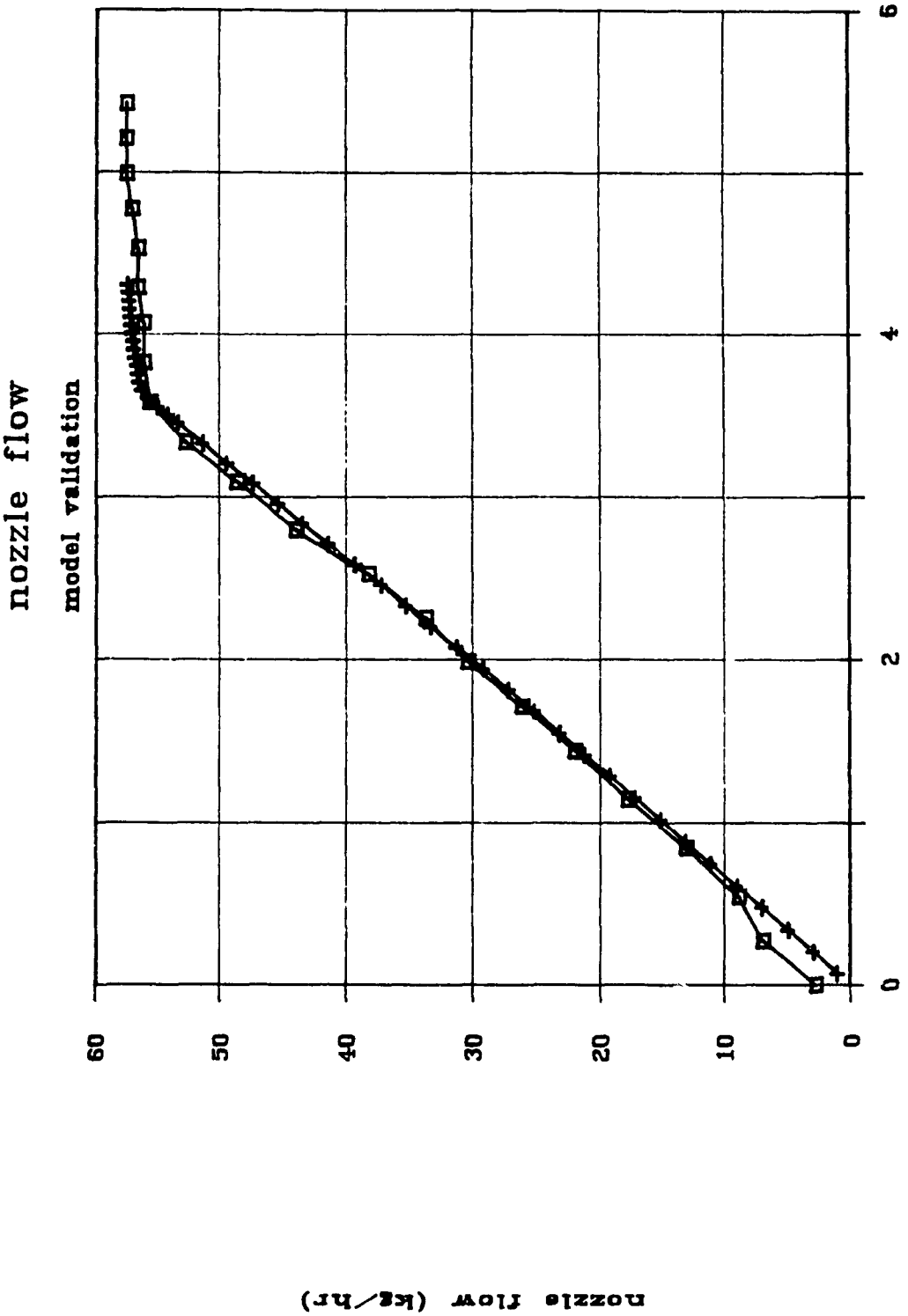

Figure 7.1 (b) Flow versus Metering Vaive Position Model Validation

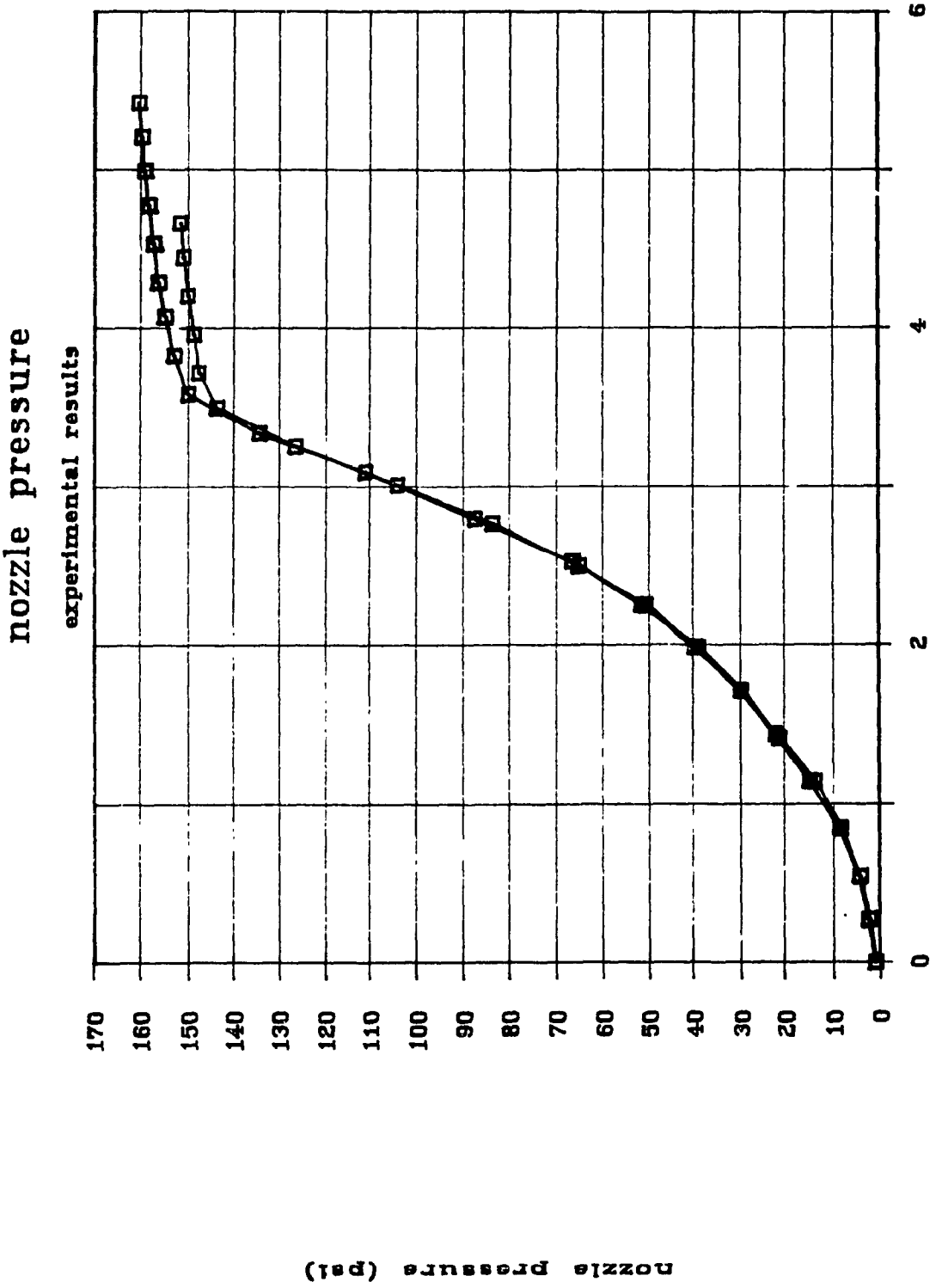

Figure 7.2 (a) Nozzle Pressure Versus Metering Valve Position - Experimental Hysterisis loop

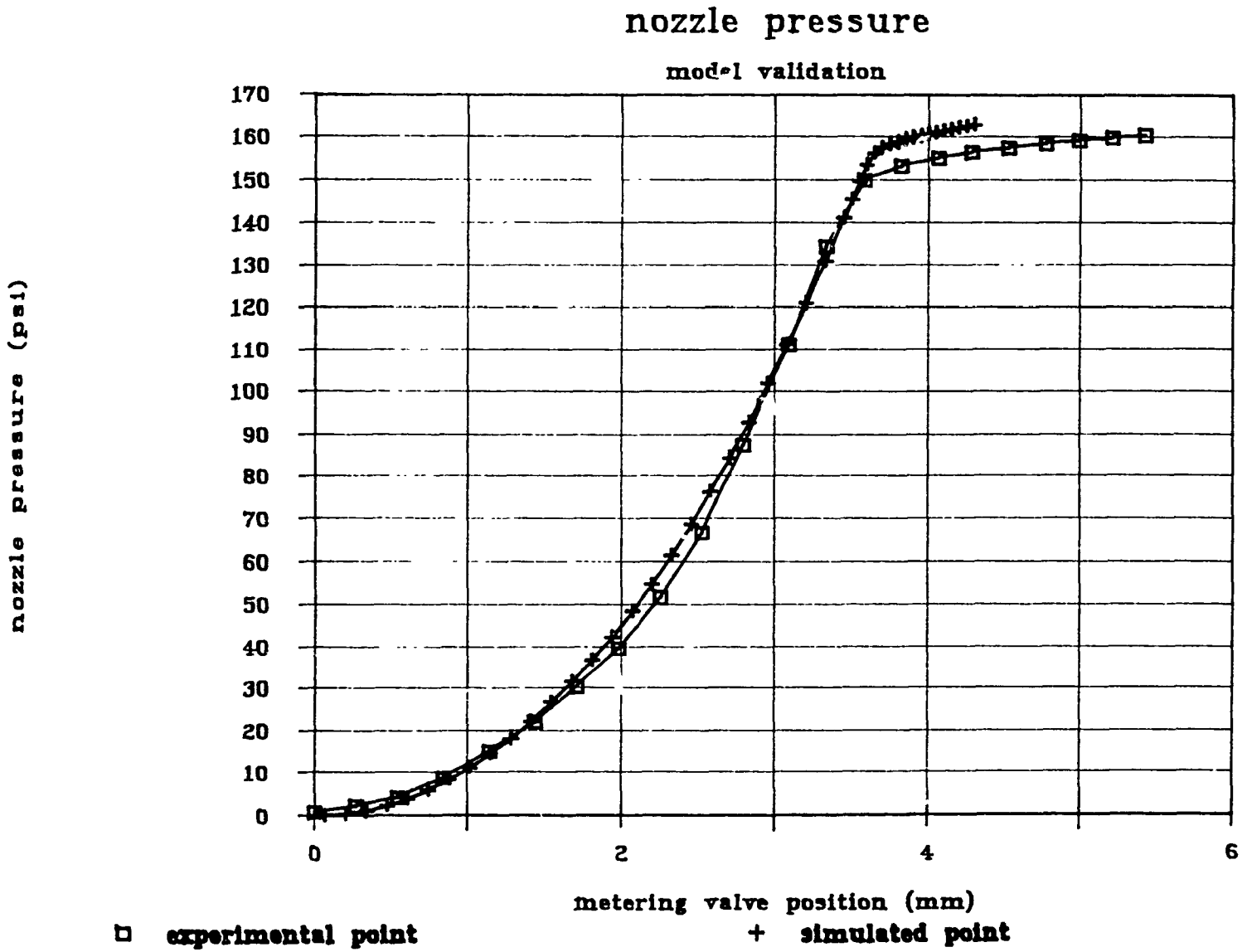

Figure 7.2 (b) Nozzle Pressure Versus Metering Valve Position - Model Validation

Figure 7.2a shows the nozzle pressure versus metering valve position. This curve is related to the flow curve by the orifice discharge equation. There is a slight hysterisis in the characteristic (more than in the flow curve because nozzle pressure is proportional to the square of the flow).

Figure 7.2b compares this curve with the simulation results. The match is good, with a maximum deviation of about 5 psi between the two curves. This is less than 3 % of the full scale.

Figure 7.3a shows the differential pressure across the metering valve versus the metering valve position. There is only slight hysterisis in this characteristic, mainly in the saturation region. For very low flow, a large pressure differential exists. This can be explained as follows. For low fuel flow, a very small diaphragm orifice flow area is required in order to keep the required differential pressure. However, when the diaphragm moves up flush with the face of the inlet of the nozzle manifold pipe, a small leakage area still exists. If the schedule requires a smaller flow, which corresponds to a smaller diaphragm orifice area than the leakage area, the diaphragm valve cannot provide it. The secondary circuit becomes a three orifice nonlinear pressure divider, with the diaphragm orifice flow area fixed at it leak level. Decreasing the metering valve flow area changes the division of the pump pressure among the three orifice. More pressure drop will occur across the metering valve as it closes. If the

metering valve closes completely, then the entire pump pressure is experienced across the metering valve and the differential pressure equals the pump pressure.

Some measures can be taken to improve this situation. If the differential pressure across the diaphragm (which is set by the spring preload on the diaphragm) would be increased, an improvement would result. With the same pump pressure and higher differential pressure, the upper diaphragm chamber pressure would be regulated about a lower value. There would be less pressure potential across the diaphragm orifice, $(P_d - P_n)$, to push the fuel through. For the same flow, the corresponding diaphragm orifice flow area would therefore be larger. Consequently, the leakage flow area of the diaphragm orifice would correspond to a lower flow. The discontinuity point in the characteristic, where the rising slope of differential pressure begins, would move to the left, closer to zero flow. However, this improvement possibility is limited. The differential pressure cannot be raised too high because of other design constraints which are discussed in chapter 11.

In saturation, the differential pressure drops as the metering valve is opened. As explained before, this is because the secondary circuit becomes a three orifice pressure divider with the diaphragm orifice fixed at the cross sectional area of the inlet of the nozzle manifold pipe. The metering valve flow area is the only variable orifice in the divider. Increasing this area changes the pressure division and results in a smaller drop across the

metering valve.

The simulated differential pressure characteristic matches the experimental result well. The low flow increase in differential pressure is not simulated, however. The decrease in differential pressure over most of the schedule as the metering valve is closed is more evident in the experimental results than in simulation.

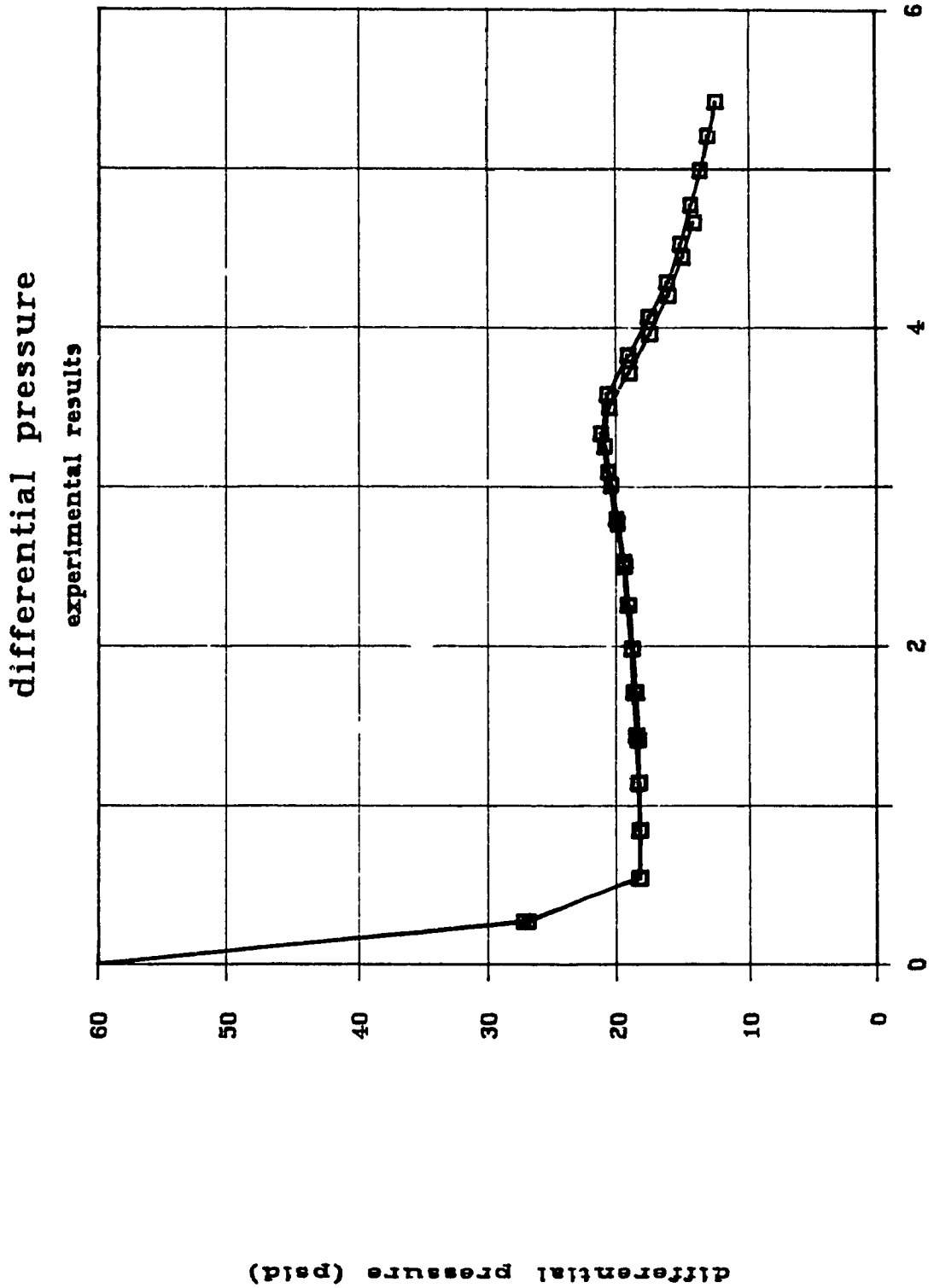

Figure 7.3 (a) Differential Pressure Across the Diaphragm Experimental Hysterisis Loop

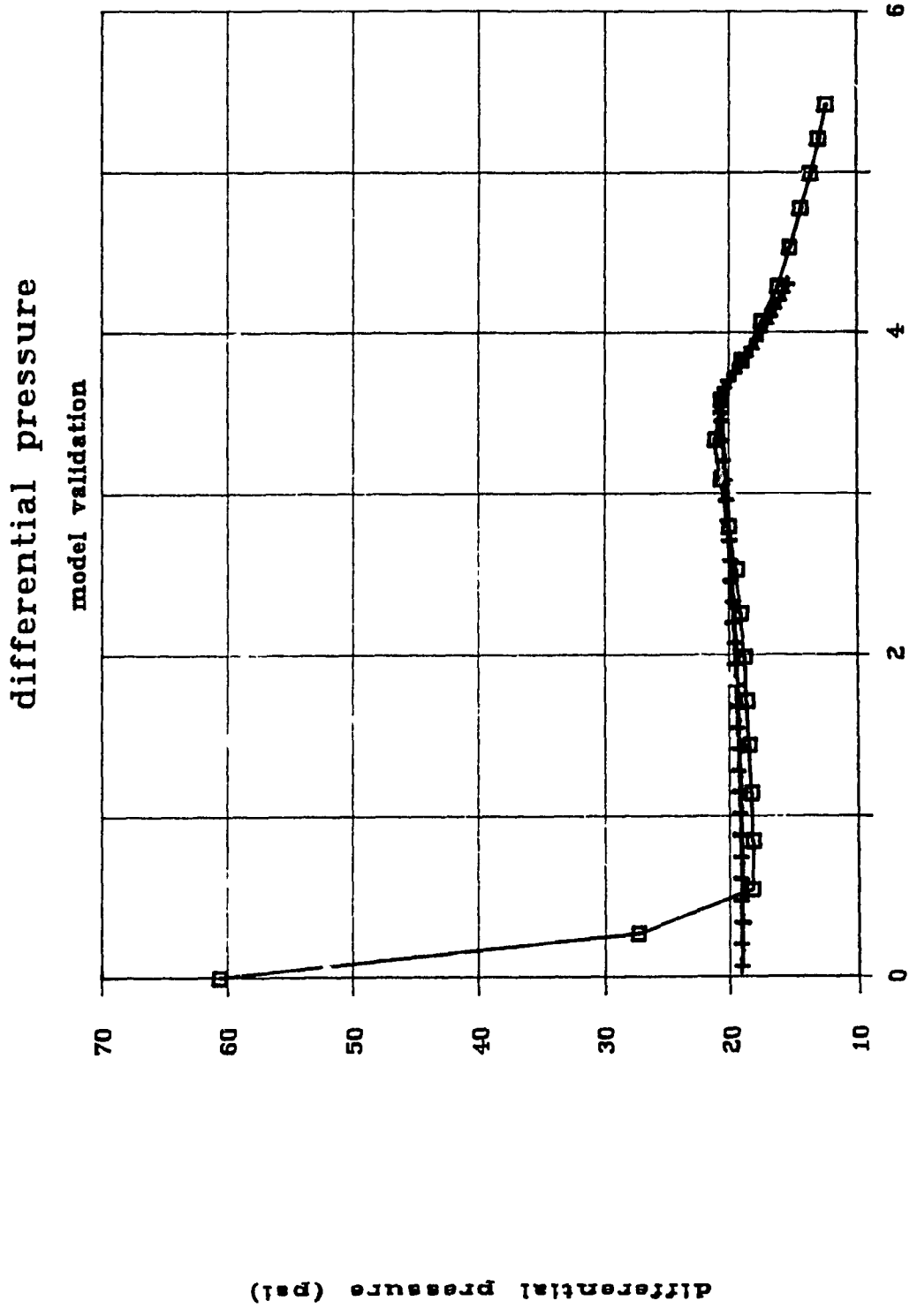

Figure 7.3 (b) Differential Pressure Across the Diaphragm Model Validation

Placing a special sealing material on the diaphragm flapper would improve the sealing. As the diaphragm pushes up against the face of the inlet of the nozzle manifold pipe, the sealing material would fill up the small gaps between the two surfaces. A smaller effective leakage area could be achieved.

Decreasing the diaphragm orifice diameter would improve the situation. The curtain area, $\pi d_n h$, is the effective flow area through the diaphragm orifice. If the diameter of the diaphragm orifice is made smaller, a larger gap would be needed to achieve the same curtain area. The minimum gap possible the leakage gap, would correspond to a smaller flow area, and therefore a smaller flow. Again, the discontinuity point of the differential pressure characteristic would move to the left. An added benefit of decreasing the diaphragm orifice diameter is that this lessens the effect of possible non-perpendicularity between the diaphragm flapper and the diaphragm orifice face.

Figure 7.4a shows the diaphragm deflection versus the metering valve position. There is no significant hysterisis in the curve. Figure 7.4b compares the simulation results and the experimental results of the diaphragm deflection. The curves match for most of the schedule, but at flow saturation of the diaphragm orifice, simulation predicts a faster increase in diaphragm deflection with metering valve position. Several reasons for this discrepancy are possible.

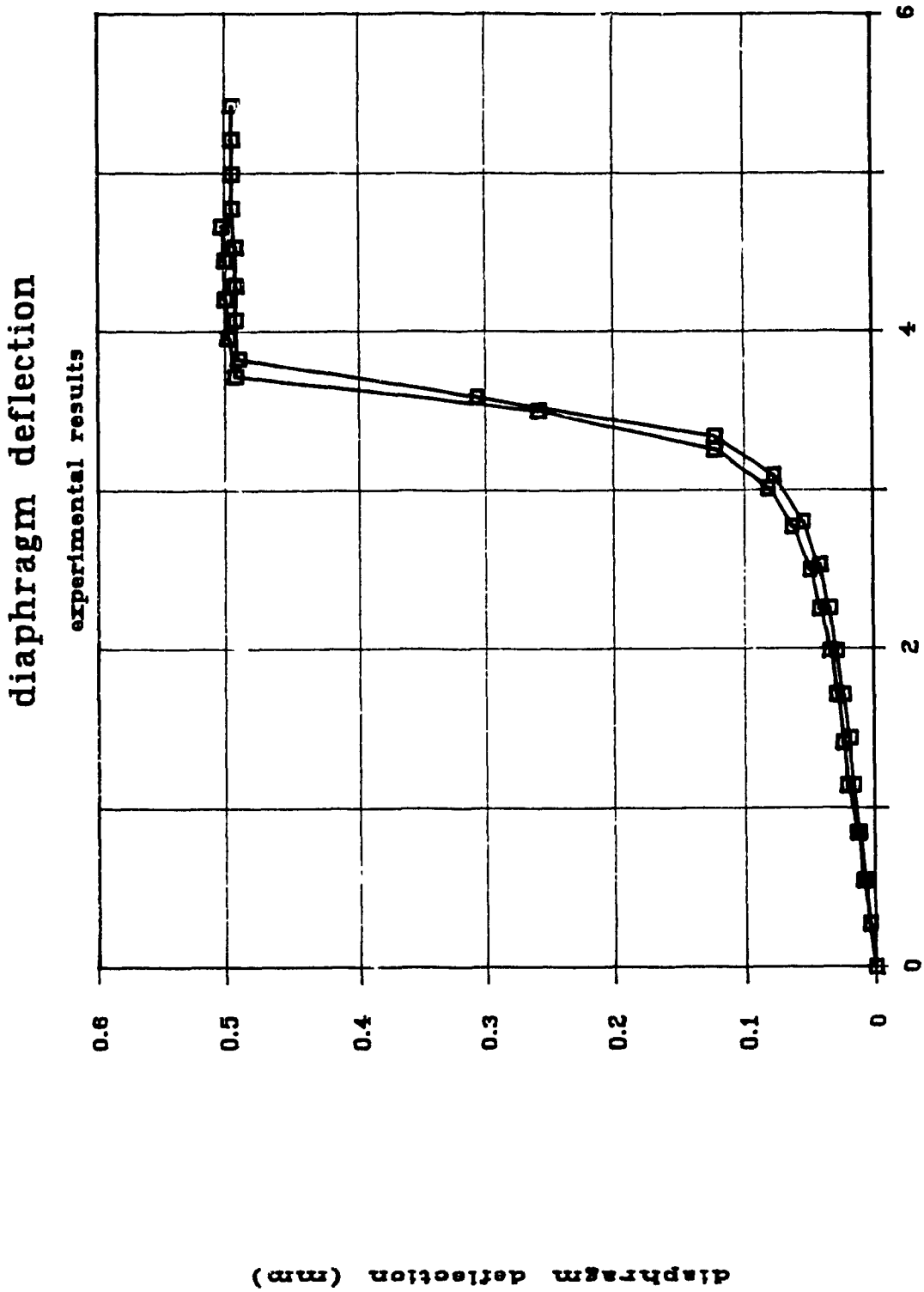

Figure 7.4 (a) Diaphragm Deflection - Experimental Hysterisis Loop

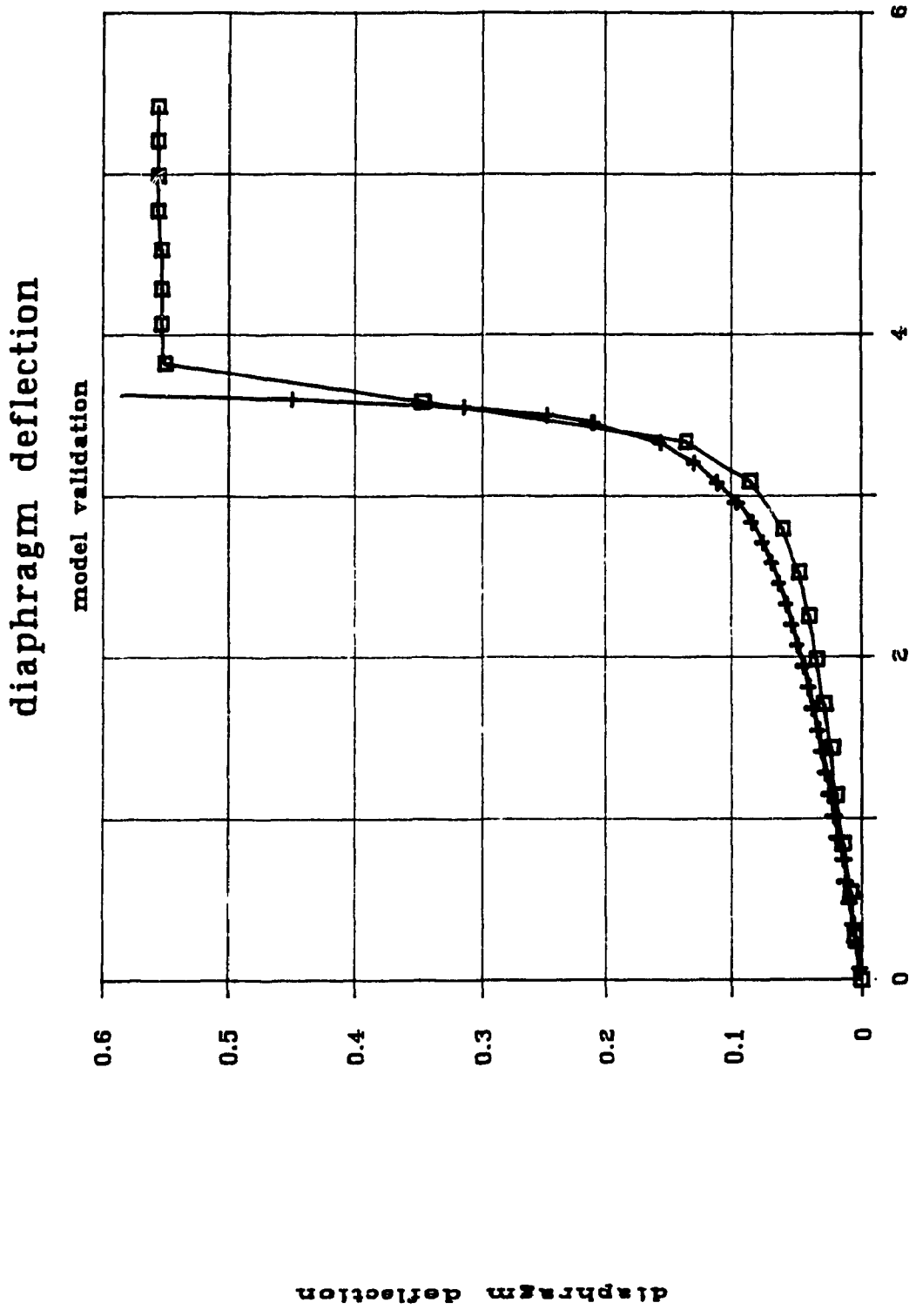

Figure 7.4 (b) Diaphragm Deflection - Model Validation

The diaphragm elasticity itself may come into play when the diaphragm is deflected by large amounts. Friction of the guide of the diapragm valve in the pilot could also be the cause. However, this discrepency should not be considered as severe because it occurs for saturation conditions. In the final design, saturation should be avoided in all operating conditions. It should be noted that the experimental diaphragm deflection is limited by a stop. Finally, Figure 7.5 shows the regulated pump pressure versus the nozzle flow. The characteristic is flat, as expected. This justifies the assumption of constant pump pressure used in the steady state simulation result. There is less than a 5 psi pressure drop over the regulated pressure range. The 5 psi change is not significant in changing the system performance (this will be shown in chapter 11 when sensitivity analysis is performed). There is some hysterisis in the characteristic due to some sticking and friction on the regulating valve. Although the nozzle flow is to some extent insensitive to the pump pressure, the lower pump pressure causes earlier flow saturation. If the regulating valve characteristic is not flat enough, it could permit the pump pressure to drop too low. The maximum flow required would then not be attainable. These considerations will be discussed later.

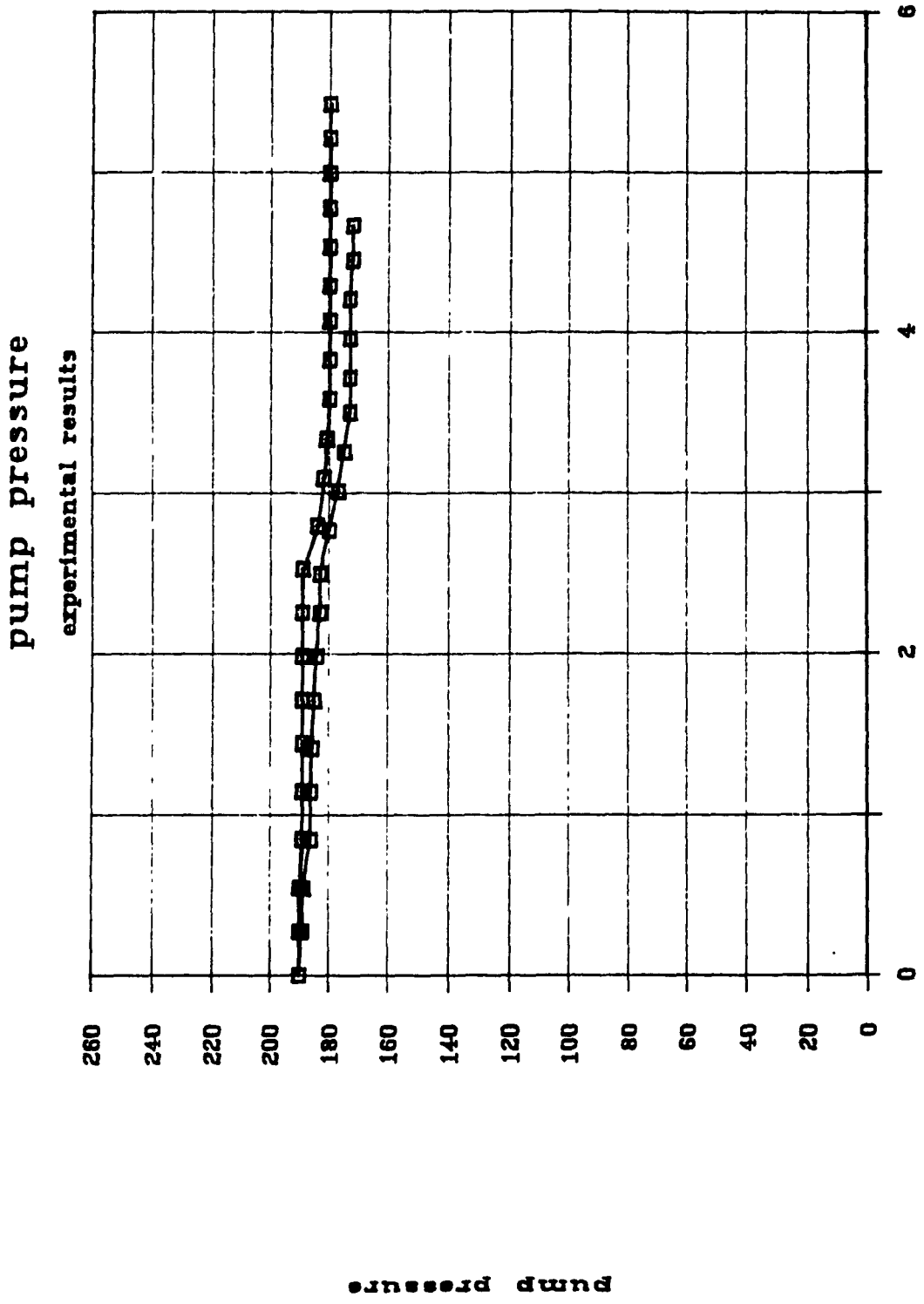

Figure 7.5 Pump Pressure Characteristic

CHAPTER 8

Dynamic Model Description and Simulation Results

In this chapter, a dynamic mathematical model of the system will be developed. Once validated, it will be used for optimization along with the steady state model described in chapter 5. Because of practical considerations, the model is validated only for the set of design parameters used in the prototype testing described in chapter 9. It is assumed that the model is valid for the range of design parameters covered in the optimization program. The calculation of simulation parameters specific to the transient response is also performed in this chapter. All other parameters used in the transient simulation are the same as those calculated in chapter 5. Some typical simulation results produced by this model are also presented in this chapter.

8.1 Model Description

Pump Pressure

Pump pressure changes little (about 5 psi) due to the effectiveness of the pump pressure regulating valve of the primary circuit. The small change in pump pressure will be neglected in the simulation. Pump pressure will be assumed constant. The negligeability of the 5 psi change in pump pressure is justified in chapter 11, when sensitivity analysis is performed.

Metering Valve Flow

The flow through the metering valve is determined by the flow equation,

$$q_{pd} = C_{dm} A_m \sqrt{(2/\rho)(P_p - P_d)} \qquad (8.2)$$

The metering Valve Flow Area is given by,

$$A_m = l \; i \; w \qquad (8.3)$$

where l, the metering valve plunger position, changes incrementally with time to meet the given fuel flow demand input according to the formula

$$l = ((\text{int}) \; f \; t) \; s \qquad (8.10)$$

where the (int) operator indicates that only the integer part of the expression f t is taken

f = the stepping frequency in steps per second

t = the running time

s = the step size

Diaphragm Valve Orifice Flow

The flow through the diaphragm orifice is given by the flow equation as,

$$q_{dn} = C_{do} A_o \sqrt{(2/\rho)(P_d - P_n)} \qquad (8.4)$$

Nozzle Flow

The flow to the nozzles is given as,

$$q_{nc} = C_{di} A_i \sqrt{(2/\rho) P_n} \qquad (8.5)$$

In steady state, the flows, (nozzle flow, diaphragm orifice flow, and metering valve orifice flow) are equal. However, during transient processes, these flows differ because of accumulation effects (fuel compressibility).

Fluid Capacitance; Upper Chamber Volume

Applying continuity to the upper chamber volume,

$$dP_d/dt = (\beta/V_d)(q_{pd} - q_{dn} + A_d(dh/dt)) \qquad (8.6)$$

where β = the effective fuel bulk modulus

V_d = volume of upper diaphragm valve chamber

The third term indicates the piston-like displacement effect of the moving diaphragm. For significant diaphragm deflections, the volume of the upper chamber changes.The volume of the upper diaphragm chamber is therefore given by,

$$V_d = V_{do} - A_d h \qquad (8.7)$$

where V_{do}= upper chamber volume with undeflected diaphragm.

Fluid Capacitance; Nozzle Manifold Volume

Relating the manifold pressure derivative to the accumulation of fuel in the manifold,

$$(dP_n/dt) = (\beta/V_n)(q_{dn} - q_{nc}) \qquad (8.8)$$

where V_n = the volume of the nozzle manifold

Diaphragm Motion

A dynamic force balance on an equivalent lumped mass approximation of the diaphragm gives,

$$M_d\ (dV/dt) = A_d P_p - P_d(A_d - A_n) - P_n A_n - K_s h - bV \qquad (8.9)$$

where M_d = effective inertia at the diaphragm center accounting for the spring mass and fluid inertia

V = (dh/dt) = diaphragm velocity

b = effective damping of the diaphragm by the fuel

To summarize, the simultaneous solution of the following set of differential equations is required.

$$M_d\ (dV/dt) = A_d P_p - P_d(A_d - A_n) - P_n A_n - K_s h - bV \qquad (8.9)$$

$$V = dh/dt$$

$$q_{pd} = C_{dm} A_m \sqrt{(2/\rho)(P_p - P_d)} \qquad (8.2)$$

$$Am = l\ i\ w \qquad (8.3)$$

$$l = ((int)\ f\ t)\ s \qquad (8.10)$$

$$q_{dn} = C_{do} A_o \sqrt{(2/\rho)(P_d - P_n)} \qquad (8.4)$$

$$q_{nc} = C_{di} A_i \sqrt{(2/\rho)P_n} \qquad (8.5)$$

$$dP_d/dt = (\beta/V_d)(q_{pd} - q_{dn} - A_d(dh/dt)) \qquad (8.6)$$

$$V_d = V_{do} - A_d h \qquad (8.7)$$

$$(dP_n/dt) = (\beta/V_n)(q_{dn} - q_{nc}) \qquad (8.8)$$

$$A_o = \frac{A_c A_n}{A_c^2 + A_n^2}$$

$$A_c = \pi d_n (h_{max} - h)$$

The control system block diagram of the dynamic model is given in Figure 8.1.

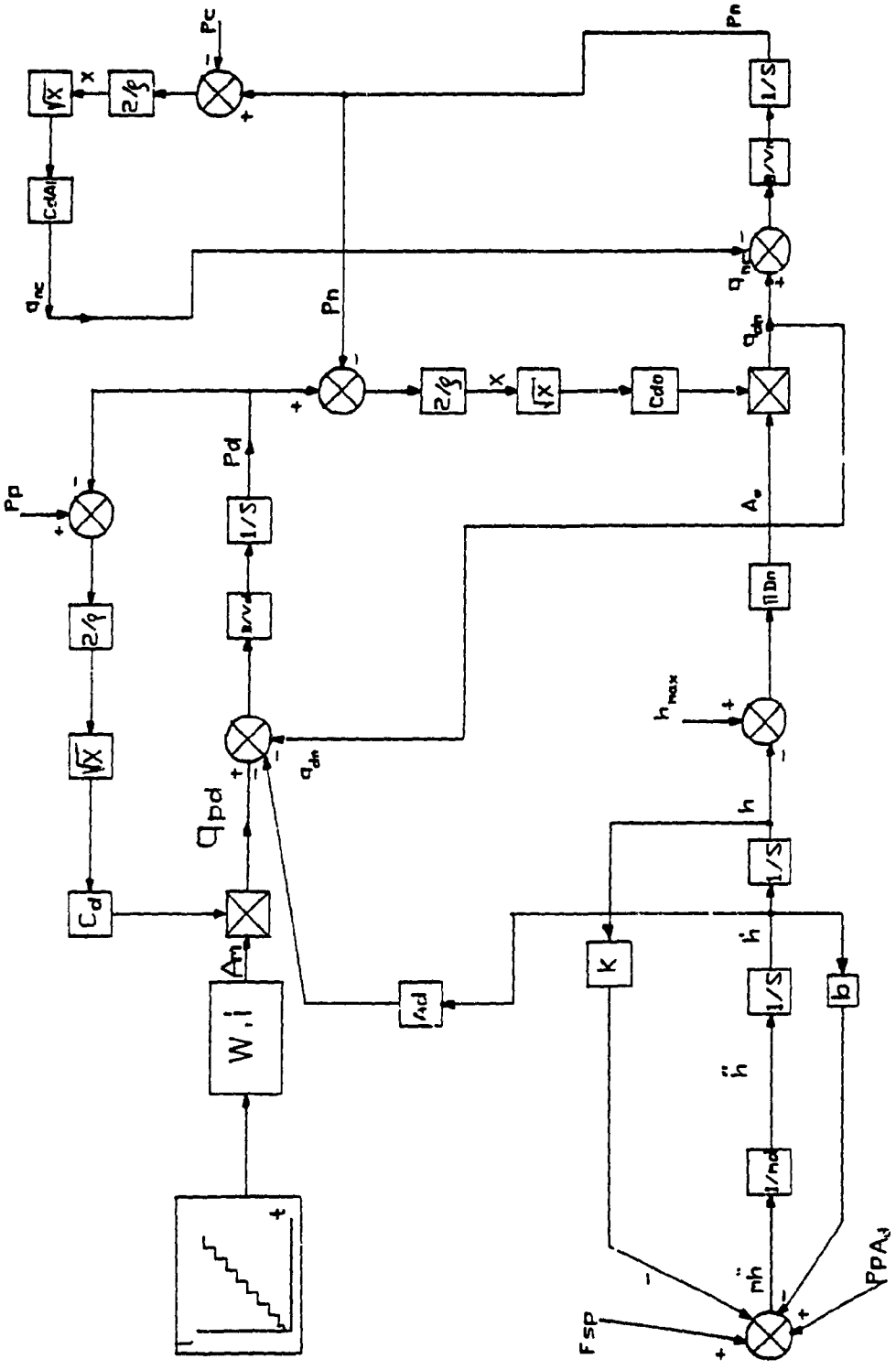

Figure 8.1 Control System Block Diagram of the Dynamic Model

8.2 Calculation of Parameters

Estimation of Effective Diaphragm Mass

The effective mass at the center of the diaphragm must take into account the mass of the diaphragm and valve guide itself, the mass of the spring preloading the diaphragm and the effective inertia of the fuel above and below the diaphragm.

The preload spring weighs about 6 g and the diaphragm and valve guide assembly weighs about 10 g. Taking 1/3 of the spring mass, the effective diaphragm mass, not including the effects of fluid inertia, is about 12 g. The actual simulation results were found not to depend strongly on the effective diaphragm mass since inertia forces are small in comparison to other forces in the system. The effective mass was tuned in the simulation program about the value of 12 g to best match experimental results.

Calculation of Nozzle Manifold Volume

The nozzle manifold volume consists mainly of 3/8 inch tubing leading out of the fuel control housing and to the nozzle simulating valve. The length of the tubing is approximately 0.8 m. The volume is therefore approximately,

$$V_n = \pi [(3/8)(.0254)]^2/4 = 7.125\ (10)^{-5}\ m^3$$

Calculation of Upper Diaphragm Chamber Volume

The upper diaphragm chamber can be crudely approximated by a one inch diameter disk that is on inch in depth. The volume of fluid in the chamber is therefore approximately,

$$V_d = (.0254)\pi(.0254)^2/4 = 1.29\ (10)^{-5}\ m^3$$

Estimation of Effective Diaphragm Damping

The damping of the diaphragm motion by the fuel is difficult to calculate analytically. This parameter was tuned in the simulation program in order to best match a variety of experimental transient response curves. However, the system response does not depend much on the diaphragm damping since damping forces are negligeable compared to pressure feedback forces.

Estimation of Fuel Compressibility

The pure bulk modulus of fuel is about $1.2\ (10)^9$ Pascals. However, the bulk modulus is greatly affected by entrapped air. For normally aerated systems, Meritt [28] recommends a reduction by about a factor of three. Thus, the bulk modulous is tuned in the simulation about the value of $4(10)^8$.

8.3 Simulation Method

The efficient solving of the nonlinear set of differential equations in the dynamic model is a challenge. The large bulk modulus of fuel and the small fluid volumes involved in the model result in large pressure derivative terms, necessitating a very small time step (about 10^{-5} seconds) for numerical stability. Optimization of the fuel control design will involve running the simulation many times with different design parameters. It was therefore critical to keep simulation time as small as possible. An efficient differential equation solver with adaptive stepsize using the Runge Kutta method was used [29]. After much code optimization for speed, a typical transient of 2.5 second duration required a simulation time of only 10 minutes.

8.4 Simulation Results

In this section, some typical simulation transient results will be plotted. The input to the simulation is a ramp change in metering valve position, which corresponds to a ramp change in fuel flow demand. The step input is a theoretical one that cannot be achieved in practice. Figures 8.1 to 8.4 show the simulation results to a positive ramp fuel flow demands. The metering valve moves from an initial position of 1.26 mm to 2.48 mm opening during these transients. The actuation time, t, can easily be calculated from the step size s =

.0254 mm, the stepping rate f = 100 Hz, and the initial (l_o) and final (l_f) plunger positions.

$$t = (l_f - l_o)/(fs) = (2.48 - 1.26)/(100\ (0254)) = 0.48 \text{ seconds.}$$

Figure 8.1 shows a typical nozzle pressure transient response to a positive ramp input. The pressure settles to its final steady state after about 1.5 seconds.

Figure 8.2 shows the corresponding nozzle flow transient, which follows the fuel flow via the discharge equation.

Figure 8.3 shows the diaphragm deflection transient. The diaphragm moves down to open up the diaphragm orifice in order to accomodate the larger flow. A slight change in the characteristic can be seen at about 0.5 seconds after actuation. This corresponds to the time the metering valve stops moving. Before this time, the diaphragm is moving to follow the metering valve motion. After this time, the diaphragm is moving due to the changing pressures in the upper diaphragm chamber and the nozzle manifold pipe. Figure 8.4 shows the differential pressure transient. The differential pressure rises slightly due mostly to the increased nozzle pressure force on the diaphragm which comes with the higher nozzle flow.

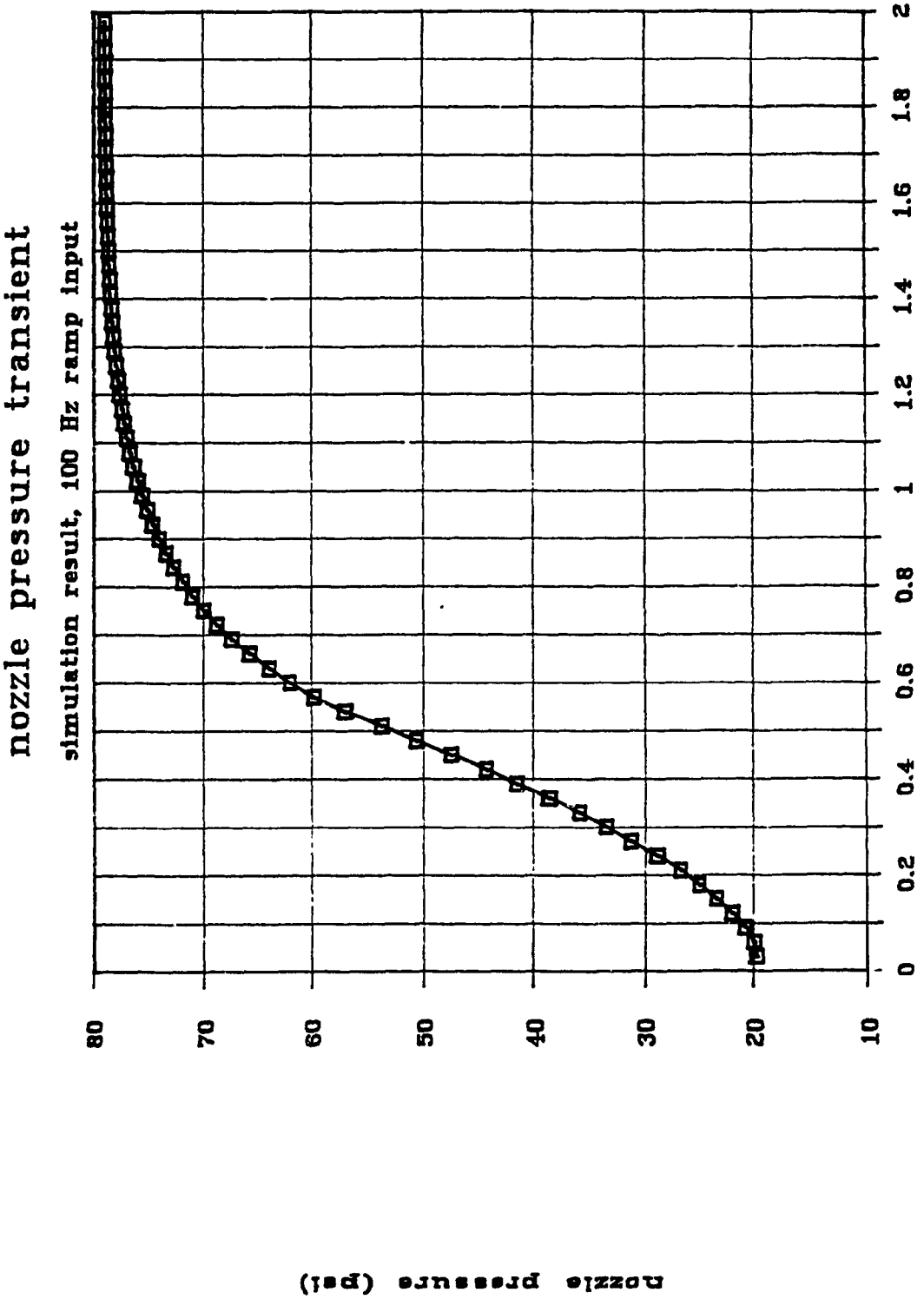

Figure 8.2 Nozzle Pressure Transient

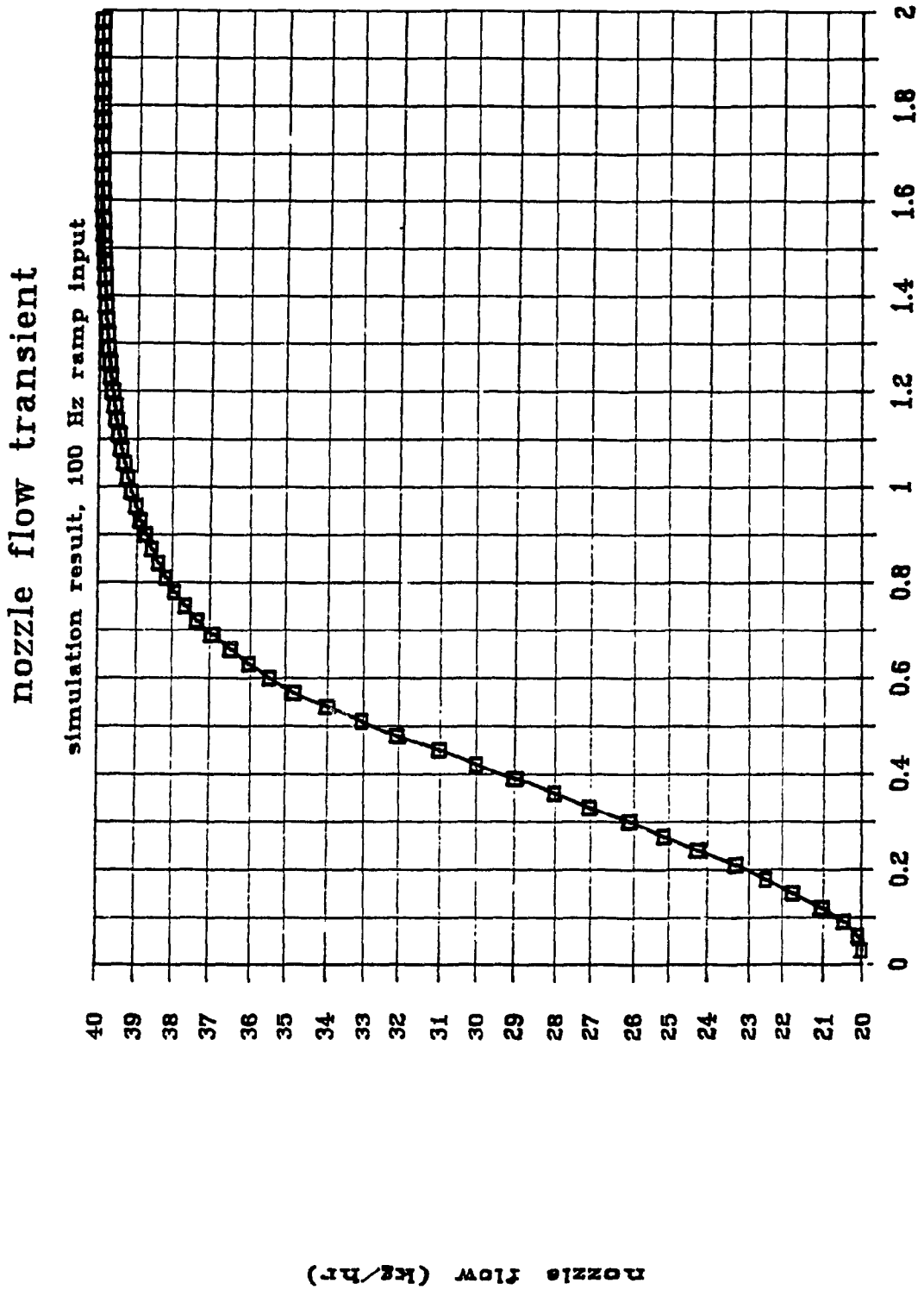

Figure 8.3 Nozzle Flow Transient

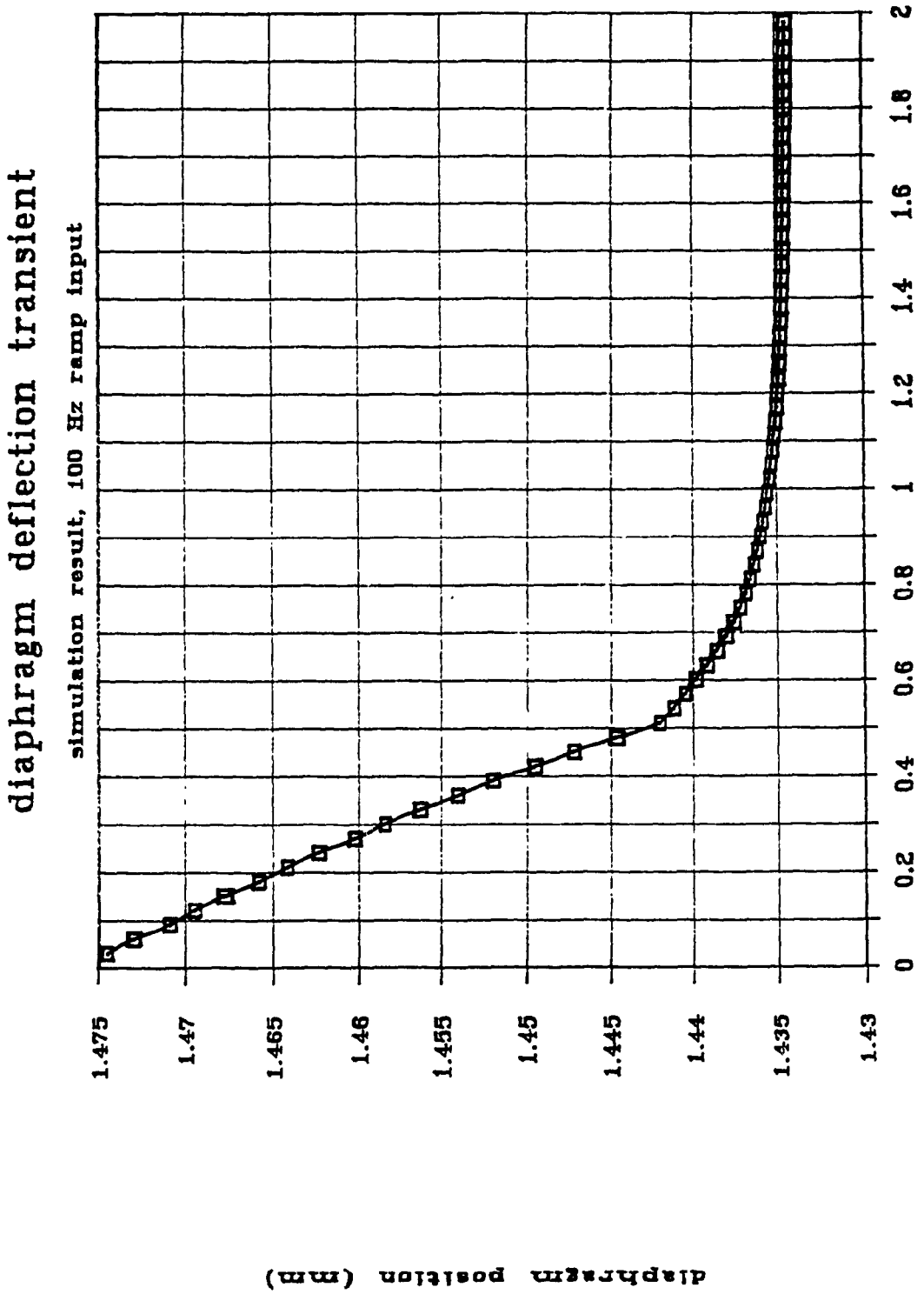

Figure 8.4 Diaphragm Deflection Transient

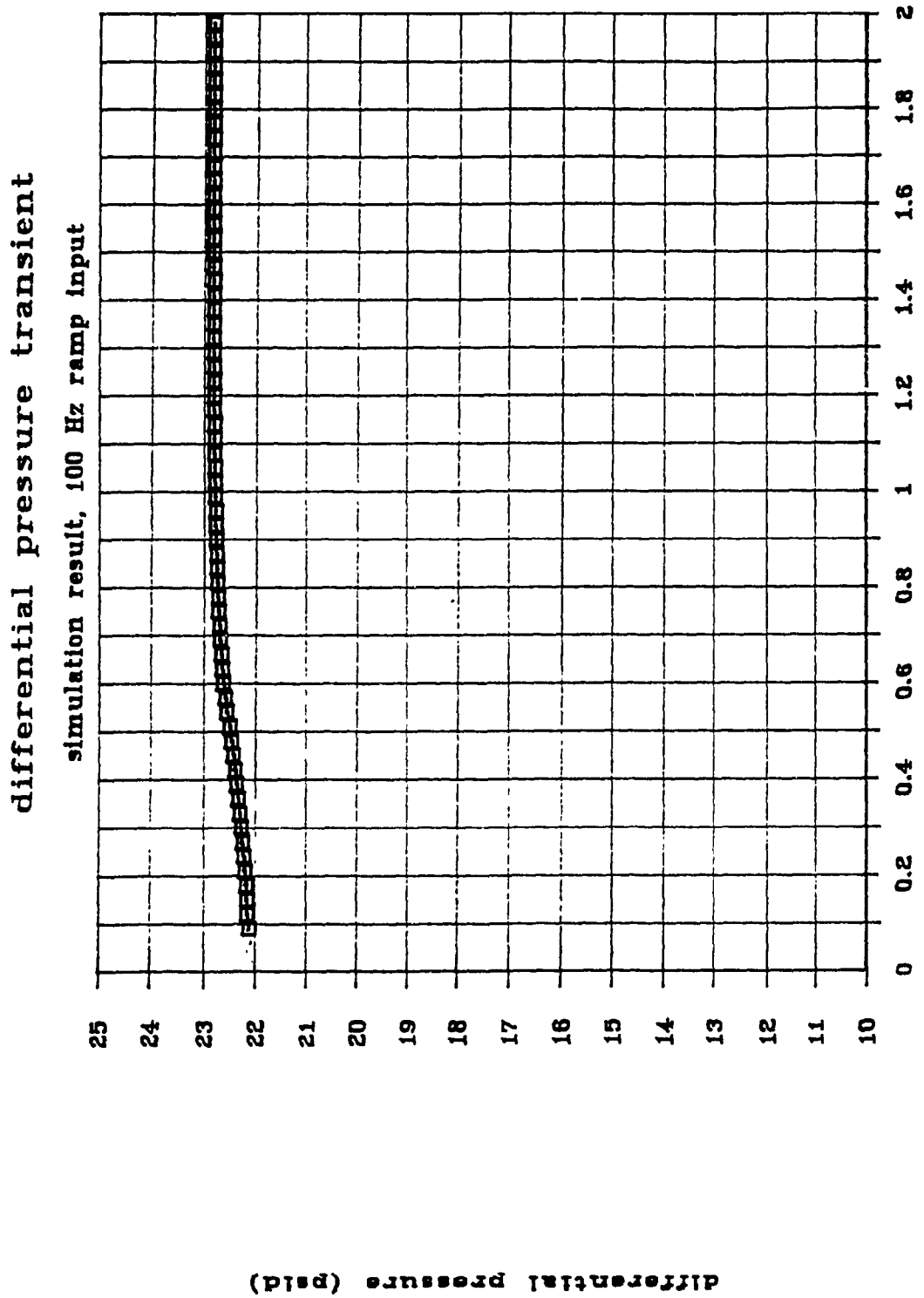

Figure 8.5 Differential Pressure Transient

CHAPTER 9

Transient Experimental Results and Model Validation

In this chapter, the transient computer simulation program described in chapter 8 will be validated against experimental results. The validation curves correspond to a positive ramp input actuation of the metering valve plunger at a 100 Hz stepping rate.

Figure 9.1 shows the model validation curve for the nozzle flow. The match between simulation and test results is very good, with the experimental curve slightly faster than predicted.

Figure 9.2 shows the model validation curve for the nozzle pressure. This curve follows the one for the nozzle flow exactly, according to the nozzle orifice discharge equation.

Figure 9.3 shows the model validation curve for the differential pressure. The experimental change in differential pressure is larger than that predicted by simulation. However, there is a similarity in trend between the two curves. The experimental curve displays some noise. This noise can be due to two causes. First, the electric disturbance caused by the fuel pump can cause electrical noise in the interface circuitry used to condition the instrument signals. Second, a fuel pump is well known to be the cause of pressure pulsations and a cause of mechanical vibration on the system [30]. Pressure waves emitted by the pump can cause the diaphragm to vibrate slightly (see Figure 9.4) which in turn causes fluctuation of the regulation of differential pressure.

Finally, Figure 9.4 shows the model validation curve for the diaphragm deflection. Again, there is some noise in the experimental curve. However, the match between experimental and simulation results can be said to be satisfactory.

It can be concluded from the validation curve that the transient model does predict all the trends noted in the experimental results. The model is sufficiently accurate for it to be used for optimization in chapter 13.

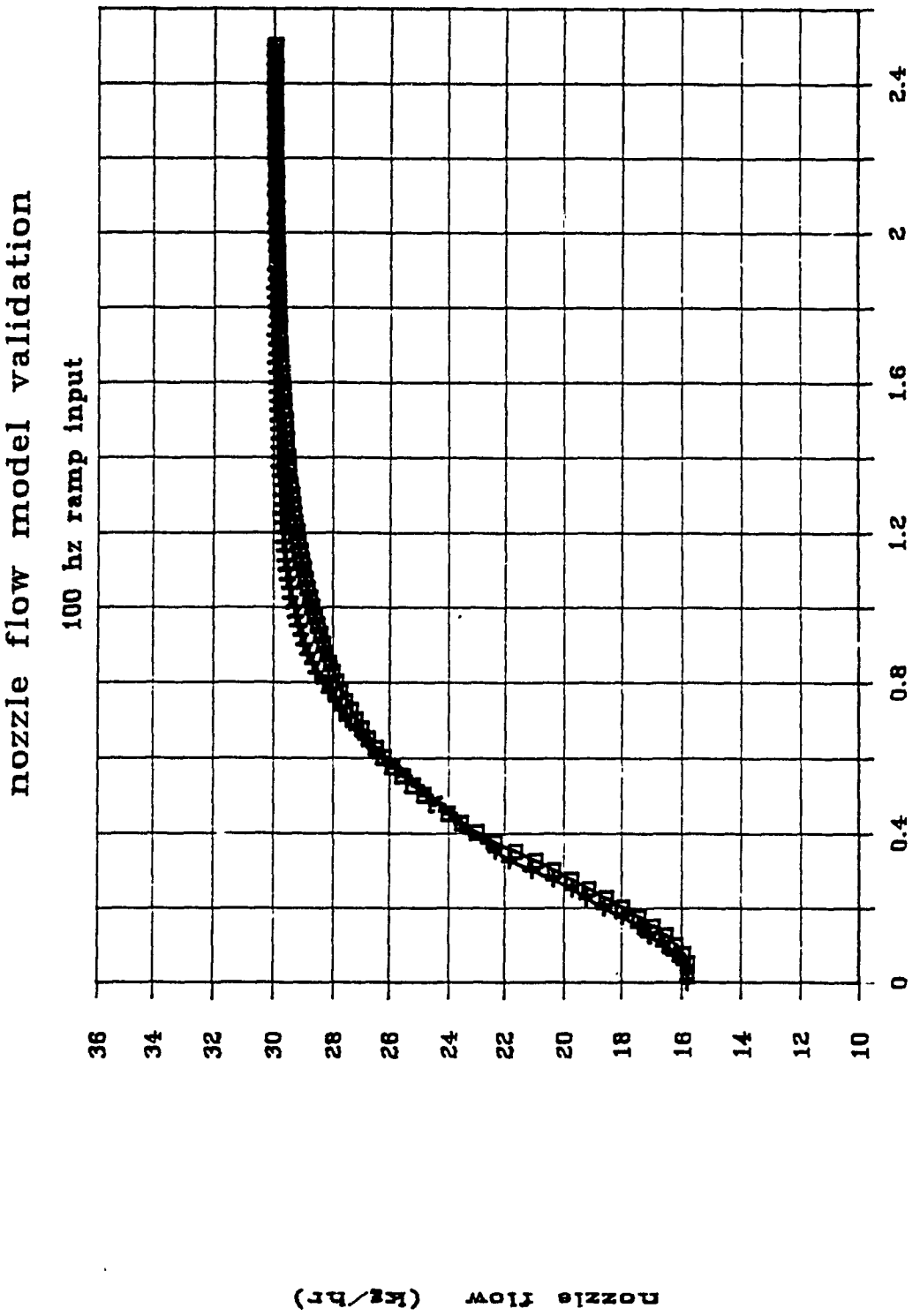

Figure 9.1 Model Validation of Nozzle Flow Transient

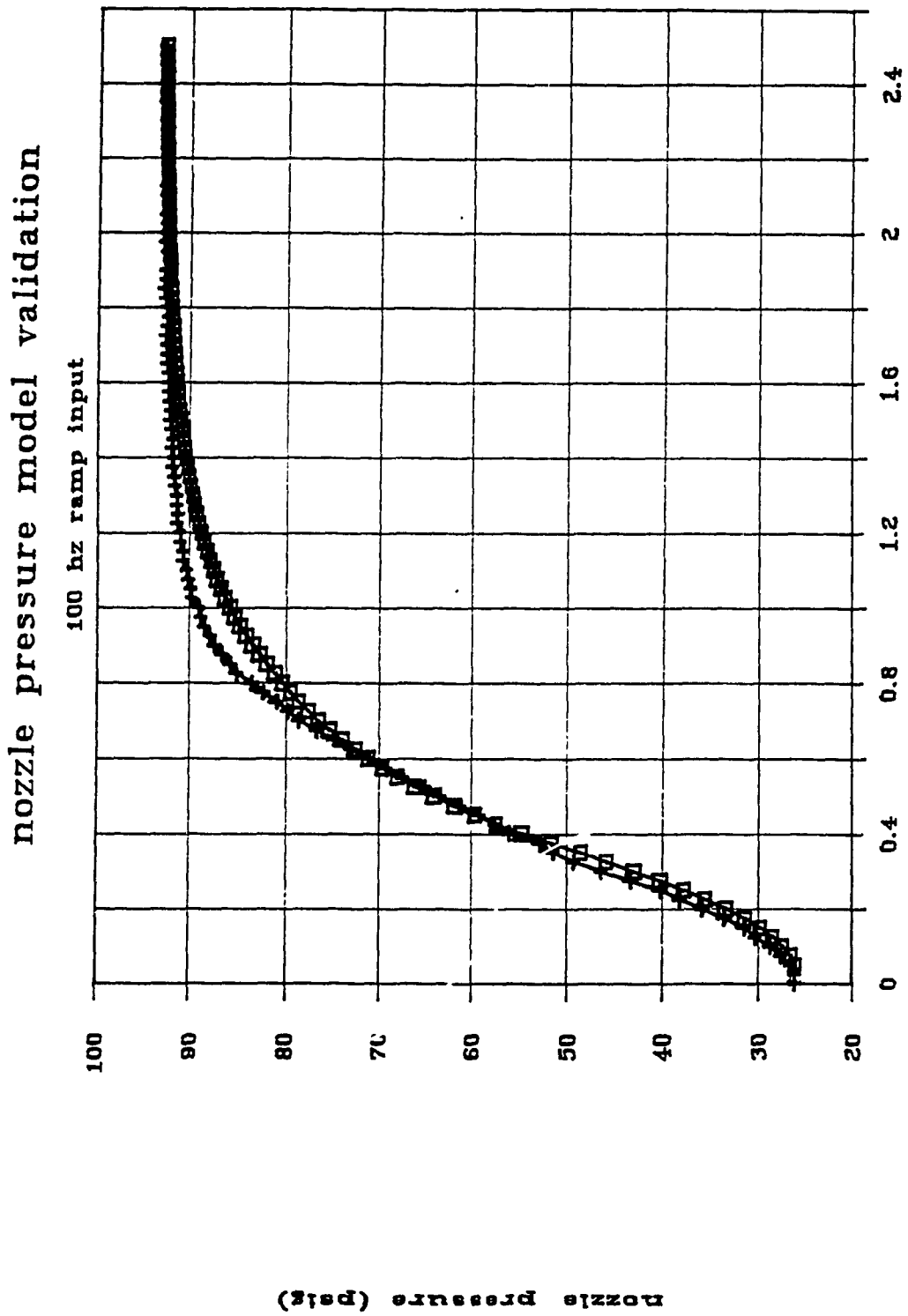

Figure 9.2 Model Validation of Nozzle Pressure Transient

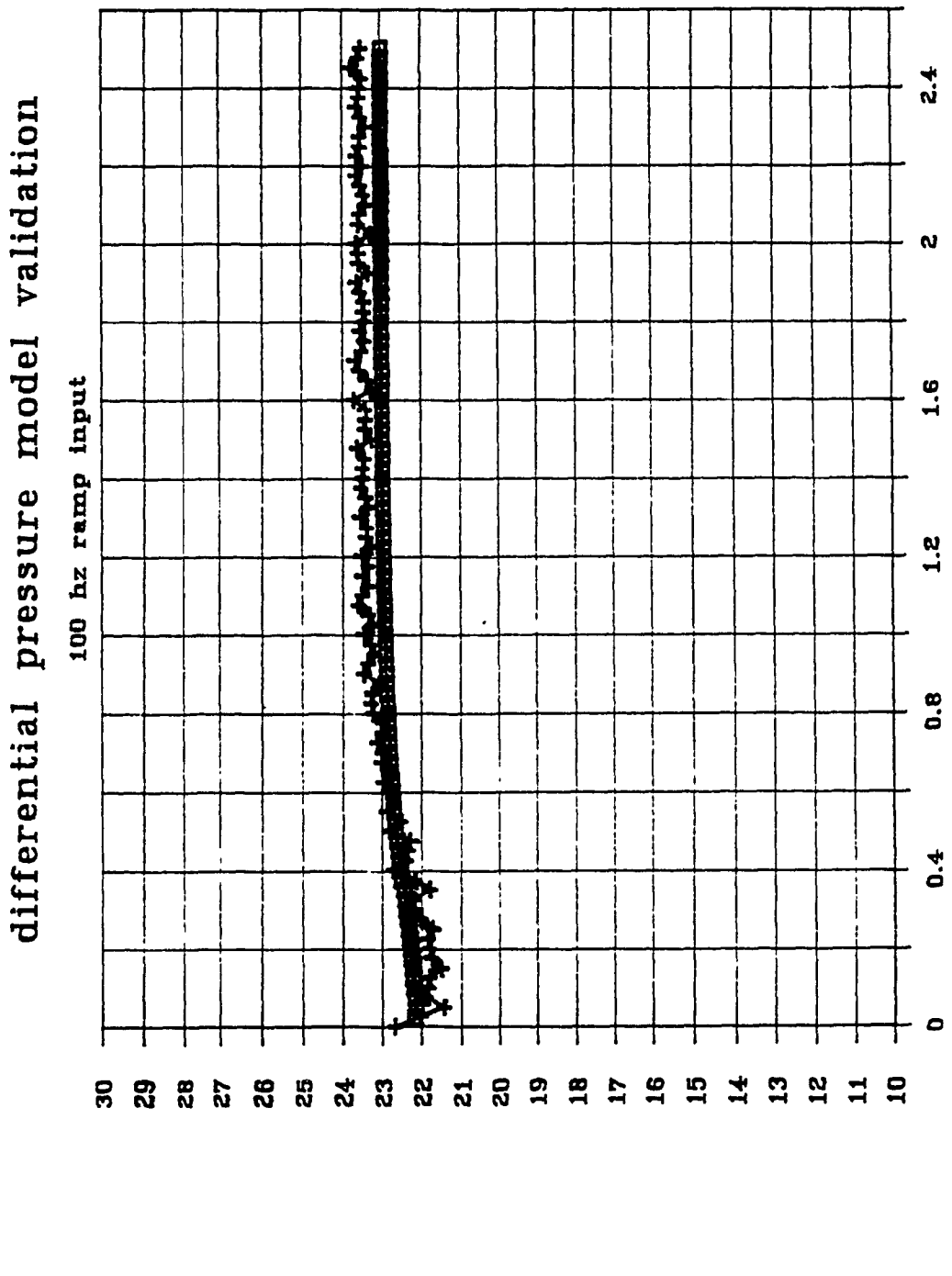

Figure 9.3 Model Validation of Differential Pressure Transient

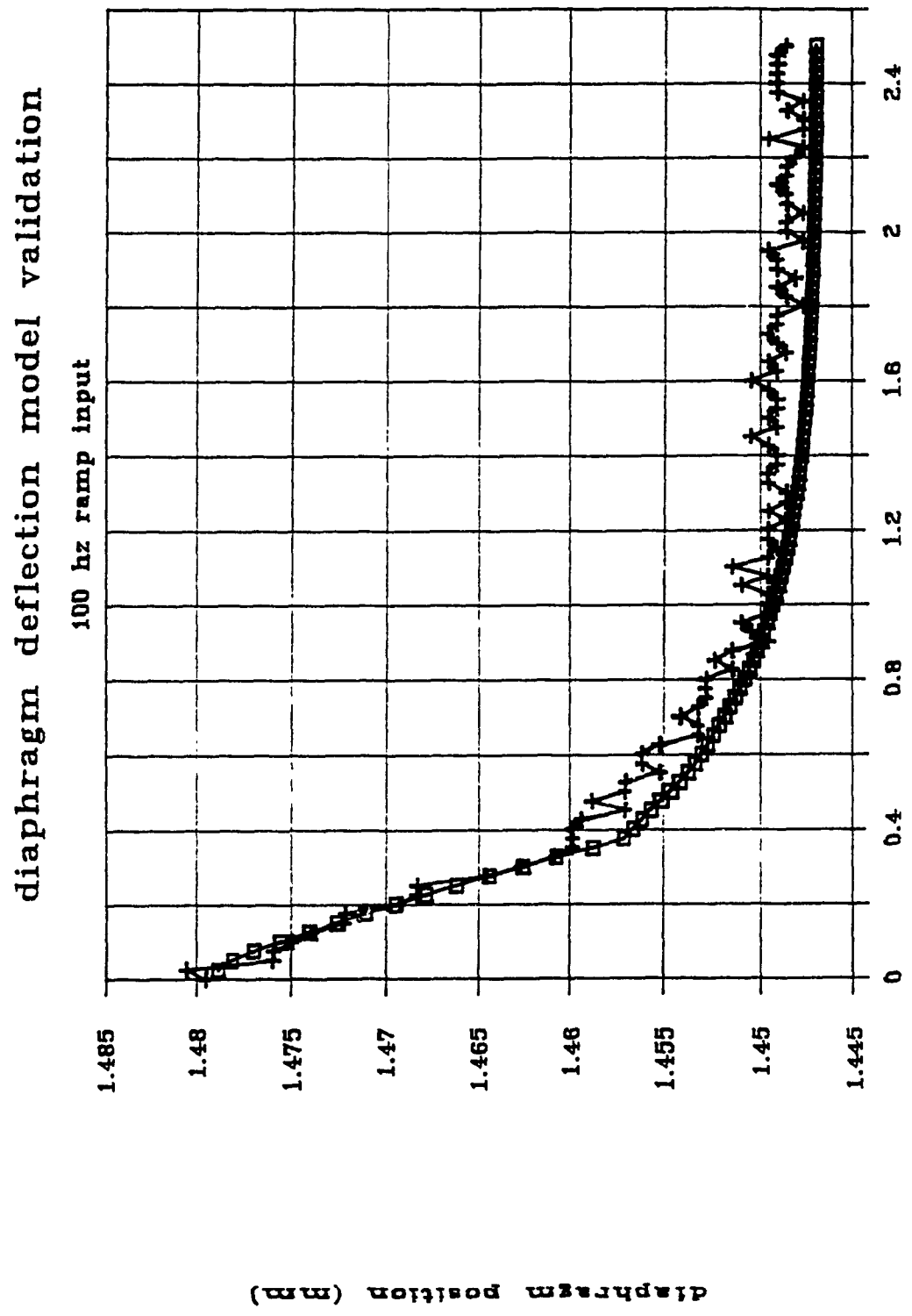

Figure 9.4 Model Validation of Diaphragm Deflection Transient

Chapter 10

Analysis on the Variation of Differential Pressure Across the Metering Valve; The First Optimization Criterion

The purpose of deriving, computer simulating, and validating the steady state and transient mathematical models capable of predicting the system performance is so that they can be used to provide insight and improve the design. Specifically, computerized design optimization of the fuel control unit is the goal. However, before an optimization scheme can be developed, the optimization criteria for a fuel control must be identified and indices must be created to suitably quantify the criteria. Three criteria were identified as important to the design of the fuel control studied in this thesis. They are:

1) The linearity of the metering valve flow schedule. That is, the fuel flow to the nozzles should be linearly relate the the metering valve positon.

2) The sensitivity of the system performance to possible parameter changes during the operational life of the fuel control.

3) The speed of the transient response to a fuel flow demand originating from the operator.

In the next three chapters, each of these three considerations will be analysed in turn. The effect of design variables on these three criteria will be investigated. Finally, in chapter 13, the three analyses will be unified in a multiobjective optimization scheme.

To have the desired (linear) metering valve fuel flow schedule, the differential pressure across the metering valve should be kept close to constant. In this chapter, the steady state simulation program validated in the chapter 7 will be used to observe how system design variables can be chosen in order to minimize the variation of differential pressure over the flow schedule. It should be noted that with the flexibility offered by electronic control, a nonlinear schedule of fuel flow versus metering valve position could be compensated for in software. However, this is an additional complication in electronic control and therefore, a linear metering valve flow schedule is a characteristic customers would prefer.

The sources of variation of differential pressure across the metering valve can be identified from a force balance equation on the diaphragm. Neglecting the flow force, which is considered small, following force equation should be written:

$$P_n A_n + P_d(A_d - A_n) + F_{sp} + K_s h = P_p A_d \qquad (10.1)$$

Expressing the forces in terms of differential pressure (P_p-P_d), the equation will change as follows:

$$P_p-P_d = F_{sp}/(A_d-A_n) + K_s h/(A_d-A_n) - (P_p-P_n)A_n/(A_d-A_n) \quad (10.2)$$

The preload force of the spring on the diaphragm is fixed, it does not vary (by definition) as the metering valve is moved. The first term on the right hand side of the above equation is therefore constant and does not contribute to the variation of differential pressure.

The second term indicates that the differential pressure tends to rise as the diaphragm moves up (when h increases and flow decreases). This effect is amplified with a stiffer spring.

The third term indicates two effects. First, for a constant pump (primary circuit) pressure, as P_n (and nozzle flow) drops, so does the differential pressure. It should be underlined that the effect of the third term and the effect of second term act in opposite directions with respect to the flow. This indicates a possibility to design the diaphragm valve so that these effects neutralize each other as much as possible. The third term also indicates the effect of the pump pressure changes, which results from the pressure regulating valve characteristic. As pump pressure increases, the differential pressure drops. For a constant metering valve position, an increase in pump pressure will cause a decrease in fuel flow to the nozzle. Therefore, the

variations in regulated pump pressure will also contribute to the changes in differential pressure. As stated by Bosch for its K-Jetronic fuel injection system [27], if area A_n is small when compared to A_d, and if the spring constant is small, deviations in differential pressure are also small and can be neglected (the second and third terms in the above equation become negligible). However, if the diaphragm valve has to be used for the larger fuel flows supplying a gas turbine engine, the diaphragm valve orifice diameter must be enlarged. Of course, the diaphragm area A_d could be also enlarged to decrease the ratio (A_n/A_d), but this would increase the overall size of the fuel control unit, making it heavy and expensive. Implementing the diaphragm valve for the fuel control design studied in this thesis, the impact of the pressure force in the valve orifice will be significant and the spring constant will not be chosen as small as possible. Rather, a higher spring constant that best compensates for the variations of the differential pressure will be chosen.

From equation (10.2), another possible solution can be proposed. The differential pressure can be made very large with a high spring preload so that the first term dominates the equation. This would also have the added benefit of speeding up the response time during transients, since less steps would be required from the stepper motor in order to vary the fuel flow. However, for a gas turbine engine, accurate fuel metering is needed, especially for

acceleration and deceleration schedules. With high differential pressure, one motor step corresponds to a larger flow change and it would be difficult to meet the required flow schedule if the resolution is too low. A second important drawback when using a high differential pressure is that a higher pump pressure would be required which needs a stronger electric pump, resulting in higher cost of the fuel system.

10.1 Study of the Impact of Design Variables

In this section, the effect of design variables on the variation of differential pressure across the metering valve will be examined. It will be evaluated by a performance index, which represents the maximum percentage variation of differential pressure over the schedule. This index will be called VAR,

$$VAR = 100 \quad | \ (\Delta p_{ext} - \Delta p_{ave}) | \ / \Delta p_{ave} \qquad (10.3)$$

where Δp_{ext} is the minimum or maximum value of differential pressure observed over the flow schedule, whichever one deviates more from the average differential pressure. Δp_{ave} is the average differential pressure over the metering valve schedule.

The effect of each variable on the VAR index will be examined by parametrically varying it while all other design variables are kept constant.

The indices from different simulation runs (with design variables altered) should be compared with the same average differential pressure setting. However, the average differential pressure over the flow schedule for a set of design variables is not known "a priori". The differential pressure is only approximately determined by the preload force F_{sp}. This approximation is given by $F_{sp} \cong (P_p - P_d)A_d$. However, for this analysis, an accurate setting of average differential pressure is needed. Therefore, for the set of parameters corresponding to the current simulation run, the spring preload force giving the desired average differential pressure is first found iteratively with a computer program. The run with this preload is used to compute the index. Figure 10.2 shows the computational scheme.

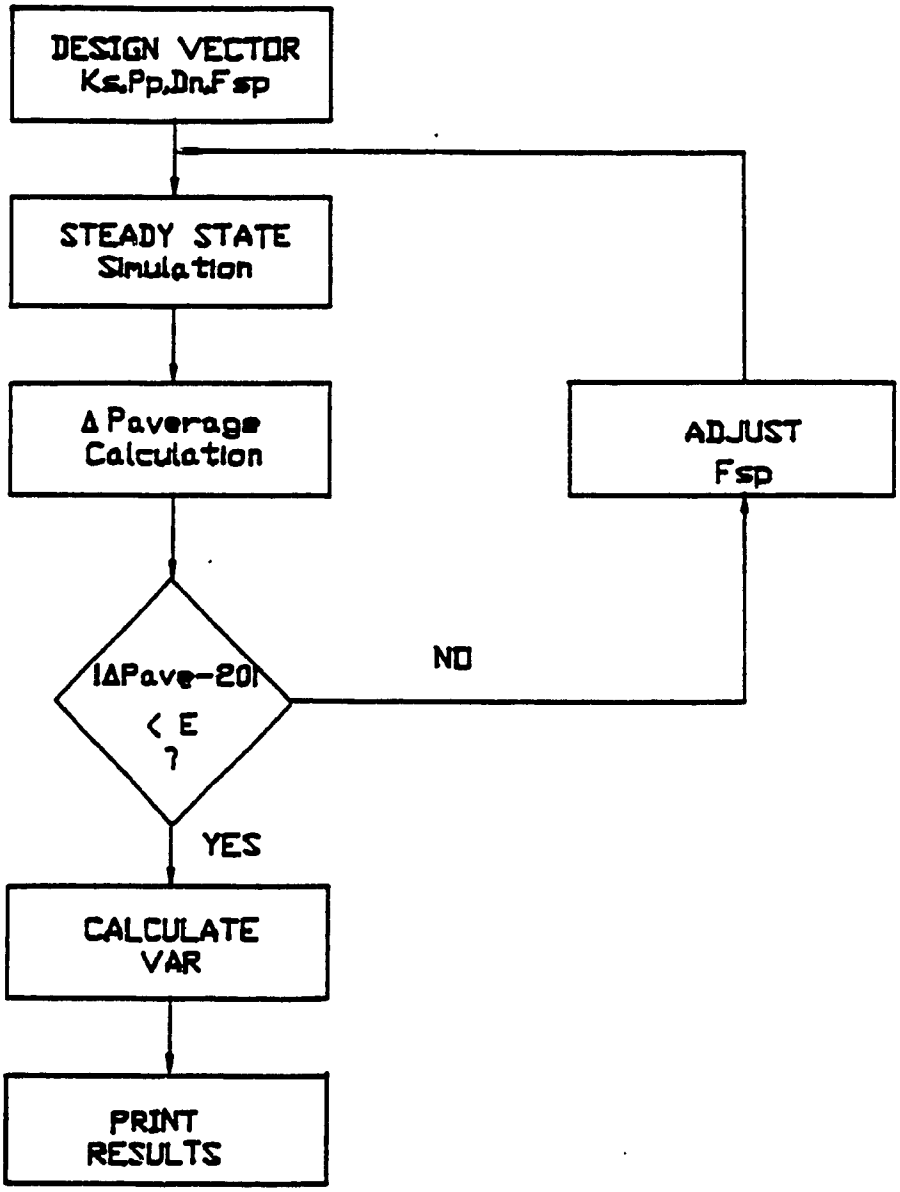

Figure 10.1 Computer Scheme to Compare Only Designs with the Required Differential Pressure

The results of the simulation studies of the effect of design variables on the VAR index are shown in Figures 10.3 to 10.5. Figure 10.3 shows that when optimizing for constant differential pressure, the smallest allowable pump pressure should be chosen to minimize the variations. The spring constant for this simulation run was fixed at 3150 N/m and the average differential pressure used for calculation of the index was 1.38 bar (20 psid). The limit on how low the pump pressure can be adjusted is set by the diaphragm valve orifice saturation condition for a particular engine's requirement. If the pump pressure is too low, the fuel control will not be able to meet the maximum flow requirements. Of course, the minimum pump pressure setting should have an acceptable safety margin to prevent the orifice saturation. The reason for the observed effect of the pump pressure on the VAR index stems from the fact that with the same differential pressure, a lower pump pressure leads to a lower upper diaphragm chamber pressure $p_d = p_p - \Delta p$. At maximum flow, therefore, there will be a smaller difference of pressure across the diaphragm orifice, $p_d - p_n$. The diaphragm orifice gap must therefore be larger in order to provide the same flow. The change in position of the diaphragm between its minimum and maximum flow openings will be also larger. The variation in differential pressure due to the $k_e h$ term of equation 10.2 becomes therefore larger and better able to compensate for the larger impact of the nozzle pressure variation on the differential pressure.

Figure 10.4 shows the effect of the spring constant on the VAR index. It shows that there is an optimum spring constant value of about 24 kN/m. With such a spring, the variations in differential pressure could almost be eliminated. In this simulation case, the differential pressure was kept at 1.38 bar (20 psid) and the pump pressure was fixed at 12.41 bar (180 psig). The reason for the effect of the spring constant can be explained as follows. For a low constant, the force variation due to the $k_s h$ term in equation 10.2 is smaller than the $p_n A_n$ term. Since these two effects act in opposite directions with respect to flow, increasing the spring constant allows better compensation of the $p_n A_n$ term, reducing the VAR index. With a very high spring constant, overcompensation takes place, the $k_s h$ variation term having a bigger effect on the VAR index than the $p_n A_n$ term.

Figure 10.5 shows the effect of the diaphragm orifice diameter on the VAR index. It shows that the variation in differential pressure increases as the diaphragm valve orifice diameter increases. This can be understood as follows. For a given flow range, the nozzle back pressure covers a range of values, depending on the size of the nozzle orifice. This variation in nozzle pressure causes a variation in the force balance on the diaphragm by virtue of the force term $P_n A_n$. If the nozzle flow area A_n is increased, then the force balance variation due to the nozzle pressure variation is also increased.

Figure 10.6 shows the effect of the spring preload on the differential pressure variation. For higher preloads, the change in differential pressure is less significant, as compared to the large nominal differential pressure. This effect produces a hyperbolic curve. For accuracy of fuel metering, the relative linearity is important, not the absolute variation of differential pressure. Therefore, higher differential pressure improves linearity of the flow schedule.

Finally, Figures 10.7 and 10.8 show the effect of potential nozzle contamination. It is well known that carbon deposits are the major cause of injector contamination in gas turbine engines. This is because the nozzle is located in the hostile environment of the combustor. Contamination reduces the effective flow area of the nozzle. A well designed fuel injection system should be to some extent insensitive to flow area changes of the nozzle. The small, 1.2 percent, increase observed in the differential pressure due to a decrease in nozzle flow area (from 0.69 to 0.58 mm^2) can be considered satisfactory. The reason for the effect of nozzle contamination on the differential pressure stems from the effect of contamination on nozzle pressure P_n. For a contaminated nozzle, P_n must rise to a higher value to produce the required fuel flow. Since the change in nozzle pressure P_n is one of the causes of the differential pressure variation, higher changes of P_n due to nozzle contamination lead to a wider variation of

differential pressure.

The orifice saturation flow value has been shown to depend mostly on pump pressure and nozzle orifice size. Figure 10.8 shows how nozzle contamination lowers saturation flow. Hence, the need for some sufficient safety margin against orifice saturation implies a higher pump pressure, despite the detrimental effect it has on the differential pressure variation it causes.

Finally, Figure 10.8 shows how the average differential pressure setting across the metering valve schedule is affected by the spring preload. It is clear that the differential pressure is almost linearly related to the spring preload.

If the transient response of the diaphragm valve is more than adequate, these steady state optimization considerations, along with sensitivity considerations covered in the next section, should govern the EFCU design. However, if they are in conflict, a compromise might have to be reached between these goals by implementing an optimization scheme which takes into account all important considerations. The trade off decisions can only be made once the specific requirements of an engine fuel supply are known.

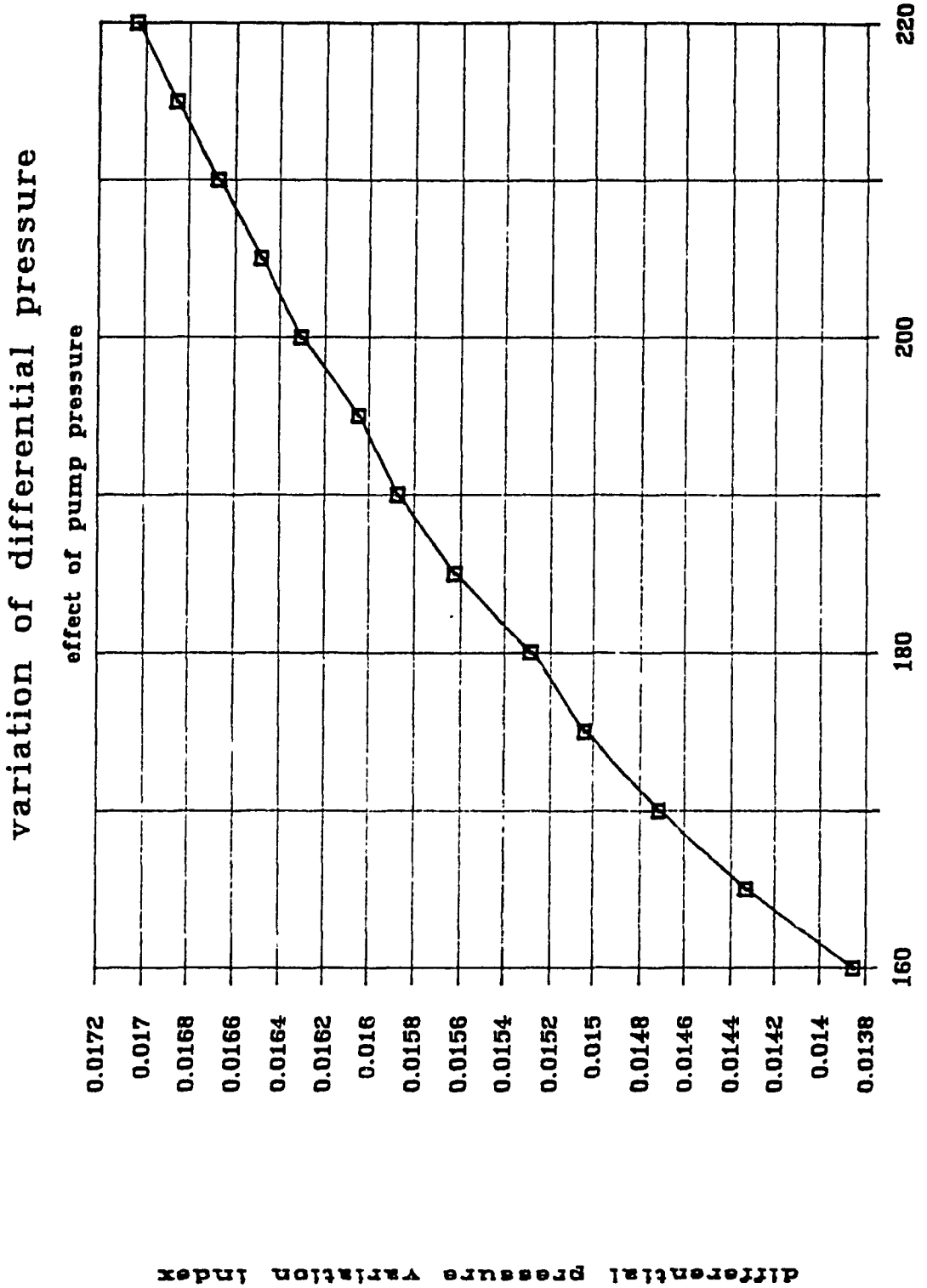

Figure 10.2 Effect of Pump Pressure on VAR Index

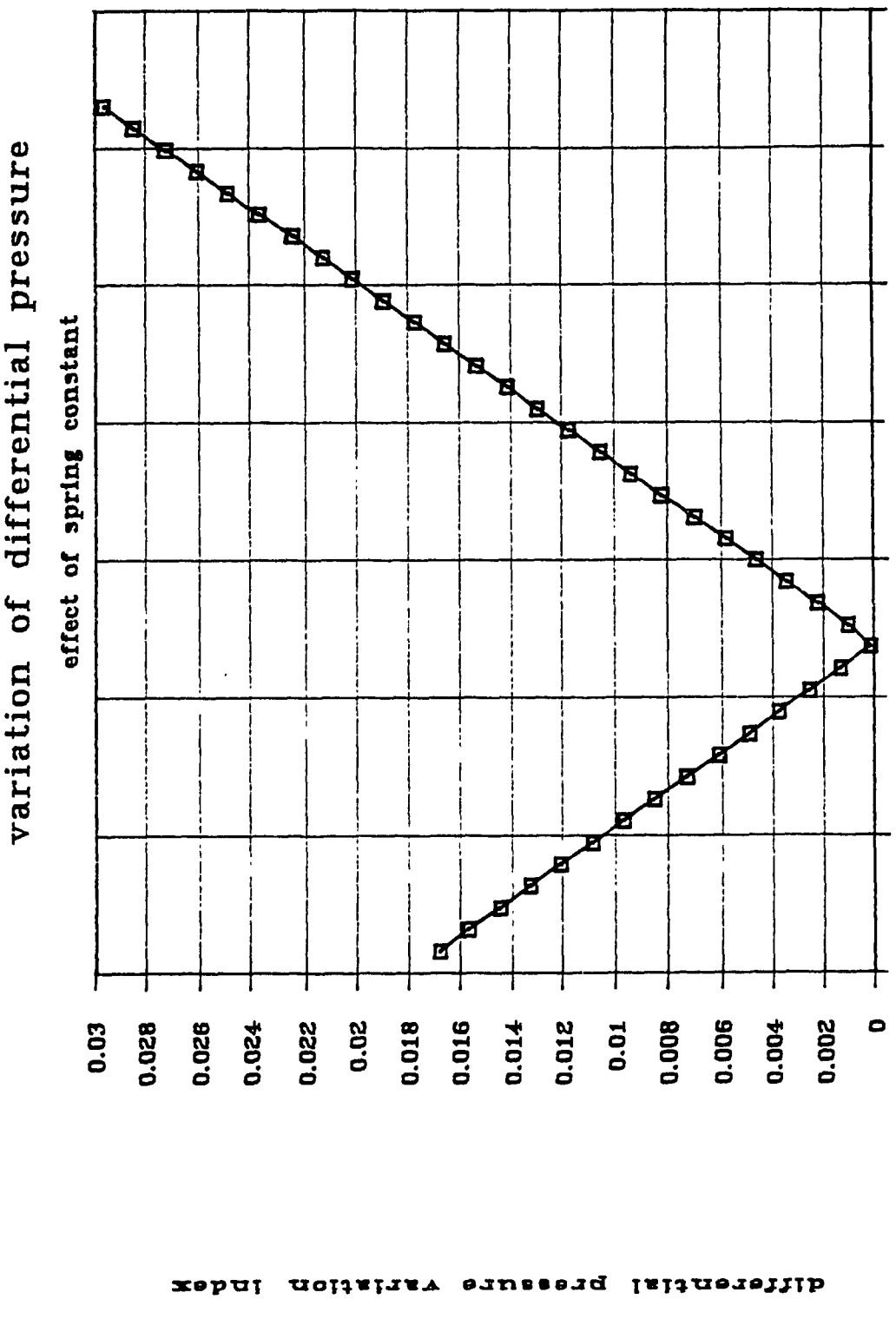

Figure 10.3 Effect of Spr ng Constant on the VAR Index

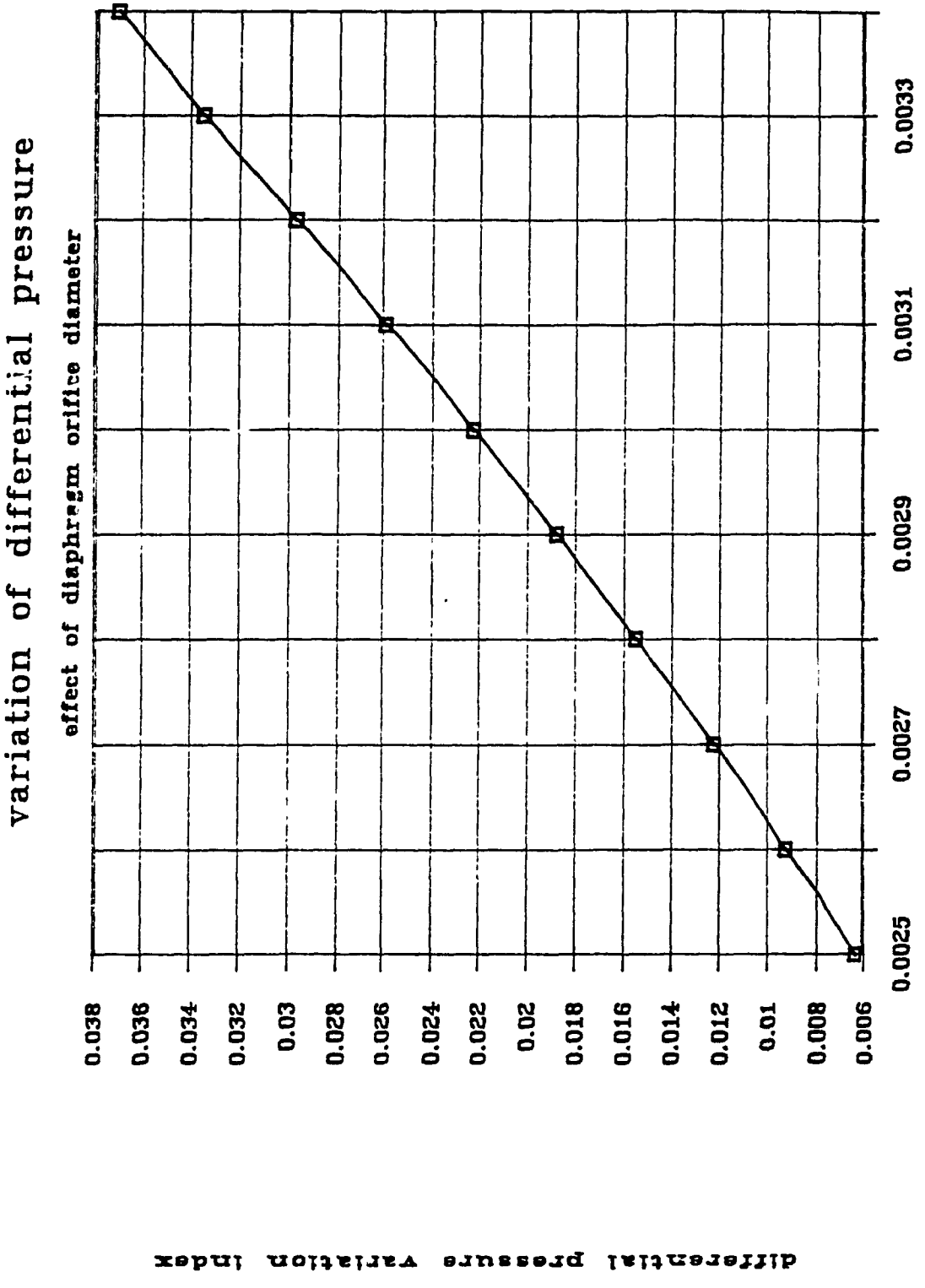

Figure 10.4 Effect of Diaphragm Orifice Diameter on VAR Index

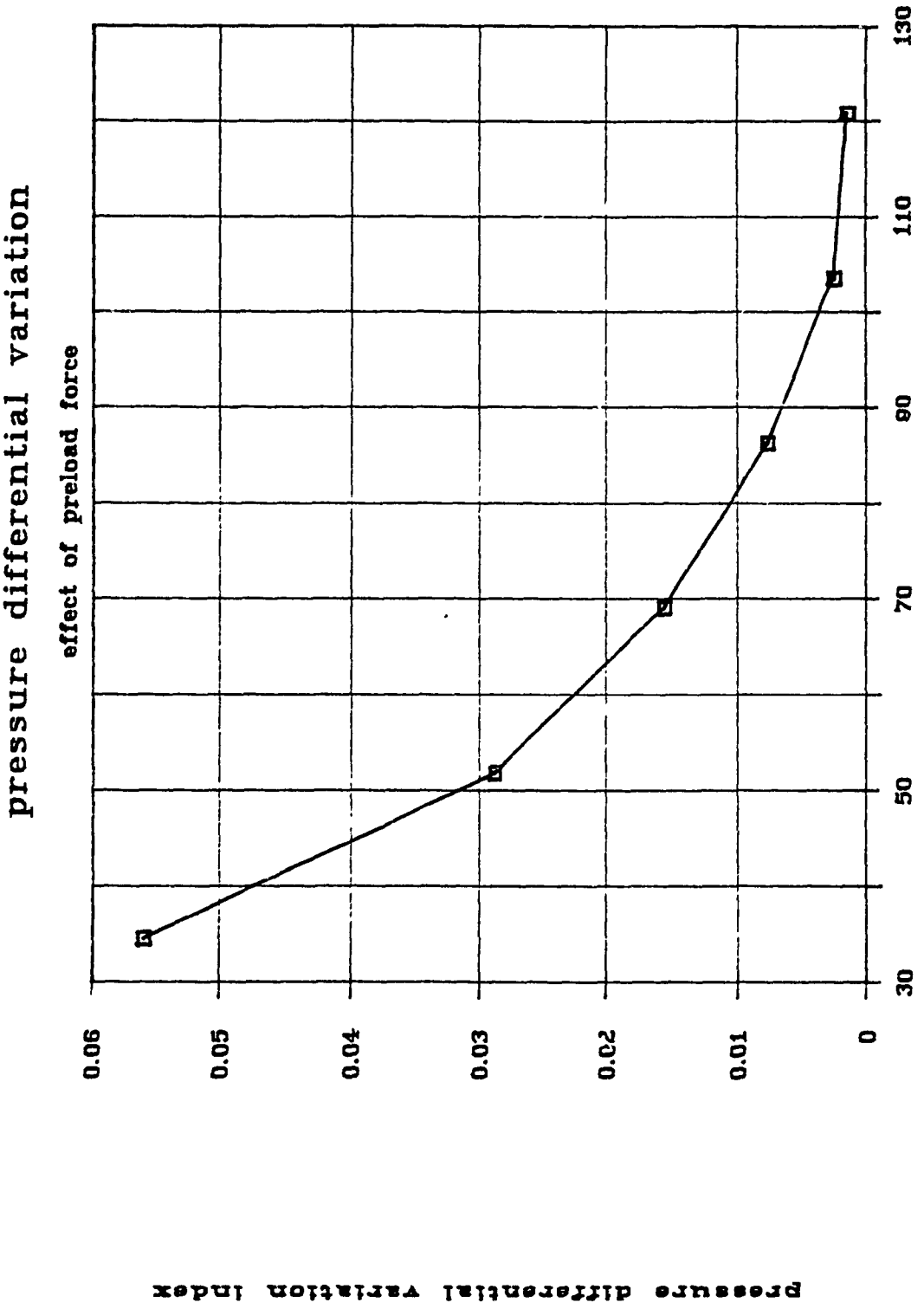

Figure 10.5 Effect of Preload Force on VAR Index

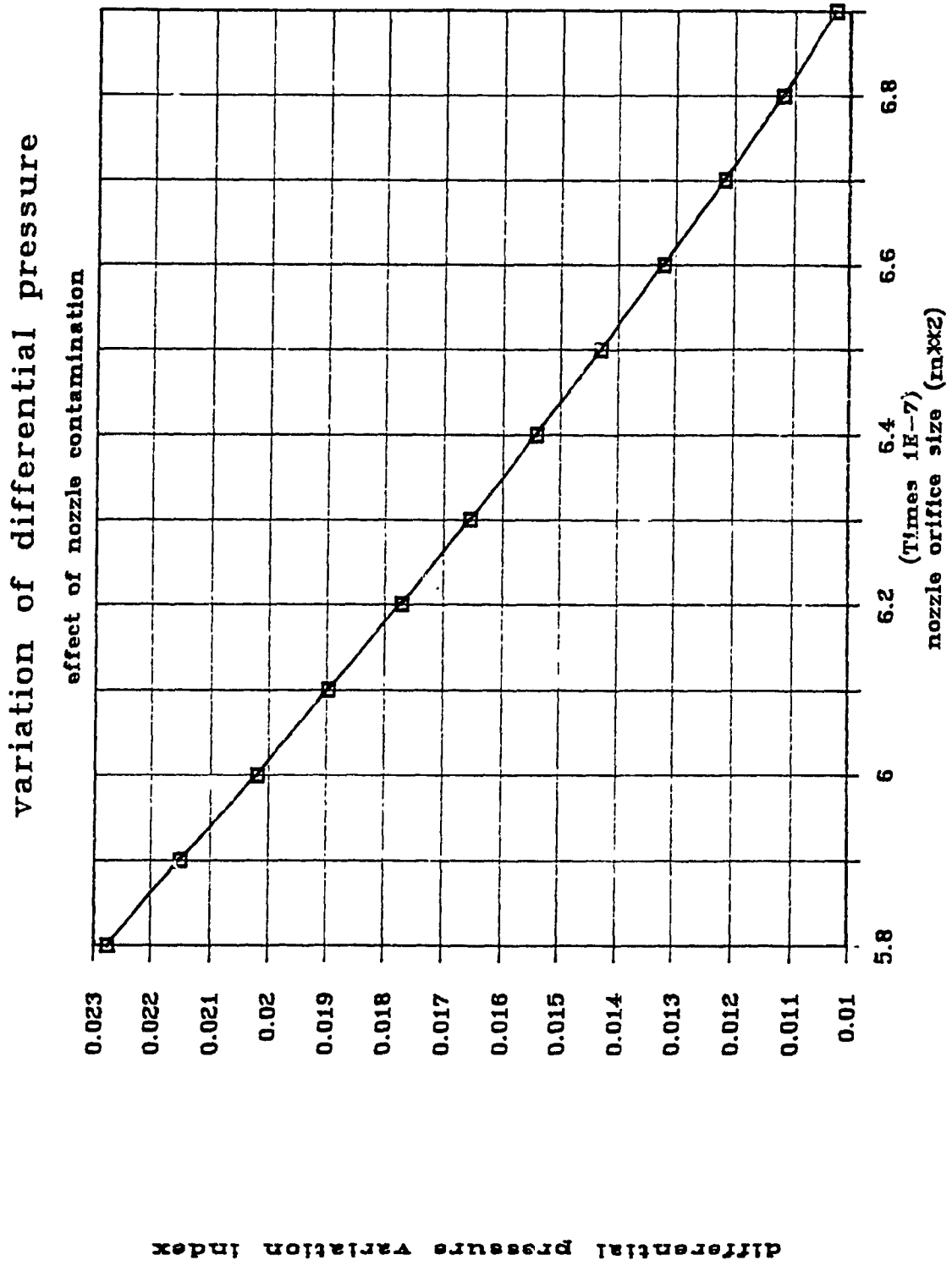

Figure 10.6 Effect of Nozzle Contamination on VAR index

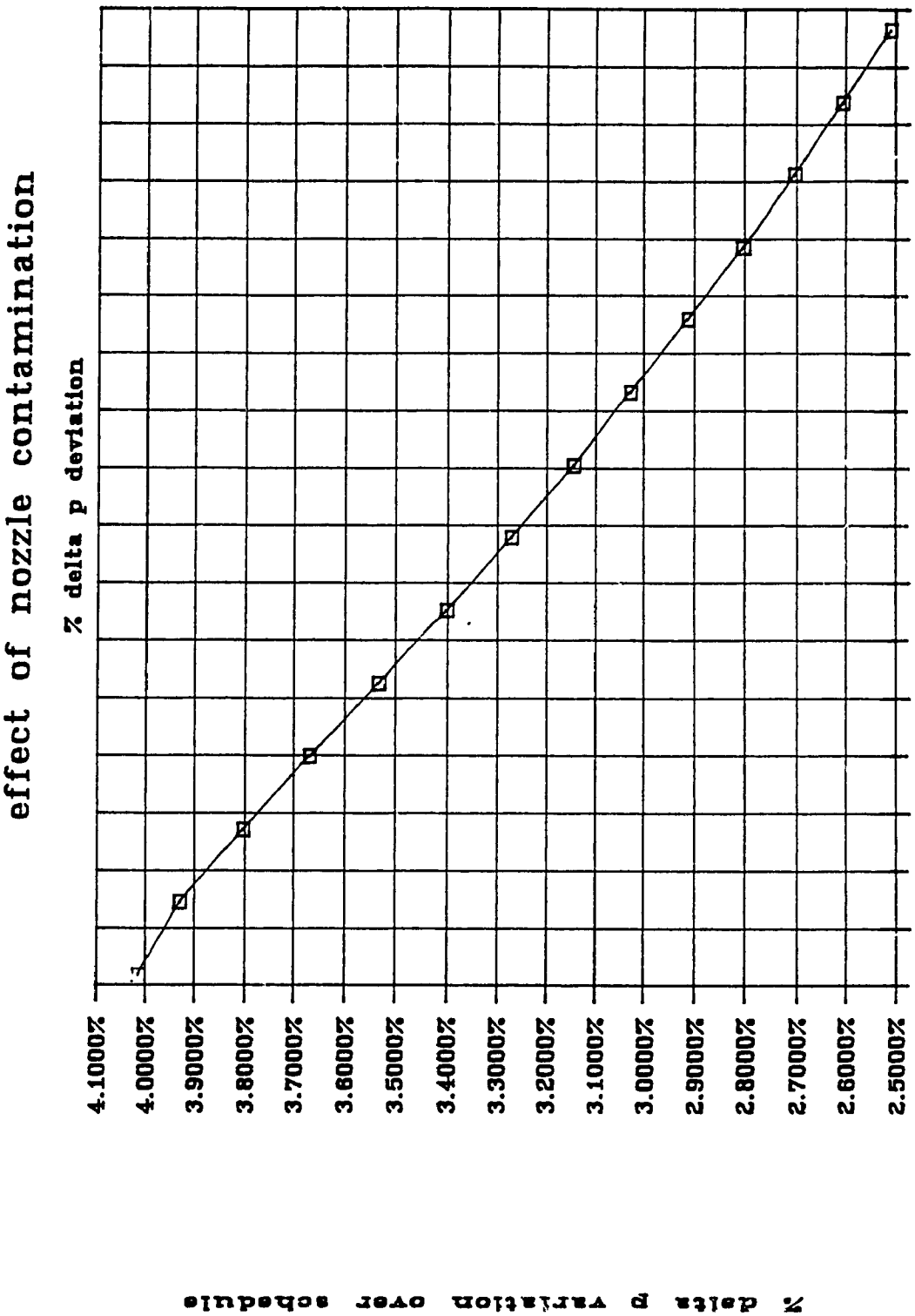

Figure 10.7 Effect of Nozzle Contamination on Saturation Flow

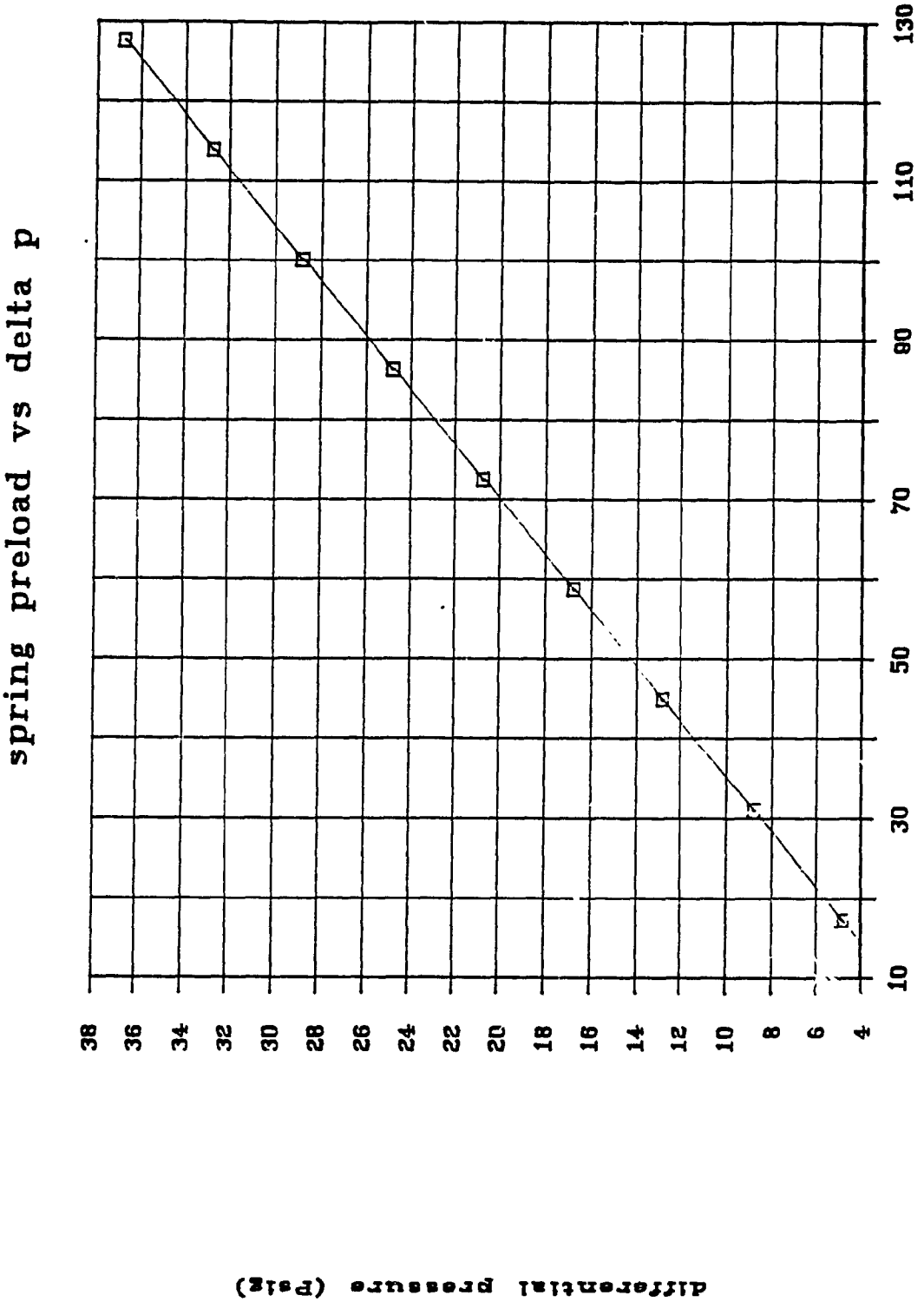

Figure 10.9 Effect of Spring Preload on Differential Pressure

Chapter 11

Sensitivity Analysis; The Second Optimization Criterion

Sensitivity considerations should be included in the design of a system. In control theory, system sensitivity is a motivation for using feedback. A closed loop system is superior to an open loop one because it is less sensitive to the design parameters variations or external disturbances.

The need for sensitivity analysis stems from the realization that system parameters can change during the operational life of a system due to environmental effects such as temperature changes, wear and contamination. For example, the fuel control may experience a temperature range of -40°C to over 30°C. This might cause a thermal expansion of the helical preload spring, altering the preload force. An incorrect differential pressure setting results, leading directly to erroneous fuel metering. Sensitivity analysis determines the impact of such inevitable changes on the system performance. A system inherently less sensitive to the design parameters variations is desired.

Another motivation for sensitivity analysis is to provide a measure of how severe model approximations are. In the steady state fuel control model, for example, the pump pressure was assumed constant since the pressure regulating valve kept the pressure constant, within 5 psi during the tests. The question arises: is this change negligible? The sensitivity analysis performed in this

chapter shows that it is, justifying the approximation.

In Operations Research, sensitivity analysis is often done as a post-optimiality analysis. That is, after an optimization has been performed, the model is investigated about the optimum design variables. Small changes from the optimal settings of each parameter are made and the new performance of the system is observed. If a large change in performance occurs due to the small change in a particular design parameter, then the system is said to be very sensitive to that parameter. On the other hand, if significant changes of a design parameter leads to a very small change in performance, the system is said to insensitive to that design parameter.

However, a different approach is taken in this research. System insensitivity should be considered as a design optimization criterion. That is, sensitivity considerations should be a factor in determining the optimal design point in the first place. For example, a particular design can be evaluated as being superior than another because of its faster transient response. However, if the slower unit reveals itself to be less sensitive to design parameter variations, it might be more desirable than the faster one. An optimization scheme should reflect this consideration. Therefore, the system sensitivity will become a criterion incorporated in the multi objective optimization scheme proposed chapter 13.

Sensitivity analysis has been already addressed informally in the chapter 10, where it was noted that a virtue of the proposed design is its insensitivity to nozzle contamination and pump pressure changes. In this chapter, these and other sensitivity considerations will be examined more quantitatively. We want to know "by how much" the system is insensitive to injector contamination, for example.

What should be made insensitive? By far, it is most important to make the metering valve flow schedule insensitive to the design parameters changes. That is, a selected metering valve position should give the same flow despite the carbon deposit contamination of the nozzle orifice, for example. We could also consider the sensitivity of the transient response to the design parameters variations. For example, the transient response, measured by the ITAE index, (see next chapter) can be slowed down by the variations in pump pressure. However, for the fuel control problem of this thesis, a slower transient response is usually not as critical as an altered final steady state. Therefore, only sensitivity of the steady state response (nozzle flow versus metering valve position) is considered in this chapter.

11.1 Sensitivity of the Metering Valve Flow Schedule

The design parameters of interest, that is those which are subject to change, are: the nozzle flow area (A_i), the spring constant (K_s), the spring preload force (F_{sp}), the pump pressure (P_p), and the metering valve area (A_m). Table 11.1 lists factors that could cause them to vary. It is desired to know how the nozzle flow, q, changes with respect to these parameters. Five derivatives, dq/dA_1, dq/dK_s, dq/dF_{sp}, dq/dP_p and dq/dA_m are being sought. These derivatives (measures of system sensitivity), depend on the steady state nominal operating point considered. These derivatives should be considered carefully. In general, the flow is a function of the "state variables", (p_n, h, and p_d) and the parameters that can changes over the operational life of the fuel control (A_i, k_s, f_{sp}, p_p, and A_m). In the above derivatives, the state variables are dependent variables and the parameters are independent variables. The above derivatives are taken with respect to one parameter with all others kept constant.

Possessing a validated computer program for the steady state system response, the derivatives can be determined by simulation. For example, a simulation run with the nominal operating point initial settings can be performed to obtain the corresponding steady state nozzle flow. Then, the parameter value can be perturbed slightly from its original setting and the simulation run repeated. The derivative of

the fuel flow with respect to that parameter can then be computed from the two runs using a finite difference approximation. As an example, a nozzle contamination case resulting in a 5% change of the nominal nozzle flow area can be considered to calculate the partial derivative of the nozzle flow with respect to the nozzle flow area.

$$(dq/dA_i)_0 = (q_L - q_0) \; / \; .05 * A_{i0} \qquad (11.1)$$

where q_0 is the flow at nominal parameter settings
q_L is the flow corresponding to the perturbed parameter settings
A_{i0} is the nominal nozzle flow area

Table 11.1 Possible Causes for Parameter Variation

Parameter	Possible Cause of Variation
P_p	- Thermal expansion of pressure regulator housing causing the change in Spring preload in primary circuit
A_m	- Contamination of metering valve - Unreliable stepper motor control/lost steps
A_i	- Carbon deposits contaminating the injector flow area
k_{sp}	- Stiffening of spring - Tolerances due to manufacturing
F_{sp}	- Temperature caused expansion of diaphragm valve housing causing the decrease in spring preload and change in differential pressure

However, this approach requires substantial computing time, since multiple simulation runs would have to be performed for different operating points and parameter changes. Fortunately, the problem can be solved analytically with some mathematical manipulations. Consider the steady state model equations,

1. Flow through metering valve = flow through diaphragm orifice

$$C_{dm}A_m\sqrt{(2/\rho)(P_p-P_d)} - C_{do}A_o\sqrt{(2/\rho)(P_d-P_n)} = 0 \qquad (11.2)$$

2. Flow through diaphragm orifice = flow through nozzle

$$C_{do}\,A_o\,\sqrt{(2/\rho)(P_d-P_n)} - C_{di}\,A_i\,\sqrt{(2/\rho)(P_n-P_c)} = 0 \qquad (11.3)$$

3. Diaphragm force balance

$$P_d\,(A_d-A_n) + K_s\,h + P_n\,A_n + F_{sp} + \rho\,V^2A_n - P_p\,A_d = 0 \qquad (11.4)$$

The "state" of the system is specified by the three state variables P_n, P_d, and h. In general, these variables are functions of each other. Implicitly differentiating the three model equations with respect to the five parameters of

concern will produce 15 equations with 15 unknown derivatives. To simplify the situation, two of the state variables can be eliminated from the formulation before differentiating. Once the sensitivities of the one remaining state variable is found, the sensitivities for the other variables can easily be obtained using the model equations. Below, the required mathematical manipulations are performed to calculate the sensitivity to nozzle contamination.

Neglecting the flow forces, the force balance equation (11.4) can be used to solve for the diaphragm deflection.

$$h = (P_p A_d - P_d A_{dn} - P_n A_n - F_{sp}) \frac{1}{K_s} \qquad (11.5)$$

where $A_{dn} = A_d - A_n$

Solving equation 2 for the nozzle back pressure (assuming equal flow coefficients),

$$P_n = \left(\frac{A_m}{A_i} \right)^2 (P_p - P_d) \qquad (11.6)$$

These two expressions can be substituted into equation (11.3) to yield an equation containing only one state variable, the upper diaphragm chamber pressure p_d.

$$A\ A_m = \pi\ D_n\ h_{max}\ B - \pi\ D_n\ C\ \ B \qquad (11.7)$$

where $A = \sqrt{P_p - P_d}$

$$B = \sqrt{P_d - \left(\frac{Am}{Ai}\right)^2 (P_p - p_d)}$$

and

$$C = \left[P_p\ A_d - P_d\ A_{dn} - (P_p - P_d)\ \ A_n\ \ \left(\frac{Am}{Ai}\right)^2 - F_{sp} \right]\ \ \frac{1}{ks}$$

The above equation can be implicitly differentiated to obtain the five derivatives of the upper diaphragm chamber pressure with respect to the five parameters of interest. Using calculus methods and taking the derivative with respect to the nozzle area A_i,

$$A_m \left(\frac{dA}{dA_i}\right) = \pi\ D_n \left(\frac{dB}{dA_i}\right) (h_{max} - C) - \pi\ D_n\ B \left(\frac{dC}{dA_i}\right) \qquad (11.8)$$

Where $\frac{dA}{dA_i} = -\frac{1}{2A}\ \ \frac{dP_d}{dA_i}$

$$\frac{dB}{dA_i} = \frac{1}{2B}\left[\frac{dP_d}{dA_i}\left[1 + \left(\frac{Am}{Ai}\right)^2\right] + 2\left(P_p - P_d\right)\frac{A_m^2}{A_i^3}\right]$$

$$\frac{dC}{dA_i} = \frac{1}{K_s}\left[\frac{dPd}{dA_i}\left[A_n\left(\frac{Am}{Ai}\right)^2 - A_{dn}\right] + 2a_n\left(\frac{Am^2}{Ai3}\right)\left(P_p - P_d\right)\right]$$

substituting into (11.8) and solving for $\frac{dP_d}{dA_i}$,

$$\frac{dP_d}{dA_i} = \frac{\pi D_n A^2\left[\frac{A_m^2}{A_i 3}\right]\left[\frac{(h_{max} - C)}{B} - \left(\frac{2B}{K_s}\right)A_n\right]}{-\frac{A_m}{2A} - \pi D_n\left[\frac{(h_{max} - C)}{2B}\left[1 + \left(\frac{A_m}{Ai}\right)^2\right] - \frac{B}{K_s}\left[A_n\left(\frac{A_m}{A_i}\right)^2 - A_{dn}\right]\right]}$$

(11.9)

Finally, the sensitivity of the nozzle flow to nozzle flow area contamination is obtained using the discharge equation and its derivative.

$$q = C_d A_m \sqrt{\frac{2}{\rho} (P_p - P_d)} \qquad (11.10)$$

$$\frac{dq}{dA_i} = \frac{- C_d A_m}{\sqrt{\frac{2}{\rho} (P_p - P_d)}} \frac{1}{\rho} \frac{dP_d}{dA_i} \qquad (11.11)$$

Similar relations for the sensitivity of the flow to the other four parameters of interest can be derived. The results are given below.

$$\frac{dP_d}{dK_s} = \frac{\pi D_n B C/K_s}{\frac{\pi D_n B}{K_s} \left[A_n \left(\frac{A_m}{A_i} \right)^2 - A_{dn} \right] - \frac{A_m}{2A} - \frac{\pi D_n (h_{max} - C)}{2B} \left[\left(\frac{A_m}{A_i} \right)^2 + 1 \right]} \qquad (11.12)$$

$$\frac{dq}{dK_s} = \frac{C_d A_m}{2 \sqrt{\frac{2}{\rho} (P_p - P_d)}} \left(- \frac{2}{\rho_f} \frac{dP_d}{dK_s} \right) \qquad (11.13)$$

$$\frac{dP_d}{dA_m} = \frac{-A - \frac{\pi D_n}{2B}(h_{max} - C)\,2\left(\frac{A_m}{A_i^2}\right)(P_p - P_d) + \frac{\pi D_n B}{K_s}\,\frac{2A_n A_m}{A_i^2}(P_p - P_d)}{\frac{-A_m}{2A} - \frac{\pi D_n (h_{max} - C)}{2B}\left[1+\left(\frac{A_m}{A_i}\right)^2\right] + \frac{\pi D_n B}{K_s}\left[A_n\left(\frac{A_m}{A_i}\right)^2 - A_{dN}\right]} \qquad (11.14)$$

$$\frac{dq}{dA_m} = \frac{C_d A_m}{2\sqrt{\frac{2}{\rho_f}(P_p - P_d)}}\left[-\frac{2}{\rho_f}\frac{dP_d}{dA_m}\right] + C_d\sqrt{\frac{2}{\rho_f}(P_p - P_d)} \qquad (11.15)$$

$$\frac{dP_d}{dF_{sp}} = \frac{\pi D_n B/K_s}{\frac{\pi D_n B}{K_s}\left[A_n\left(\frac{A_m}{A_i}\right)^2 - A_{dN}\right] - \frac{A_m}{2A} - \frac{\pi D_n}{2B}\left[\left(\frac{A_m}{A_i}\right)^2 + 1\right](h_{max} - C)} \qquad (11.16)$$

$$\frac{dq}{dF_{sp}} = \frac{C_d A_m}{2\sqrt{\frac{2}{\rho_f}(P_p - P_d)}}\left[-\frac{2}{\rho_f}\left(\frac{dP_d}{dF_{sp}}\right)\right] \qquad (11.17)$$

$$\frac{dP_d}{dP_p} = \frac{-\frac{A_m}{2A} - \frac{\pi D_n (h_{max} - C)}{2B}\left(\frac{A_m}{Ai}\right)^2 - \frac{\pi D_n B}{Ks}\left[A_d - A_N\left(\frac{A_m}{Ai}\right)^2\right]}{-\frac{A_m}{2A} - \frac{\pi D_n (h_{max} - C)}{2B}\left[1 + \left(\frac{A_m}{Ai}\right)^2\right] + \frac{\pi D_n B}{K_s}\left[A_n\left(\frac{A_m}{Ai}\right)^2 - A_{dN}\right]}$$

(11.18)

$$\frac{dq}{dP_p} = \frac{C_d A_m}{2\sqrt{\frac{2}{\rho_f}(P_p - P_d)}}\left(\frac{2}{\rho_f}\right)\left(1 - \frac{dP_d}{dP_p}\right)$$

(11.19)

In general, these sensitivities are a function of the flow operating point considered. Considering the sensitivity to flow contamination, an entirety sensitivity index can be defined by integrating and averaging the flow sensitivity to injector contamination over the whole flow schedule. However, this approach would require much computing time, which will become an important consideration when multiobjective optimization is performed in chapter 13.

The simplified approach taken here is to use a "typical" operating point in the most important region of operation. It is assumed that the sensitivities at other

operating points follow the same trends. Taking a fuel flow of 35 kg/hr as an arbitrarily chosen operating point and using the nominal design parameters, the sensitivity equations were solved and the results plotted in the sensitivity histogram of Figure 11.1

The sensitivity of the flow rate to the metering valve flow area is the greatest (103%). This is because with essentially constant differential pressure, a change in metering valve flow area leads directly to erroneous metered flow. The result differs from the expected 100% sensitivity because the differential pressure changes slightly as the flow changes.

Changes in the diaphragm valve preload force exerted by the helical spring have the second biggest impact on the flow (57% sensitivity). A change in the spring preload force due to thermal expansion of the valve housing, for example, alters the differential pressure across the diaphragm and, therefore, indirectly alters the metered fuel flow.

As expected, the sensitivity of the fuel flow rate to the nozzle contamination is rather low (-3.8%). The negative sign implies that, as the nozzle becomes contaminated (area A_1 decreases), the nozzle flow actually increases. This has been confirmed experimentally. Also, the pump pressure increases in the primary circuit lead to a decrease in the metered flow (-5.7% sensitivity) and the diaphragm valve spring constant increases lead to

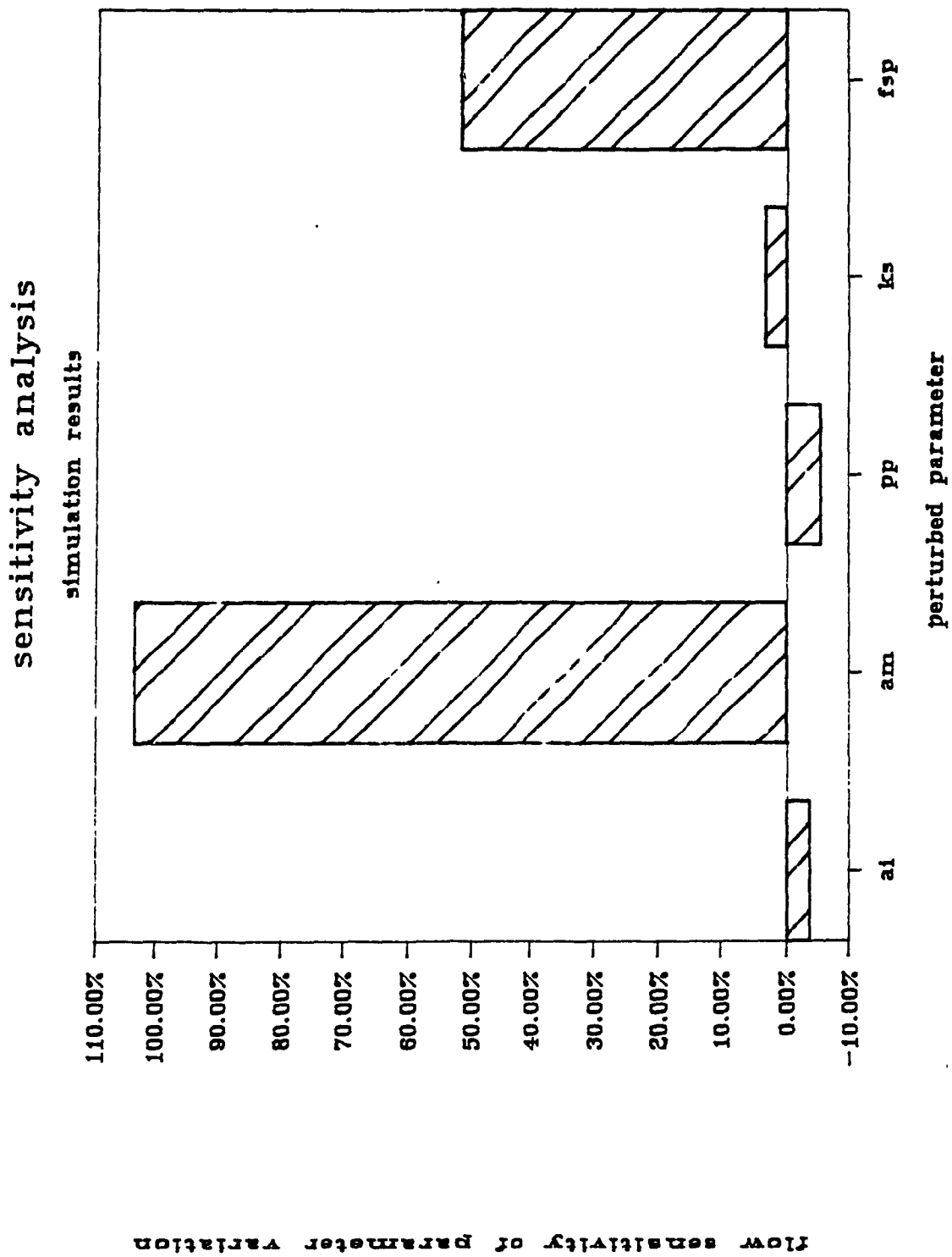

Figure 11.1 Sensitivity Histogram

an increase in flow (3.5% sensitivity).

Note that the sensitivity figures are expressed in terms of percent of the nominal value. For example, the sensitivity of the flow rate to the nozzle flow area changes is defined by,

$$SENSQA_i = (dq/dA_i)(A_i/q)\ 100\ \% \qquad (11.21)$$

A numerical example can be used to clarify the interpretation of the sensitivity index. If the nominal flow is 35 kg/hr and the nominal nozzle area is $0.6333 \cdot 10^{-6}$ m^2, and if contamination reduced the nozzle area to $0.60 \cdot 10^{-6}$ m^2, the sensitivity index can be used to determine the change in flow dq due to the contamination.

$$dq = (-.037)\left(\frac{0.6 - 0.633}{0.633}\right)(35) = 0.07 \text{ kg/hr}$$

The scheme developed to derive the sensitivities requires the knowledge of a fixed steady state operating point. That is, the set of state variables, P_n, P_d, and h required for the operating point nozzle flow at steady state condition must be selected. This set depends on the value of the design parameters chosen. For example, a design with a higher pump pressure will have a different set of state

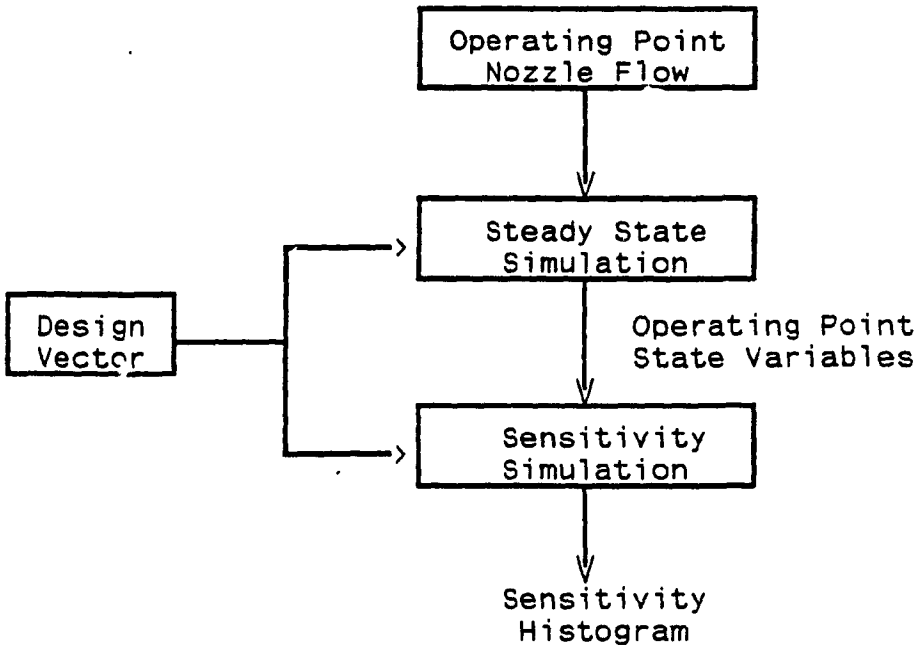

Figure 11.2 Computational Scheme for Sensitivity Calculations

variables for a steady state nozzle flow of 35 kg/hr. Therefore, the solution of the steady state simulation program is first run to find the steady state operating point, as shown in the flow chart in Figure 11.2.

It would be desired to have a single index as a measure of the overall system sensitivity. This index will later be used in a multiobjective optimization scheme. The index is found by taking a weighted sum of the individual system sensitivities to different parameter changes. These weights should reflect the likelihood and severity of each parameter change. For example, it is considered relatively improbable that the helical spring constant will change significantly during the operational life of the fuel control. The corresponding sensitivity is therefore assigned a small weight of 10%. Injector contamination, on the other hand, is a well known and rather inevitable phenomenon. It is therefore assigned a large weight of 50%. Preload changes of the helical spring are also inevitable because of thermal expansion resulting from the ambient temperature changes, for example. However, these changes can be compensated using special bimetallic disks provided in the design (Figure 11.3). Sensitivity to preload changes is therefore given a weight of only 15%. The sensitivity of the system response to the regulated pump pressure changes is given a weight of 25% because there is no protection against the impact of thermal expansion on the spring preload in the

pressure regulator of the primary circuit. Also, sticking of the plunger of the pressure regulator has been observed experimentally as affecting the regulated pressure level. The overall sensitivity index is therefore defined as,

$$SENS = 0.1\left|\frac{dq}{dk_s}\right|\left(\frac{k_s}{q}\right) + 0.5\left|\frac{dq}{dA_1}\right|\left(\frac{A_1}{q}\right) + 0.25\left|\frac{dq}{dp_p}\right|\left(\frac{p_p}{q}\right) + 0.15\left|\frac{dq}{df_{sp}}\right|\left(\frac{f_{sp}}{q}\right) \qquad (11.21)$$

The "design vector", the set of the design parameters under the designer's control, in this case includes the spring constant k_s, the spring preload force F_{sp}, the diaphragm valve orifice diameter d_n, and the pump pressure P_p. The impact of each of these design variables on the combined sensitivity index as well as on the individual sensitivity indices, is plotted in Figures 11.5 to 11.8.. Figure 11.5(a) shows the effect of the diaphragm valve orifice diameter on the overall sensitivity index. Increasing the diameter increases the sensitivity index. Figure 11.5(b) shows the effect of the diaphragm valve orifice diameter on the particular sensitivities making up the composite index. The relation seems to be positive monotonic in every case (recall that negating a function reverses the monotonicity). The reason for such behavior can be understood by examining the force balance on the

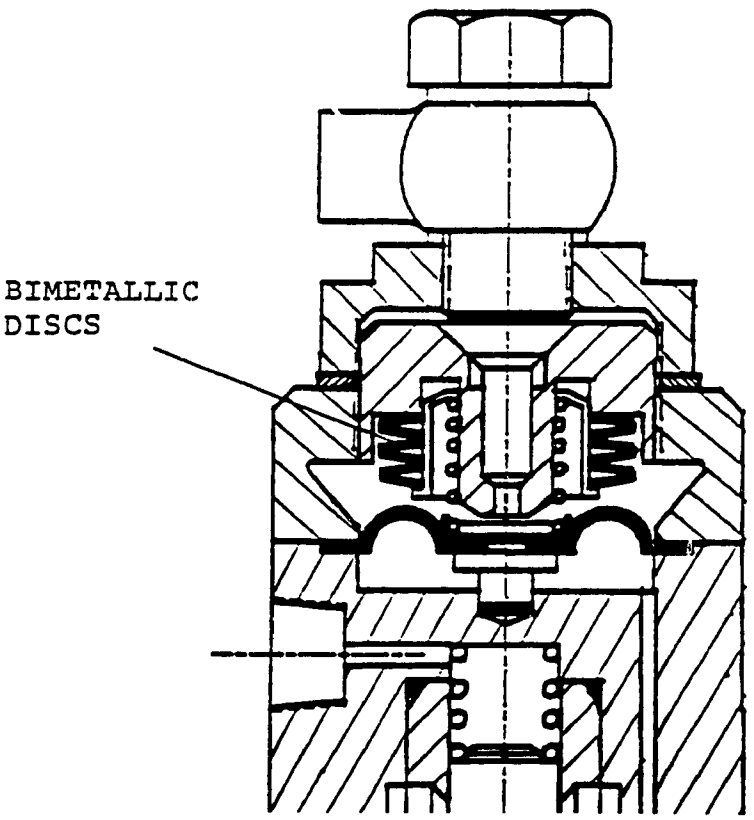

Figure 11.3 Bimetallic Temperatur Compensating Disks

diaphragm. Solving 11.3 for the differential pressure,

$$P_p - P_d = F_{sp}/(A_d - A_n) + K_s h/(A_d - A_n) - (P_p - P_n)A_n/(A_d - A_n) \quad (11.22)$$

Regarding nozzle contamination, the resulting change in nozzle pressure affects the differential pressure (which is directly related to the flow). The third term indicates that differential pressure increases with the nozzle manifold inlet cross sectional area A_n. Decreasing A_n increases the impact of the third term and hence, the sensitivity to the nozzle contamination. However, for a contaminated nozzle, the diaphragm has to move a larger distance over the schedule because there is a smaller pressure drop across the diaphragm orifice. A smaller A_n amplifies the second term and hence its contribution to the sensitivity. This effect outweighs the first effect for the design parameters that the plots were made for.

The increase in sensitivity to the pump pressure changes with diaphragm valve orifice diameter is also due to the fact that the decrease of the diaphragm valve orifice diameter amplifies the second term, which involves the pump pressure indirectly. That is, a higher pump pressure lead to a larger movement of the diaphragm. Similar reasoning can be used to explain the other trends in the plot.

Figure 11.6(a) shows that a low pump pressure gives the best composite sensitivity index. Figure 11.6(b) shows the impact of the pump pressure on the individual sensitivities. gain, the relation is positive monotonic in every case.

Figures 11.7(a) and 11.7(b) show that it is best to use a large preload force from the sensitivity point of view. This result is expected because a parameter change which causes a shift in the force balance on the diaphragm will not have as severe impact on the flow. This is because with the large nominal differential pressure set by the high preload, a change in the force balance causes a small relative change in differential pressure. It is the change in differential pressure relative to its nominal setting that determines the flow sensitivity.

Figures 11.8(a) and 11.8(b) show that a large spring constant should be used from the sensitivity point of view. However, Figure 11.8(b) shows that not all the individual sensitivities making up the composite sensitivity index exhibit the same monotonicity. Namely, the sensitivity of the flow to spring constant changes has opposite monotonicity with respect to the spring constant than all the other sensitivities. However, this component has low weight in the composite index, so it has little impact on the overall trend shown in Figure 11.8 (a)

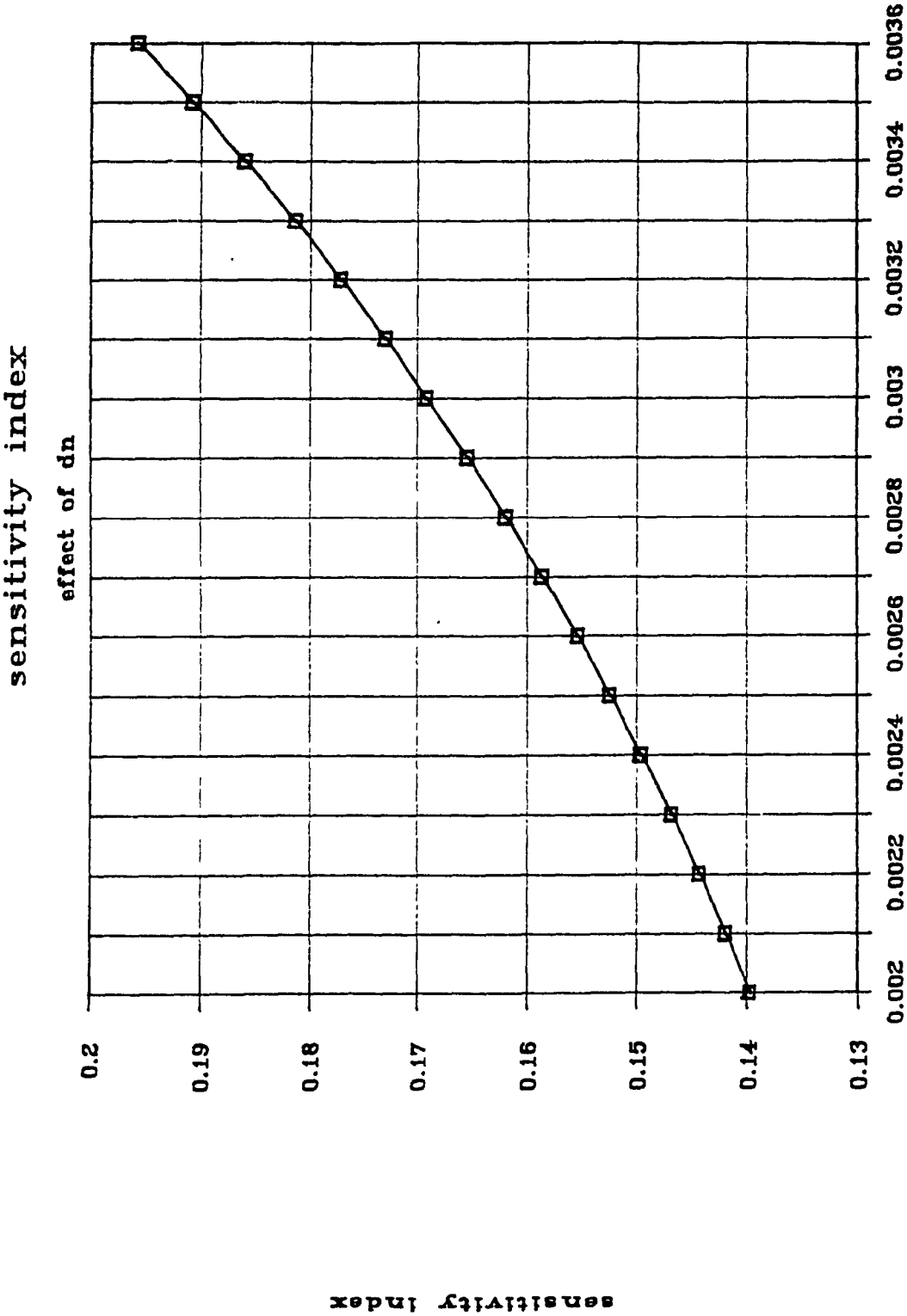

Figure 11.5(a) Effect of Diaphragm Valve Orifice on the Flow Sensitivity

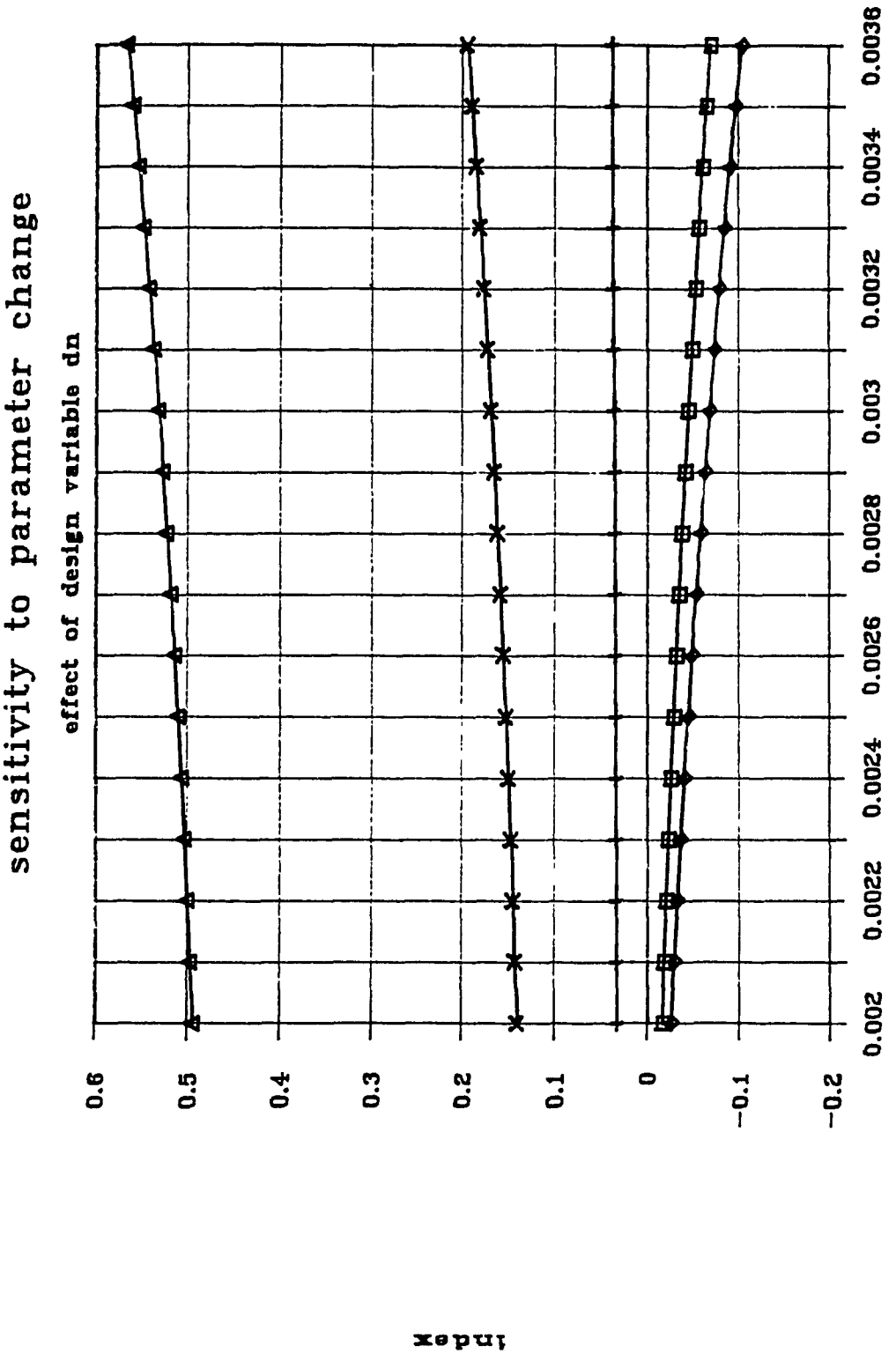

Figure 11.5(b) Effect of Diaphragm Valve Orifice on the Flow Sensitivity

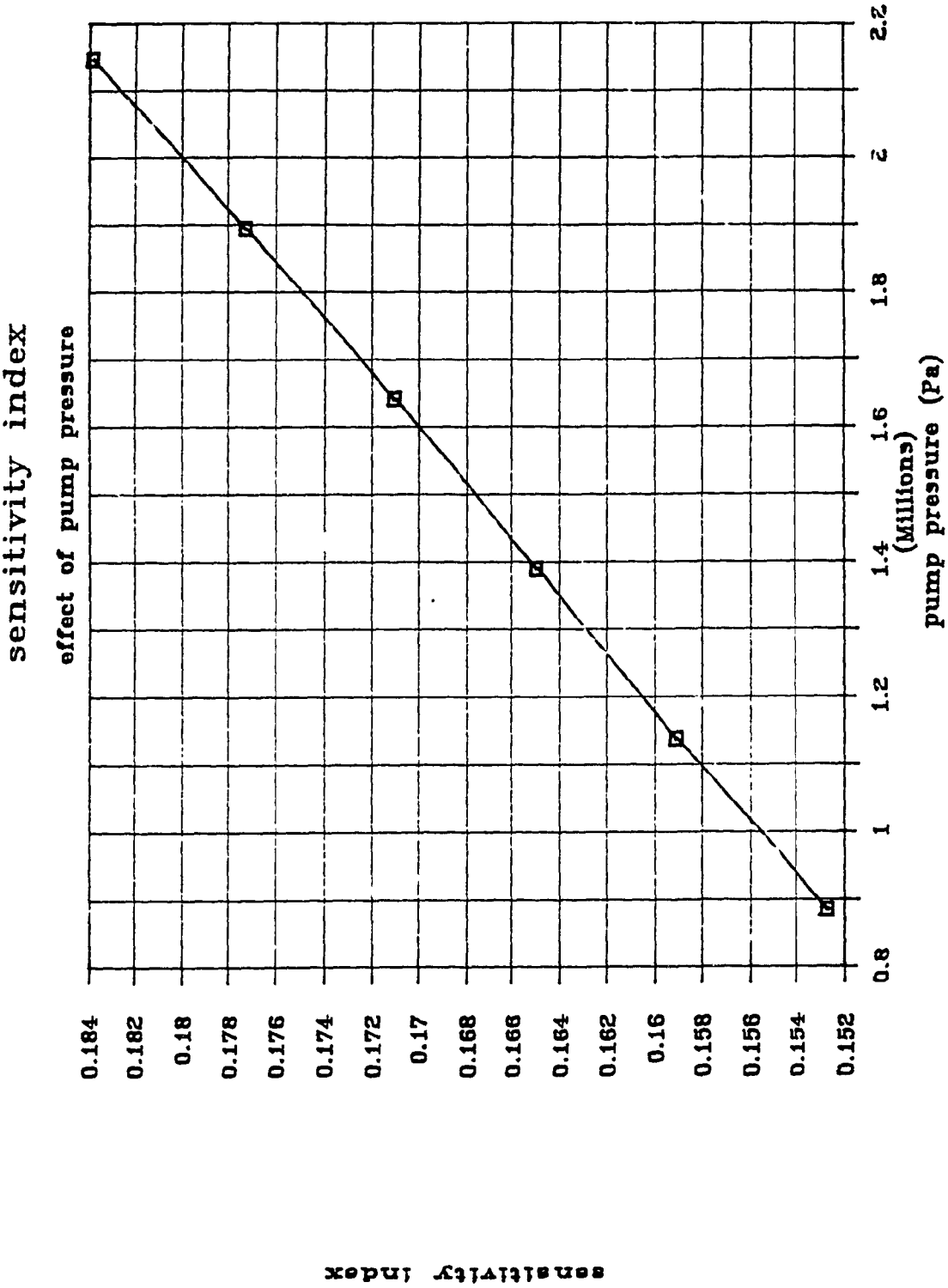

Figure 11.6 (a) Effect of Pump Pressure on Flow Sensitivity

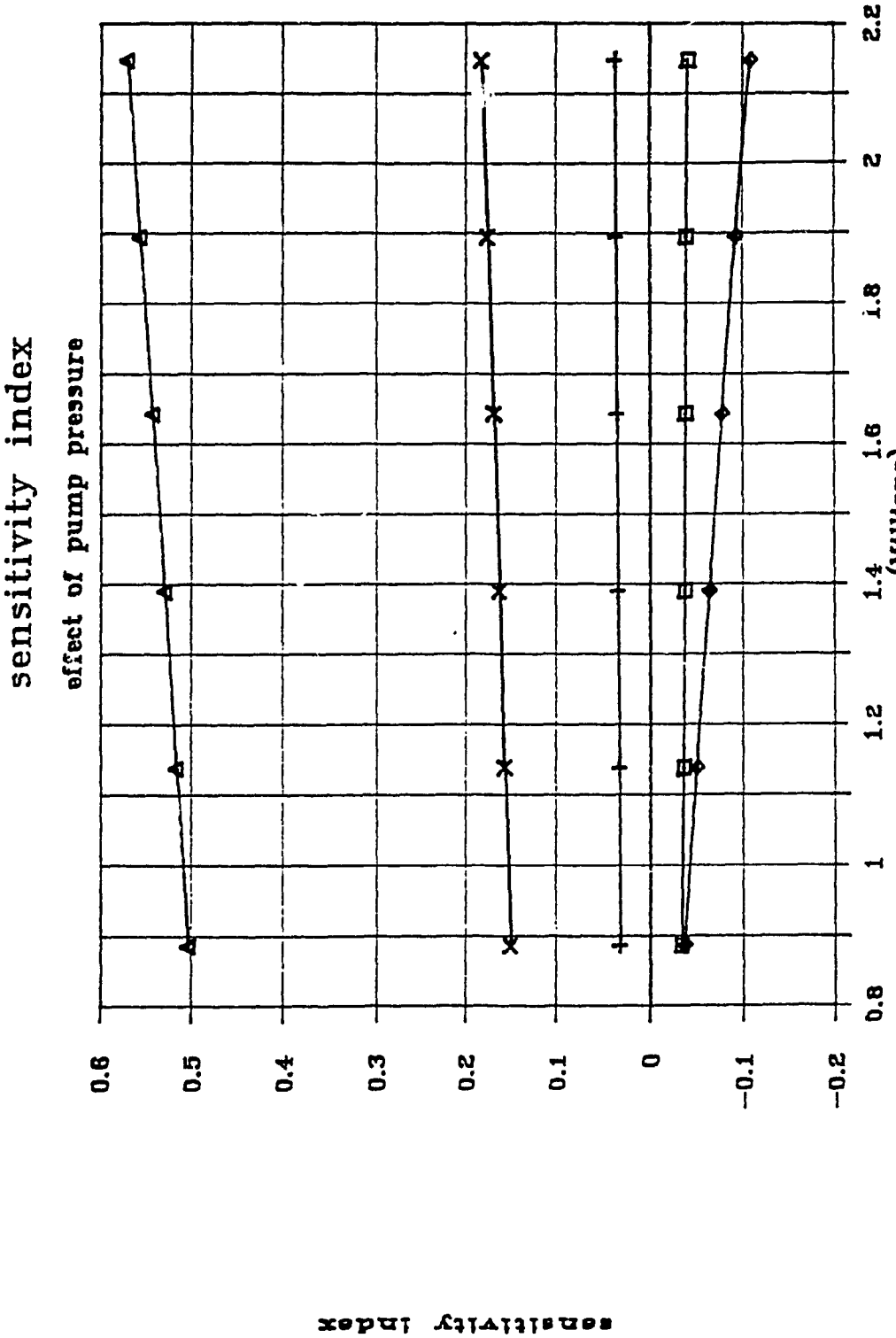

Figure 11.6 (b) Effect of Pump Pressure on Flow Sensitivity

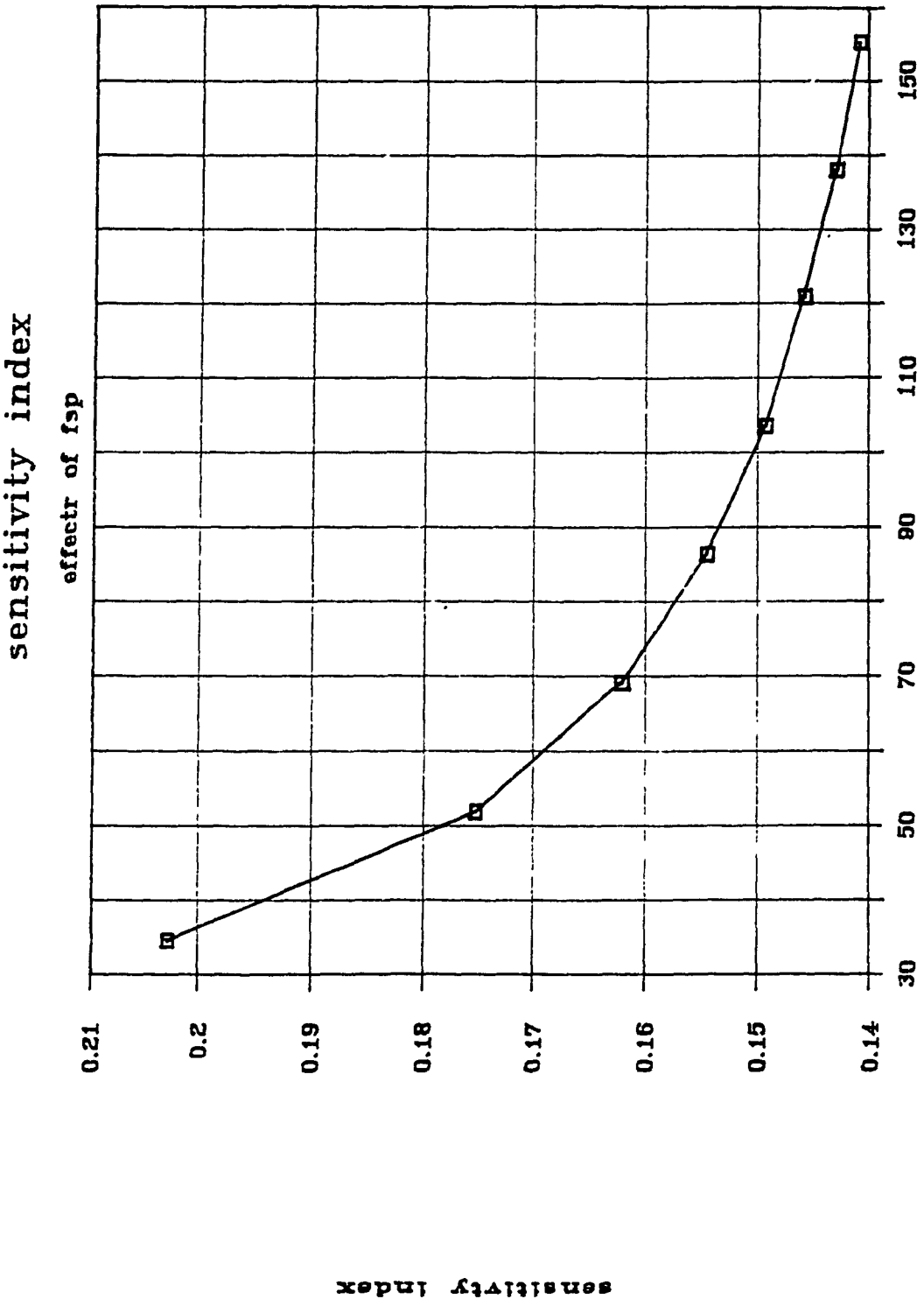

Figure 11.7 (a) Effect of Spring Preload on the Flow Sensitivity

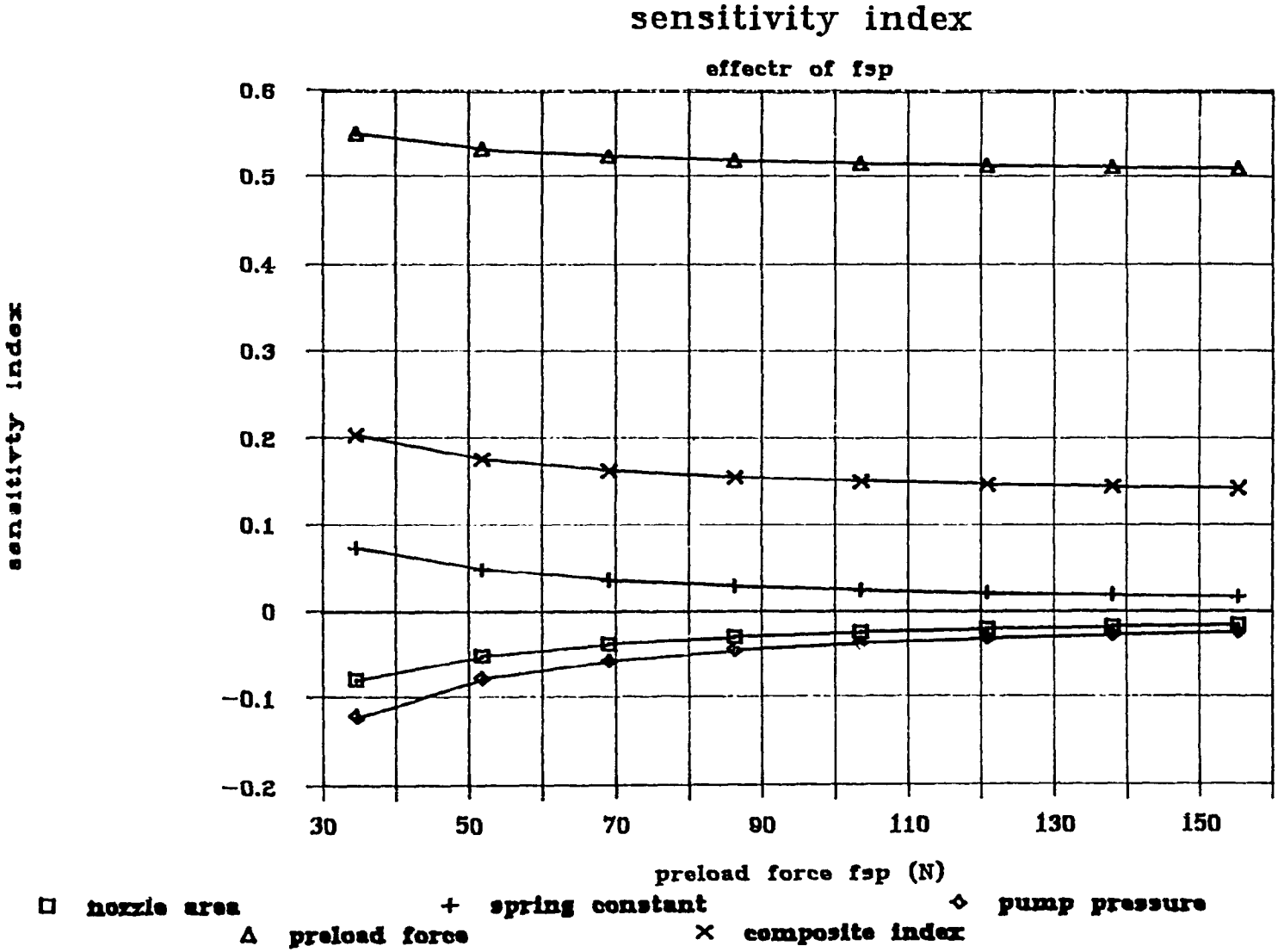

Figure 11.7 (a) Effect of Spring Preload on the Flow Sensitivity

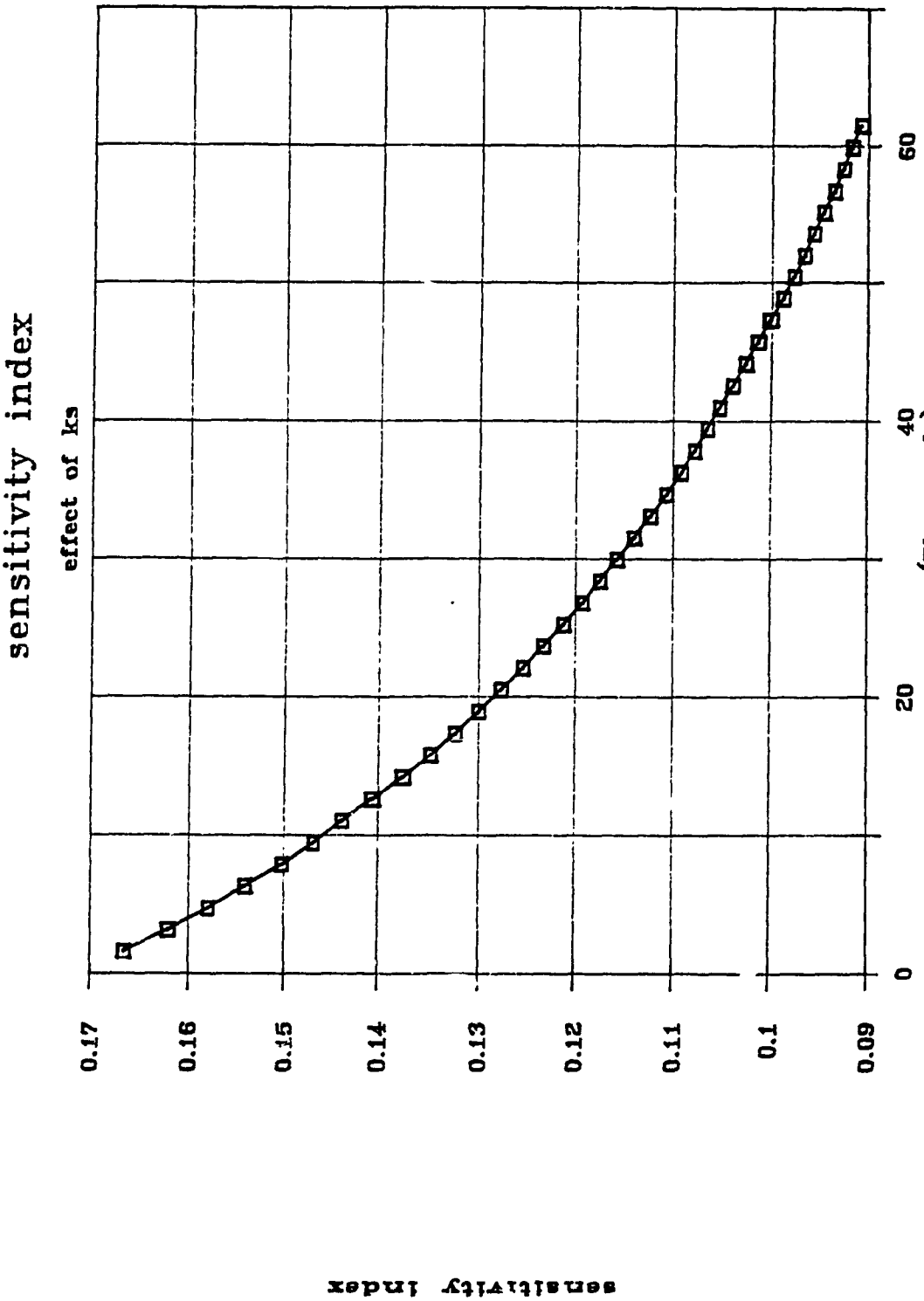

Figure 11.8 (a) Effect of the Spring Constant on The Flow Sensitivity

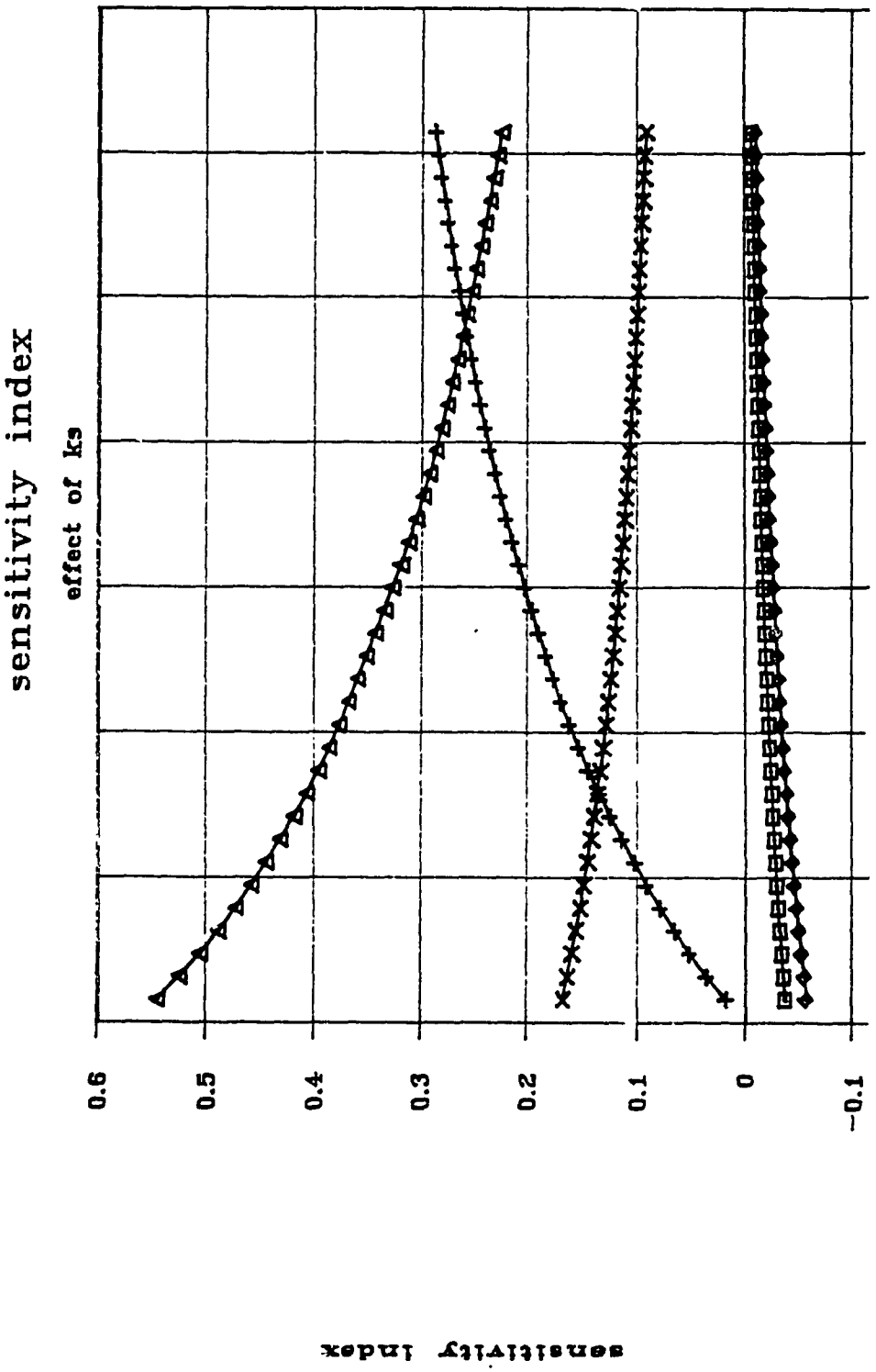

Figure 11.8 (b) Effect of the Spring Constant on The Flow Sensitivity

Chapter 12

An Analysis of the Dynamic System Performance; The Third Optimization Criterion

In this chapter, the transient response of the system will be investigated. First, an index will be defined to suitably quantify the transient performance. Then, the effect of design variables on the transient performance index will be investigated. The dynamic mathematical model of the system, which was described and validated in chapter 9 will be used.

The Transient Response Index

An ITAE (Integral of the Absolute value of the Error multiplied by Time) was created as the performance index. The integral is calculated from the simulation using rectangular integration.

$$ITAE = \sum_{i=1}^{K} \frac{|Pn_f - Pn_i|}{Pn_f} \cdot t \cdot \Delta t_i \qquad (12.1)$$

where Pn_f is the final steady state nozzle manifold pressure

Pn_i is the nozzle manifold pressure at the i-th step of the simulation

t is the running simulation time

Δt_i is the current time step

K is the number of simulation steps

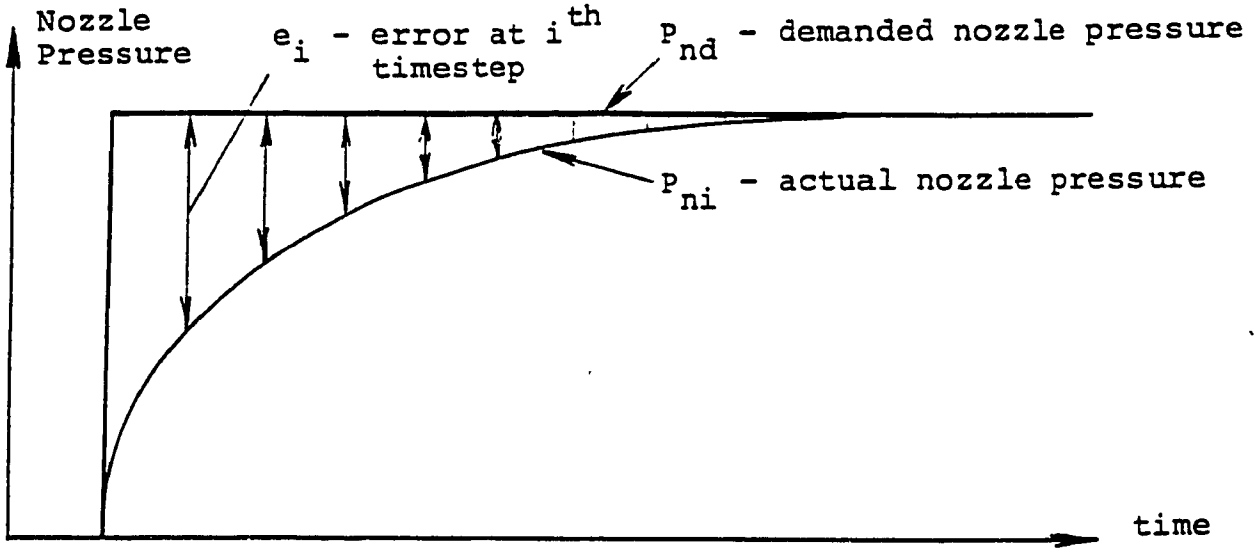

Figure 12.1 Calculation of ITAE Index

Note that the fuel flow could be used in calculating the ITAE index in place of the nozzle pressure. However, since the flow is proportional to the square root of the nozzle pressure, the nozzle pressure based ITAE index provides more selectivity. that is, the difference between indices from two simulation runs will be greater with the nozzle pressure based ITAE index. The final time to end the simulation was chosen as 1.5 seconds. This allowed ample time for settling of the dynamic response.

The ITAE index emphasizes errors which occur later in the response since the error is multiplied by time. Other indices commonly used in control theory such as the IAE (integral of the absolute error) and the ISE (integral of the square of the error) indices could also be used, each possessing certain advantages and disadvantages.

A step input was created as a reference input by selecting a very high stepping rate in the simulation program. Although the "step input" is not achievable in practice (the stepper motor stalls at high stepping frequencies) it provides a suitable criterion to differentiate a "fast" design from a "slow" one.

Consideration should be given to the fact that not all simulation time steps, Δt_i, are equal, since the simulation program uses an adaptive step size technique, i.e. the program itself controls the step size. However, it was found that the steps taken are still small enough to create negligible integration errors in calculation of the index.

In general, it is desired to minimize the ITAE index. The "best system" in this sense, is the fastest one. However, since designing exclusively for speed of response could compromise other design goals, optimization will not be performed on the transient response in this section. In the next section, the ITAE index will be considered simultaneously with the VAR and SENS indices in a multi objective optimization scheme.

Figures 12.2 to 12.6 show the effect of design variables on the transient response. The effect of all variables was investigated in sequence with all other variables fixed at nominal settings. Only the feasible design range was investigated.

Figure 12.2(a) shows the effect of the spring constant on the ITAE index. A higher constant gives a faster response. Figure 12.2(b) shows two typical transients, one with a low spring constant, and the other with a high spring constant - demonstrating the improvement in ITAE index due to the increased spring constant.

This effect can be understood by considering the mechanism by which the diaphragm valve regulates the flow. At steady state, the forces on the diaphragm are balanced and the diaphragm is at a particular location corresponding to the metering valve position. The flow into the upper diaphragm chamber equals the flow out of the chamber and into the nozzle manifold. When the metering valve is suddenly opened (a step input) more flow enters the upper

diaphragm chamber, causing a difference between the flow in and out of the chamber. Fuel starts to accumulate in the chamber, resulting in a pressure rise. Because the metering valve position changed, the diaphragm is no longer in a steady state position. The increased upper chamber pressure changes the force balance on the diaphragm and pushes the diaphragm down to its new equilibrium position. However, because the diaphragm is still in transient, there also exists a change in the spring force, described by $k_s(h - h_*)$, where h_* is the new equilibrium location corresponding to the new metering valve position. This aids the pressure force in pushing the diaphragm to its new equilibrium position. With a stiffer spring, the restoring force of the spring is greater, speeding up the transient response. It should be noted that the spring constant also has an effect in determining the final steady state position of the diaphragm. However, this effect is rather minor.

Figures 12.3(a) and (b) show a result that is at first glance, surprising. The speed of response improves as the diaphragm valve orifice diameter is decreased. This despite the fact that with a smaller orifice diameter, the diaphragm has to move a larger distance to cover the same curtain area. The explanation for this result again lies in considering how the diaphragm valve regulates the flow. When the metering valve is suddenly opened, more flow enters the

upper diaphragm chamber, causing the upper diaphragm chamber pressure to increase. The increased upper diaphragm chamber pressure leads to a force imbalance on the diaphragm. Assuming that the upper chamber pressure momentarily increases by an amount of Δp_d, the imbalanced force, resulting from this is $\Delta p_d(A_d - A_n)$. It is mainly this force that restores the equilibrium by pushing the diaphragm to the new required steady state position. If the diaphragm valve orifice diameter is decreased, the area A_n decreases and the imbalance force due to Δp increases because the term $(A_d - A_n)$ increases. Equilibrium is, therefore reached in shorter time. Of course, if the area A_n decreases, the force due to the nozzle manifold pressure $p_n A_n$ decreases too. But, this is not enough to compensate for the increase of the pressure force $\Delta P_d(A_d - A_n)$. The diaphragm thus experiences a stronger acceleration. The effect explained outweighs the fact that the diaphragm does not have to move as far when the diaphragm valve orifice is small.

Figures 12.4(a) and (b) show that for the range considered, the diaphragm mass has little effect on the transient response. This indicated that the pressure forces dominate. The model can be approximated by a first order system. The effect that ism demonstrated shows that the mass should be made small to speed up transients.

Figures 12.5(a) and (b) show that the pump pressure has little effect on the transient response. The ITAE index changes by less than 0.2 % for a 50 psi change in pump pressure.

Finally, Figures 12.6(a) and (b) show that increasing the spring preload force increases the speed of transient response. The input for this simulation was the more realistic ramp input so that the following effect could be demonstrated. With a larger differential pressure across the metering valve, a smaller change in metering valve flow area is required to achieve the same change in fuel flow. Thus, in exposing the metering valve slits, the stepper motor has to push the plunger a shorter distance. This speeds up the response time. This effect seems to be the dominant one, especially at lower stepping rates where the difference in the arrival time of the metering valve plunger to its final steady state position between different preload settings is larger.

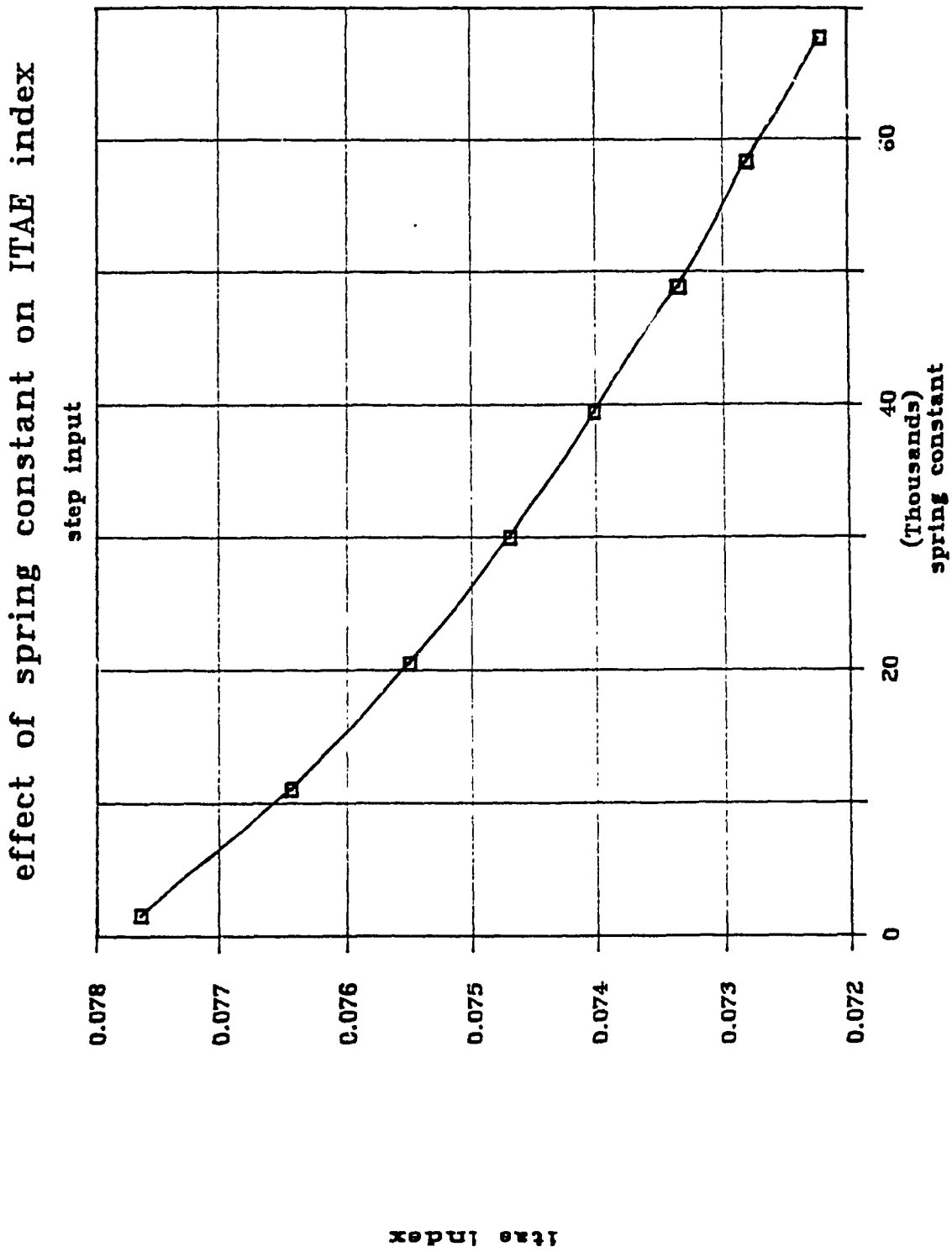

Figure 12.2 (a) Effect of Spring Constant On Transient Response

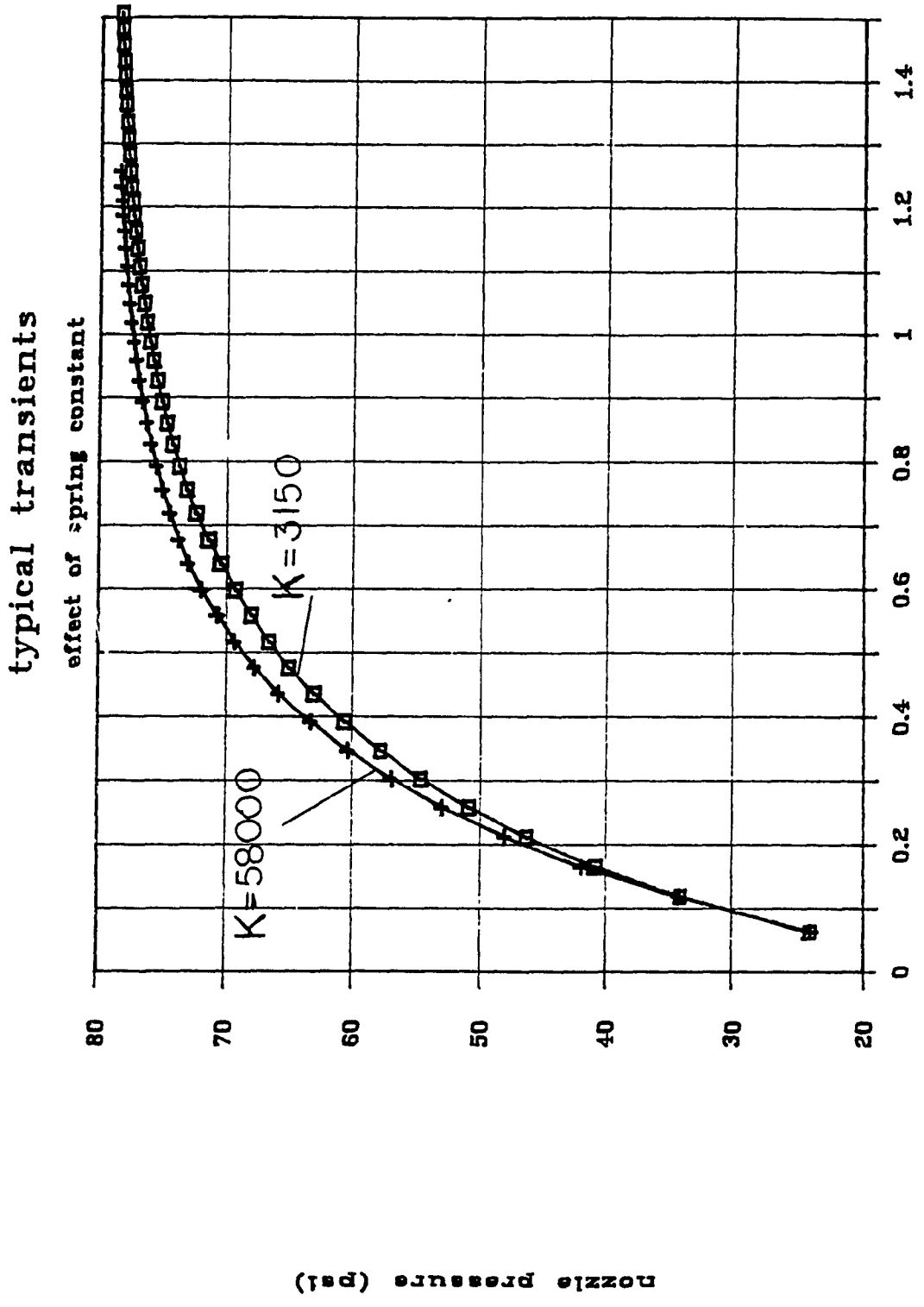

Figure 12.2 (b) Effect of Spring Constant On Transient Response

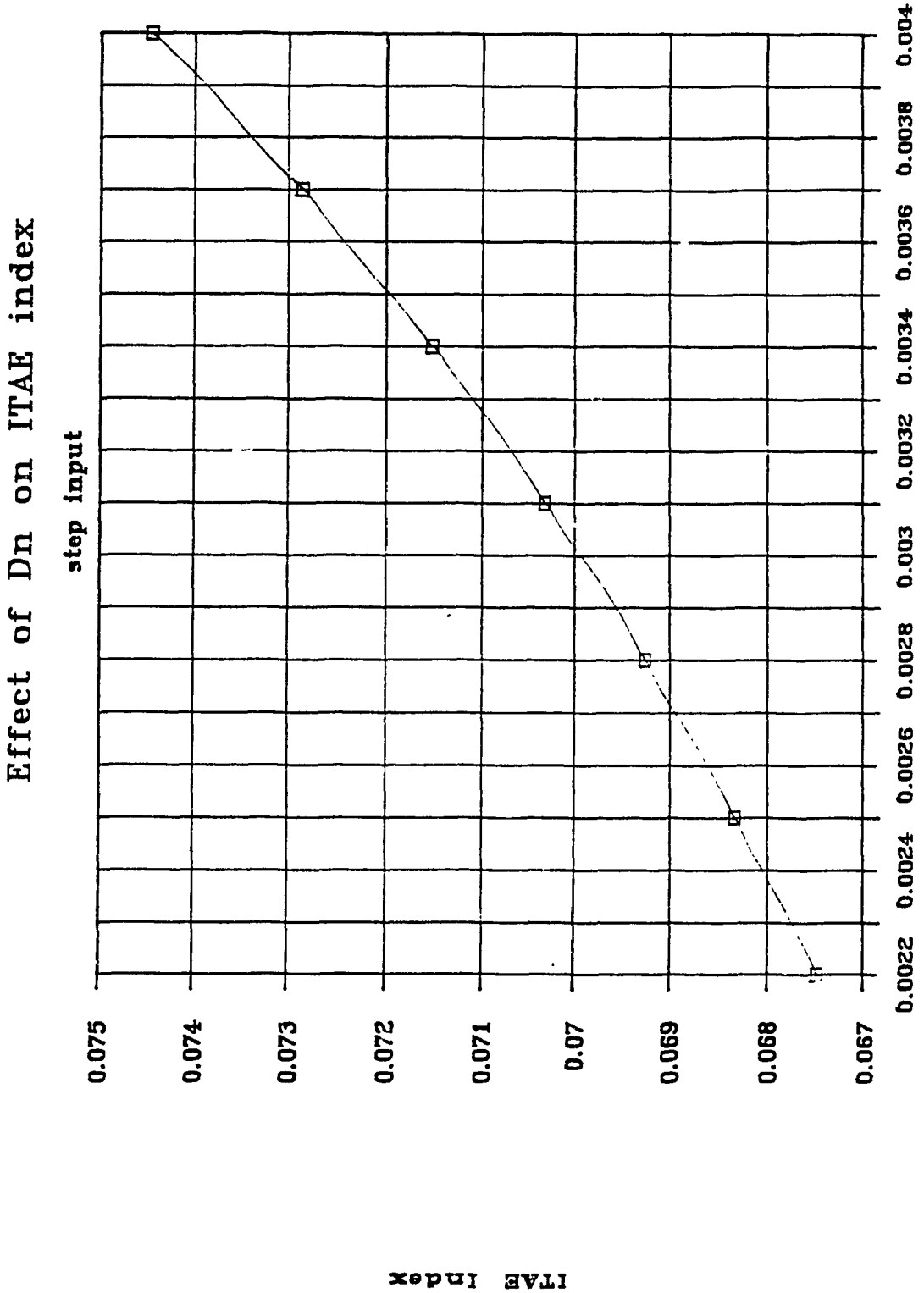

Figure 12.3 (a) Effect of Diaphragm Orifice Diameter on Transient Response

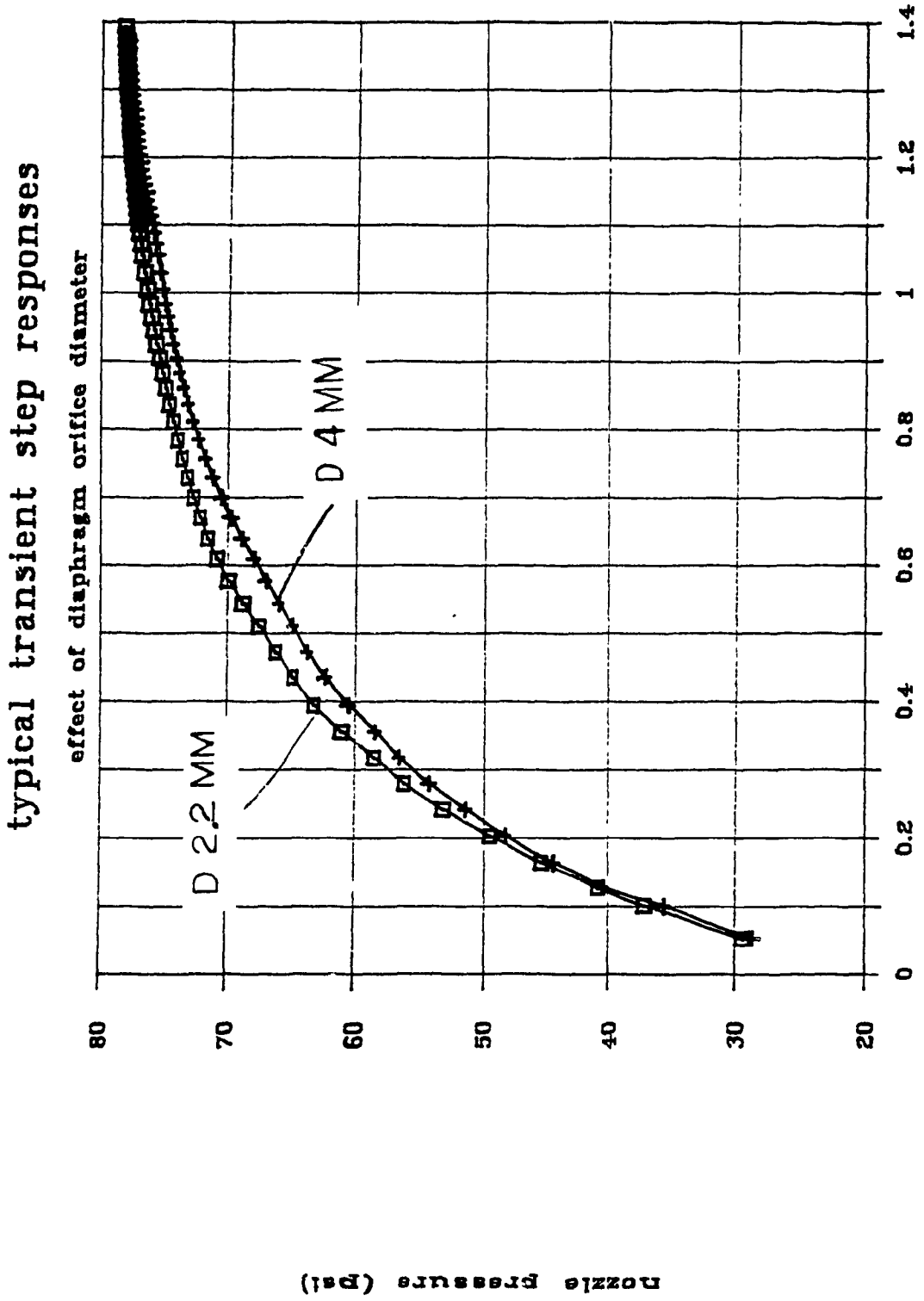

Figure 12.3 (b) Effect of Diaphragm Orifice Diameter on Transient Response

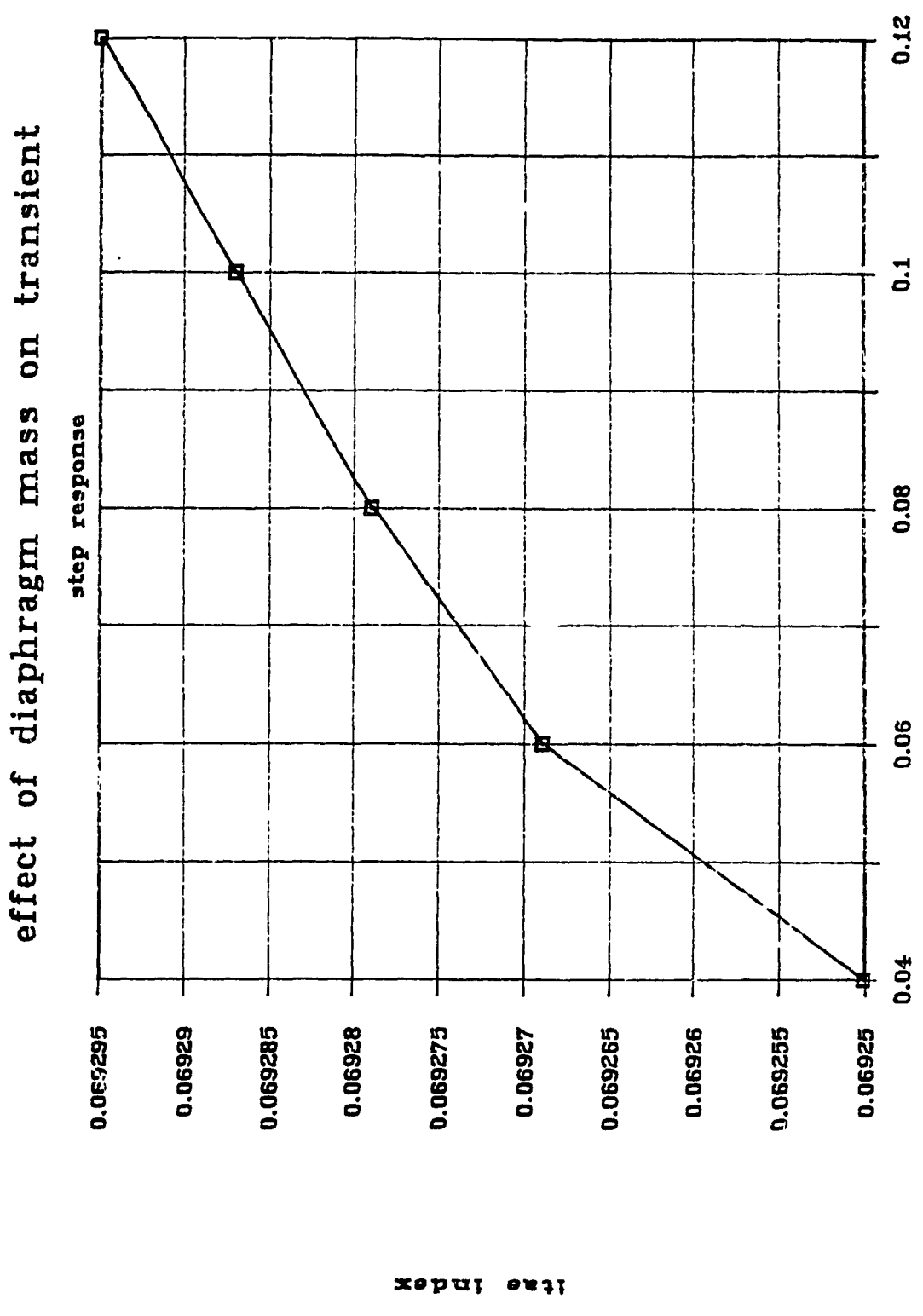

Figure 12.4 (a) Effect of Diaphragm Effective Mass on Transient Response

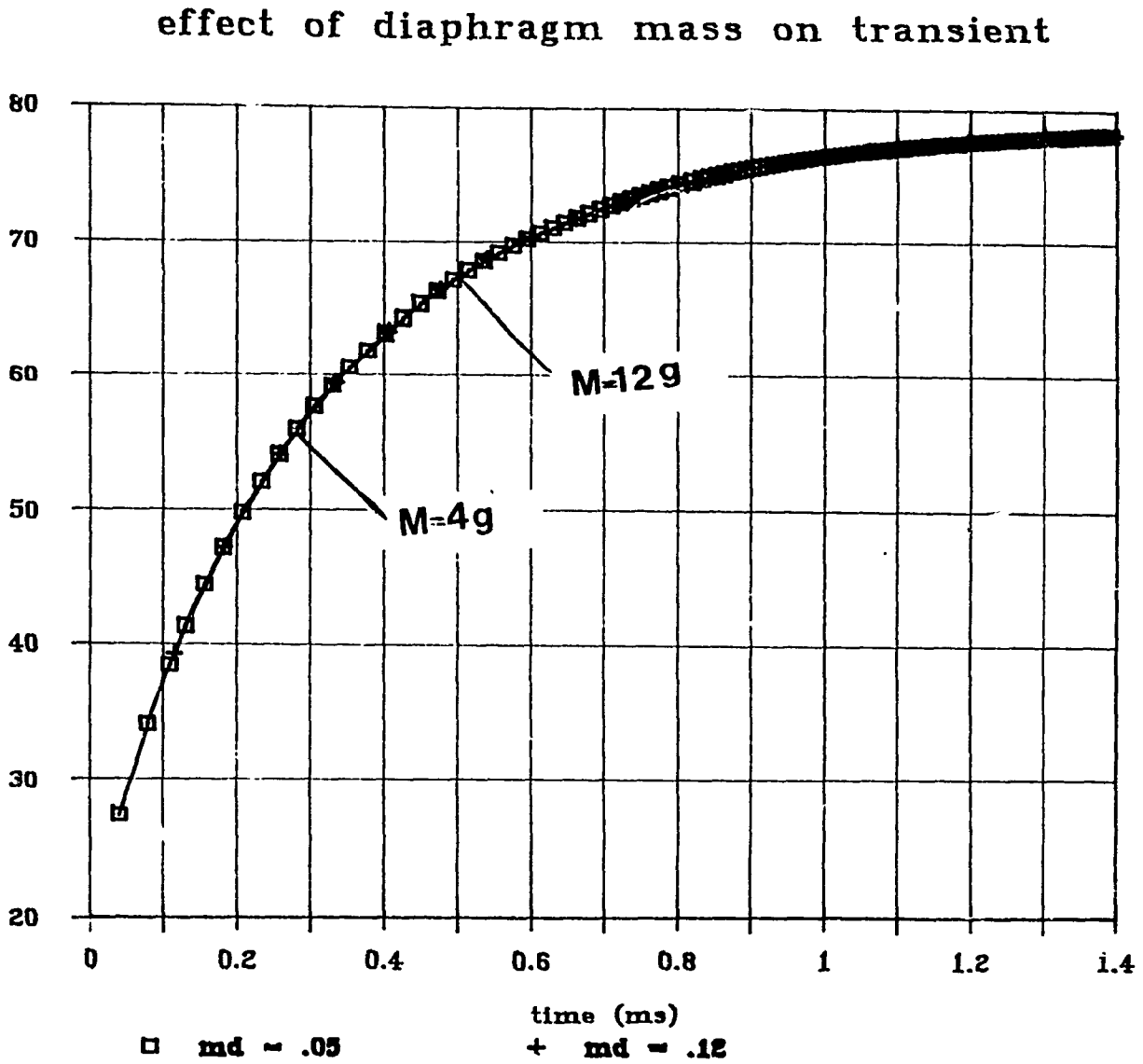

Figure 12.4 (b) Effect of Diaphragm Effective Mass on Transient Response

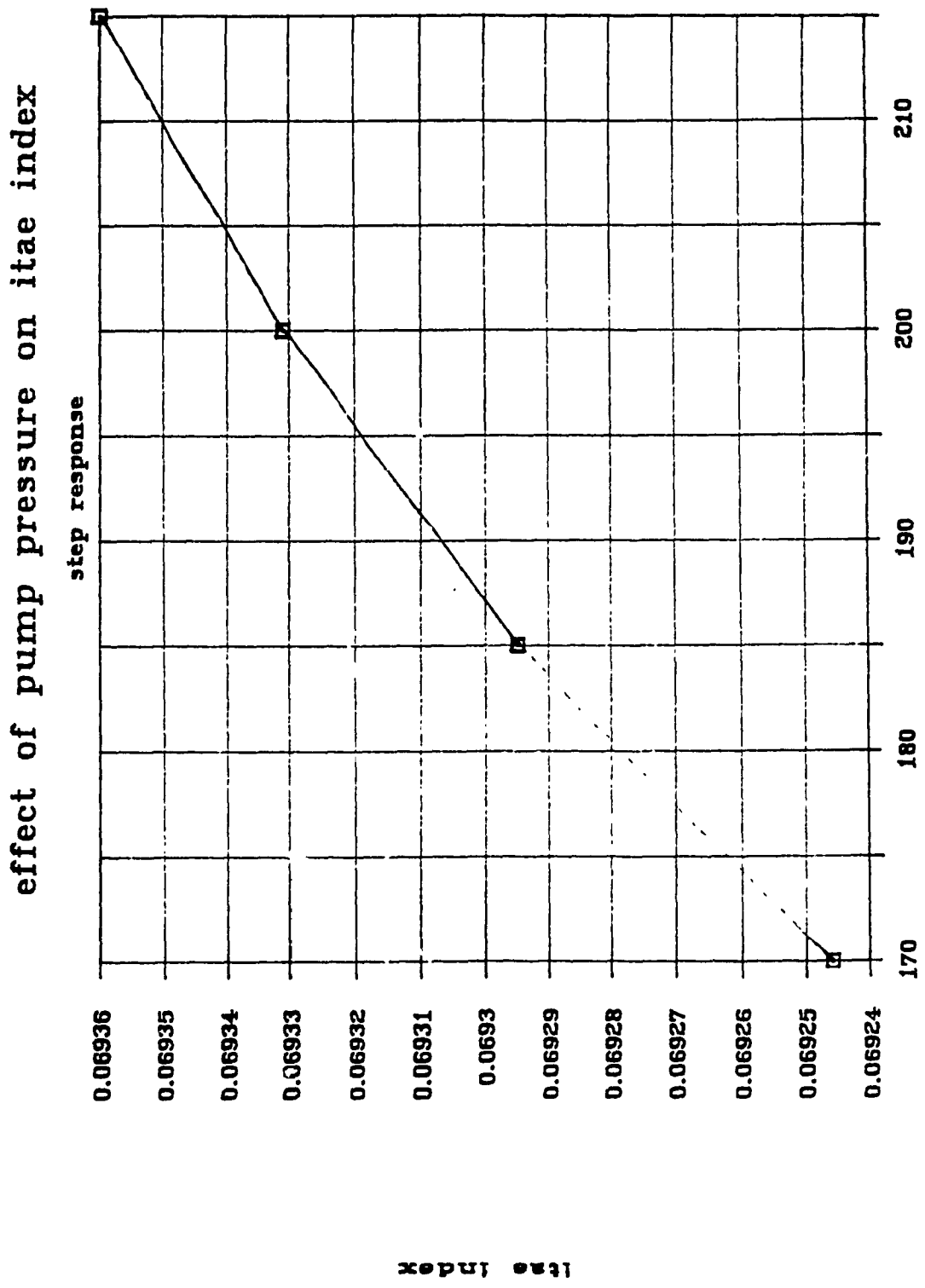

Figure 12.5 (a) Effect of Pump Pressure on Transient Response

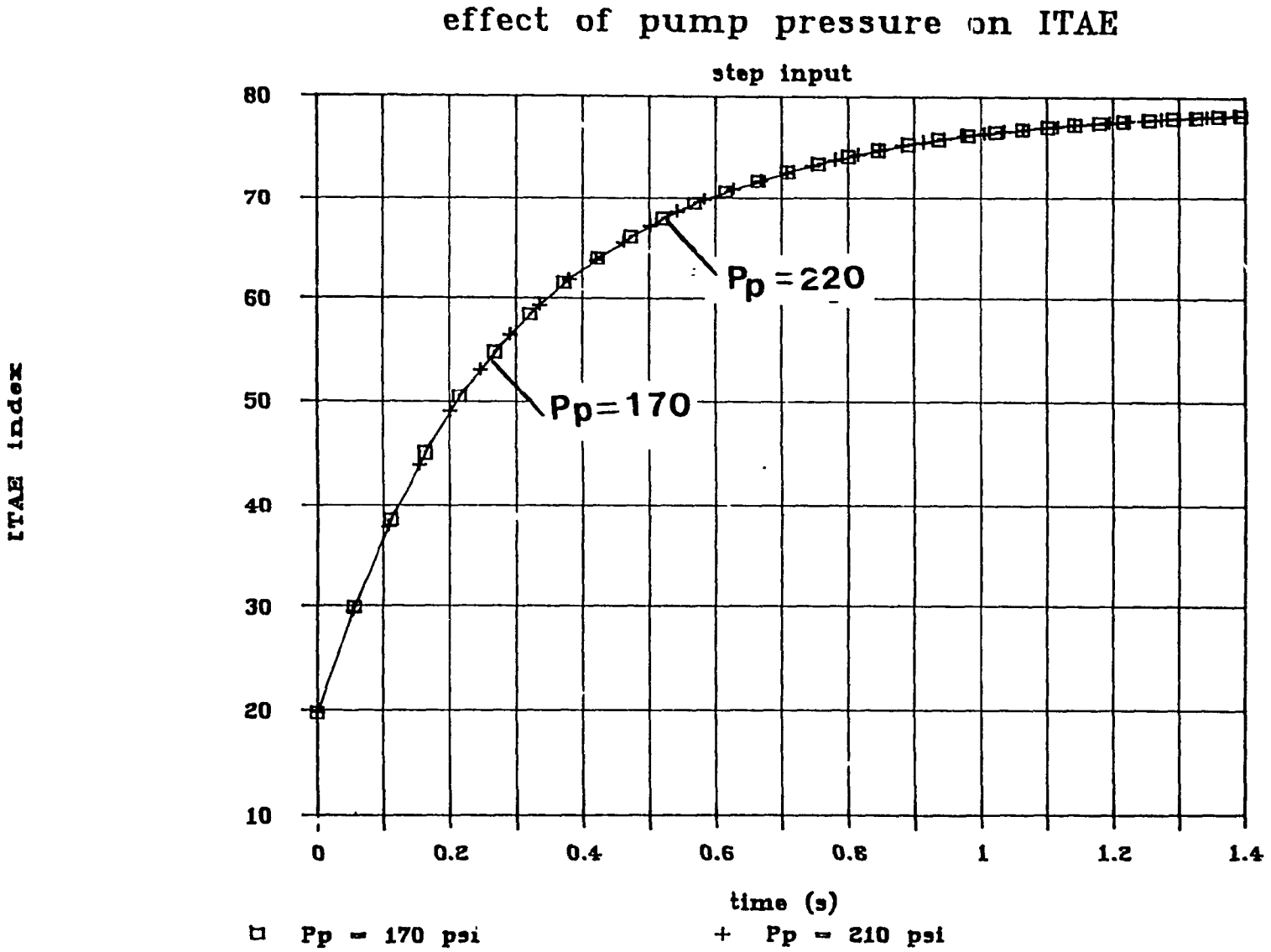

Figure 12.5 (b) Effect of Pump Pressure on Transient Response

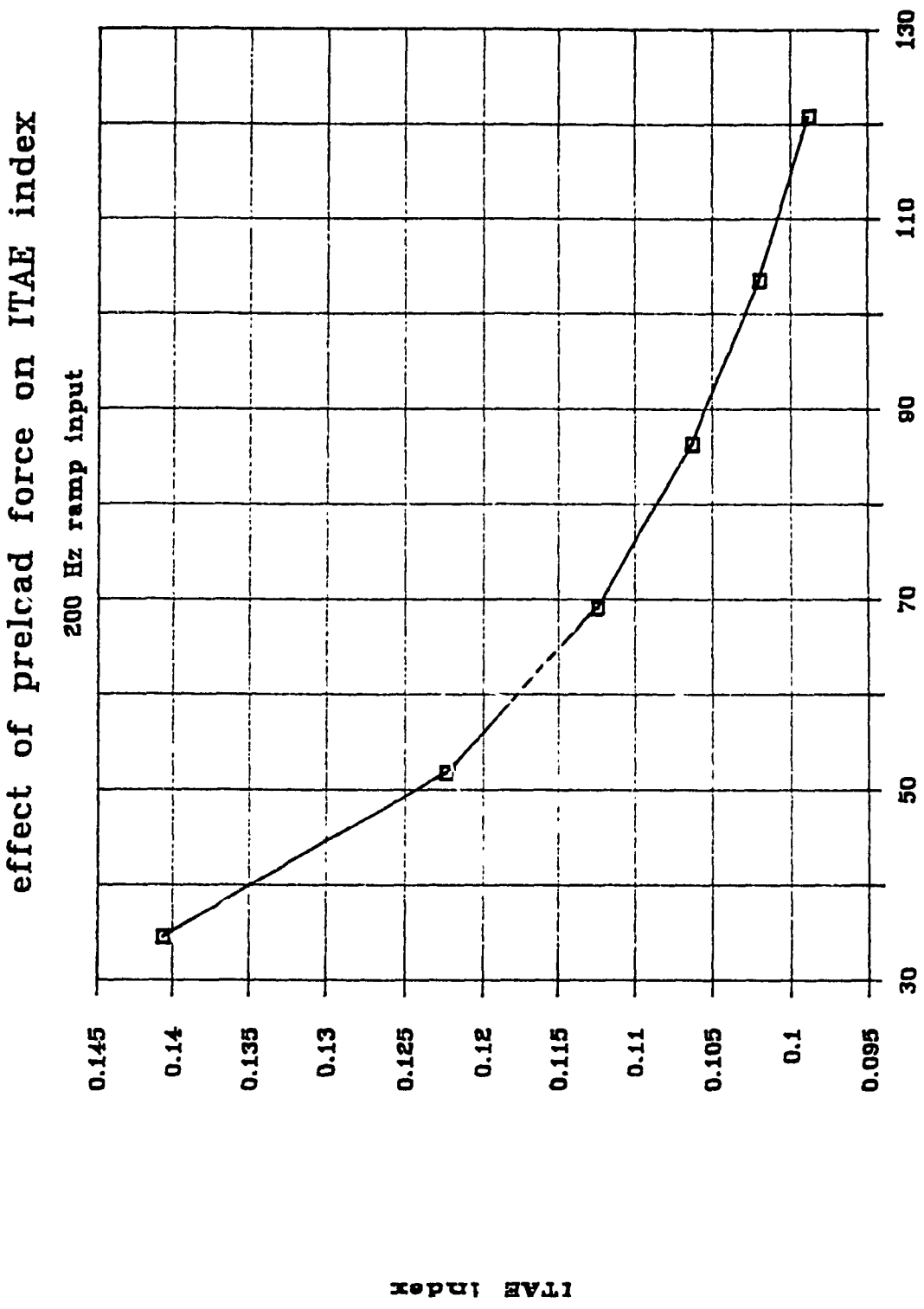

Figure 12.6 (a) Effect of Preload Force on Transient Response

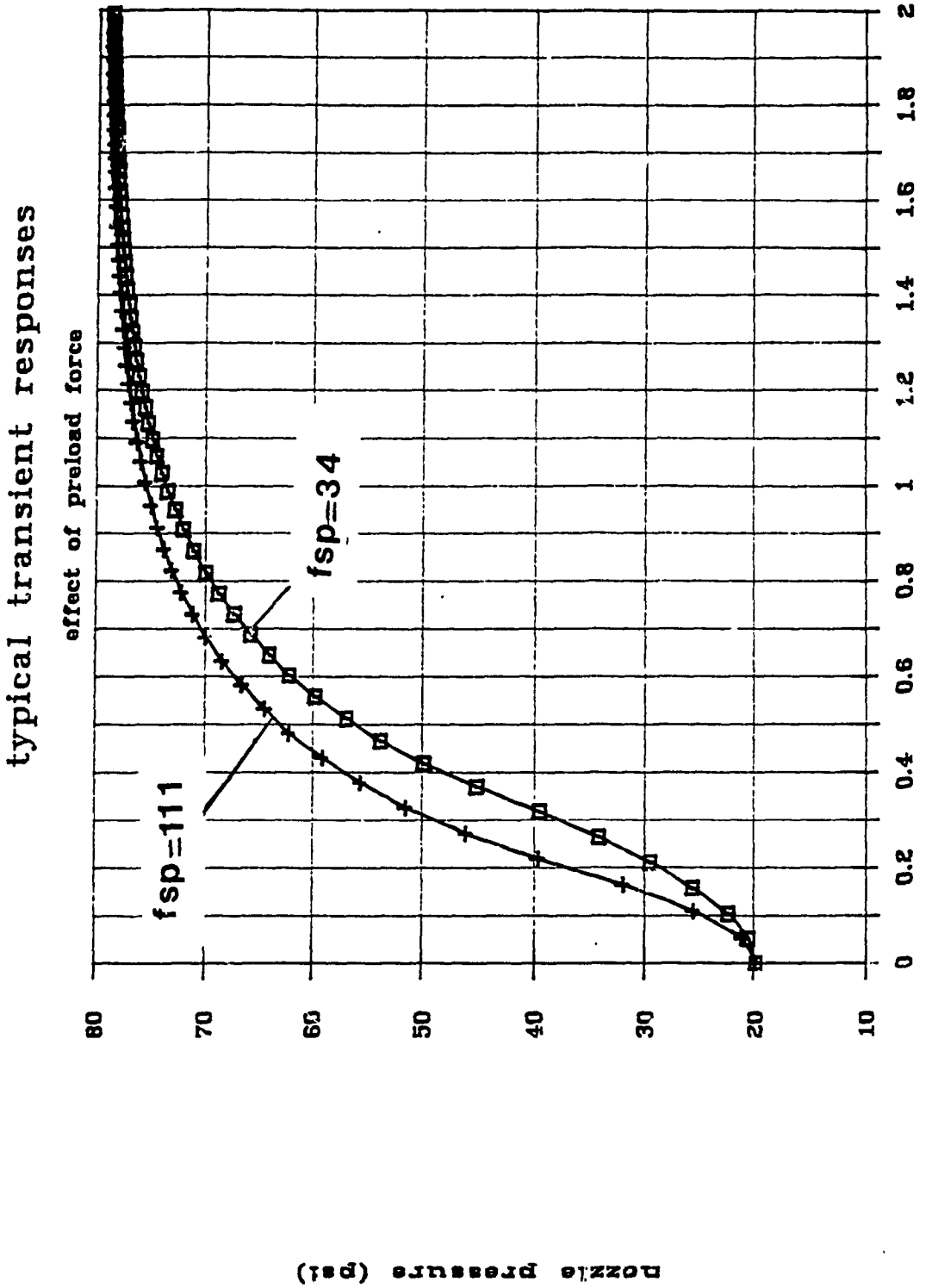

Figure 12.6 (b) Effect of Preload Force on Transient Response

Chapter 13

A Multiobjective Optimization Scheme

13.1 Introduction

The fuel control unit for gas turbine engines must have the qualities discussed in the previous chapters. It must respond quickly to a step change in fuel flow demand, as measured by the ITAE transient performance index introduced in chapter 12. The unit should provide an accurate fuel flow rate at steady state conditions with a close to linear metering valve fuel flow schedule. That is, it should minimize the variations of differential pressure across the metering valve when the flow rate changes so that the fuel flow to the nozzles is linearly related to the metering valve position. This was measured by the variation index VAR described and calculated in chapter 10. Finally, for the reasons discussed in chapter 11, it is desirable to have a system that is as much as possible insensitive to design parameter variations that may occur over the operational life of the system. This was measured by the sensitivity index SENS. The trends displayed by each of these criteria with respect to the design variables were investigated seperately in the three previous chapters in order to gain insight on the behaviour of the system.

Having identified the important optimization criteria and having validated models for each criteria: speed of

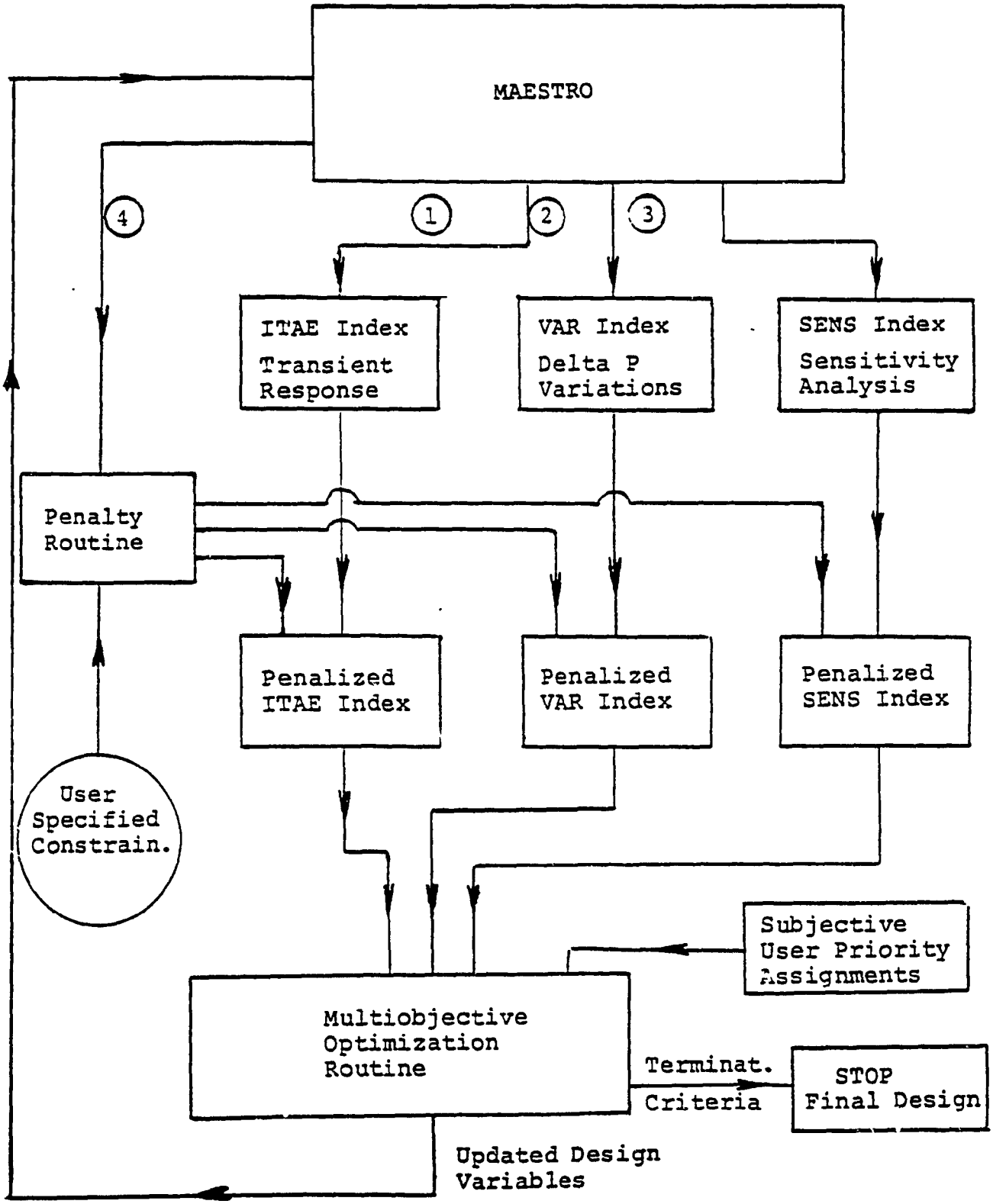

Figure 13.1 The Multiobjective Optimization Scheme

transient response, fuel flow linearity, and sensitivity to design parameter variations, all these programs will now be combined in a unified optimization scheme that will consider the three criteria simultaneously. This scheme is snown in Figure 13.1. A control routine, MAESTRO, directs the overall program logic. In order to have a fair comparison between different sets of design variables, the optimization scheme should compare the designs with the same average differential pressure setting. The preload needed to achieve this setting is a function of the design variables. Therefore, the preload required with the current design variable set is first found. This is done iteratively with the steady state simulation program as shown in Figure 10.2. Then, the subroutine for the ITAE index evaluation is executed. This involves the solution of the set of differential equations in the dynamic FCU model. The input to this routine is a reference step change in fuel flow demand. The ITAE index is calculated based on the resulting transient response. However, the steady state simulation program must first be run to determine the initial and final metering valve positions corresponding to the levels of fuel flow demand. The initial and final metering valve positions depend on the current design parameter set for the FCU. A flow step change from 20 to 40 kg/hr is used as a reference. MAESTRO then calls subroutine VAR which solves the steady state model for the entire range of metering valve positions with 1 kg/hr increments in fuel flow. The

maximum percentage deviation of the differential pressure is computed as the VAR index. Finally, MAESTRO calls on the subroutine SENSITIVITY, which performs some sensitivity studies on the system design. It calculates the composite sensitivity index, SENS, of the nozzle flow to the design parameter variations at the operating point of 35 kg/hr. For the sensitivity calculations, however, the steady state simulation program is first run to determine the "state" variables corresponding to the current design vector, as was explained in chapter 11.

The three indices are then passed on to the multiobjective optimization routine (MOR), which updates the design vector according to the value of the current design vector and the values of current and and past index calculations. The MOR also checks for termination of the optimization process; i.e. when there will be no further improvement in the objectives. The whole process is iterative, with the MOR continually feeding MAESTRO with new sets of design variables and MAESTRO requesting index calculations from the subroutines under its command.

In this chapter, single criterion optimization will first be described. Then, a description of multi- objective analysis will follow. A fuel control multi- criteria optimization problem will then be formulated and solved. Results will be presented.

An important distinction should be made regarding the terminology used in the following analysis. Following the recommendations of Papalambros and Wilde [32], a "variable" will refer to quantities that can be changed by the designer. These include the spring constant, k_s, the pump pressure, p_p, the diaphragm orifice diameter, d_n, the preload force f_{sp}, and the effective diaphragm mass m_d. "Parameters" will refer to quantities that are considered fixed in the analysis. That is, the possibility to change these quantities is not in the designer's power. Examples of model parameters include the diaphragm diameter d_d, the nozzle orifice size A_i, the bulk modulus of fuel β, and the metering valve slit width, w. However, it should be noted that in sensitivity analysis, some of the parameters are considered as "variables". For example, the effect on the nozzle flow of variations of the parameter A_i were investigated in chapter 11.

13.2 Single Criterion Optimization

The general problem of single-objective mathematical programming is to search for the optimum (minimum or maximum) of a function of several variables that are limited by equations or inequalities called constraints. The problem can be expressed as,

$$\text{minimize } f(x)$$

subject to,

$$g_i(x) < 0 , \quad i = 1, 2, \ldots, p$$

$$h_k(x) = 0 , \quad k = 1, 2, \ldots, m$$

$$x_j > 0 , \quad j = 1, 2, \ldots, n$$

where $f(x)$ is the objective or merit function, $g_i(x)$ are the inequality constraints and $h_k(x)$ are the equality constraints. The "design vector", x, is the set of decision variables. The functions $f(x)$, $g(x)$, and $h(x)$ can be either linear or nonlinear functions of the decision variables. The feasible space χ is the set of all design vectors that satisfy both the equality and inequality constraints. Each point in the feasible design space is called a "design

point". The optimization problem then seeks to find a design vector x_* in the feasible space that minimizes the function f(x). Various numerical methods are used to find this optimum. These search methods can be divided into two groups; those that use gradient information and those that use only function evaluations. Every method, however, must check certain mathematical conditions to ensure that optimality has been achieved. A review of various optimization techniques is given in reference [33].

13.3 Multiobjective Optimization

In design, the choice of objective function depends on the nature of the problem. Traditionally, in solving design problems, decision makers have considered a single objective in their analysis. For example, a typical objective was to minimize weight or cost, subject to design constraints. When confronted will multiple goal problems, typically the most important criteria was treated as the objective function only. The other criteria were limited within certain values in the constraint set. This was due to both the lack of powerful computing means and the lack of a theoretical framework to attack the problem. However, in some cases, there may be more than one criterion of importance in the analysis. There may be cases where optimization with respect to a particular criterion may lead to results that are unsatisfactory with respect to another

criterion. For example [33], a gear pair may have to be designed to achieve the two goals of minimum weight and maximum transmission efficiency. In the last two decades, there has been an increased awareness of the need to identify and to consider simultaneously several objectives. This became possible with the development of inexpensive and powerful computing. The new techniques have been developed mostly for application in large scale systems such as water resource management and economic studies. Since mechanical design is itself a decision making process, these developments can successfully be applied to smaller scale problems such as the mechanical design of a fuel control unit. This is the idea investigated in this chapter.

The multi-objective nonlinear programming problem differs from the single objective optimization problem in that it is characterized by a p-dimensional vector of objective functions [34],

$$z(x) = [z_1(x), z_2(x), z_3(x), \ldots, z_p(x)]$$

where p is the number of design criteria or goals.

This may be considered as a vector-valued objective function of a vector variable subject to the same type of constraints as in single criterion optimization. It is desirable to minimize, for example, everyone of these

objectives. However, it may not be possible to minimize all the objectives simultaneously. Improving one objective may reduce the possibility of achieving another. In this case, the goals are said to be incongruent. This is usually the case in design, indicating that a trade-off or compromise must be reached by the decision maker.

In the fuel control design problem of this thesis, the objective function vector contains the three design criteria that have been explored separately in the last three chapters.

$$z(x) = [VAR(x),\ SENS(x),\ ITAE(x)]^T$$

The design vector, x, consists of the spring constant, K_s, the preload force setting, f_{sp}, the diaphragm orifice diameter d_n, the pump pressure, p_p, and the effective diaphragm mass, m_d. It is represented as,

$$x = [K_s,\ f_{sp},\ d_n,\ P_p,\ m_d]^T$$

Each of the objective functions is a function of the design vector. These relationships have been explored in the three previous chapters.

In general, for the multiobjective optimization case, an "optimum" can only be found once the "preference structure" is articulated by the designer. That is, the multiobjective optimization method must somehow solicit from the designer a statement about which of the objectives are preferred (more important) and by now much. The word "optimum" is not used in the formulation of the multiobjective analysis problem since one cannot in general optimize a priori a vector of objective functions (without the articulation of a preference structure). The term that will be used here is to max- or min- dominate.

There are many possible designs that could satisfy the design constraints. The set of all such dsigns is called the feasible space. However, even before a preference structure is defined, the feasible space can be reduced to the set of "nondominated" solutions. This important idea in multiobjective programming can be explained as follows: Consider a design vector x_i and the corresponding values of the objective functions, VAR_i, $SENS_i$, and $ITAE_i$. Suppose that a small change is made to the design vector, the new one being denoted x_{i+1} and the corresponding new values of the objective functions are VAR_{i+1} $SENS_{i+1}$ and $ITAE_{i+1}$. Suppose further that each one of the objective functions "improved" (i.e. their numerical value decreased) as a result of the small change in design vector. Then, there is no doubt that the second design vector is better than the

first in every respect, no matter what importance we give to each criterion. The second design vector "dominates" the first, and the first vector can be removed from consideration as the final design. In general, for any design vector, if it is possible to make a small change that will cause all the objective functions to improve, then it is a "dominated" solution. If, on the other hand, a design vector has the characteristic that any small change imposed on it causes at least one on the objectives to "get worse", than it is a " nondominated" solution and therefore, until further analysis is performed, it must be retained as a candidate for the final design.

More formally [34] , for a given set of feasible solutions χ , the set of nondominated solutions is denoted S and is defined as follows (assuming that more of each objective function is desireable):

$$S = \{x: x \in \chi \text{ , there exists no other } x' \in \chi \text{ such that } z_q(x') > z_q(x) \text{ for some } q \in \{1,2,\ldots,p\} \text{ and } z_k(x') \geq z_k(x) \text{ for all } k \neq q \}$$

Once the entire nondominated set of solutions is found, the decision maker must pick the final design from this set, based on his subjective evaluation of the relative importance of the criteria. There are different multiobjective analysis techniques available that find the

nondominated set. The main difference between them lies in how the decision maker inputs his subjectivity into the analysis. In general, the simplest techniques to solve the multiobjective analysis problem eventually convert the problem to a form that can be numerically solved using single criterion mathematical programming optimization techniques.

The Weighing Method

The simplest way to solve the multiobjective optimization problem is to convert the vector valued objective function into a scalar function by application of weights. The problem then becomes a single criterion optimization problem for which the solution algorithms are well known. For example, for the fuel control design problem, the new scalar objective becomes,

$$f(x) = w_1 VAR + w_2 SENS + w_3 ITAE$$

where the weights w_1, w_2, and w_3 obey the relation

$$w_1 + w_2 + w_3 = 1$$

It can be shown that the solution to this problem is nondominated if the weights are all nonnegative [34]. The entire nondominated set can be generated by parametrically varying the weights between zero and one and solving the resulting single criterion optimization problem each time. Conceptually, the generation of the nondominated set using the method of weights appears simple. However, in practice the generation procedure is quite demanding. Several weight sets can generate the same nondominated point. The parametric variation of weights in discrete steps is very expensive computationally if very small steps are used. Using large steps, on the other hand, may result in skipping of some nondominated extreme points.

The weighting method provides less insight into the design optimization then other methods and the assignment of the preferred weighing of objectives by the designer can be very subjective and difficult. Another problem is that the goals are often noncommensurate. That is, the goals cannot be measured with comparable units. This makes the task of assigning weights even harder. For example, values of the sensitivity index cannot be directly compared with values of the ITAE or VAR indices. The weighing method is therefore not used in this analysis.

The ε-Constraint Method (Haimes 1973) [34]

The ε-constraint method is more appealing for application in the fuel control design problem of this thesis than the weighing method because the decision maker's subjective input is in the form of proposed limits to each objective function rather than relative worths or weights. This is usually much easier to do. For example, in the fuel control design problem, the designer needs only to specify that the VAR index should be less than 2%, that the SENS index should be less than 15% and the ITAE index should be less than .02. These limits can sometimes be inferred from the customer's required specifications, making the job even easier. This is less difficult than specifying the relative importance of the three objectives. Another advantage of the ε-constraint method is that it gives the designer the "goal achievement" of his design. In other words, it reveals how much of each objective was achieved compared to the maximum achievable. The variation of the used in this thesis will be explained below with reference to the fuel control design problem of this analysis.

Let the three constraints, or "acceptability limits" of the three objectives, VAR, SENS, and ITAE be denoted ε_1, ε_2, and ε_3, respectively. The first step in this procedure is to solve three separate single criterion optimization problems. The objective function in each case is one of the three design criteria, with the other two objective functions included in the constraint set, restricted by the

corresponding ϵ-constraints. The three preliminary optimization problems can be formulated:

1. minimize VAR(x)

subject to

$$\text{SENS}(x) < \epsilon_2$$

$$\text{ITAE}(x) < \epsilon_3$$

design constraints

2. minimize SENS(x)

subject to

$$\text{VAR} < \epsilon_1$$

$$\text{ITAE} < \epsilon_3$$

design constraints

3. minimize ITAE(x)

subject to

$$\text{SENS} < \epsilon_2$$

$$\text{VAR} < \epsilon_1$$

design constraints

In the above formulation, the "design constraints" refer to the set of constraints on the system design that will be described later in this chapter. The solution to each of these three problems can be found using standard numerical search techniques. The three respective minimums of the objective functions are denoted VARMIN, SENSMIN, ITAEMIN. Of course, when the three objectives are considered simultaneously, tradeoffs and compromises must occur between the objectives. These three minimums will typically not be achieved simultaneously in the multiobjective optimization. They represent the best that could have been achieved for one objective if it were not limited by other incongruent objectives in the analysis. Also, it should be noted that these minimums depend on the values of the assigned ε-constraints. The next step in this method is to define a scalar surrogate goal function,

$$G(x) = [\ VAR(x)/VARMIN + SENS(x)/SENSMIN + ITAE(x)/ITAEMIN\ ] \quad (13.1)$$

Note that the terms VARMIN, SENSMIN, and ITEAMIN are constants in this case. Note that each term in the goal function should be greater than one and the minimum each term can be is one. The goal function is now minimized using single criterion optimization. The resulting optimum design vector and objective function values are recorded.

The goal achievement for each objective is then checked, VARMIN/VAR_*, SENSMIN/$SENS_*$, and ITAEMIN/$ITAE_*$ (the asterisk denotes the final design point generated by the multiobjective optimization method). These will be fractions, with values of less than one. If all three goals were perfectly congruent, then each of these goal achievements would be unity. If all the goals achievements are satisfactory, the problem could be considered solved. However, if the decision maker is not satisfied with a particular goal achievement, he could modify the corresponding ε-constraint and try to solve the problem once more.

In general a nondominated set of solutions can be obtained as follows [34]. The user specifies maximum and minimum acceptability limits for each ε-constraint. By parametrically varying each ε-constraint between its upper and lower limits and re-solving the problem each time, a nondominated set could be generated. The designer chooses his final design by examining this set of nondominated solutions and the corresponding goal achievements which each of the solution produces.

Note that the ε-constraint method can be considered as a type weighing method where, for example, the weight w_1 = 1/VARMIN.

13.4 Description of Design Constraints and Problem Formulation

In this section, the design constraints imposed on the design variables will be described. Then, the formal statement of the multiobjective analysis problem will be developed. Monotonicity analysis will be used to simplify the model in the next section before the numerical optimization is performed.

Flow Resolution Constraint

To achieve acceptable flow resolution with the incremental motion of the stepper motor, one step, s, should cause a change of flow, $\dot{q}_s$, that is less than 0.4 kg/hr. This is necessary in order for the fuel control to accurately meter fuel to the combustor during acceleration and deceleration, avoiding stall or flameout. A constraint is therefore imposed on the spring preload force, f_{sp}. Using the approximation f_{sp}/A_d for differential pressure, the constraint can be expressed as

$$\dot{q} = c_{dm} s\, w\, i \sqrt{(2/\rho)\,(f_{sp}/A_d)} < (0.4)/\,[(3600)(770)] \qquad (13.2)$$

Diaphragm Orifice Diameter Lower Limit

The diaphragm orifice lower limit is governed by the saturation condition for the diaphragm orifice. The critical flow area through the diaphragm orifice should be the curtain area formed by the clearance between the diaphragm and the face of the orifice. The most crucial test for this occurs at maximum flow. Expressing the upper diaphragm chamber pressure as $p_p - \Delta p$, the flow equation can be used to determine the maximum flow area, A_{or}, through the diaphragm valve. Recalling that maximum flow (54 kg/hr) corresponds to a nozzle pressure of 150 psi, the flow equation gives,

$$(54)/((3600)(770)) = c_{do} A_{or} \sqrt{(2/\rho)\,(p_p - \Delta p - (150)(6895))} \qquad (13.3)$$

The diaphragm valve orifice diameter must be large enough so that the cross section area of the orifice is still smaller that the curtain area at maximum flow. This constraint is expressed as:

$$\frac{\pi d_n^2}{4} > A_{or} \qquad (13.4)$$

where A_{or} is given by equation (13.3).

Pump Pressure Constraint

The lower limit for the pump pressure is governed by the diaphragm valve orifice saturation constraint. The pump pressure should be adequate to push the fuel through the system with the given nozzle size. Assuming that at maximum flow the nozzle orifice is much smaller that the diaphragm valve orifice, the constraint can be approximated as follows,

$$c_d A_{ic} \sqrt{(2/\rho)(p_p - \Delta p)} \quad > \quad (54)/[(770)(3600)] \tag{13.5}$$

where A_{ic} is the effective orifice for the diaphragm valve orifice and nozzle orifice in series at maximum flow.

An upper limit is imposed on the pump pressure because of the extra energy and therefore cost of pumping at high pressure. A stronger electric motor would be required, adding to the cost of the system. An upper limit of 220 psi is chosen.

$$P_p \quad < 220 \text{ psi} \tag{13.6}$$

Other Constraints

Besides the constraints outlined above, upper and lower limits should be imposed on the design variables in order to reflect manufacturing limitations, limited availability of components and geometrical restrictions. These "side" constraints are listed below.

Upper and Lower Spring Constant Limits

$$k_s^l < k_s < k_s^u \tag{13.7}$$

Upper and Lower Effective Diaphragm Mass Limits

$$M_d^l < M_d < M_d^u \tag{13.8}$$

Upper Diaphragm Orifice Limit

$$D_n < D_d \tag{13.9}$$

Lower Preload Force Limit

$$f_{sp} > f_{sp}^u \tag{13.10}$$

The superscripts in the above constraints denote upper and lower limits, which will be given numerical values after model simplification is done in the next section.

The formal statement of the multiobjective analysis problem for the fuel control unit design is presented below.

Min-Dominate $Z(X) = [VAR(X), SENS(X), ITAE(X)]$

subject to,

$$q_{step} = c_{dm} s\, w\, i \sqrt{(2/\rho)(f_{sp}/A_d)} < (0.4)/[(3600)(770)] \quad (13.11)$$

$$(54)/((3600)(770)) = c_{do} A_{or} \sqrt{(2/\rho)(p_p - \Delta p - (150)(6895)} \quad (13.12)$$

$$\frac{\pi d_n^2}{4} > A_o \quad (13.13)$$

$$c_d A_{ic} \sqrt{(2/\rho)(p_p - \Delta p)} > (54)/[(770)(3600)] \quad (13.14)$$

$$P_p < 220 \text{ psi} \quad (13.15)$$

$$k_s^l < k_s \quad (13.16)$$

$$k_s < k_s^u \quad (13.17)$$

$$M_d^l < M_d \quad (13.18)$$

$$M_d < M_d^u \quad (13.19)$$

$$D_n < D_d \quad (13.20)$$

$$f_{sp} > f_{sp}^u \quad (13.21)$$

13.5 Model Simplification; Monoticity Analysis

In general, there are two types of techniques that can be used in optimization. One deals with numerical iterative computation driven by "local knowledge" or information, that is, knowledge pertaining to a single point in the design space and in the neighborhood of this point. All traditional mathematical programming methods use this approach. The other approach is characterized by examination of mathematical properties of the entire model and makes use of "global knowledge" or information, that is, knowledge pertaining to all points of the design space [32]. Without computing function values or derivatives numerically, some problems can be examined for certain mathematical properties that can be used to find or simplify the solution.

It is assumed that the problem formulation results in a well bounded model. That is, none of the design variables will turn out to be zero or infinity when the problem is solved. This will be the case if no important constraints are omitted and if the system is accurately modeled. The most useful "mathematical property" or "global knowledge" in simplifying design models is monotonicity. A function $f(x)$ is said to be increasing with respect to a positive finite variable x if for every $x_2 > x_1$, there is an inequality $f(x_2) > f(x_1)$ [32]. Similarly, a function is said to be decreasing with respect to a positive finite variable x if for every $x_2 > x_1$, $f(x_2) < f(x_1)$. A monotonic function is one that is

either increasing or decreasing.

Monoticity can be a very useful property to exploit in optimization because of the First Monoticity Principle of Papalambros and Wilde, [32] which states,

> " In a well-constrained objective function, every increasing (decreasing) variable is bounded below (above) by at least one active constraint."

The major value of this principle is that it can sometimes prove that a constraint is active without finding the optimum first.

In the case of the fuel control unit design, it is difficult to decide on the monoticity of the objective functions with respect to different variables. In general, simulation has to be used and the objective function value has to be plotted versus the variable of interest. However, if the objective function appears monotonic with respect to the variable on the plot, one has to be careful about making conclusions. In order for the function to be monotonic, it has to behave monotonically no matter what the other design parameter settings are. In general, the plots made in the previous sections when each objective function was analyzed individually cannot provide a proof of monoticity. However, if there is strong physical justification for believing that the relation will always be monotonic, then an assumption can be made with small risk.

In the fuel control design problem, it is clear that the spring preload force should be made as large as possible in order to speed up the transient response. This was shown in Figure (12.6). The reasoning is simple. With higher preload and hence differential pressure, the stepper motor has to move less far in exposing the metering valve slits. This speeds up the response, especially at lower stepping rates. In the case of the VAR index, a large preload was also shown to be beneficial (Figure 10.6). A large differential pressure results from a large spring preload, and hence the changes in the force balance lead to a smaller relative change in the differential pressure since the nominal setting is higher. It is the relative change in differential pressure that determines the linearity of the flow over the schedule with respect to the metering valve position. Finally, a high spring preload has also been shown to improve the sensitivity index (Figure 11.7). The reason is similar to that for the VAR index. With a high differential pressure, the diaphragm force balance alterations caused by parameter changes do not cause as serious a change in the relative differential pressure. Since each objective requires the preload force be made as large as possible, and since there is strong physical justification for this behavior, it is safe to assume that goal achievement is monotonic with respect to the preload force. Simply, the preload should be as high as possible. Using the First Monoticity Principle, there must be an

active constraint binding the preload from above.

Only the flow resolution constraint (See equation 13.11) can fulfill this function. Therefore, it must be active, i.e. satisfied by equality. The optimum preload given this constraint is therefore calculated from

$$q_{step} = c_{dm} s\, w\, i \sqrt{(2/\rho)(f_{sp}/A_d)} = (0.4)/\,[(3600)(770)] \qquad (13.22)$$

Substituting $c_{dm} = 0.6$, $i = 6$, $w = 0.08$ mm $s = .0254$mm $\rho = 770$ kg/m^3 and $A_d = 309.$ mm^2, the preload force becomes about 46.3 N/m and the differential pressure is about 22 psi. The preload force can now be removed from the set of design variables since its optimum value is determined.

Considering now the pump pressure, it was shown that for the range of pressures considered, the pump pressure has little effect of the transient response time. In fact , the slight effect demonstrated (Figure 12.5) showed that decreasing the pump pressure decreases the ITAE index. Lowering the pump pressure was also shown to have a positive effect on the VAR index (Figure 10.3). The reason for this effect can be understood as follows. If the pump pressure is low, the upper diaphragm chamber pressure is lower for

the same differential pressure setting across the metering valve. At maximum flow, therefore, there will be a smaller pressure drop across the diaphragm orifice. The diaphragm must open up more the curtain area and hence its total displacement over the flow range is larger. The force term $k_s h$ is therefore larger due to the larger h variation. This effect helps to compensate for the larger nonlinearity in flow causes by the nozzle pressure impact term $p_n A_n$ (which acts in the opposite direction). Therefore, in optimizing the VAR index, it is best to use the lowest allowable pump pressure. For the case of sensitivity of the nozzle flow to the design parameters variations, a lower pump pressure has also proved beneficial (Figure 11.6). Again, the reason is similar to that for the VAR index. It stems from the fact that a lower pump pressure leads to a larger movement of the diaphragm, h. For example, consider the sensitivity of the flow to injector contamination and the effect that the pump pressure would have on this sensitivity. If the nozzle gets contaminated, the nozzle manifold pressure will rise. This will cause an increase in the differential pressure and thus an increase in the flow. However, due to this increase in nozzle pressure, the pressure difference across the diaphragm orifice drops. The diaphragm orifice must therefore move down to support the flow. This decreases the spring force term $k_s h$, offsetting partially the impact of the increased $P_n A_n$ term. The more the diaphragm moves in reaction to this disturbance, the

better the compensation the $k_s h$ term performs, diminishing the change in fuel flow due to the contamination. For a lower pump pressure and therefore a lower upper chamber pressure p_d, a given nozzle contamination and increase in pressure p_n leads to a bigger relative change in the pressure difference across the diaphragm orifice (as compared to what it was before contamination). Therefore, with lower pump pressure, the diaphragm moves more in reaction to nozzle contamination and therefore is better able to reduce the increase in differential pressure across the metering valve. Similar reasoning can be applied to the other components of the composite sensitivity index. In conclusion, for all three design criteria, it seems to be best to have the lowest possible pump pressure. This is also advantageous from the cost point of view, since less energy will be needed for pumping. Applying again the first monotonicity principle, we conclude that there must be an active constraint binding the pump pressure from below. The only constraint available is the flow saturation constraint, which ensures that the pump pressure is adequate to supply the maximum fuel flow. It must be active. Since the differential pressure is approximately set by the preload force determined earlier, the pump pressure can be determined as,

$$c_d A_{ci} \sqrt{(2/\rho)(p_p - \Delta p)} = (54)/[(770)(3600)] \qquad (13.23)$$

Substituting c_d = 0.6, A_{ci}= the effective orifice for the diaphragm and nozzle orifice in series at maximum flow = 0.6 mm^2, ρ = 770 kg/hr, and Δp = 22 psi, the pump pressure is determined as, p_p = 175 psi. However, a safety margin is recommended against saturation, so that the pump pressure will be set at 180 psi.

The final simplification that will be done involves the effective diaphragm mass. In general, the designer can control this variable by adding or removing mass to the valve guide stem. The mass comes into play only in the transient response criteria. It does not enter in the formulation of the steady state model . The impact of the mass on the transient response was found to be very small for the range of masses involved. Because of the very small mass involved, the inertia force is insignificant in the force balance. The system can be approximated by a first

order system, where only fluid transients and flow equations are involved in the model. The small impact that the mass has indicates that the mass should be made as small as possible to improve the ITAE index (Figure 12.4). Therefore, the mass should be fixed at the lowest value possible that does not cause manufacturing inconveniences. The effective diaphragm mass used in simulation is 20 g. It should be acknowledged that the mass could have an important effect on the possible impact of vibrations on the system.

The model has been simplified to one with only two design variables; the spring constant and the diaphragm orifice diameter. The index VAR is not monotonic with respect to the spring constant (Figure 10.4), and thus monotonicity analysis cannot help here. The objective functions seem to all be monotonic with respect to the diaphragm orifice diameter (Figures 10.5, 11.5, and 12.3). However, as explained in chapter 12, two opposite trends can be identified in the case of the transient response. The fact that with a larger diameter, the diaphragm has to move a shorter distance to cover the same curtain area seems to indicate that a large diameter should be used to increase the speed of response. On the other hand, a small diameter leads to a larger force unbalance during transients, which speeds the up the return of the diaphragm to its equilibrium position. For the nominal parameter settings, the second effect dominates and simulation shows that a smaller diameter improves the ITAE index. However, the trend may

reverse as design parameters take on other values. It is therefore unwise to make conclusions about monoticity on such limited evidence. Therefore, the diaphragm orifice diameter is left as a variable in the problem formulation.

Simplifying the lower diaphragm orifice size limit,

$$(54)/((3600)(770)) = 0.6\ A_o \sqrt{(2/\rho)\ (180-22-(150))(6895)\ (13.24)}$$

$$\frac{\pi d_n^2}{4} > A_o$$

Substituting numerical values and using a 25 % safety factor, to the condition becomes

$$d_n > 2.0 \text{ mm}$$

The reduced problem in two variables is formulated below.

$$\text{Min-Dominate} \quad Z(X) = [VAR(X),\ SENS(X),\ ITAE(X)]$$

$$\text{subject to,} \qquad (13.25)$$

$$d_n > 2.0 \text{ mm}$$

$$k_s^l < k_s$$

$$k_s < k_s^u$$

$$D_n < D_d$$

The upper and lower limits for the spring constant are arbitrarily chosen as 100000 N/m and 1000 N/m. These limits reflect the availability of spring constants.

13.6 The Numerical Search Technique

The multiobjective analysis scheme presented in the previous section converted the multiple objective constrained optimization problem into a single objective one, minimization of the surrogate goal function. Also, the theory of monotonicity analysis was used in connection with the studies of the three previous chapters in order to simplify the model. The problem has been reduced to a

workable form, with only two design variables, the spring constant and the diaphragm orifice diameter, left in the formulation. In this section, the numerical search technique used to solve the constrained optimization problem will be described.

The Penalty Function Method

The constraints were dealt with by using the exterior penalty function method, a type of sequential unconstrained optimization technique. This method has the advantage over other methods of relative simplicity. The constrained problem (13.25) is converted into an unconstrained one by adding to the objective function penalties for constraint violation. The penalized objective function in this case is given by

$$f(x) = G(x) + w_i\, r \sum \max\,[g(x),\, 0] \qquad (13.26)$$

The penalty functions, or barrier functions, $w_i r\, g_i(x)$, are zero when the constraint $g_i(x)$ is not violated and very large when it is violated. The parameter r is a very large number that is sequentially made larger. A series of unconstrained minimizations of the penalized objective function tends to a local constrained minimum of the goal function G(x) as the parameter r approaches infinity. The theoretical proof of this convergence, when all problem

functions are continuous, has been demonstrated by Fiacco and McCormick [36]. They also prove that the first order and second order conditions for optimality are satisfied. Box et al [37] indicate faster convergence when all problem functions are scaled to the same order of magnitude. The weights (w_i) are used for this purpose. However, no effective method exists for selecting these weights. The penalty functions create steep valleys at the constraint boundaries which may cause computational problems if the penalty factor r is too large. The barrier functions ensure that most successive design vectors x stay inside the feasible region.

Special consideration must be given to the fact that the optimization code may venture into design vectors that would cause the computer program to crash. For example, this may result from taking the square root of a negative number or dividing by zero. Therefore, a check is first made to ensure that the new design vector will not cause a crash. If any of the design parameters, d_n or k_s are beyond the "crash limits ", then the values sent to the subroutines are the limiting ones. The actual design vector, however, is used in the calculation of the penalty functions.

The Search Algorithm

In the case of the fuel Control Optimization Problem of this thesis, special problems exist in numerically searching for the optimum design vector. The objective function in this case consists of three simulation subroutines which are very expensive computationally. In order to get results in a reasonable amount of computation time, the code had to be written very efficiently. The time for one function evaluation was reduced to 2.5 minutes on an IBM AT computer with a math coprocessor. The function evaluation involves simulation of the transient response to a step input for 750 ms, and performance of the sensitivity and linearity analyses required to calculate the three indices, VAR, SENS, and ITAE. Because the objective function is not analytic, derivatives of it with respect to the design variables cannot be easily obtained. Derivative information could only be obtained by changing slightly the design variable of interest and reevaluating the objective function. The partial derivative of the objective function with respect to that variable could then be found using a finite difference approximation. It was decided, however, to use a numerical search technique that does not require derivative information. There is still some question whether it would be faster to incur the extra computing expense of calculating derivatives in order to take advantage of the faster convergence properties of gradient methods.

Powell1's method [36] was used. The method involves a series of line minimizations along a set of mutually conjugate directions. The initial search directions were set to the unit vectors. The line minimizations were done by Brent's Method [36]. A bracketing routine is used to find the interval that Brent's Method should search [36]. Termination occurs when the function changes by a very small percentage after an update.

13.7 Optimization Results

In this section the results of the computer optimization will be presented. The subjective acceptability limits for the three criteria were set based on observing several system responses and on experience in working with the fuel control. The limits are

ε_1 : acceptability limit for VAR index = .02

ε_2 : acceptability limit for SENS index = 0.13

ε_3 : acceptability limit for ITAE index = 0.025

The results for the three preliminary optimization problems are plotted in Figures 13.2 to 13.5. First, in optimizing for the VAR index, it was found that the optimum diaphragm orifice diameter was 2.0 mm and the optimum spring constant was 17238 N/m. With these values, the variation of differential pressure across the metering can be almost eliminated, the VAR index reducing to a minimum value of VARMIN = 0.000734. Figure 13.2shows the progress of the optimization process. The initial VAR index is about 0.025. This corresponds to the initial design parameters of d_n= 2.8 mm and k_s = 2150 N/m. First, the diameter is changed with the spring constant fixed. The initial attempts at d_n fluctuate wildly (because of the large penalty function applied to the objective function until) the process converges to a diameter of about 2.0 mm. Then, the spring constant is altered briefly with the new diaphragm orifice diameter fixed. This is because the initial search directions were set to the unit vectors. After about 40 iterations, the optimization program decides on its own best search directions and alters both k_s and d_n simultaneously until convergence. Similar optimizations were done for the SENS index and the ITAE index, with the resulting optimums SENSMIN = 0.0732 and ITAEMIN = .0227 (Figures 13.3 and 13.4). The optimum design variables were d_n= 2.0 mm and k_s = 45208 N/m when optimizing for SENS and d_n = 2.0 mm and k_s = 40989 N/m when optimizing for ITAE.

Finally, the goal function was defined as

$$G(x) = \frac{VAR(x)}{.000734} + \frac{SENS(x)}{.0732} + \frac{ITAE(x)}{.0227}$$

Figure 13.5 shows the results of optimizing the goal function (it is desired to minimize this function). The goal function was reduced to a value of 3.53 (a minimum value of 3.0 would indicate perfect goal congruency). The final design variables were d_n = 2.0 mm and k_s= 17850 N/m. It should be noted that the lower limit constraint on the diaphragm orifice diameter is active in this case, but none of the constraints on the spring constant are active. The corresponding values of the objective function are VAR_* = .000742, $SENS_*$ = .114 and $ITAE_*$= .0232. The goal achievements can be computed as follows,

Goal achievement for VAR = $VARMIN/VAR_*$ = .000734/.000742

= 98.9 %

Goal achievement for SENS = $SENSMIN/SENS_*$ = .0732/.114

= 64.2 %

Goal achievement for ITAE = $ITAEMIN/ITAE_*$ = .0227/.0232

= 97.8 %

It should be noted that this is only one of many possible nondominated solutions. If, for example, it is desired to have a better SENS index, the ϵ_2 constraint can be decreased and the problem resolved.

In conclusion, it is recommended that the pump pressure be 180 psi, the preload force be 78 N, the effective diaphragm mass be 20 g,. the diaphragm orifice diameter be 2.0 mm, and the spring constant 17850 N/m.

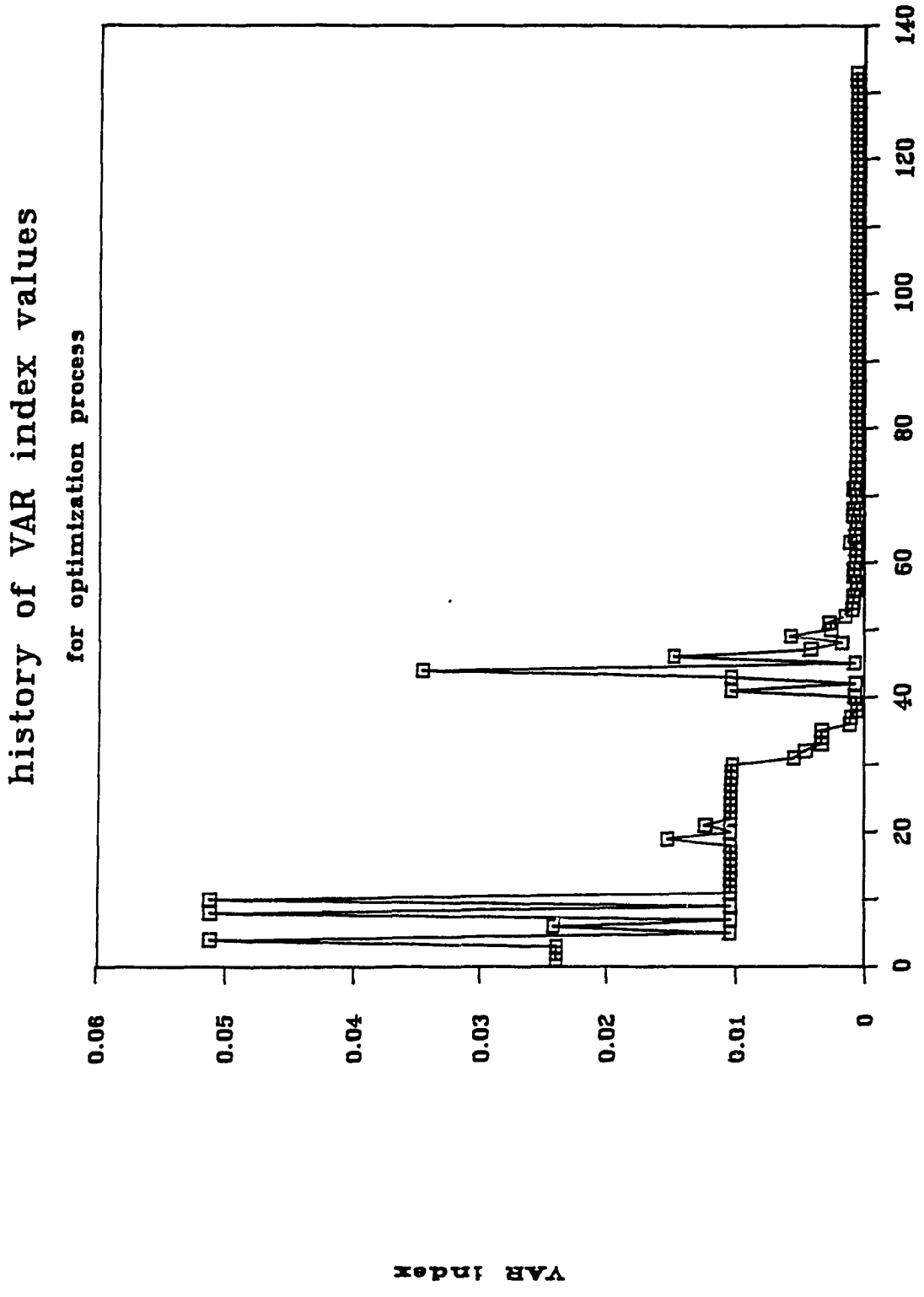

13.2 (a) Optimizing for VAR - History of Var index Values

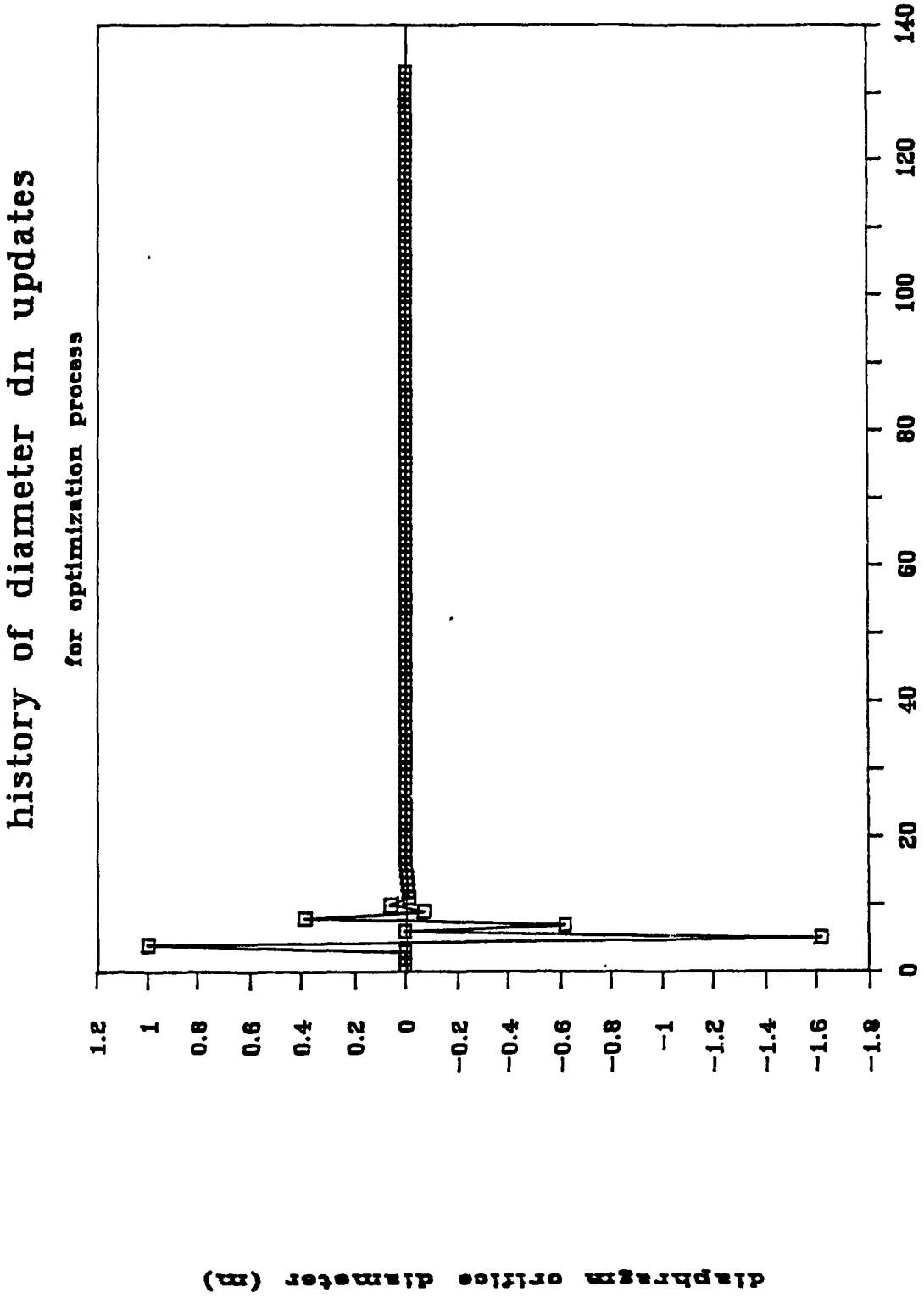

13.2 (b) Optimizing for VAR - History of Diameter d_n updates

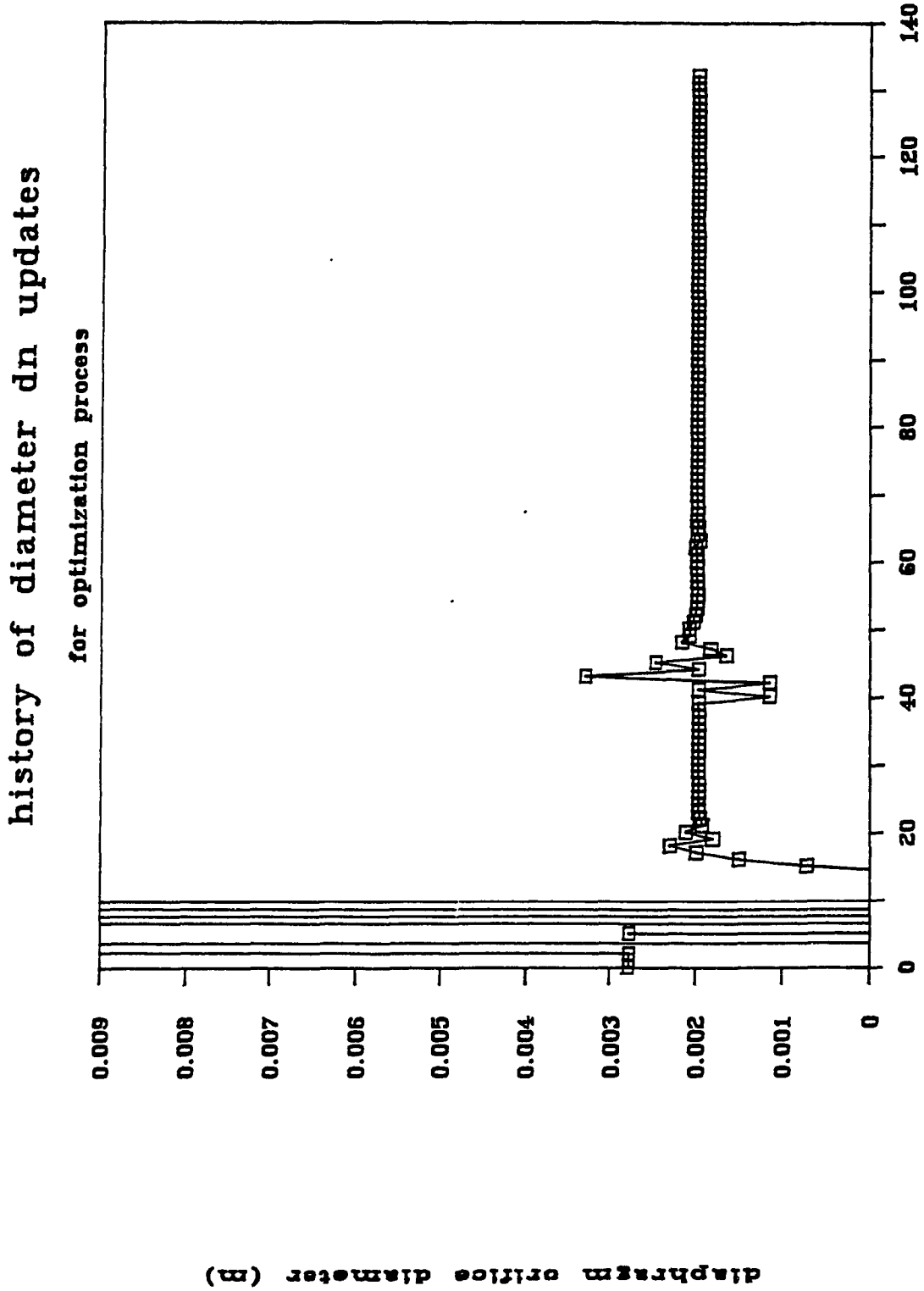

13.2 (c) Optimizing for VAR - History of diameter dn Updates (detail)

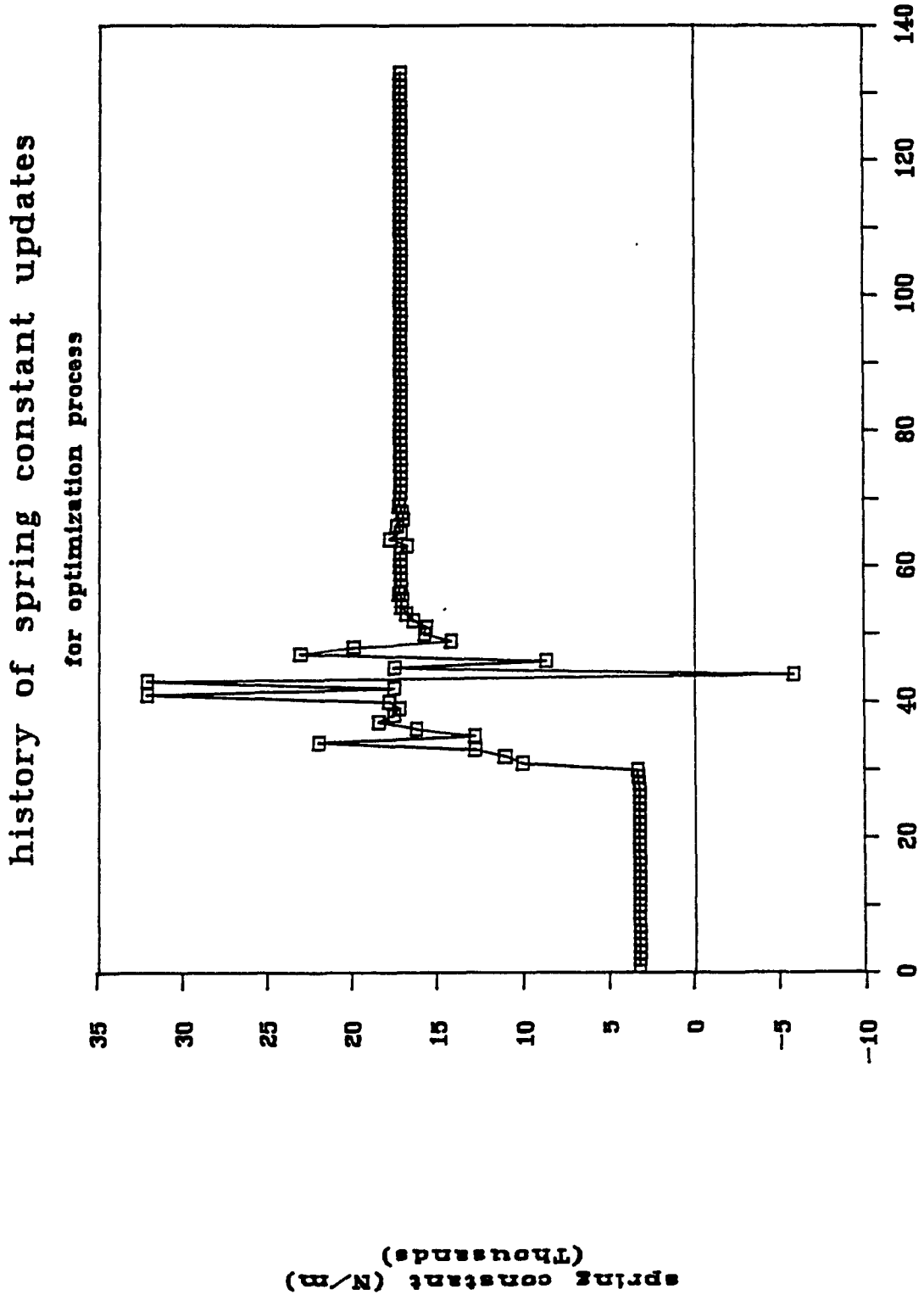

13.2 (d) Optimizing for VAR - History of Spring Constant Updates

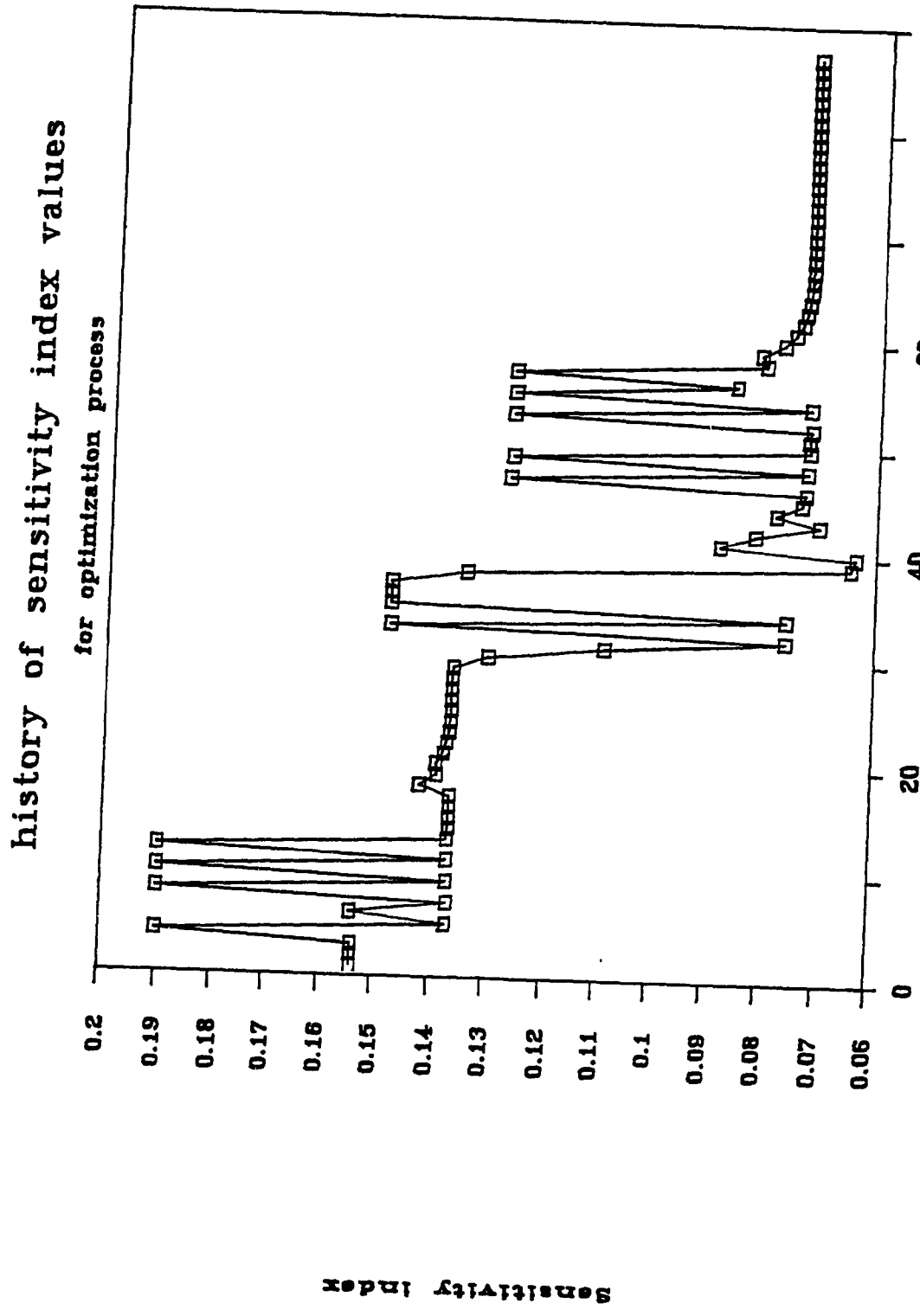

13.3 (a) Optimizing for SENS - History of SENS index values

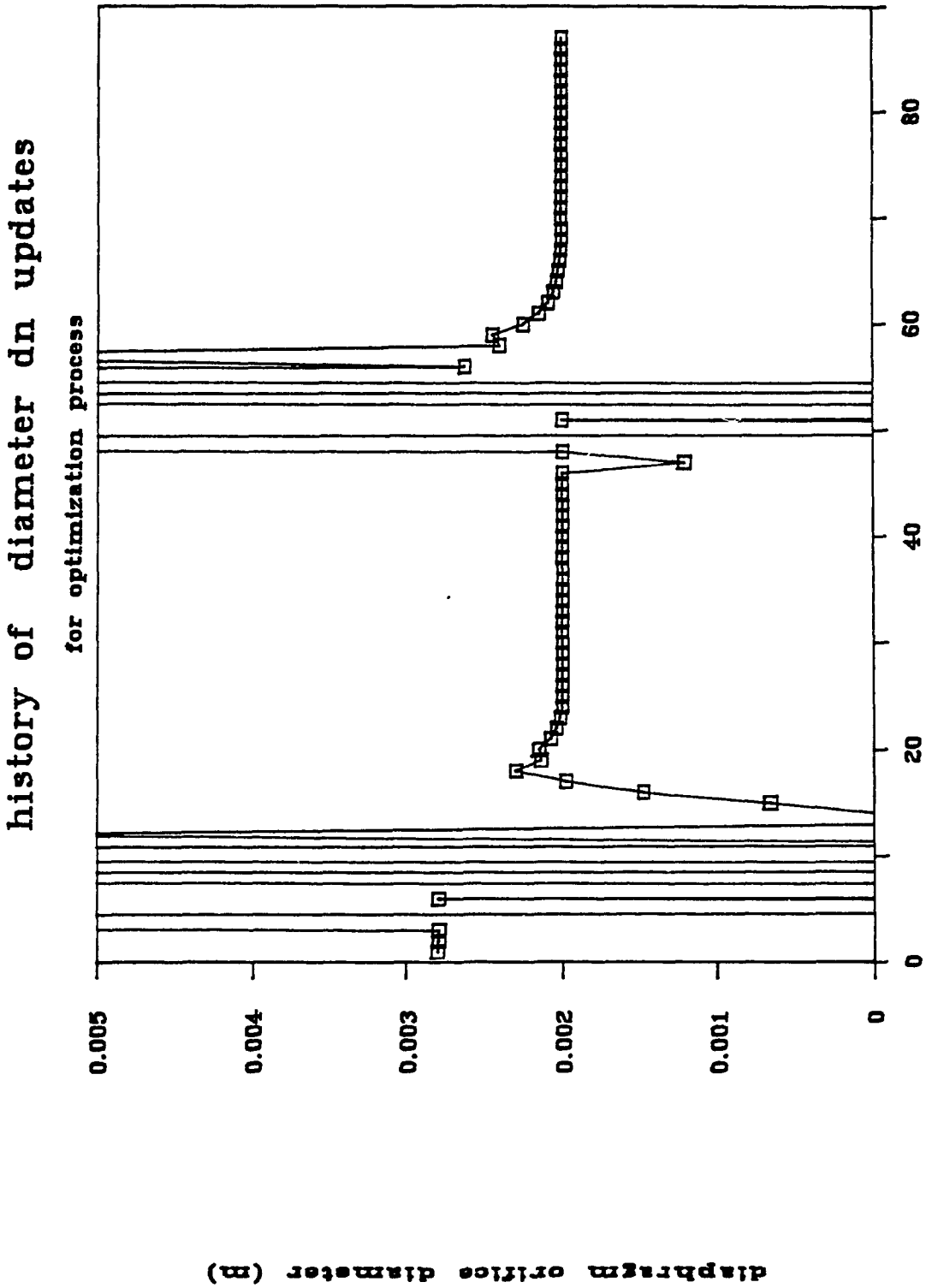

13.3 (b) Optimizing for SENS - History of Diameter Dn Updates

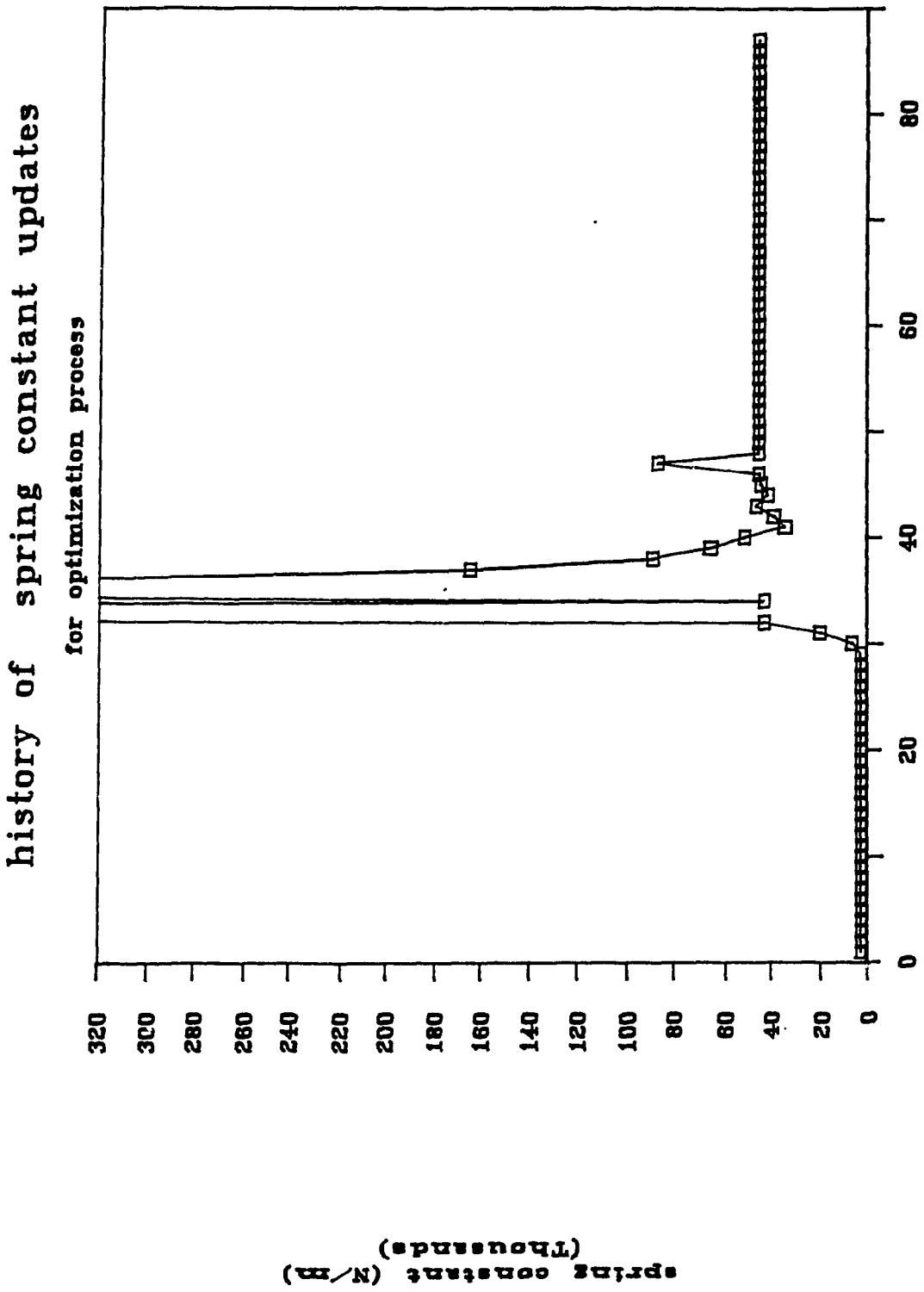

13.3 (d) Optimizing for SENS - History of Spring constant updates

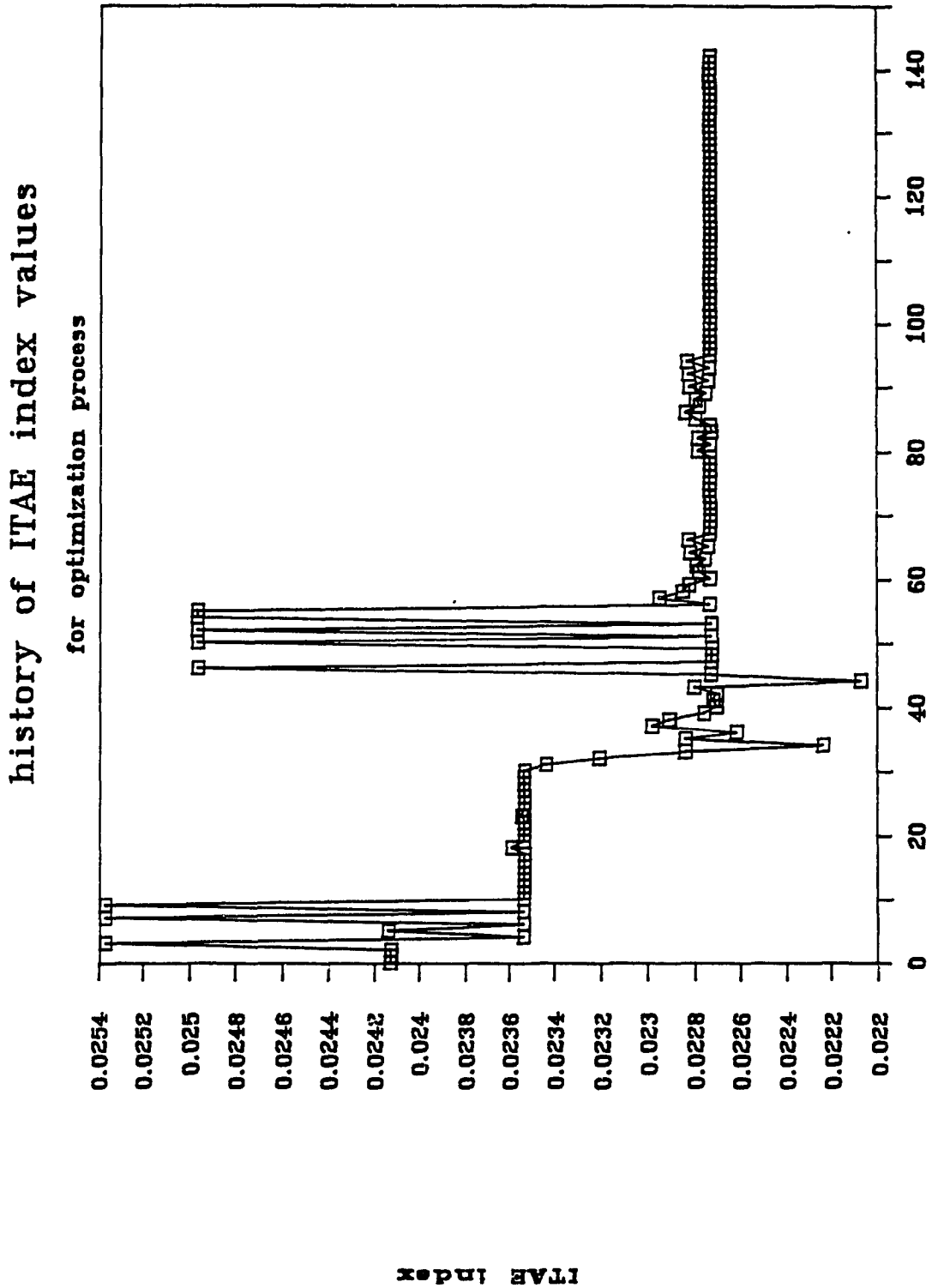

13.4 (a) Optimizing for ITAE - History of ITAE Index Values

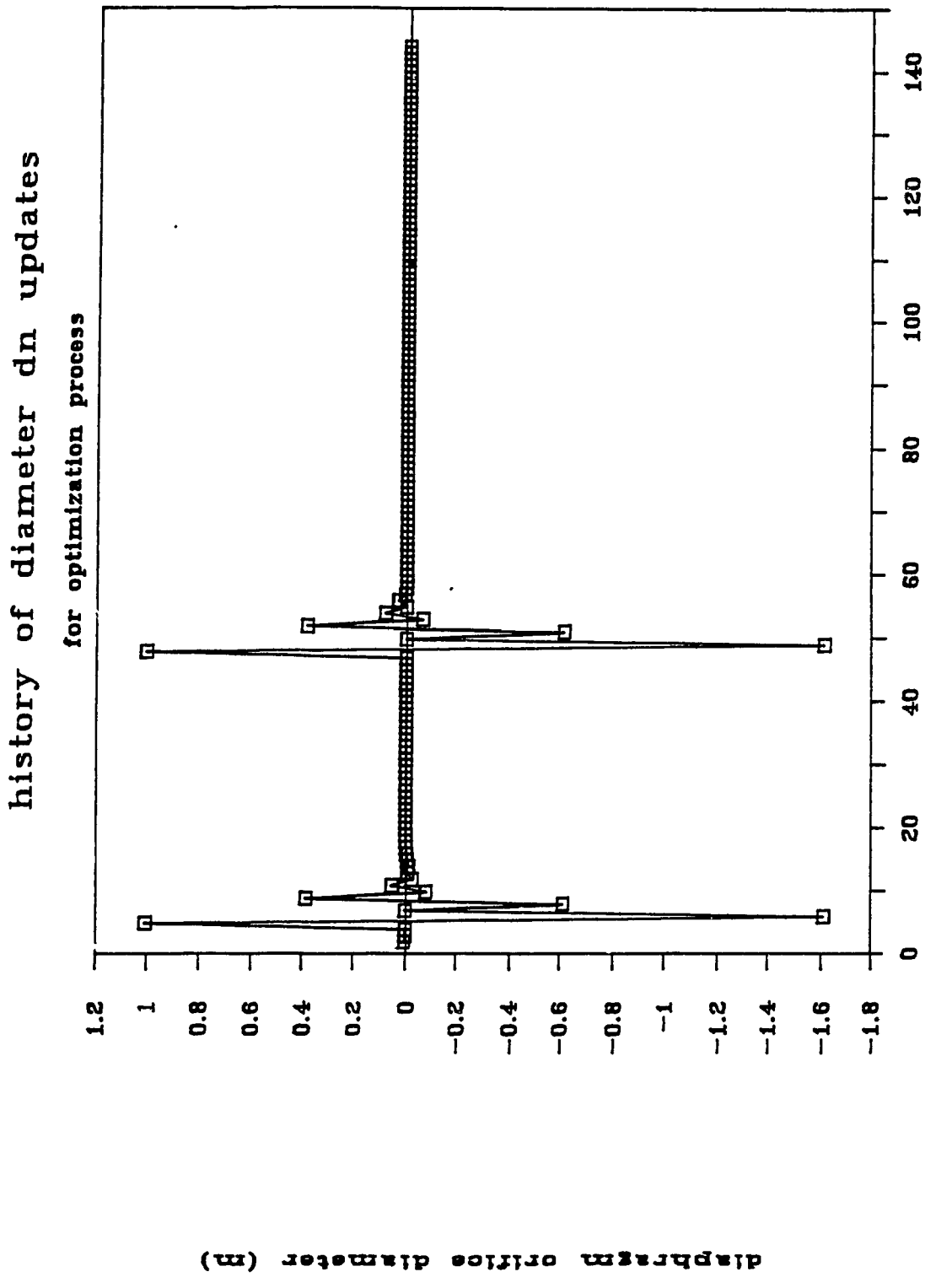

13.4 (b) Optimizing for ITAE - History of diameter Dn Updates

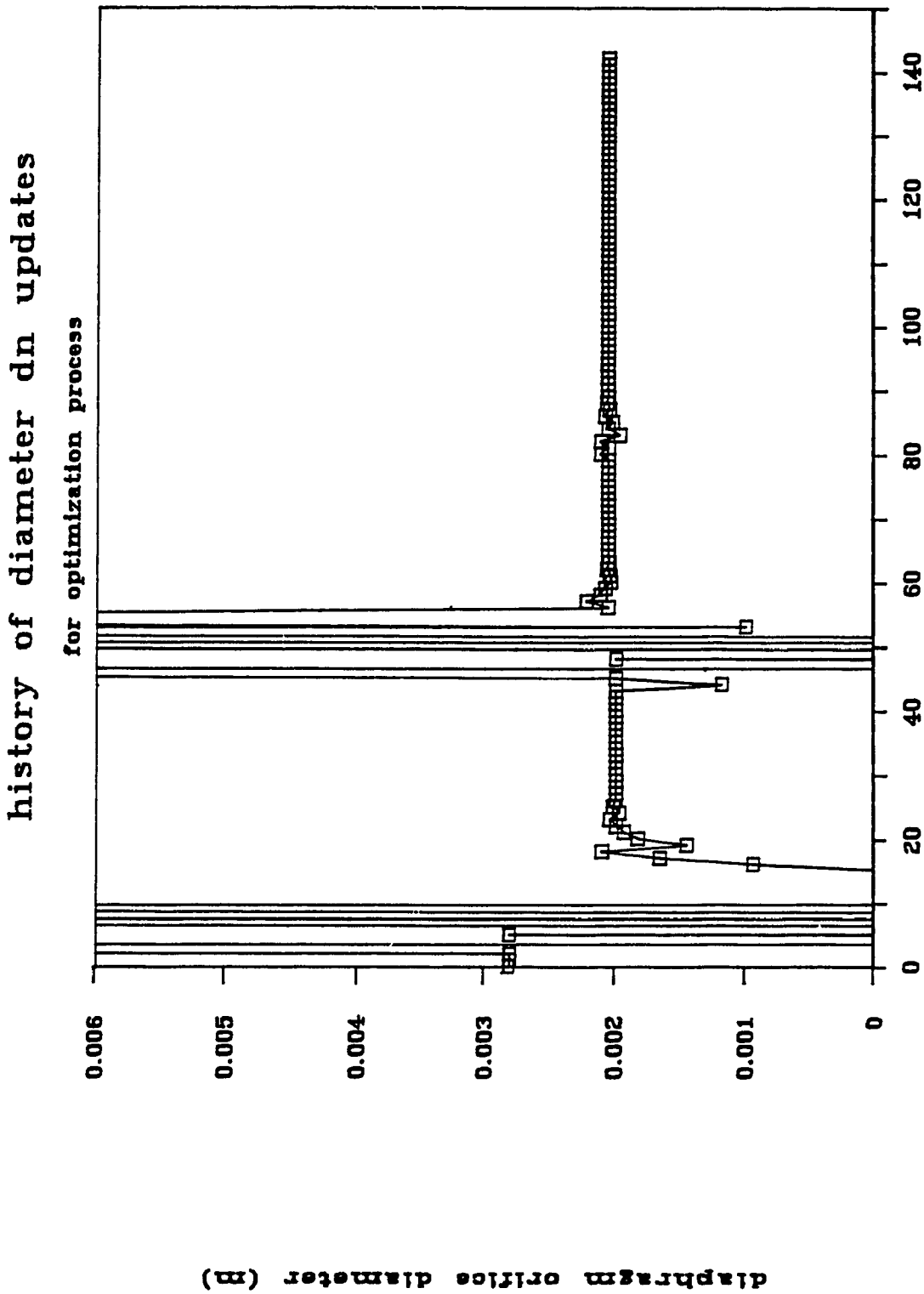

13.4 (c) Optimizing for ITAE - History of Diameter Dn Updates (detail)

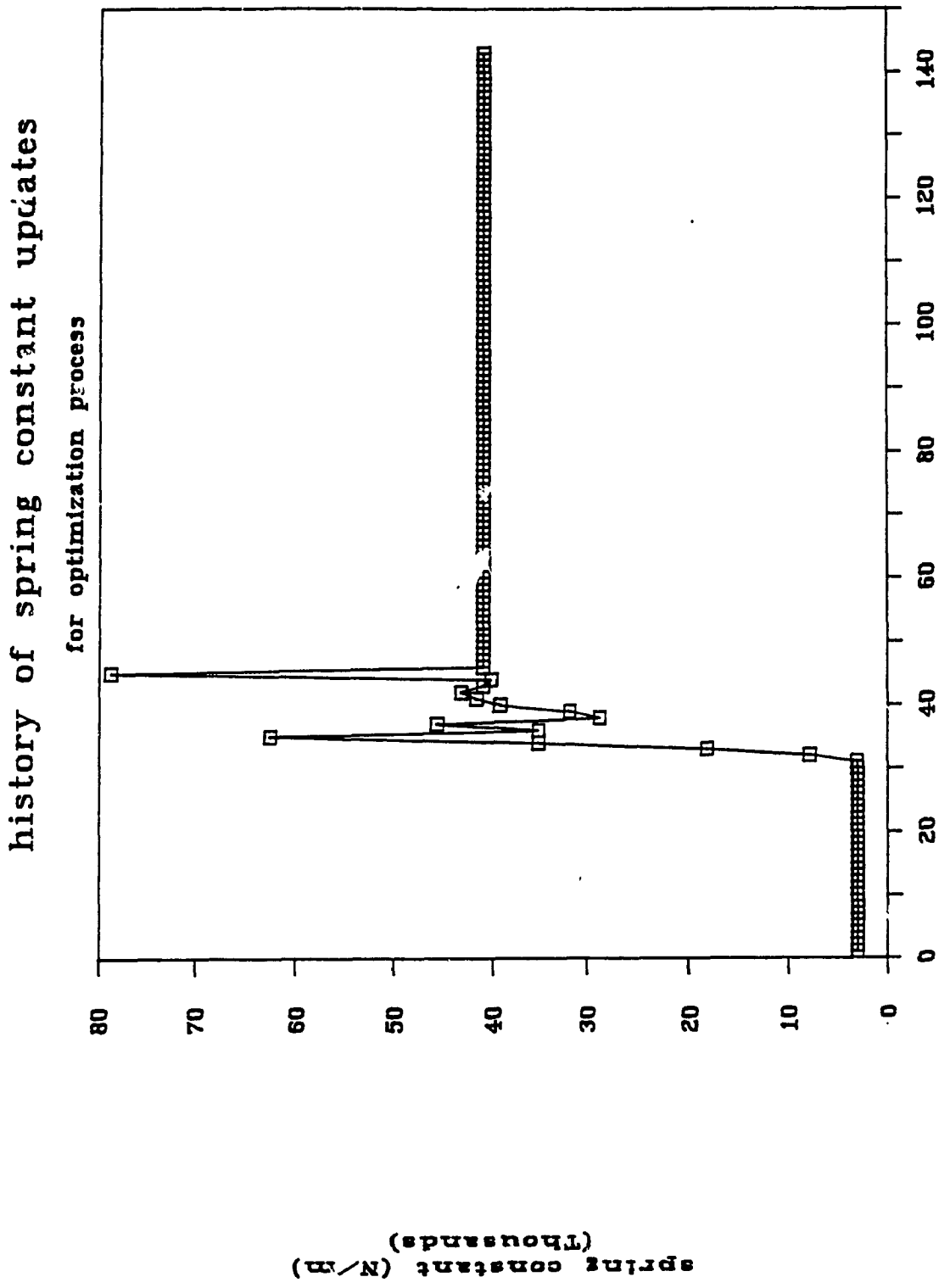

13.4 (d) Optimizing for ITAE - History of Spring Constant Updates

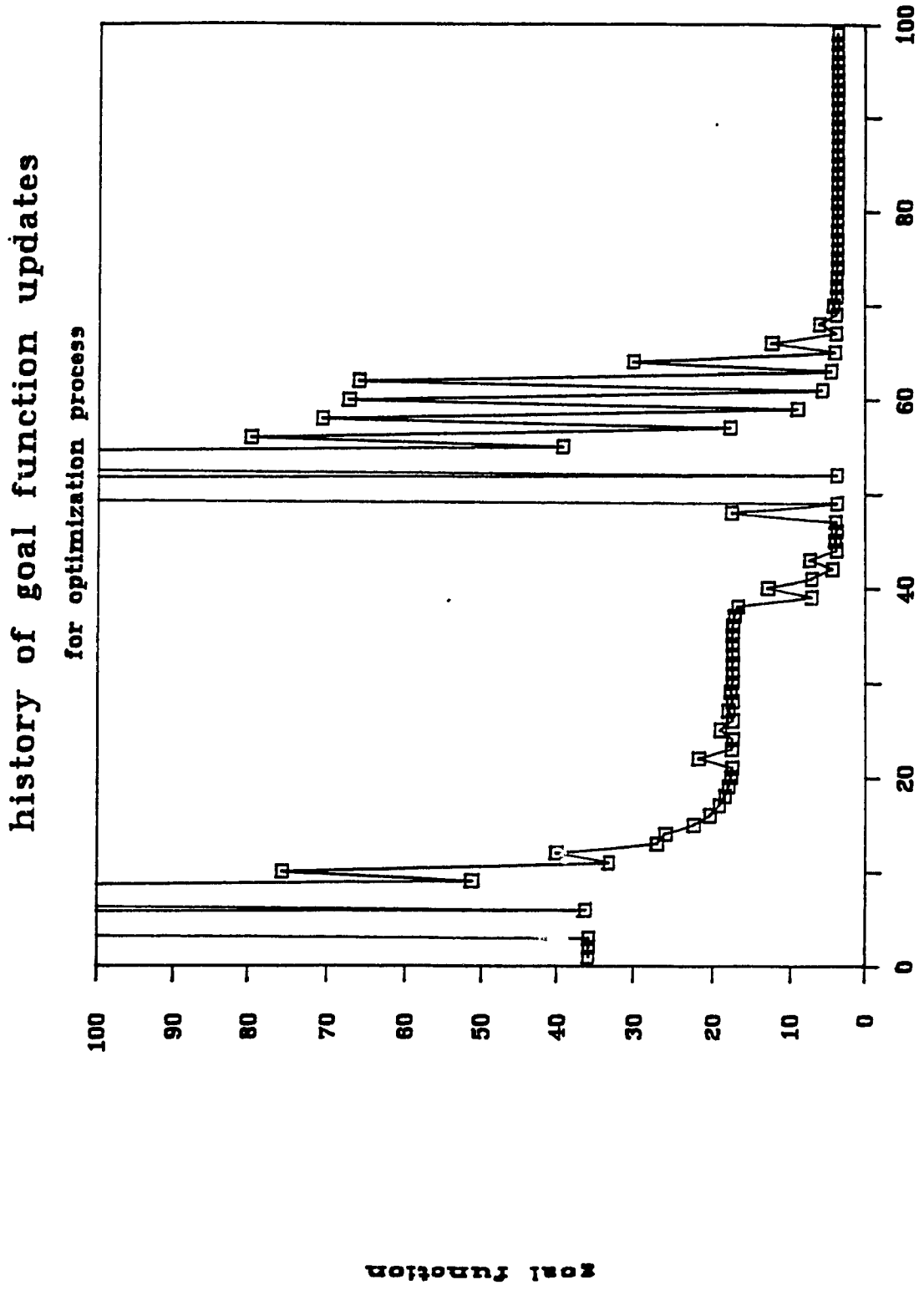

13.5 (a) Optimizing for Goal Achievement - History of Goal Function Values

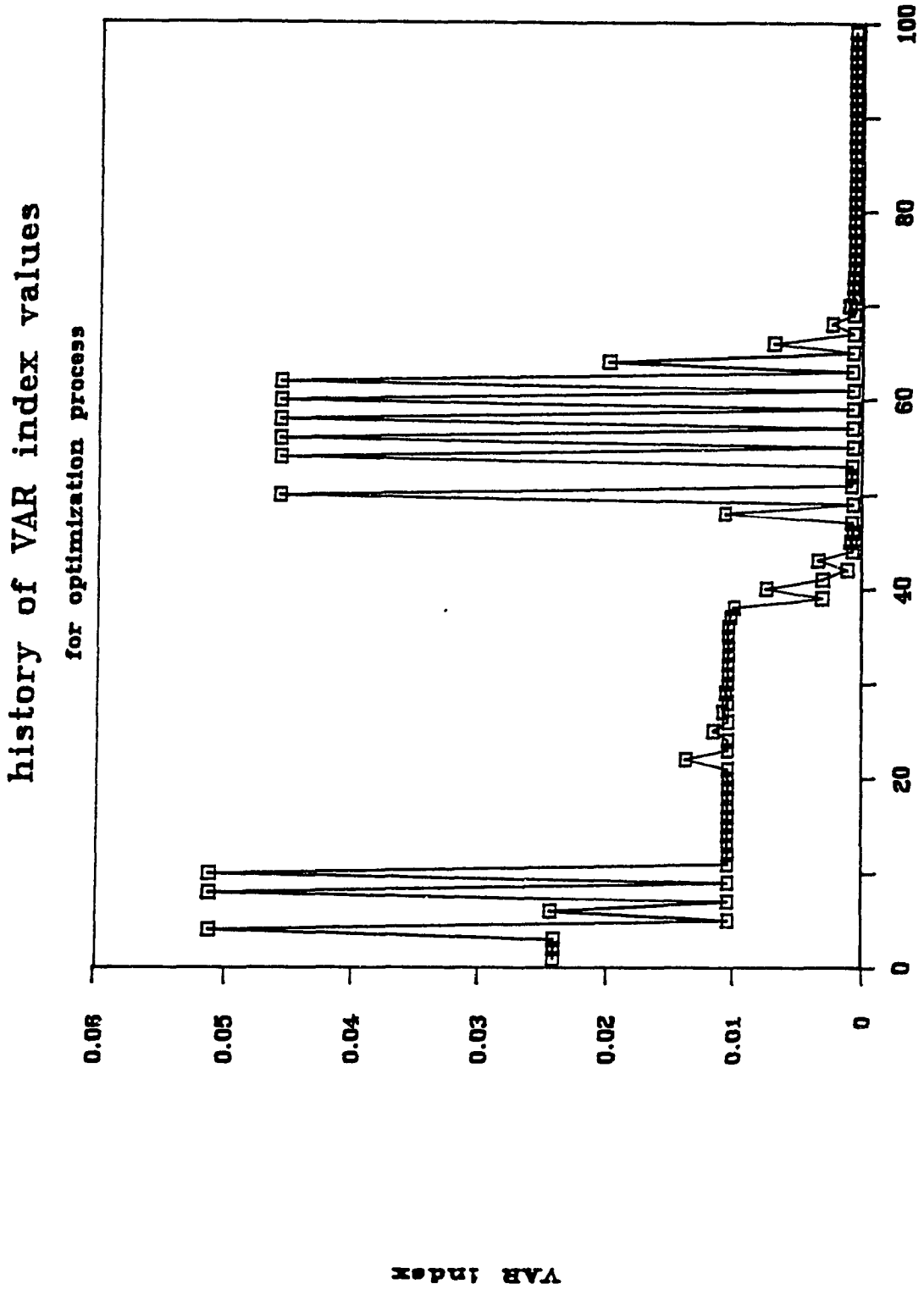

13.5 (b) Optimizing for Goal Achievement - History of VAR Index Values

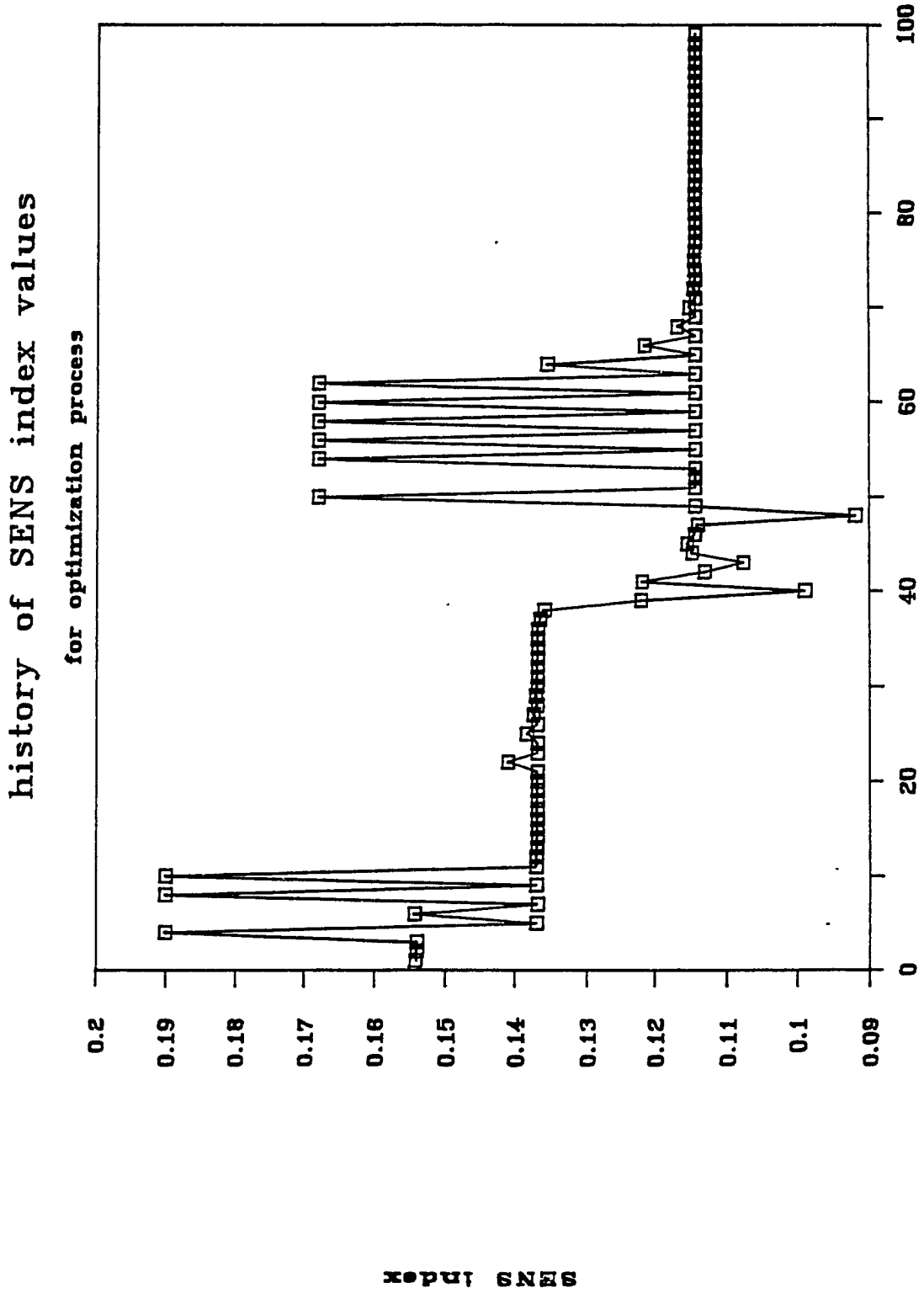

13.5 (c) Optimizing for Goal Achievement - History of SENS Index Values

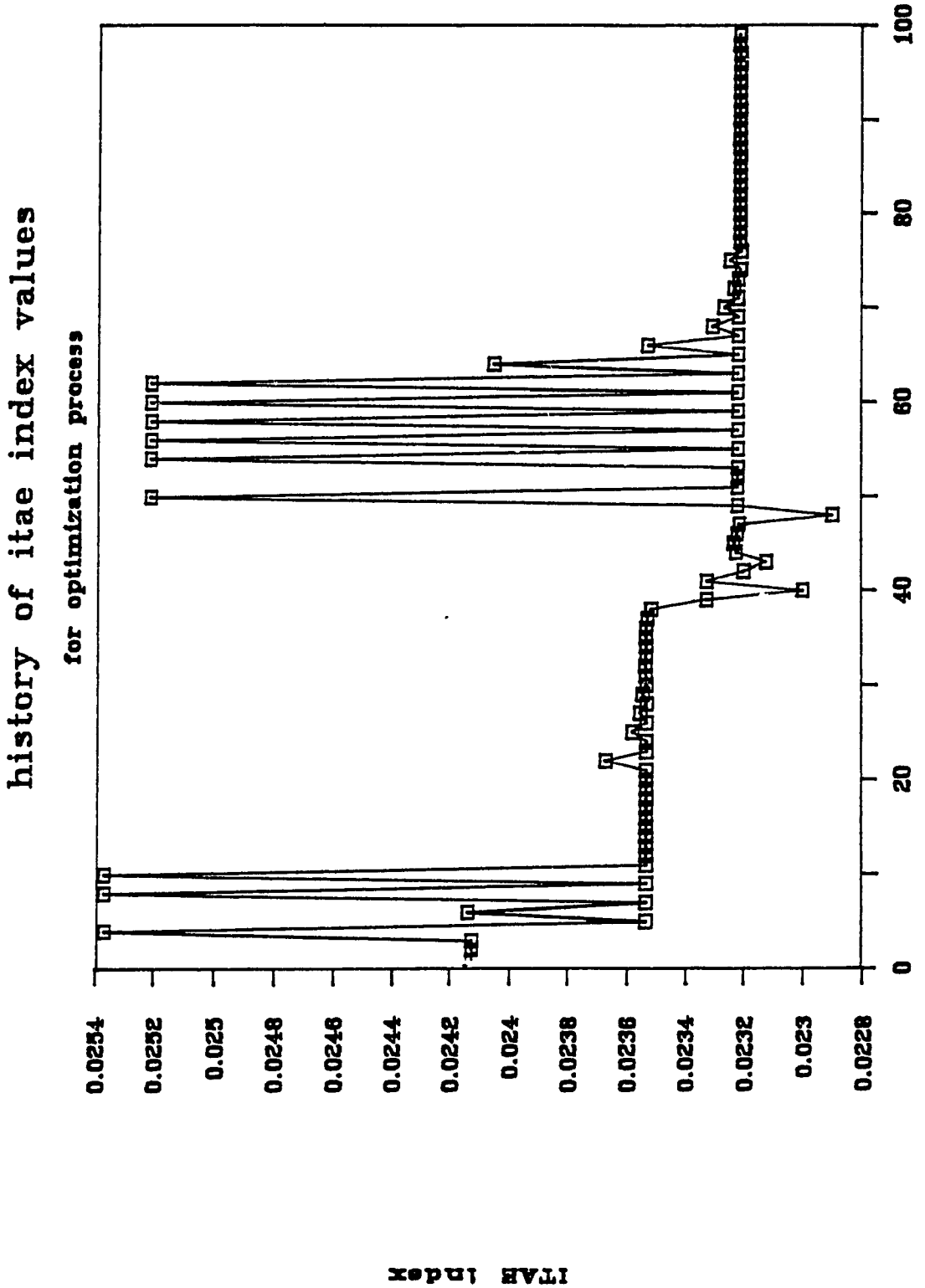

13.5 (d) Optimizing for Goal Achievement - History of ITAE Index Values

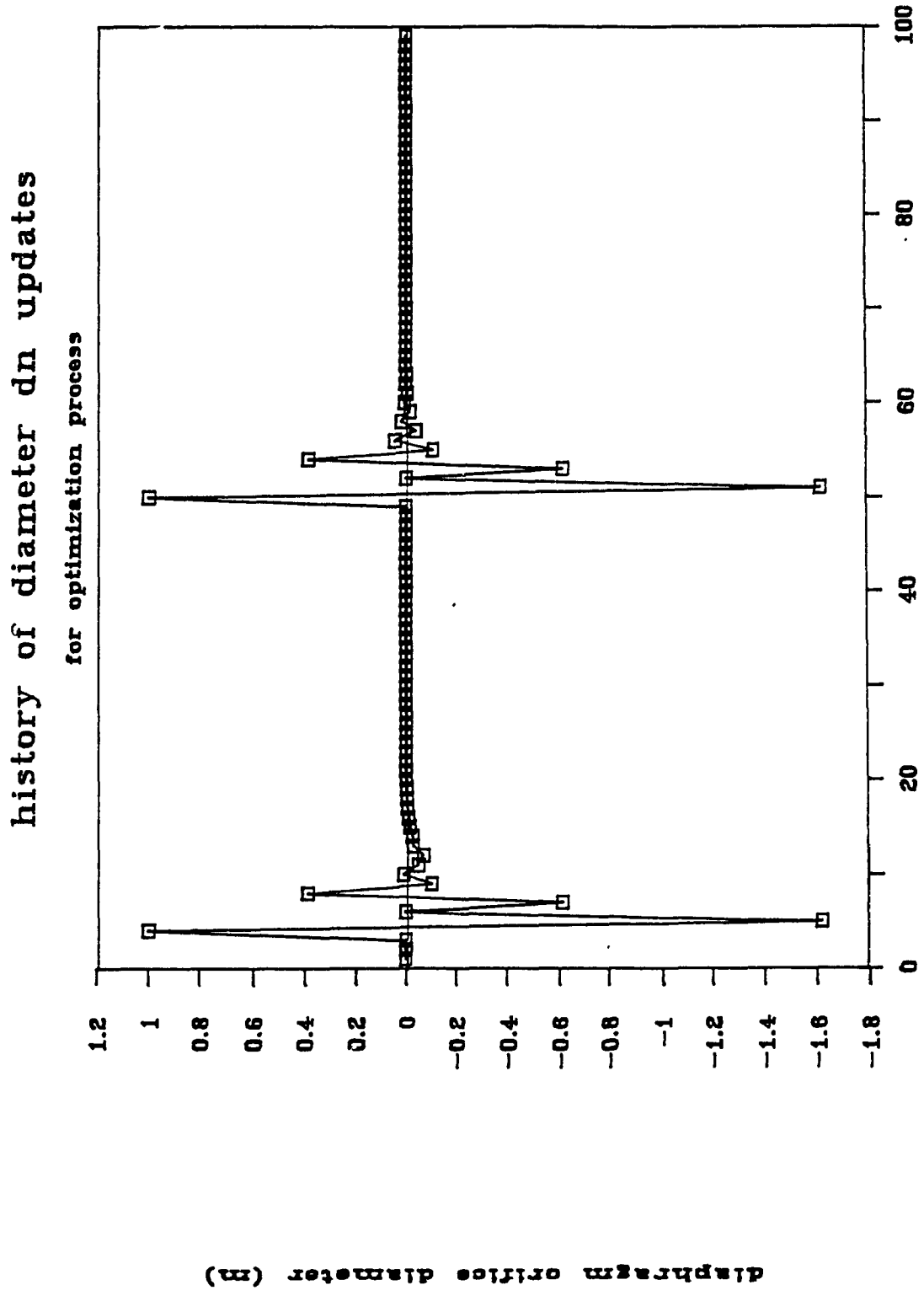

13.5 (e) Optimizing for Goal Achievement - History of Diameter Dn Updates

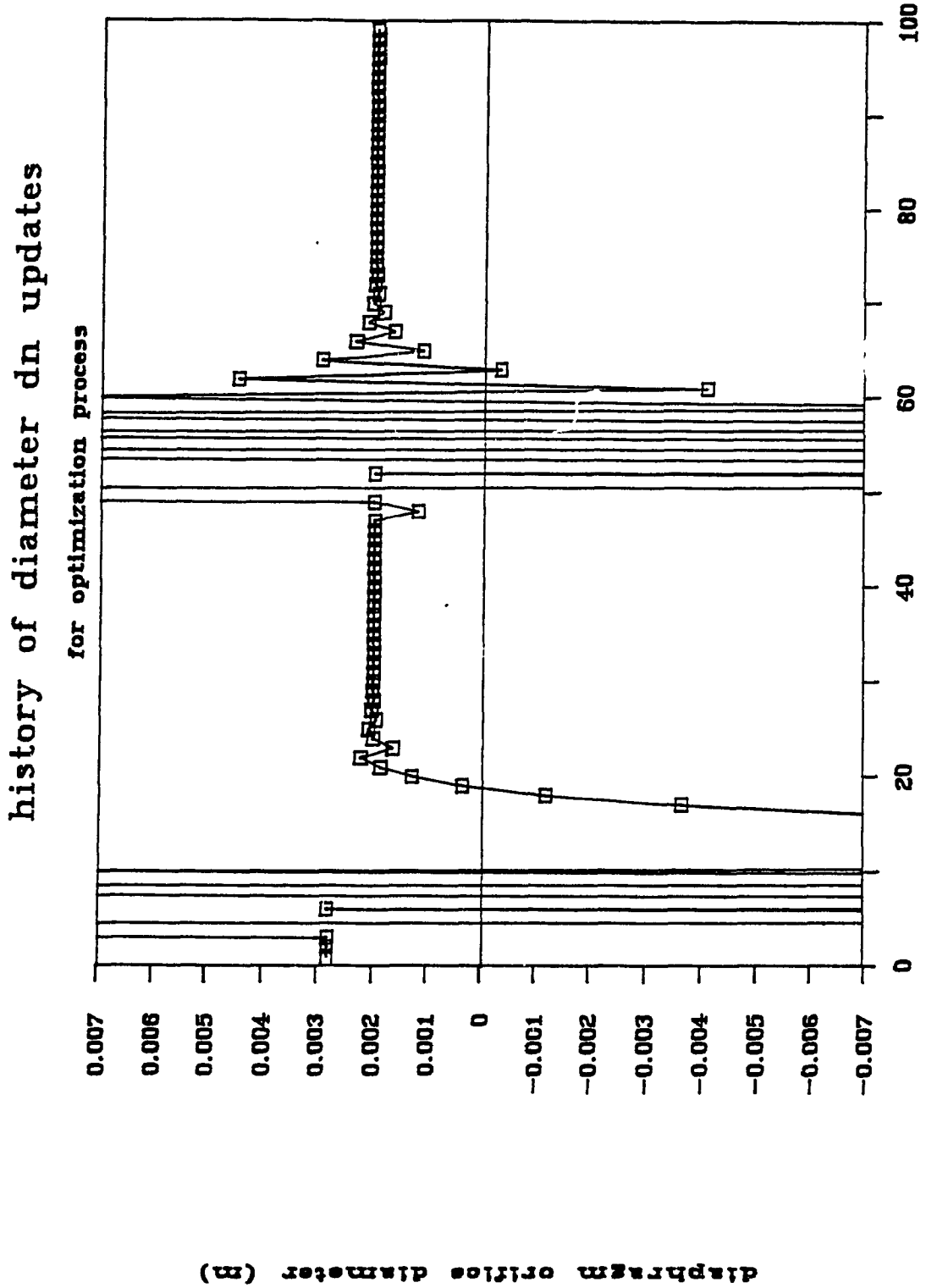

13.5 (f) Optimizing for Goal Achievement - History of Diameter Dn Updates (detail)

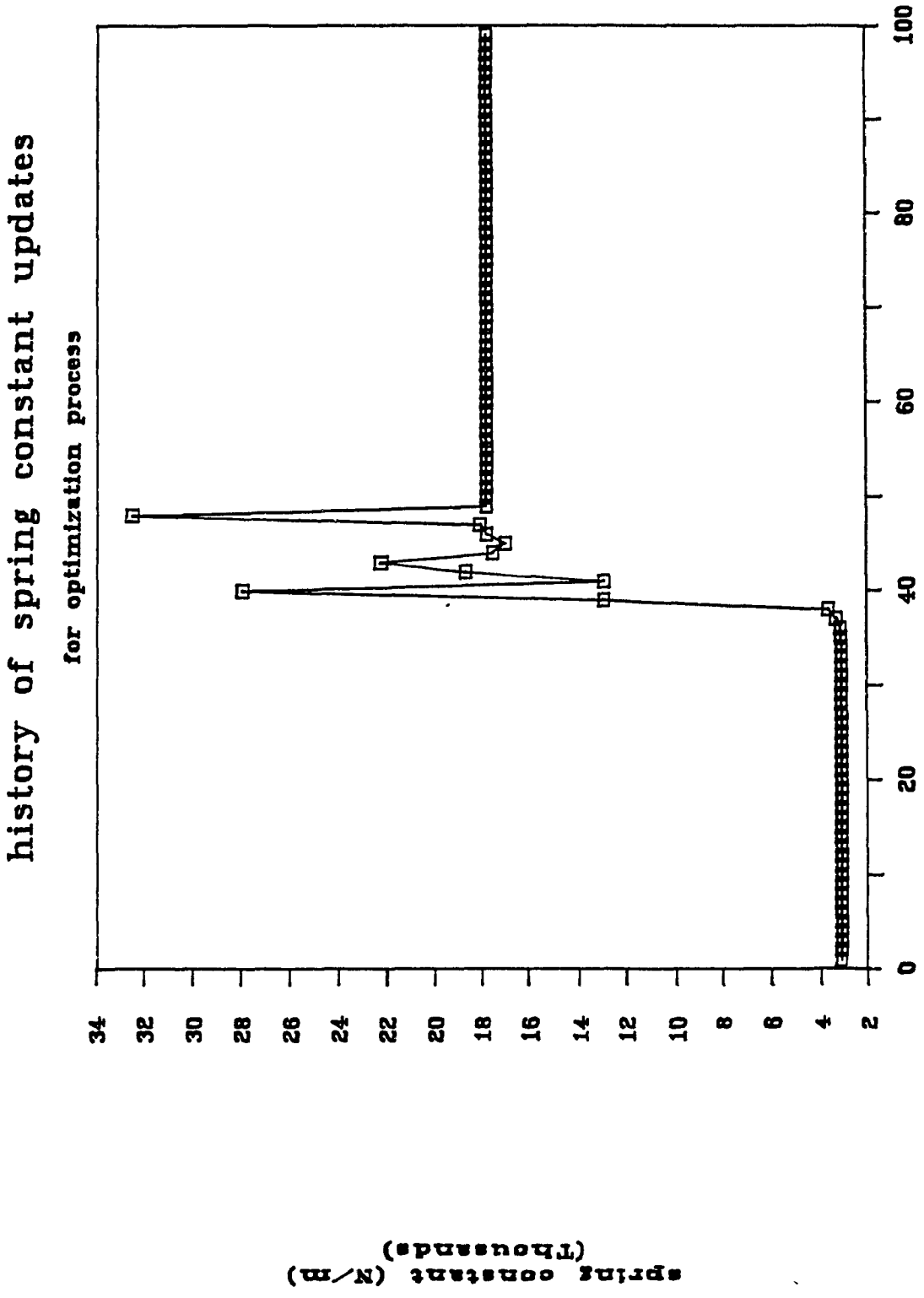

13.5 (g) Optimizing for Goal Achievement - History of Spring Constant Updates

Chapter 14

Summary, Conclusion and Recommendations

A new electronic fuel control system design for small gas turbine engines has been studied experimentally and analytically. The unit was shown to be capable of meeting the fuel flow demands of a small gas turbine. It is inexpensive because it uses mass produced components from automotive fuel injection technology. Also, since the design incorporates some proven reliable concepts used in mass produced automotive fuel injection systems, the reliability prospects of the design are good. The steady state and transient computer simulation models were shown to accurately predict the system performance. This allowed the use of the models for computer aided design optimization. Three criteria, linearity of the metering valve flow schedule, sensitivity and speed of transient response, were identified as the most important design optimization goals. Indices were created to suitably quantify these goals. The effect of design variables on these indices was studied. It was found that the variation of differential pressure across the metering valve over the flow schedule could be minimized by careful selection of design variables. A mathematical method was formulated to derive the system sensitivity to design parameter changes during its operational life. These analyses required only the steady state model equations. The effect of design variables on the transient response of the system was also studied.

A method to consider simultaneously all the design goals was developed. Computer codes for the various analyses performed in the thesis were unified in a multiple objective optimization scheme. This scheme solicits (from the designer) subjective acceptability limits for each of the design criteria. It then proceeds to recommend a nondominated design based on these limits. Monotonicity analysis was successfully used to simplify the optimization model. A search technique was implemented to numerically find the optimum design point.

This study indicates that the design parameters of the system can be suitably selected in order to improve all of the design criteria.

The analysis performed in this thesis should be verified experimentally byrebuilding the fuel control unit with the recommended design variables testing it. tests to ensure that the computer still accurately predicts the performance. The analysis used in this thesis is quite general and can be applied to the development of any new fuel control according to customer specifications.

More sophisticated multiobjective analysis techniques could be explored where the designer enters his subjectivity into the analysis at different stages. A more efficient optimization scheme should be found and with the help of a faster computer, the entire nondominated set of designs should be found and presented to the designer, who would make his final decision based on these results.

Further work on this project is recommended. Multiobjective optimization is a growing area of research and should be explored further. More sophistigated techniques than the one used in this thesis are presented in the literature. Follow up work wouldinclude the addition of a microcontroller to the fuel metering unit. A computer engine model can be linked to the fuel control unit model and microcontroller to study the closed loop behaviour of the system, thus including the engine dynamics. Much research must be done in programming the controller. One interesting possibility is to adapt multiobjective optimization techniques to deal with the optimal digital control of the system.

References

1. H. Cohen, C.F.C. Rogers, and H.I.H. Saravanamutoo, "Gas Turbine Theory", Longmon Group Ltd, London, 1972.

2. H.I.H. Saravanamutoo, "Gas Turbine Performance and Design", Lecture Notes, Carleton University, Ottawa, Canada, 1985.

3. R.G. Moore, "Fuel System Requirements for Small Gas Turbine Engines", SAE paper No. 740381, 1974

4. T. Krepec, "Fuel Control Systems for Combustion Engines", Lecture Notes, Concordia University, 1988

5. W.C. Peck, "Microelectronics in Fuel Controls", SAE paper No. 650529, 1965.

6. R. Falk, "Digital Electronics Applied to the Control of Gas Turbine Engines", SAE paper 650528, 1965.

7. K. B. Swonger and M.F. Huffman, "Low Cost Control System for Expendable Turbine Engines" , AIAA/ASME/SAE/ASEE 25 Joint Propulsion Conference, Monterey, CA, July 10-12, 1989.

8. A.I. Georgantes and T. Krepec, "Investigations on an Electronically Controlled Metering Valve in a Fuel Control Unit for Small Gas Turbine Engines", Proceedings of the 1987 ASME International Conference and Exhibition, ASME, New York, August 9-13, 1987.

9. F. C. Zuliani and G. N. Kline, "Microcomputer Brings Digital Power to Small Gas Turbine", SAE paper 821402, 1982.

10. G. D. Cropper, "Electronic Fuel Controls for Missile and RPV Gas Turbines", SAE paper 751061, 1975

11. A.I. Georgantes and T. Krepec, "Low Cost Electronic Fuel Control Unit for Small Gas Turbine Engines of Remotely Piloted Vehicles", Progress Report no. 1 to Bendix, Avelex, Concordia University, 1987.

12. M. McGlone, R. Miller, J. Davies, P. Adams, "Full Authority Fault Tolerant Electronic Engine Control Systems for Advanced High Performance Engines (FAFTEEC)", SAE paper 821398, 1982.

13. S. Janic, "Full Authority Digital Control for a Small Turbine Helicopter Engine", SAE paper 831476, 1983.

14. A. Georgantas and T. Krepec, "Diesel Injection Pump Conversion for Alternative Applications", Proceedings of the Tenth Congress of Applied Mechanics, London, Ontairio, June 2 - June 7, 1985 , p. b141.

15. A. Georgantas, M. Krepec and T. Krepec, "New Possibilities in Fuel Flow Modulation for Small Gas Turbine Engines", Proceedings of the Tenth Congress of Applied Mechanics, London, Ontairio, June 2 - June 7, 1985 p. b181.

16. A.I. Georgantas, T. Krepec, and R.M.H. Cheng, "Interaction of Two Electronic Actuators Employed in a Fuel Control Unit for Small Gas Turbine Engines", Proceedings of the 1988 ASME International Computers in Engineering Conference and Exhibition, ASME, San Francisco, August 1-4, 1988.

17. A.I. Georgantes and T. Krepec, "Investigations on an Electronically Controlled Metering Valve in a Fuel Control Unit for Small Gas Turbine Engines", Proceedings of the 1987 ASME International Conference and Exhibition, ASME, New York, August 9-13, 1987.

18. G. Carrese, A. Georgantes, and T. Krepec, " A New Multivariable Controller Tuning Method for the Digital Controller of a Small Gas Turbine Engine", Proceedings of the 1989 ASME International Computers in Engineering Conference and Exhibition, ASME, Anneheim, CA, August 1-4, 1989.

19. A.I. Georgantes, G. Carrese, and T. Krepec, "Designing and Tuning the Digital Controller of an Electronic Fuel Control Unit for Small Turbine Engines", SAE paper no. 892255, 1989.

20. A.I. Georgantes and T. Krepec, "Low Cost Electronic Fuel Control Unit for Small Gas Turbine Engines of Remotely Piloted Vehicles", Progress Report no. 1 to Bendix, Avelex, Concordia University, 1987.

21. A.I. Georgantes, G. Carrese and T. Krepec, "Low Cost Electronic Fuel Control Unit for Small Gas Turbine Engines of Remotely Piloted Vehicles", Progress Report no. 2 to Bendix, Avelex, Concordia University, 1988.

22. A.I. Georgantas, G. Carrese and T. Krepec, "Low Cost Electronic Fuel Control Unit for Small Gas Turbine Engines of Remotely Piloted Vehicles", Progress Report no. 3 to Bendix, Avelex, Concordia University, 1989.

23. A.I. Georgantas, G. Carrese and T. Krepec, "Low Cost Electronic Fuel Control Unit for Small Gas Turbine Engines of Remotely Piloted Vehicles", Progress Report no. 4 to Bendix, Avelex, Concordia University, 1989.

24. K. B. Swonger and M.F. Huffman, "Low Cost Control System for Expendable Turbine Engines" , AIAA/ASME/SAE/ASEE 25 Joint Propulsion Conference, Monterey, CA, July 10-12, 1989.

25. O. Glockler, H. Knapp, and H. Manger, "Present and Future Status of Gasoline Fuel Injection systems for Passenger Cars", SAE paper 800467, 1980.

26. Bosch, "Automotive Handbook", Robert Bosch, Stuttgart, 1986.

27. W. Maisch, "KE-Jetronic, A New Continuously Injecting Electronically Controlled Multipoint Injection System with Limp Home Capability", SAE paper 820253, 1982.

28. R. Schwartz, G. Stumpp, and H. Knapp, "K-Jetronic - Kontinuierliche Benzineinspritz ung von Bosch", Automobiltechnische Zeitschrift, VDI 75, 1973, 11

29. M. F. Spotts, " Design of Machine Elements", sixth edition, Prentice Hall, Inc, Englewood, CA, 1985.

30 U. Kemmner, M. Rollwage, and K. Rose, "New Generation of BOSCH Electric Fuel Pumps- Improvement in Hot-Fuel Handling and Noise", SAE paper no. 870120, 1987.

31. H. P. Press, B. P. Flannery, S.A. Teukolsky, W. T. Vettering, "Numerical Recipes in C " Cambridge University Press, Cambridge, 1988

32. P. Y. Papalambros and D. J. Wilde, "Principles of Optimal Design" , Wiley, New York, 1988.

33. S.S. Rao, "Optimization, Theory and Applications", second edition, Wiley Eastern Ltd, New Delhi, 1984.

34. A. Goicoechea, D. Hansen,and L. Duckstein, "Multiobjective Decision Analysis with Engineering and Business Applications",

35. M. E. Elliot, "Model Choice in Decision Making in Natural Resource Systems", Phd Thesis, University of Arizona, 1981.

36. A. V. Fiacco and G. P. McCormick, "Nonlinear Programming", Wiley, New York, 1968.

37. M. Box, D. Davis, "Nonlinear Optimization Techniques", Oliver and Boid, Tweeddale, 1968.

38. H. E. Meritt, "Hydraulic Control Systems", John Wiley and Sons, Inc, New York, 1967.